ABSTRACT

Title of Document: BUILDING A MAP OF THE DYNAMIC RIBOSOME.

Suna Pelin Gulay, Doctor of Philosophy, 2015

Directed By: Professor Jonathan D. Dinman
Cell Biology and Molecular Genetics

Our understanding of the static structure of the 80S eukaryotic ribosome has been enhanced by the emergence of high resolution cryo-electron microscopy and crystallography data over the past 15 years. However our understanding of the dynamic nature of the ribosome has lagged. High-throughput Selective 2'-Hydroxyl Acylation analyzed by Primer Extension (hSHAPE) is easily amenable for interrogation of rRNA dynamics. Here we report an improved method of hSHAPE data analysis and apply it to translation initiation and elongation complexes of the yeast ribosome to identify the changes in rRNA flexibility that occur during these processes. Most importantly, we have obtained complete analyses of tRNA binding and intersubunit bridge dynamics, as well as overall expansion segment dynamics, as the ribosome progresses through the translation elongation cycle. The results from these analyses suggest that (1) the yeast P site tRNA binding site is a "hybrid"

between the prokaryotic and mammalian P sites, (2) there may be substates of intersubunit rotation, (3) expansion segments may have roles in accommodation. We are also able to identify a network of information pathways that connect elongation factor binding sites to all tRNA binding sites, five intersubunit bridges and two expansion segments. Future directions of this project will focus on improving the visualization of our data to better reflect the highly dynamic nature of the yeast ribosome and to reveal the underlying causes of the observed rRNA flexibility changes.

BUILDING A MAP OF THE DYNAMIC RIBOSOME

By

Suna Pelin Gulay

Dissertation submitted to the Faculty of the Graduate School of the
University of Maryland, College Park, in partial fulfillment
of the requirements for the degree of
Doctor of Philosophy
2015

Advisory Committee:

Professor Jonathan Dinman, Chair
Associate Professor Douglas Julin
Assistant Professor Vincent Lee
Professor Anne Simon
Associate Professor Richard Stewart

Dedication

I would like to dedicate this dissertation to my family, especially my sister Ece, for lending me her ear at every petty annoyance, my fiancé Darryl, for his immense support throughout my studies, peaking in the last three months, and Şeker. This would not have become a reality if it were not for all of you.

Acknowledgements

First and foremost, I would like to thank my advisor, Dr. Jonathan Dinman, for giving me years of guidance and support, and fulfilling every last-minute request of edits or recommendation letters without fail. I learned how to be a scientist from working with you.

I would also like to thank my committee for their time and assistance in improving my research. Special thanks to Dr. Anne Simon and Dr. Vincent Lee for their support of my future career.

A big thank you to everyone in the department I had the pleasure of interacting with through teaching assistantships and administrative processes, especially Dr. John Buchner, Dr. Michelle Brooks, Ms. Gwen Warman and Ms. Molly Burke. You made my life easier in ways I cannot express.

Thank you to everyone that made contributions to my scientific endeavors, including classmates, alumni from Dinman lab, and collaborators at UMD, NIH, LANL. I am looking forward to continue working with you all.

Last but not least, very sincere thanks to my support system: friends and family that helped make UMD my home away from home. A special note of appreciation goes to my "Dinman lab family": Dr. Sharmishtha, Alicia, Carol, Cassie, Drs. Trey & Lara, Vivek, Ryan, and Joe. You all made for an enjoyable experience both in and outside the lab. It was a crazy ride, and I appreciate you being there to experience it with me. We will always be close friends and colleagues.

Table of Contents

List of Tables

List of Figures

List of Abbreviations

1M7	1-methyl-7-nitroisatoic anhydride
AC	Accommodation corridor
Ac-Phe-tRNA	N-acetyl-phenylalanyl tRNA
ANI	Anisomycin; used to denote a complex prepared with this antibiotic
ASL	Anticodon stem loop
CHX	Cycloheximide; used to denote a complex prepared with this antibiotic
CP	Central protuberance
Cryo-EM	Cryogenic electron microscopy
CTD	Carboxyl terminal domain
CTT	Carboxyl terminal tail
DC	Decoding center
EF	Elongation factor
ES	Expansion segment
GAC	GTPase associated center
hSHAPE	Highthroughput selective 2’-hydroxyl acylation analyzed by primer extension
IF	Initiation factor
ln	Natural log
LSU	Large subunit
NGD	No-go decay

NTD	Amino terminal domain
NTT	Amino terminal tail
ORF	Open reading frame
Phe-tRNA	Phenylalanyl tRNA
PIC	Preinitiation complex
Postacc	Used to abbreviate “postaccommodation” complex
Posttrans	Used to abbreviate “posttranslocation” complex
Preacc	Used to abbreviate “preaccommodation” complex
Pretrans	Used to abbreviate “pretranslocation” complex
PTC	Peptidyltransferase center
RF	Release factor
smFRET	Single molecule Förster resonance energy transfer
SRL	Sarcin-ricin loop
SSU	Small subunit
TC	Ternary complex

Chapter 1: Introduction

1.1. The Ribosome and its static structure

Protein synthesis, also called translation, is a crucial step in the central dogma of molecular biology. It involves the decoding of genetic information carried by the messenger ribonucleic acid (mRNA) by the the ribosome, employing transfer RNAs (tRNA) carrying amino acids and protein factors that regulate different steps. To understand translation, it is critical to understand the structure, both static and dynamic, of the ribosome. The ribosome is a ribonucleoprotein complex consisting of two subunits, each of which are composed of ribosomal RNA (rRNA) and proteins. The two subunits and the fully associated ribosome are named after their sedimentation values. Bacterial 70S ribosomes are made up of the 50S and 30S subunits. The 50S subunit is composed of 33 proteins, 5S rRNA (121 bases) and 23S rRNA (2904 bases), while 30S is composed of 21 proteins and 16S rRNA (1542 bases) (Figure 1) [1]. Eukaryotic 80S ribosomes are made up of the 60S and 40S subunits. In lower eukaryotes, such as *Saccharomyces cerevisiae*, 60S consists of 46 proteins, 5S (121 bases), 5.8S (158 bases) and 25S rRNA (3396 bases), while 40S consists of 33 proteins and 18S rRNA (1800 bases) (Figure 1) [1]. Higher eukaryotes, such as *Homo sapiens*, have even larger ribosomes, in which 60S is composed of 47 proteins, 5S (121 bases), 5.8S (156 bases) and 28S rRNA (5034 bases), and 40S is composed of 33 proteins and 18S rRNA (1870 bases) [1]. Although the primary sequences of the rRNAs can vary greatly among different species and are used to determine phylogenetic relationships, they all fold into complex secondary structures

that are highly conserved in all domains of life, and can further fold into conserved tertiary structures. The eukaryotes have extra rRNA regions in addition to the core structure. These are called "expansion segments" (ES) (Figure 1), which get longer and more complex as we go higher in the assumed hierarchy of species.

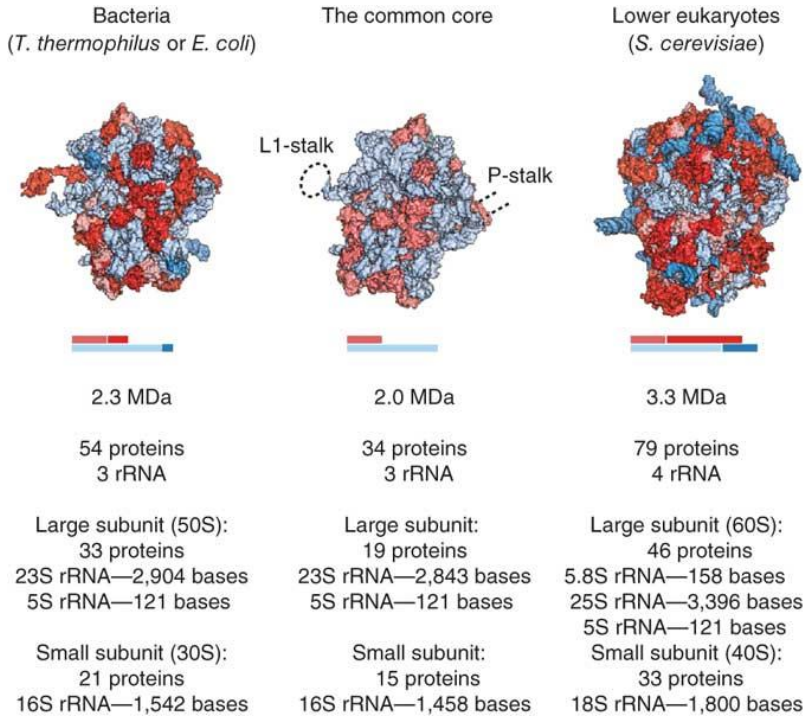

Figure 1. The features of bacterial and yeast ribosomes.

Comparison of the features of the 80S ribosomes from bacteria and *Saccharomyces cerevisiae*, and the common core between these are shown. Red and blue mark the rRNA and the proteins, respectively, with lighter colors used to indicate the elements of the common core while the brighter colors show the additional components in each ribosome type. The relative ratios of the conserved and additional elements are shown below the structures. Most of the eukaryote specific rRNA components consists of expansion segments (ES). Image modified from Melnikov et al, 2012 [1].

The architecture of the whole ribosome has prominent features that were first identified by electron microscopy. These features, now known to be dictated by rRNA domains, include the central protuberance (CP), the L1 stalk, and the L7/L12 stalk (the P stalk in eukaryotes) in the large subunit (LSU). In the small subunit (SSU), the prominent structures are named mostly after body parts (Figure 2). Of these, the "head," the "body," and the "neck" are the most functionally critical.

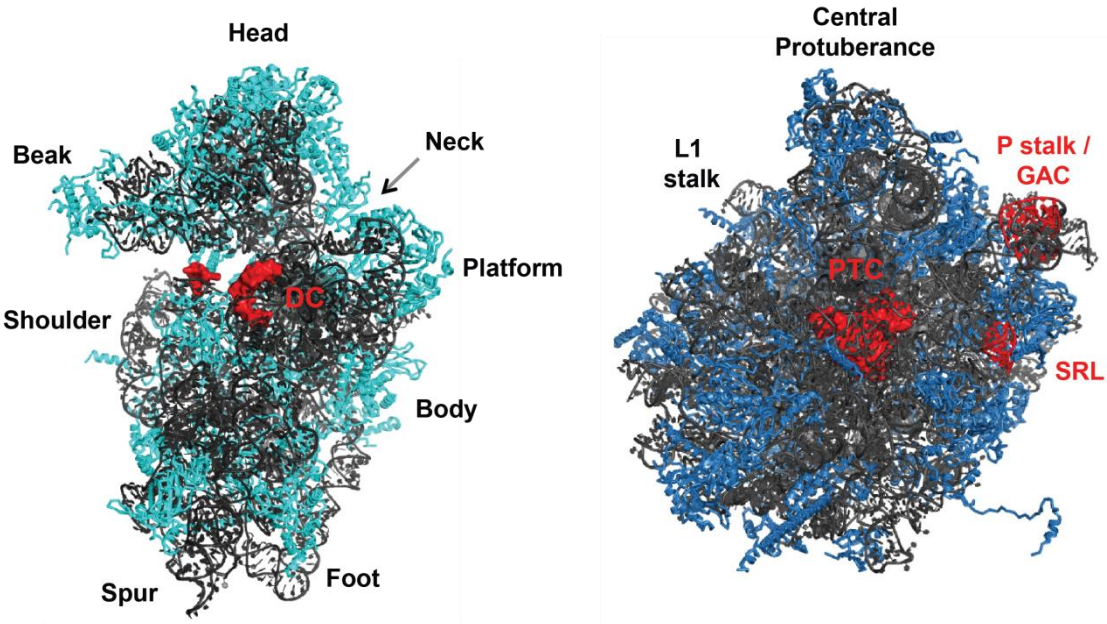

Figure 2. Ribosomal subunits and functional sites.

Shown left is the 40S "small" subunit, right is the 60S "large" subunit. Structurally important regions are labeled in black. Proteins are shown in tones of blue, rRNA is shown in grey. Functionally important sites are shown in red: DC stands for decoding center, PTC stands for peptidyltransferase center, GAC stands for GTPase associated center, SRL stands for sarcin-ricin loop. The structurally important, dynamic element P stalk forms the GAC. GAC and SRL together form most of the elongation factor (EF) binding site. Image generated by PyMOL, structure from Ben-Shem et al, 2011 [2].

The ribosome is a ribozyme, as the rRNA component harbors its catalytic site: the peptidyltransferase center (PTC) where peptide bond transfer between the growing peptide chain and a new aminoacyl residue occurs. In addition, while not directly catalytic, the GTPase associated center (GAC) which stimulates GTP hydrolysis by elongation factors, and the decoding center (DC) where the new aminoacyl tRNA recognizes and binds its codon on the mRNA template, as well as large portions of the elongation factor, mRNA, and tRNA binding sites are mainly composed of RNA. Similarly, a critical structural element required for elongation factor binding called the sarcin-ricin loop is composed of a loop at the end of Helix 95 (H95) of the large subunit, taking its name from the fact that ribotoxins α-sarcin and ricin cleave this region. tRNA binding sites are the A ("aminoacyl") site where

the incoming aminoacyl tRNA binds, the P ("peptidyl") site where the growing peptide chain is found attached to a tRNA, and the E ("exit") site from which deacylated tRNAs leave the ribosome (Figure 3). Another important regulatory region that consists of rRNA is the accommodation corridor (AC), or the path of rRNA nucleotides that act as a gate to the acceptor stem and the CCA end of the incoming aminoacyl tRNA on its journey to the PTC.

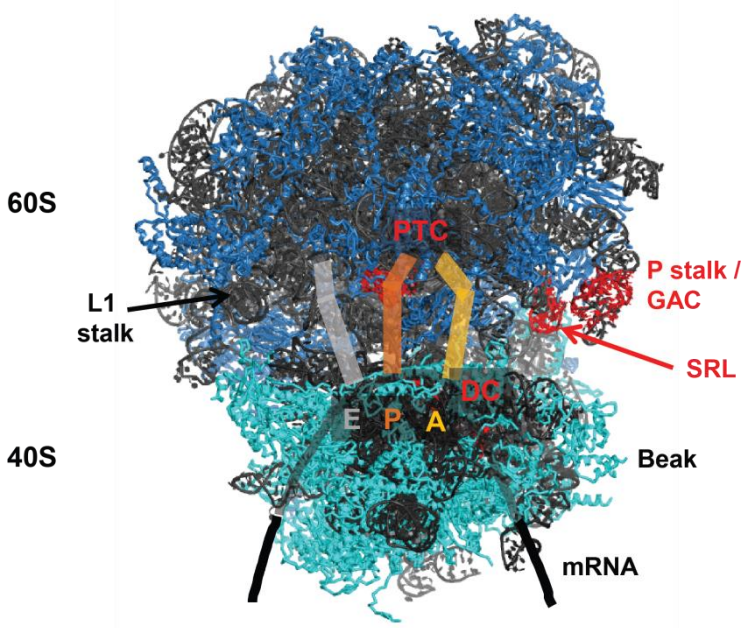

Figure 3. 80S ribosome and tRNA, mRNA, EF binding sites.

Fully associated 80S ribosome viewed from 40S head - 60S central protuberance side. Some structural elements are noted in black. Proteins are shown in tones of blue, rRNA is shown in grey. Functional sites are marked with red. mRNA (thick black line) winds around the neck of 40S, to which the tRNAs bind (blocks of varying colors). A, P, E sites are shown in different colors. PTC: peptidyl transferase center, DC: decoding center, GAC: GTPase associated center, SRL: sarcin-ricin loop. GAC and SRL form most of the elongation binding site.

The rRNA folds into many domains that confer both rigidity and flexibility to the ribosome, as well as forming the functional sites and pockets mentioned above. These domains are shown in Figure 4. The rRNA harbors many modified nucleotides, including ribose 2'-O-methylated bases and pseudouridines; these are important for ribosome function, as loss of base modifications cause translational fidelity defects [3–

[7]. Another extraordinary feature of the rRNA is the presence of noncanonical base pairs [8]. At the secondary and tertiary levels, numerous structural motifs and long distance interactions are important both functionally, as indicated by their presence at the catalytic sites, and structurally [8]. The most common of these are the A-minor motifs and interactions. In these motifs, single-stranded adenosines reach into the minor groove of a helix, making hydrogen bonds and van der Waals contacts with both the bases and the riboses of the interacting nucleotides. A-minor interactions are seen between the PTC adenines and the 3' CCA ends of tRNAs, and between the DC adenines and the codon:anticodon duplex. Other motifs and interactions throughout the rRNA include tetraloops, E-loops, U- and K-turns, purine stacks, coaxial stacking, and ribose zippers [8,9].

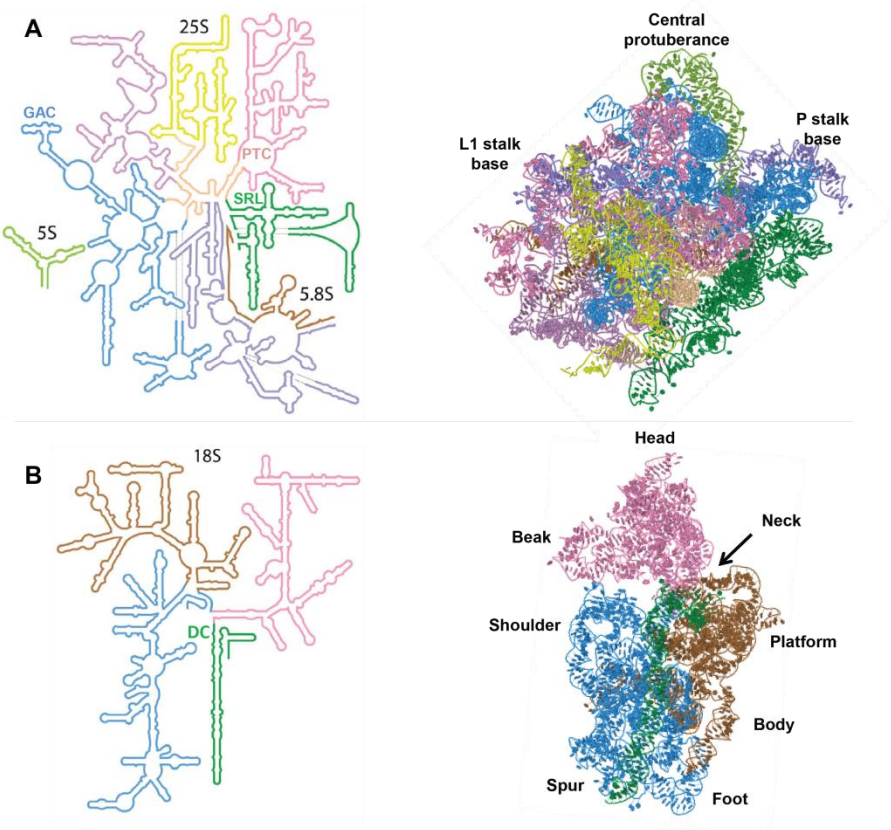

Figure 4. Yeast rRNA domains on 2D and 3D maps.

A. Two dimensional view of 25S rRNA domains is shown on the left, and the three dimensional view (in a similar angle to Figure 1) is shown on the right, keeping the same color code to mark the places of different domains. B. Two dimensional view of 18S rRNA domains is shown on the left, and the three dimensional view (similar angle to Figure 1) is shown on the right. The domains fold separately both at the secondary and tertiary levels, and dictate the structural elements of the whole ribosome (especially true for 18S domains). Functional sites are noted on the 2D maps; structurally important regions are noted on the 3D maps. Two dimensional views are from Petrov et al, 2014 [10], three dimensional views are generated using Ribovision [11].

All prominent structural features of the large subunit are functionally important, and their protein counterparts are just as critical as the rRNA. For example, the L1 stalk includes the ribosomal protein L1, and the L7/L12 contains heterodimers of L7 and L12 proteins bound to L10 in prokaryotes, and the acidic P proteins in eukaryotes. Intersubunit bridges forming the fully associated ribosomes are other regions in which proteins take part (Figure 5) [2]. Bridge B1b/c is solely formed by protein-protein interactions. The eukaryotic ribosomes have more intersubunit bridges compared to the bacterial ribosomes, and these "eukaryote specific" bridges generally have a protein component. Finally, uL4 and uL22 are important components of the peptide exit tunnel where the growing peptide chain resides, in addition to the rRNA bases that line this region.

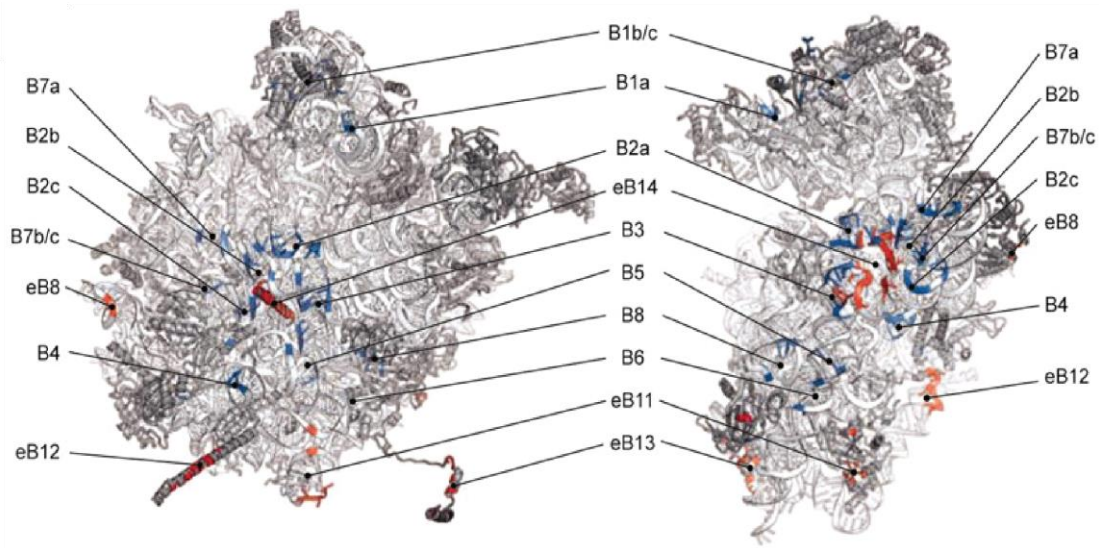

Figure 5. Intersubunit bridges of the yeast ribosome.

Conserved bridges are shown in blue, eukaryote specific bridges are shown in red. Except B1b/c, all bridges have an rRNA component, with the eukaryote specific bridges solely consisting of rRNA:protein interactions. Image from Ben-Shem et al, 2011 [2].

1.2. Translation

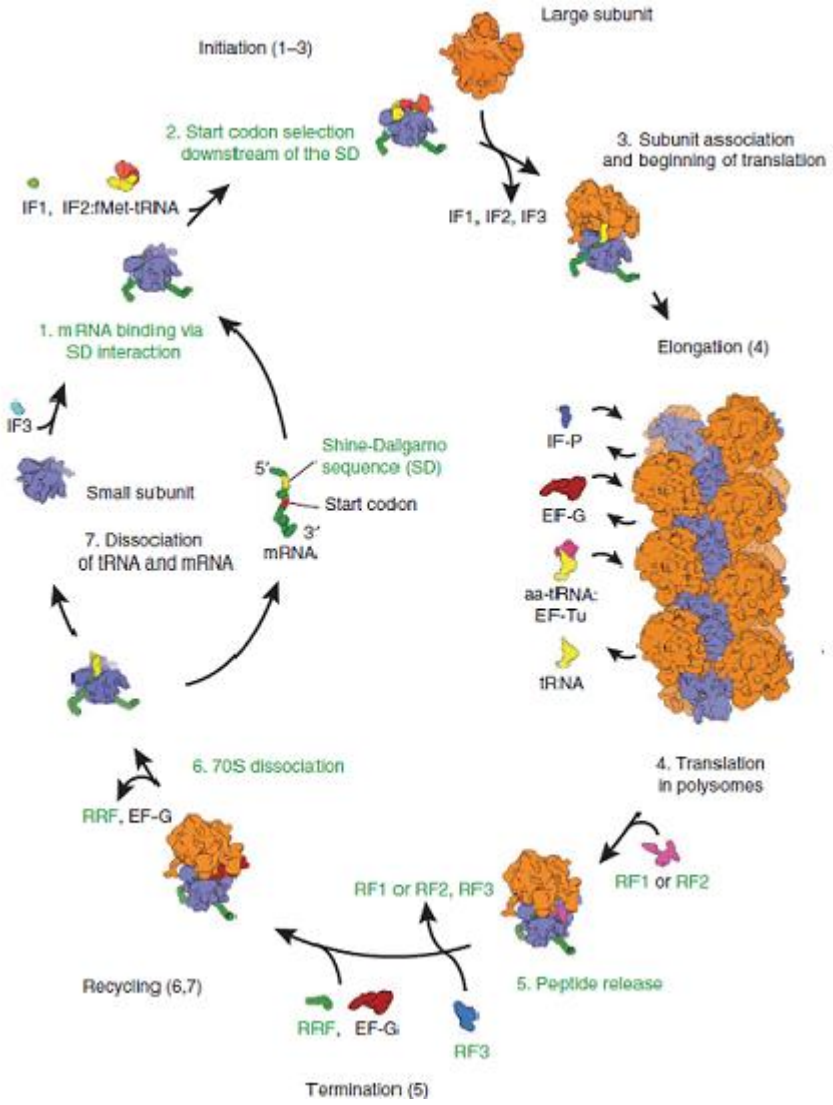

Figure 6. Overview of translation in bacteria.

A simplified version of the whole translation process in bacteria is shown, and comprises of initiation, elongation, termination and recycling. Steps 1-3 above form initiation, step 4 belongs to elongation, step 5 and 6 are termination and recycling, respectively. Please see text for more detailed information on each part of translation. Image modified from Melnikov et al, 2012 [1].

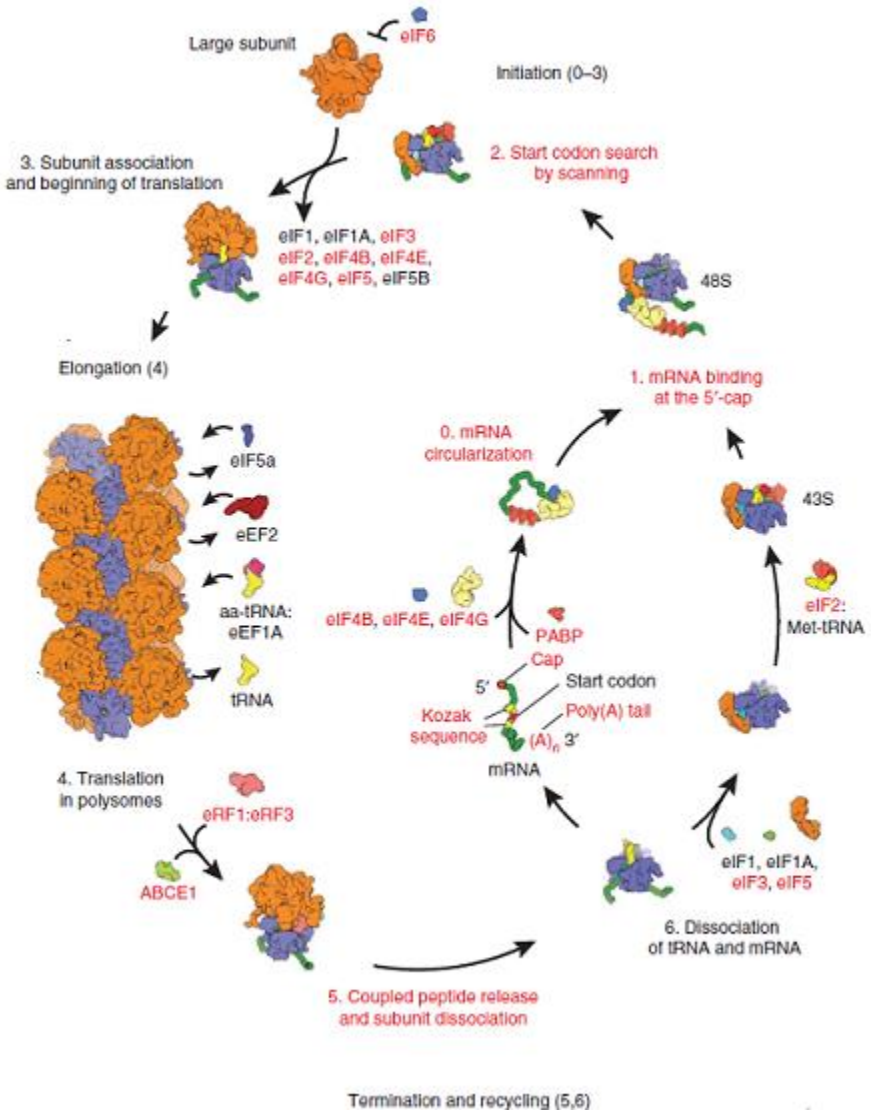

Figure 7. Overview of translation in eukaryotes.

A simplified version of the whole translation process in eukaryotes is shown, and comprises of initiation, elongation, termination and recycling. Steps 0-3 above form initiation, step 4 belongs to elongation, step 5 and 6 are termination and recycling. Please see text for more detailed information on each part of translation. Image modified from Melnikov et al, 2012 [1].

Protein translation occurs in four main steps: Initiation, elongation, termination and recycling. During initiation, the mRNA binds to the ribosomal small subunit and the initiator tRNA binds to the start codon, thus defining the translational reading frame. The elongation cycle begins when the next aminoacyl tRNA binds to its codon on the mRNA, and continues until a stop codon is reached. Most of peptide synthesis occurs during this step of translation through peptide bond transfer.

Termination occurs when the stop codon is recognized by a variety of *trans*-acting factors, resulting in release of the amino acid chain. This is followed by ribosome recycling, which frees the ribosome from the newly translated polypeptide and the mRNA, allowing the cycle to be repeated. Overviews of the bacterial and eukaryotic translation are shown in Figure 6 and Figure 7.

1.2.1. Initiation

The key processes of translation initiation in both prokaryotes and eukaryotes are the SSU recruitment to the start codon and subunit association. For the first process, the protein coding RNAs of most prokaryotes have a highly conserved purine-rich sequence, Shine-Dalgarno (SD) sequence, located approximately 8 nucleotides upstream of the start codon AUG. This is complementary the 3' end of 16S rRNA, and base-pairing between the two positions the ribosomal small subunit in close proximity with the translation start site. The start codon is heavily biased towards AUG in *E. coli*, however GUG and UUG can be favored in other organisms such as *Actinobacteria* spp. Metagenomics analyses have shown that not all genes have the SD sequence, revealing the presence of SD-independent translation initiation pathways in bacteria [12]. Ribosomal protein S1 is thought to be the key component of such SD-independent pathways, as ribosomes with S1 can translate messages with weak SD sequences whereas S1-depleted ribosomes cannot, and S1 variants may be employed for efficient translation of messages from different prokaryotic species [12–14].

Prokaryotic initiation requires three proteinacious initiation factors: IF1, IF2, and IF3. These, in complex with the SSU, form the pre-initiation complex, to which

the mRNA binds through SD-antiSD interactions [15]. IF3 is an anti-association factor that keeps the two ribosomal subunits separate during initiation and recycling, in accordance with its primary binding site on the interface surface of 30S [15–17]. IF1 binds to and blocks the A site of SSU, as well as stimulating activities of the other initiation factors. In this respect, it cooperates with IF2 to ensure the correct positioning of the initiator tRNA in the P site. IF1 also induces structural rearrangements in the SSU, some at the A site, and some longer distance changes that influence association and dissociation of the ribosomal subunits [15,16]. IF2 is a GTPase and its main role is to recruit the initiator tRNA, a formylated methionine tRNA (fMet-tRNA^{fMet}) in prokaryotes, to the P site. Its C terminus is highly conserved in different species, as well as kingdoms, and contains the recognition site for fMet-tRNA^{fMet}. The G domain, containing the GTP binding pocket, is structurally related to the G domains of other transacting factors [15,16]. Structural studies indicate that the positioning of IF2 on SSU changes depending on whether it is bound to GTP (ie. before GTP hydrolysis), GDPCP (mimics hydrolyzed GTP, before phosphate release), or GDP (after phosphate release) [15,16]. GTP hydrolysis of IF2-GTP might be enhanced during LSU joining [16]. It results in the dissociation of the three initiation factors, and the complete association of 70S ribosomes, allowing translation elongation to resume.

SSU recruitment to the start codon occurs in two steps in eukaryotes: Recruitment of the SSU to the 5’ end of the message (which requires mRNA activation), and scanning for the start codon. Switching from a scanning-permissive state to scanning-restrictive state upon start codon recognition requires structural

rearrangements within SSU, in addition to the changes in the components of the large initiation machinery. These make eukaryotic initiation overall much more complex than the prokaryotic translation initiation.

Most eukaryotic mRNAs are also posttranscriptionally modified, the most common being addition of a 7-methylguanosine cap to the 5' end, and a polyadenine tail to the 3' end, except histone encoding mRNAs which are not polyadenylated. These modifications are thought to be important for labeling nuclear-encoded mRNAs as "self", and to facilitate translation initiation, as different factors bind to these regions (eIF4E and poly(A) binding proteins, respectively), and are bridged by the large scaffolding protein eIF4G to effectively bring together the ends of the mRNA together, forming the closed loop mRNP. The whole eIF4 complex (eIF4F) also includes eIF4A, an ATP-dependent DEAD box RNA helicase important to resolve the secondary structure of the mRNA, and eIF4B, the cofactor of eIF4A and an RNA binding protein that helps to anchor the mRNA and the 18S rRNA. The positioning of the eIF4F complex targets the ribosomal subunit to the 5' end of the mRNA, while the closed loop possibly allows for efficient reinitiation on the same message.

Another anchoring protein for binding of the small subunit onto the "activated" mRNA is eIF3, which is a component of the 43S preinitiation complex (43S PIC). Formation of 43S PIC will be discussed in more detail in Section 3.1, and entails binding of eIF1, eIF1A, eIF3, eIF5 and the ternary complex of eIF2, GTP and Met-$tRNA_i^{Met}$ to the 40S subunit. eIF1 and eIF3 are known to stimulate ternary complex binding to 40S, with the initiator tRNA positioned over the P site [18]. eIF2

and eIF5 are known to interact, and this may be how eIF5 is recruited to the ribosome [19]. eIF1A and eIF1 are the eukaryotic homologs of bacterial IF1 and IF3, respectively. In addition to functions homologous to their bacterial counterparts (blocking of the A site, and preventing association of ribosomal subunits, respectively), they are important in scanning, start codon recognition and the related structural rearrangements.

After 43S PIC is recruited onto the mRNA, scanning for the start codon AUG starts. Scanning on structured messages is powered by ATP hydrolysis, which is mostly required by eIF4A and eIF4B [20]. During scanning, 43S PIC/mRNA is in an open conformation induced by eIF1, eIF1A and stabilized by eIF3. eIF1 is also important in monitoring tRNA/mRNA interactions, as it regulates the P_{out} and P_{in} states of the tRNA, where P_{in} is the fully accommodated state of the initiator tRNA. The conformations of the SSU and the initiator tRNA allow the PIC to move on the mRNA, until an AUG in good context is encountered. The optimal start codon context entails the Kozak consensus sequence, (gcc)gccRcc<u>AUG</u>G, where R is a purine and the AUG is underlined. Another event that takes place during scanning is the GTP hydrolysis of the G protein eIF2 by the GTPase activating protein (GAP) eIF5. The inorganic phosphate (P_i) resulting from GTP hydrolysis is not readily released, however, and P_i release is thought to be the "committing" step of the initiation, as it occurs upon start codon recognition and eIF1 dissociation, signaling the formation of correct tRNA/mRNA interactions.

Upon start codon recognition, 48S PIC forms. The SSU assumes a "closed conformation," possibly provided by the eIF1A-eIF5 interaction. This conformation

is not permissive for scanning. The initiator tRNA commits to the P_{in} state, which is thought to stabilize the closed conformation. After P_i release, eIF5 and eIF2-GDP dissociate as well and are replaced by eIF5B-GTP. eIF5B is homologous to the C terminus of prokaryotic IF2, and recruits the large subunit to the 48S complex. eIF1A is thought to contribute to subunit association [21]. The LSU is prevented from associating earlier due to interactions with eIF6 [22]. eIF6 dissociates upon phosphorylation involving RACK1 (Receptor for Activated C Kinase 1) which is a scaffolding protein associated with protein kinase C and an ancillary protein of SSU [23,24]. GTP of eIF5B is hydrolyzed upon LSU joining. eIF5B-GDP and eIF1A dissociate and the ribosome is now ready to resume with the elongation cycle.

Even though ribosomal scanning is the main hypothesis for start codon recognition in eukaryotic translation initiation, a recent study indicates another mechanism called “RNA looping” by the authors [25], whereby a reporter gene may be translated independently of the 5’ end of mRNA through looping of the mRNA portion between the ribosome binding site and the start codon. This hypothesis, as well as the mathematical model that is associated with it, explains the effect of 5’ untranslated region length on efficient translation initiation as well.

1.2.2. Elongation

The elongation cycles of bacteria and eukaryotes are functionally identical, the only difference being the names given to the transacting factors that take part in the process. The elongation factors of prokaryotes and eukaryotes are homologous in sequence and function. An overview is shown in Figure 8.

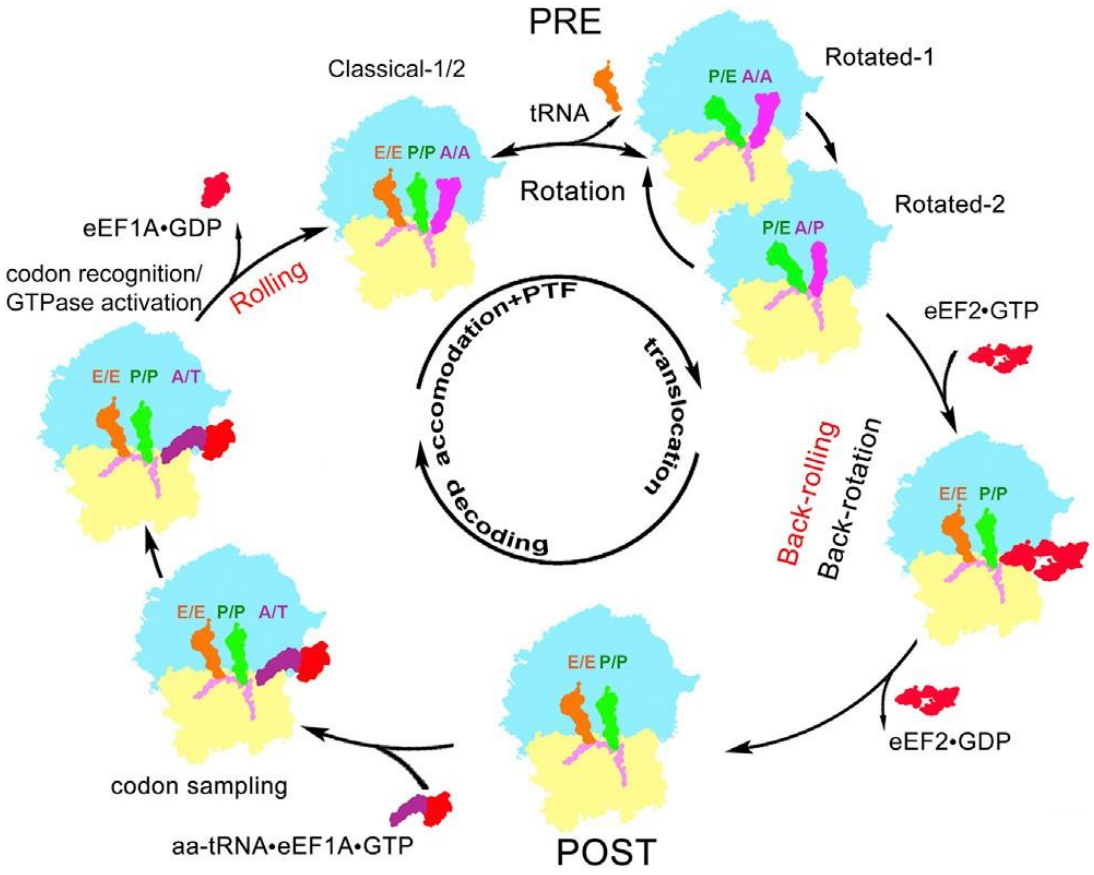

Figure 8. Eukaryotic translation elongation cycle.

The ribosome before and after translocation is traditionally named "PRE" and "POST." In "POST" conformation, it has an open A site and a peptidyl tRNA or initiator tRNA on the P site. A ternary complex composed of aminoacyl tRNA, eEF1A and GTP binds during the decoding step, followed by GTP hydrolysis and accommodation of the incoming tRNA to the LSU A site. This is coupled to a "rolling" motion in mammalian ribosomes. Peptidyl transfer (PTF) takes place upon correct positioning of the tRNA CCA ends. At this point, any deacylated tRNA remaining on the E site is detached, allowing for the "rotation" motion. Rotation is coupled to tRNA CCA end movement to the next site on LSU. The rotated conformation locks upon binding of eEF2-GTP. Upon GTP hydrolysis, translocation of tRNA anticodons : mRNA codons occur, opening up the A site for the cycle to be repeated. eEF2 function is coupled to the reversal of the earlier rolling and rotation motions. Image from Budkevich et al, 2014 [26].

1.2.2.1. Decoding, accommodation and peptidyl transfer

The cycle begins as a new aminoacyl tRNA, dictated by the next codon on the mRNA in a process known as "decoding," is brought to the A site of the ribosome in a ternary complex with the elongation factor Tu (EF-Tu in bacteria, eukaryotic elongation factor 1A or eEF1A, in eukaryotes) and GTP. The interaction of the

aminoacyl tRNA anticodon with the mRNA codon is accompanied by the movements of SSU rRNA nucleotides G530 (G580 in yeast), A1492-93 (A1755-56 in yeast) and LSU nucleotide A1913 (A2256 in yeast).

In the vacant ribosomes, the three adenines normally form stacking interactions with each other. Upon binding of the anticodon to the codon, A1913 rotates freeing the nucleobases of A1492-93 to "flip out", G530 switches to *anti*-conformation from *syn*-, forming a part of the stabilization network of the codon-anticodon duplex [27–32]. There are two schools of thought on the roles of these nucleotides during decoding. Earlier research suggested that these occur in response to cognate aminoacyl tRNA anticodon - mRNA codon interactions and can discriminate against near-cognate ones, by resulting in the "closure" of the small subunit whereby the shoulder moves towards the neck [27,29,30]. However recent research suggests that these structural changes take place whether or not there is a cognate or near-cognate tRNA in the A site. In fact, some of these start happening after the initiator fMet-tRNA^{fMet} has bound to the P site, and these nucleotides may actually form a "static" part of the DC [28,31,32].

Right after decoding, the tRNA is conformationally distorted, or "bent," with its anticodon stem loop bound to the mRNA codon in the decoding center and its acceptor stem bound by the protein factor in the GTPase associated center [33]; this is also known as the A/T state (Figure 9). Structural and mutational studies indicate that Domain I of EF-Tu is responsible for GTP binding, rearrangements in this domain causing a "hydrophobic gate" of amino acids to open and allow the catalytic amino acid (His84) to come in contact with GTP. His84 is thought to position and activate a

water molecule for GTP hydrolysis. The ribosome may be contributing to this process as well, as GAC is known to stimulate hydrolysis 2500 fold in bacteria, and SRL is located adjacent to the nucleotide binding pocket.

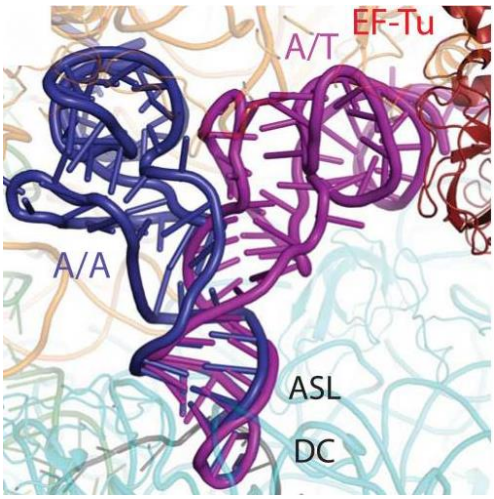

Figure 9. The structure of A/T state tRNA.

The "bent" structure of A/T state tRNA is shown. This conformation is assumed when the elongation ternary complex binds the ribosome and before GTP hydrolysis by EF-Tu (eEF1A in yeast). The bending occurs in the anticodon stem (purple tRNA) and is due to the localization of the anticodon to the SSU A site, while the CCA end of the tRNA is bound to the elongation factor. Upon GTP hydrolysis and EF-Tu dissociation, accommodation occurs and A/A state is achieved (dark blue tRNA). Image from Schmeing et al, 2009 [33].

Upon GTP hydrolysis and release of inorganic phosphate, the affinity of the protein factor for the aminoacyl-tRNA is decreased and it detaches from the ribosome. The acceptor stem of the aminoacyl-tRNA moves into the PTC through a corridor of rRNA nucleotides from LSU helices 89-92, propelled by the "bent" conformation. This process is known as "accommodation" and is complete when the 3' end of the incoming tRNA is placed in a position favoring peptide bond transfer in the PTC.

Peptide bond transfer involves a nucleophilic attack by the amino group of the A site tRNA aminoacyl residue on the carbonyl carbon of the peptide on the P site tRNA resulting in formation of an amide bond and transfer of the peptidyl group onto

the A-site tRNA. This occurs through the formation of a zwitterionic tetrahedral intermediate (Figure 10), followed by deprotonation into a second intermediate (not shown) and finally the decomposition of the second intermediate into products. The nucleophilic attack and formation of the intermediates have been shown to be the rate limiting step on the ribosome, whereas the final breakdown occurs in a separate, rapid step [34–36]. The rate limiting step proceeds through a concerted proton shuttle mechanism (Figure 11).

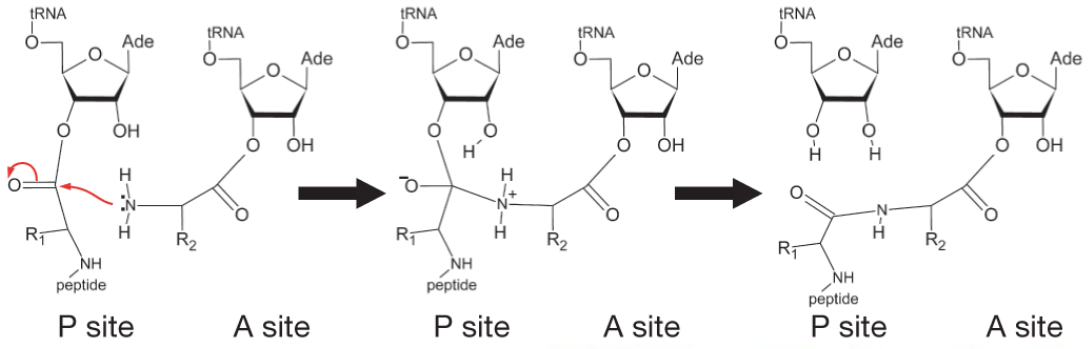

Figure 10. The peptidyltransfer reaction.
Image from Scott A. Strobel, via [37].

Despite decades of study, the precise role of the PTC is not entirely clear, as catalysis is achieved through the substrates themselves (e.g. possibly the 2'-hydroxyl group of A76 of the peptidyl tRNA [38]), implying an indirect role for the ribosome [39]. A2451 in bacteria (A2820 in yeast) is within hydrogen bonding distance of the nucleophilic amino group of the aminoacyl tRNA, however it does not have a direct effect on peptide bond formation [40]. Even though the adenine is conserved in all domains of life, the effects of A2451 on peptidyl transfer have been largely attributed to the ribose 2'-hydroxyl group through atomic mutagenesis [41]. Overall, the PTC is thought to be important in accurate positioning of substrates and in water exclusion

[38,42,43]. According to this view, A and P loops (LSU Helices 92 and 80, respectively) are more crucial than any individual nucleotide for peptide bond formation [44].

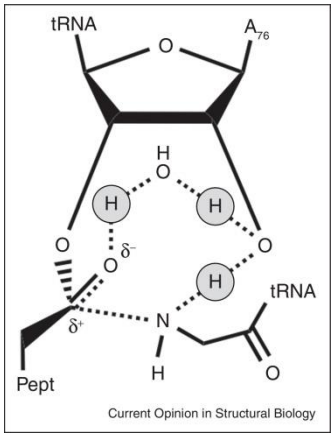

Figure 11. The concerted proton shuttle.
Protons of the concerted shuttle are circled. Image from Rodnina, 2013 [36].

1.2.2.2. Rotation and translocation

After peptide bond formation, the next step is to move the mRNA and the tRNAs by one codon on the ribosome, opening up the A site again for a new aminoacyl tRNA to bind. This process is called "translocation." It occurs as a result of both movements within the ribosome, specifically rotation, and by the action of another elongation factor, EF-G in bacteria or eEF2 in eukaryotes.

After accommodation and during peptidyl transfer, the tRNAs are in the so-called "classical" A/A and P/P states. Upon peptidyl transfer, the small subunit rotates (5-8°) with respect to the large subunit [26,45]; this correlates with movement of the CCA ends of the A site and P site tRNAs to P and E sites, respectively. The new conformation of the tRNAs are called "hybrid" A/P and P/E states. Due to the structure of the E site, the P/E state can only be assumed by a deacylated tRNA, hence it has to occur after peptidyl transfer. The change in tRNA conformation seems to be coupled to movement of L1 stalk in a manner to stabilize the P/E hybrid state [46].

The elongation factor (i.e. EF-G and eEF2) functions in the movement of the tRNA ASL and the corresponding mRNA codons to the P and E sites [47], and elongation factor binding locks the ribosome into the rotated state. Domain IV of the elongation factor, and possibly a conserved histidine residue at the tip of this domain (His699 in yeast; posttranslationally modified to diphthamide [48]), is inserted into the decoding center, and is thought to displace the decoding center rRNA nucleotides [47]. Domain III contacts both SSU and LSU, allowing the factor to "sense" ribosome conformation [47]. Domain G harbors the GTP binding site as well as switch regions that prevent premature GTP hydrolysis [47]. Domain II contains structural elements that contact both the shoulder of SSU and switch I region before GTP hydrolysis, hence these elements may be how GTP hydrolysis, ribosome conformation, and translocation are coupled [47]. Upon GTP hydrolysis, the ribosome is unlocked with additional tRNA hybrid states shown in bacteria [42,49–51], and translocation occurs possibly as a result of: 1) interaction of the tip of domain IV with the P site codon-anticodon duplex pushing it "forward", 2) the back-rotation of small subunit, 3) interaction of L1 with P/E tRNA pulling it "forward", and 4) interplay between A and P sites (shown in a recent study [51]).

The release of E site tRNA and the presence of a ribosomal E site at all are active questions in the field. In fungi, an additional elongation factor, eEF3, was found to bind close to the E site on posttranslocation ribosomes. It was proposed that this factor may function in E site tRNA release in fungi, possibly through L1 mobility [52]. eEF3 is fungi-specific, does not have a homolog in bacteria or in mammals, and is required for protein synthesis [52,53].

1.2.3. Termination and Ribosome Recycling

Translation elongation cycle is repeated until a stop codon (UAA, UGA or UAG) is encountered. These codons are not recognized by tRNAs but by release factors (RF's). In bacteria, type I release factors RF1 (specific for UAG and UAA) and RF2 (specific for UGA and UAA) recognize stop codons [36,54]. The codon specific motif of RF1 is PVT of domain 2, whereas it is SPF for RF2. When the RFs bind to the ribosome, these motifs are located in the 30S decoding center. Thr186 of RF1 selects for an adenine in the second position of the stop codon, whereas the Ser206 can form hydrogen bonds with either adenine or guanine in this position. Additional selection occurs at the third position, where Thr194 and Gln181 of RF1 allow for either adenine or guanine, whereas Val203 of RF2 restricts this to an adenine. The first position of the codon is universally restricted to a uridine since a common element in both RF's can form hydrogen bonds with the Watson-Crick edge of this nucleotide [54].

Peptide bond hydrolysis from the P site tRNA is achieved through the conserved GGQ motif found in domain 3. This motif locates to the PTC and functions in correct positioning of the substrates for hydrolysis. The glutamine component selects for water as the nucleophile and excludes larger molecules. This component further aids in the hydrolysis reaction by providing a hydrogen bonding network for stabilization of the transition states [36,54]. Unless the stop codon is recognized, the GGQ motif does not locate to its correct place, as the structural rearrangements occurring upon stop codon recognition are required for the correct positioning of this motif [54].

Hydrolysis of the peptide bond occurs through a tetrahedral intermediate that breaks down into the free peptide product and deacylated tRNA. It does not require proton shuttling as only one proton needs to be transferred [35,36]. The PTC also plays a role in peptide bond hydrolysis, specifically nucleotides A2451 (A2820 in yeast), U2506 (U2875 in yeast), U2585 (U2954 in yeast), and A2602 (A2971 in yeast) [35,44]. Additionally, coupling of stop codon recognition to peptide bond hydrolysis requires rearrangements in the decoding center nucleotides including A1492-93 (A1755-56 in yeast) of 16S rRNA and A1913 (A2256 in yeast) of 23S rRNA [54].

After peptide bond hydrolysis, RF1 and 2 remain tightly bound to the ribosome. A class II RF, RF3, which is an EF-G-like GTPase, is necessary for the release of RF1 and 2. This is thought to occur by rotation of the small subunit upon GTP hydrolysis, weakening the bonds of RF1 and 2 with the ribosome [54].

The process of ribosomal subunit dissociation and release the deacylated tRNA remaining on the ribosome is called "recycling" and occurs through the combined action of ribosome recycling factor (RRF), EF-G, and IF3 in bacteria. RRF and EF-G function in dissociation of the ribosomal subunits in a GTP-dependent manner, whereas IF3 stabilizes this dissociation by binding to the 30S subunits and preventing the subunits to reassociate until initiation [55]. IF3 is also required for ejection of deacylated tRNA and the mRNA from the ribosome, and this constitutes the rate limiting step of recycling [56]. It is thought that EF-G induces structural rearrangements similar to the unlocking observed during translocation, rather than translocation itself, during recycling, even though RRF mimics an A site tRNA and binds to the A site [56]. In turn, RRF interacts with intersubunit bridges B2a and B3,

and the combined action of EF-G and RRF alters these bridges, resulting in dissociation of the subunits [56].

Termination and recycling events in eukaryotes remain active areas of research. In eukaryotes, termination is catalyzed by the collaboration of eRF1 and eRF3. eRF1 is a class I RF and is responsible for stop codon recognition and peptide bond hydrolysis, whereas eRF3, a class II RF, is an EF-Tu-like GTPase. eRF1 is tRNA-shaped like its bacterial counterparts, although it has no evolutionary relationship to these proteins [53]. It decodes stop codons through a highly conserved NIKS motif of its amino terminal domain via interactions resembling those of codon:anticodon [57]. Another motif that is implicated in stop codon recognition is YxCxxxF. The middle (M) domain of eRF1 resembles the acceptor stem of a tRNA and extends into the PTC, with a GGQ motif in this region being responsible for peptide bond hydrolysis [58]. This reaction appears to occur as it does in bacteria.

eRF3 interacts with carboxyl terminus and M domain of eRF1. eRF1 acts as a GTP dissociation inhibitor. GTP hydrolysis by eRF3 promotes eRF1 function by positioning the M domain into the PTC [59], essentially like GTP hydrolysis by EF-Tu aiding in the accommodation of the aminoacyl tRNA CCA end into the PTC. eRF3 does not promote dissociation of eRF1 from the ribosome, in fact, eRF1 has been shown to remain associated with the ribosome following termination and to be required for recycling [60,61].

Following termination in eukaryotes, the ribosome can either be recycled or translation can be “reinitiated” on the same circular message [62]. Reinitiation is thought to occur through the interaction of eRF3 with PABP [63].

Recycling in eukaryotes consists of separate steps of subunit dissociation, catalyzed by ABCE1/Rli1 [61], a cytosolic, essential ATP binding cassette family protein, and deacylated tRNA ejection followed by dissociation of 40S subunit from mRNA [64]. Mechanistic insights into recycling in eukaryotes come from studies on the no-go decay (NGD) pathway. Dom34 and Hbs1, key components of NGD, are related to eRF1 and eRF3 respectively, but instead of catalyzing peptide release, they catalyze subunit dissociation in stalled ribosomes. This observation and subsequent research showed that the eukaryotic release factors are able to promote subunit dissociation at slow rates themselves [65]. ABCE1/Rli1 is proposed to increase the rate of subunit dissociation through ATP hydrolysis and possibly by rearrangements of the intersubunit bridges [66–69]. It also functions in an ATP-independent manner to promote peptide release during termination, hence possibly staging the sequence of events of termination and recycling [53,70]. Structural studies provide support for an EF-Tu-like function for eRF3 in promoting eRF1 M domain localization to the PTC, as well as a model in which upon GTP hydrolysis by eRF3, no factor dissociates but ABCE1/Rli1 binds, facilitating eRF1 M domain positioning, hence promoting peptide release, and subsequently, ribosome recycling [66–69].

After subunit dissociation, eIF3 is thought to prevent the reassociation of subunits [53]. Release of deacylated tRNA and mRNA possibly occur through an open conformation of the 40S subunit brought about by Ligatin (also known as eIF2D) and the related protein pair MCT-1/DENR [71]. Release of tRNA and mRNA has also been shown to be stimulated *in vitro* by canonical initiation factors eIF1, eIF1A and eIF3 [60].

1.3. Translation Inhibitors

Translation inhibitors comprise approximately half of the available antibiotics. As a general rule, the inhibitors that bind to the small subunit bind around the neck, as this is the region of the SSU that interacts with mRNA and tRNA anticodon. The inhibitors that target the large subunit tend to bind in the vicinity of the PTC and the peptide exit tunnel, where the CCA end of the tRNA and the growing peptide chain are located. Hence, most known translation inhibitors act during elongation cycle of translation, and modify codon:anticodon interactions, block tRNA localization to the PTC, or block the new peptide chain from growing [72]. Bacterial translation inhibitors are shown in Figure 12. Due to the conserved nature of the bacterial and eukaryotic ribosomal catalytic sites, a number of these (sparsomycin, aminoglycosides, etc) are also are toxic to eukaryotic cells. For example, ribotoxins such as α-sarcin cleave the SRL of the LSU rRNA, abolishing the ribosome's ability to stimulate GTP hydrolysis activity. Puromycin is a structural analog of the 3' end of tyrosyl-tRNA and it triggers premature release of the peptide chain by forming an amide linkage with it. Sparsomycin is a nucleotide analogue that binds at the PTC and inhibits tRNA binding at the A site, while promoting translocation and stabilization of the tRNA at the P site. Aminoglycosides such as paromomycin bind at the SSU rRNA whereby promoting near-cognate tRNA binding, and in some cases, inhibiting small subunit rotation, thereby inhibiting translocation [73,74].

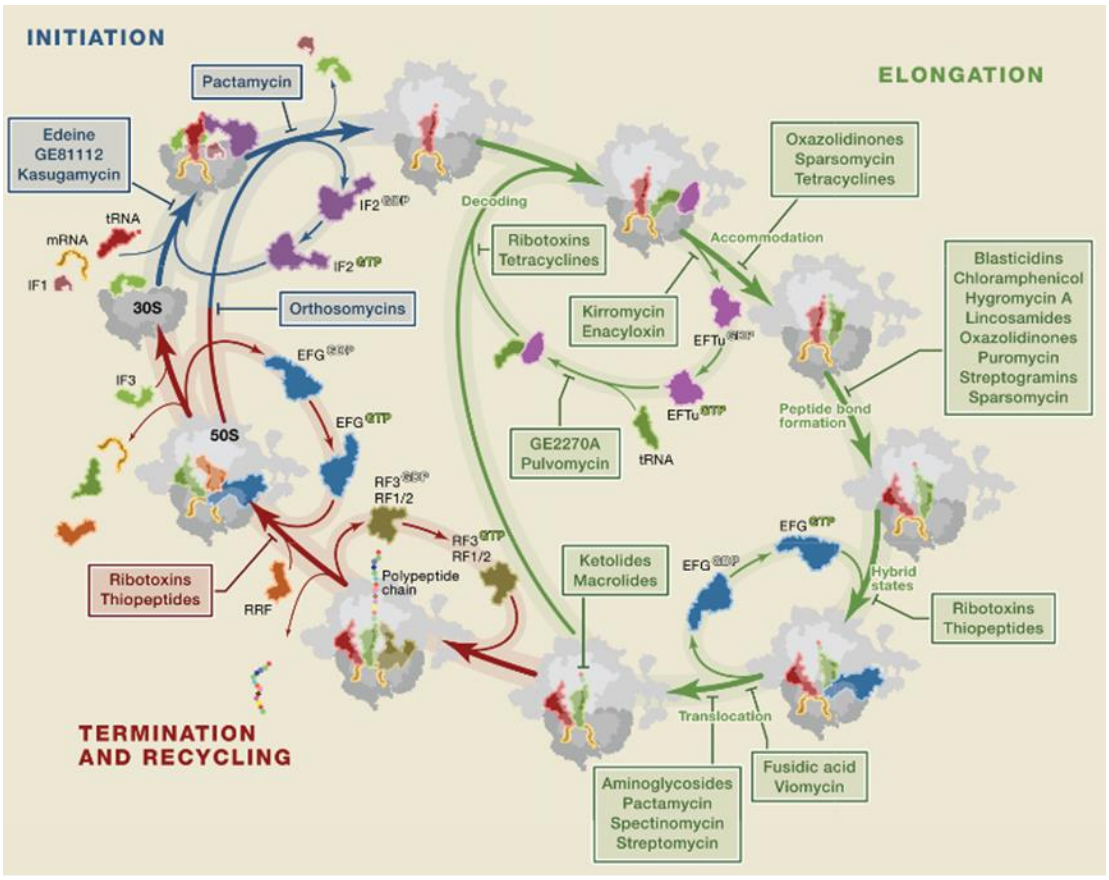

Figure 12. Bacterial and broad-spectrum translation inhibitors.

The steps of translation inhibited by different translation inhibitors are shown, and color coded according to the phase of translation. Image from Sohmen et al, 2009 [72].

There are also eukaryote specific translation inhibitors, a comprehensive structural study of which was recently published [75]. The binding sites of, and the steps blocked by these inhibitors are shown in Figure 13. Interestingly, most eukaryote specific inhibitors bind to the LSU, some of which bind to the E site, thereby inhibiting translocation. The most well-known examples of these are cycloheximide and lactimidomycin. These antibiotics are closely related but lactimidomycin has an additional lactone ring, slowing its insertion into the E site, making it a "slow" inhibitor that can only block translocation during the first elongation cycle, as it cannot effectively compete with tRNA In contrast, cycloheximide is very efficient at this and can block translocation at any stage during the elongation cycle. A number of

the eukaryote specific translation inhibitors bind to the PTC as well, mostly in the vicinity of the 3' end of A site tRNA. Some of these, such as T-2 toxin and verrucarin A, form extensive interactions with the rRNA bases of the A site and extend towards and/or into the peptide exit tunnel. Most of the A site blockers are inhibitors of peptidyl transfer and some are competitors of accommodation (eg. anisomycin) [76,77].

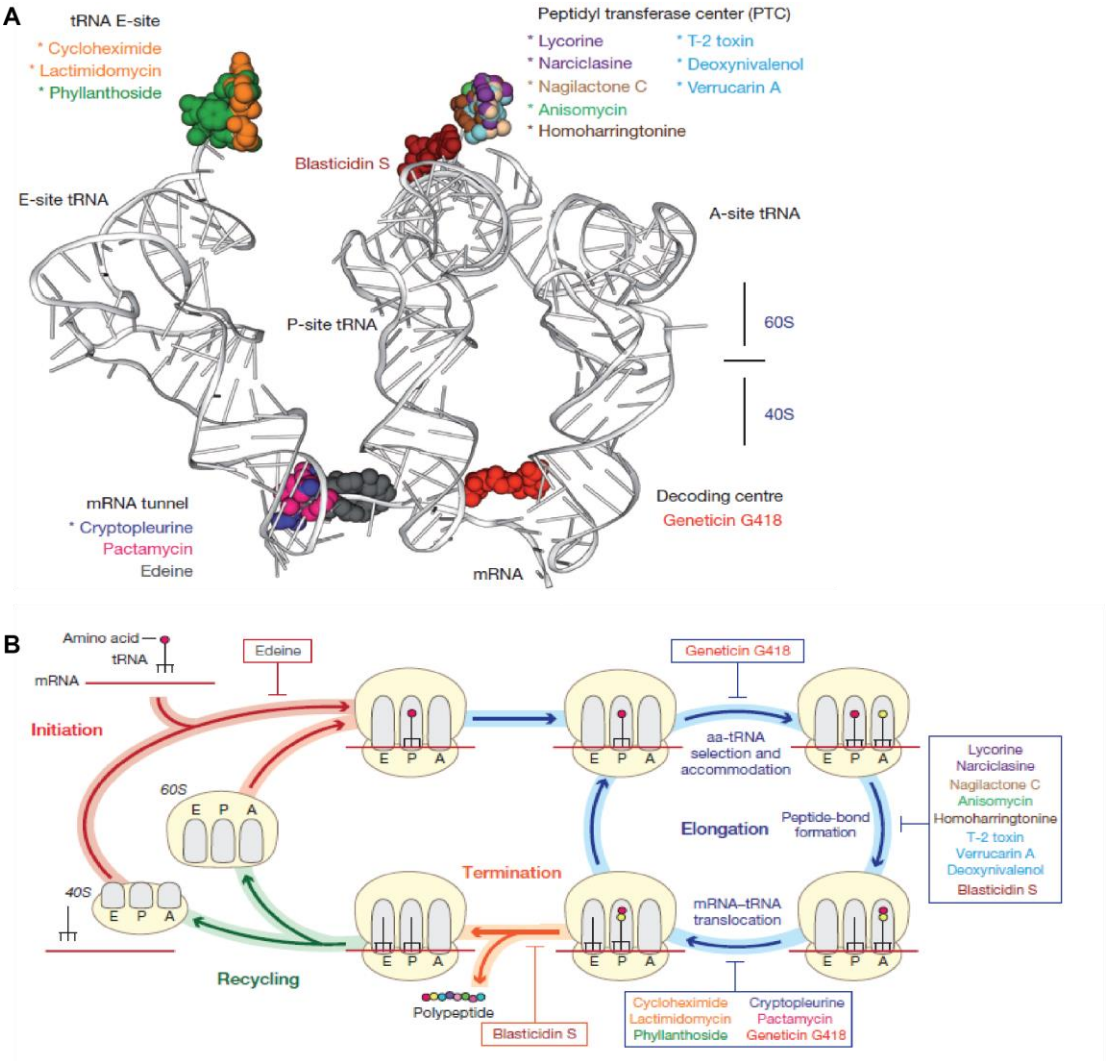

Figure 13. Eukaryote specific antibiotics.

A. The binding sites of the antibiotics studied in de Loubresse et al, 2014 [75]. B. The step of translation blocked by the antibiotics shown in A. Out of these, edeine, geneticin G418, pactamycin and blasticidin S are broad-spectrum antibiotics and inhibit translation in prokaryotes as well. Image modified from de Loubresse et al, 2014 [75].

1.4. Translational dynamics

As discussed in Section 1.2, translation is a highly dynamic process. Translational dynamics may refer to time dependent changes in either composition or conformation of the translational machinery [78]. Compositional dynamics are determined by bimolecular association and dissociation rate constants, and are affected by intermolecular collision frequencies, electrostatic interactions, proper binding orientations, and energy barriers for dissociation of noncovalent intermolecular interactions. These events are related to tRNA or protein factor binding. Single molecule, fluorescence techniques have been especially helpful in determining the order of binding of bacterial initiation factors to the ribosome, as well as the hydrogen bond energies of mRNA or tRNA-ribosome interactions, uncovering the mechanism of mRNA secondary structure unwinding on the ribosome, and the mechanism of IRES-mediated translation. Structural studies with cap-dependent eukaryotic initiation complexes are underway to determine the mechanistic aspects of eukaryotic initiation factor binding.

Conformational dynamics encompass electronic motions, bond vibrations, local conformational changes of protein side chains, nucleic acid bases or sugars, and larger rearrangements such as domain movements. These occur on an intramolecular level, such as tRNA, translation factor, or ribosome dynamics. As most of these are functionally important, they were discussed above in subsection 1.2.2. Elongation. Examples of the changes in tRNA conformation include the switch from the "bent" A/T state during the decoding step to A/A state before peptidyl transfer, as well as the formation of hybrid A/P and P/E states simultaneously with ribosomal rotation,

requiring rearrangements of the acyl moieties with respect to key rRNA nucleotides. Studies of translation factor dynamics focus mainly on EF-G. Domain IV, which shows molecular mimicry with the tRNA anticodon arm, undergoes a hinge-like motion with respect to domain G (GTPase domain) upon GTP hydrolysis, disrupting the interactions between the tRNA at the A site and the mRNA, and driving translocation. Another large conformational change is seen in domain II of RRF, induced by EF-G domain IV movement during recycling, which results in disruption of ribosomal intersubunit bridges.

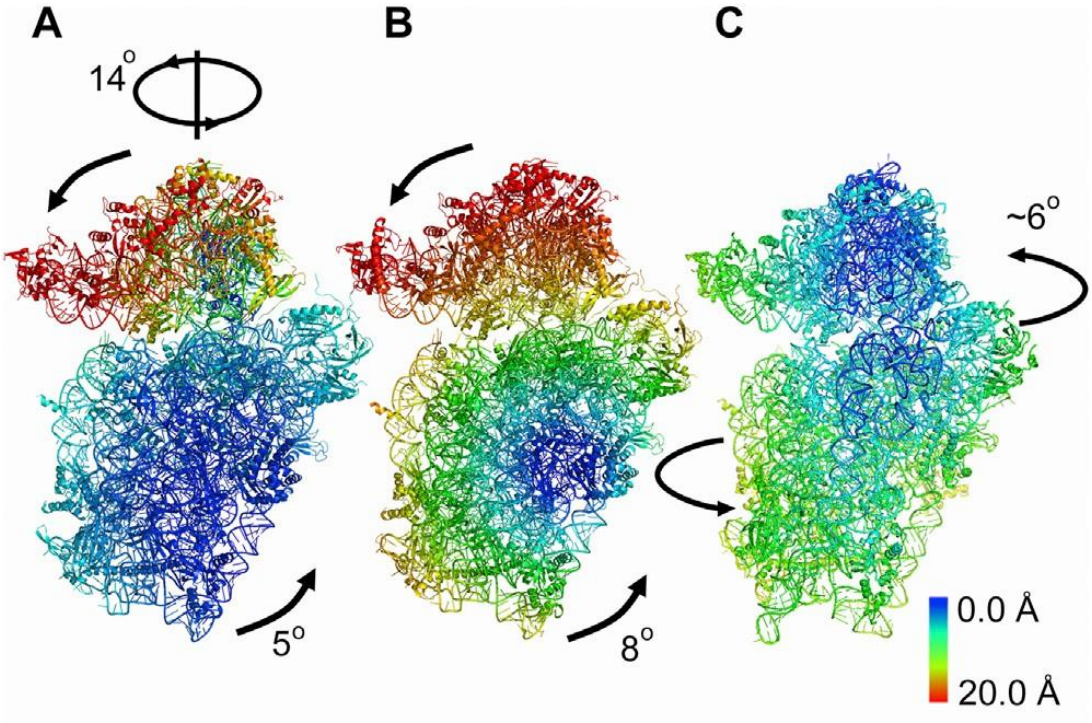

Figure 14. Motions of the small subunit color coded by the level of displacement.

A. Fully ratcheted state, observed in bacterial 30S, characterized by rotation with respect to the 50S, and a swivel movement of the head domain with respect to the body. **B.** Rotated state, observed in bacterial and eukaryotic small subunits, characterized by rotation with respect to the large subunit. **C.** Subunit rolling with respect to 60S, recently described in mammalian 40S. Image from Budkevich et al, 2014 [26].

Structural studies have found evidence of both intersubunit and intrasubunit ribosomal dynamics. Intersubunit conformational changes (Figure 14) are mainly brought about by rotation (shown in ribosomes from various organisms) and rolling

(shown in mammalian ribosomes) of the small subunit with respect to the large subunit. Rotation (a motion of 5°-8°) and the recently described rolling (a motion of 6°) occur in planes that are perpendicular to each other. Even though rolling occurs during accommodation of aminoacyl tRNA to the A site, the reversal of both rolling and rotation occurs during translocation, hence both motions are thought to prepare the ribosome for translocation [26].

One type of intrasubunit movement in the small subunit occurs at the decoding center, as A1755-56 (A1492-93 in bacteria) "flip" in response to tRNA binding [79]. Another important motion, observed in bacteria, is the head swivel which is the 14° movement of the head domain with respect to the body of the small subunit, occurring in the "rolling" plane. This is also thought to be important in translocation. Low resolution structural studies have provided insight into ribosomal dynamics during eukaryotic initiation [80,81]. Upon eIF1 and eIF1A binding, a connection between the head and the shoulder is observed on the solvent side, involving the 18S rRNA and S3. The beak and the platform also exhibit altered conformations. A so-called "latch," formed by interactions between h18 and h34 and thought to clamp around mRNA to prevent dissociation, is "closed" in empty 40S, but "open" or not visible in the 40S-eIF1-eIF1A complex, possibly to allow mRNA binding. While there is evidence indicating eIF1's involvement in influencing the conformation of the platform and the positions of the mRNA and the initiator tRNA (whereas eIF1A acts like IF1 and seemingly only blocks the A site), both factors are required for the full conformational change. These changes are observed in the 43S preinitiation complexes (ie. in the presence of other initiation factors and initiator tRNA) as well,

resulting in the opening of the head-body-platform junction and hence the mRNA entry channel, and permitting mRNA binding and scanning for the start codon.

The intrasubunit motions of the large subunit are mostly observed in the so-called "hinge" regions, the L1 and L7/L12 stalks (P stalk in eukaryotes), and show changes in conformation throughout the bacterial translation [82–84]. Information on their conformations and functions during eukaryotic translation remains limited as their high intrinsic mobilities have interfered with structural studies, however they are thought to act similar to their bacterial counterparts. The L1 stalk, formed by the protein L1 and H76-78 in both bacteria and eukaryotes, becomes especially mobile after peptidyl transfer and upon rotation, moving towards the CP, and locks in this position upon EF-G binding [78]. After GTP hydrolysis and simultaneously with translocation, it goes back to its original position, "pulling" the P/E tRNA to the E site as it does so, or possibly out of the ribosome since the original position is permissive for bacterial E site tRNA release [78]. L7/L12 stalk is formed by H33-34 (GAC) at its base, the long α helix of L10 bolstered by L7/L12 NTD dimers at its middle, and L7/L12 CTDs at the tip (bound to the NTD dimers by long, disordered flexible linkers) [83]. A similar structure is formed by the acidic phosphoproteins P0, P1, P2 in the eukaryotic ribosomes, according to low resolution structural studies. The CTDs in the resulting structure are very flexible and are thought to capture elongation factors, as L7/L12 stalk forms part of the factor binding site. This stalk also has been observed to move towards CP upon TC binding [78,83]. Another important large subunit motion occurs during accommodation. H92, or the "A loop," switches from a conformation that impedes tRNA accommodation to the PTC to a permissive

position, resulting in the opening of a 3D gate, formed by U2492 (U2861 in yeast) of H89, and C2556 and C2573 (C2925 and C2942 in yeast) of H92 [83,85,86]. This gate, and the whole AC, a corridor of 20 conserved rRNA bases spanning H89-H93 that interact with the tRNA during accommodation, "closes" again after the tRNA CCA end has completely moved into the PTC.

1.5. Experimental approaches related to the ribosome structure and function

The last five to six decades have seen major breakthroughs in the research of translation and ribosomes, allowing us to have an atomic resolution view of the static ribosome and to identify many steps and components of translation [87]. The advent and commercialization of electron microscopy and ultracentrifugation fueled this research area in the 1950's. Biochemical and molecular biology approaches, made possible by the use of radioactive labeling, from 1950's to 2000's resulted in the discovery of tRNA and mRNA, elucidation of the genetic code and the protein composition of the ribosome, reconstitution of bacterial ribosomes *in vitro*, and the sequencing of the large rRNAs. Biophysical approaches yielded important results as well. In the late 1960's, small angle X-ray and neutron scattering techniques (SAXS and SANS, respectively) allowed the overall shapes of the ribosome and its subunits to be observed, enabling generation of a "neutron map" of the positions of the proteins in the small subunit. This is also when Förster resonance energy transfer (FRET) started to be used in this research area to locate ribosomal proteins. The use of FRET began to flourish in the mid-2000's, and has been enhanced by the recent development of single molecule techniques. In the mid-1970's and 1980's, advances in electron

microscopy made it possible to identify the shapes and interactions of the ribosomal subunits, the locations of specific proteins and resulted in the discovery of the peptide exit tunnel. These advances also laid the foundation of the single particle reconstruction techniques of today. Cryogenic electron microscopy (cryo-EM), developed in mid-1990's and still used today with major improvements primarily driven by advances in computational technologies, opened the door to structural dynamics studies. 1980's and 1990's also saw the extensive use of chemical and enzymatic structure probing methods, resulting in the identification of A, P, E sites on the rRNA, as well as the hybrid states of tRNA binding. The use of nuclear magnetic resonance (NMR) has been helpful in analyses of rRNA fragments and ribosomal protein / RNA fragments. The application of X-ray crystallography to the field began with crystals of isolated ribosomal proteins, and moved to the whole ribosome in the 1970's when the first useful, but poorly diffracting crystals of ribosomes were obtained. The diffraction resolution continually increased. The incorporation of the phases of the electromagnetic waves, and not just the intensities, resulted in a breakthrough in the field in 1998, resulting in the publication of the first atomic resolution structures of the ribosomal subunits in 2000. Overall this method contributed immensely to the determination of the atomic structure of ribosomes from all domains of life.

Today the static structures of the 70S and 80S ribosome are well known thanks to continued improvements to X-ray crystallography, while cryo-EM and single molecule studies continue to be promising to study ribosomal dynamics. Additional visualization of dynamics is made possible by molecular dynamics (MD)

simulations, especially when coupled to cryo-EM, single-molecule FRET (smFRET), and highthroughput versions of chemical probing techniques. The following subsections will focus on the key methods to study ribosome structure and dynamics.

1.5.1. X-ray crystallography

Different forms of electromagnetic radiation are useful to visualize objects, requiring the wavelength of the radiation to be comparable to the smallest features to be resolved. In biological molecules, the smallest features of interest are atomic bond lengths (1-2 Å in length), rendering X-rays suitable. X-rays may be produced by in-house rotating anodes, or by synchrotrons. Upon interaction of X-ray waves with the electrons of matter, the electrons become secondary sources of electromagnetic radiation, scattering the incident radiation. Scattering from one molecule is generally too weak to measure, hence the successful use of X-rays has first been described on crystals, which contain millions of ordered and repeating molecules. X-ray scattering off the regularly repeating assembly of molecules in a crystal allows reconstruction of electron densities, finally arriving at the distribution of the atoms [82].

X-ray crystallography is undoubtedly a very powerful technique especially for *de novo* structure determination, as it does not have a size limitation, as long as well-diffracting crystals may be prepared. The structures of many proteins, including the Nobel prize winning hemoglobin, have been discovered by this technique [88]. However, and even though the X-ray structure of the ribosome were also awarded the Nobel prize, obtaining well-diffracting crystals, especially as they pertain to ribosomes, is a difficult process, and requires very homogeneous samples. Homogeneity may be achieved by employing thermophilic bacteria and archaea,

whose ribosomes are highly stable and resistant to degradation [82]. Obtaining homogeneous ribosomes from eukaryotes is still challenging, as the only known method in use is glucose starvation of yeast [82]. This causes ribosomes to be "locked" with the Stm1 protein, a suppressor of ribosome activity [2]. While glucose starvation stabilizes yeast ribosomes in a single, homogenous population, these ribosomes cannot be used to make complexes because their ligand binding sites are occupied by Stm1 and they are in a permanent "rotated" conformation [2]. Furthermore, X-ray crystallography is not suitable for studies of dynamics, in any domain of life, as molecules may behave differently in crystals and in solution, and more than one diffraction experiment on separate subsets of homogeneous ribosomes would be required to really get a sense of the change in the "motion" of molecules.

1.5.2. Cryo-EM

Cryogenic electron microscopy (cryo-EM) is another structure determination method that is suitable for use with dynamic systems. A dilute solution of a biological complex is flash frozen in a thin layer of vitreous ice (e.g. using liquid ethane) on an electron microscopy grid, and 2-dimensional (2D) images (micrographs) are collected under 50,000x or more magnification by transmission electron microscopy (TEM). The signal to noise ratio with this method is low, resulting in low contrast images, requiring hundreds of thousands of images to be collected. Contrast transfer functions of these are calculated to explore the relationship between the object of interest and the contrast, and to correct for the low contrast. Particles in the micrographs are then classified according to orientation, averaged, and merged. Three-dimensional (3D) density maps are obtained upon image processing [84].

The power of cryo-EM in ribosome studies comes from the natural contrast between the phosphate backbone and proteins [84]. Cryo-EM also does not have a size limitation. Common image processing methods to obtain 3D information from 2D images include random conical tilt (RCT) and common line (CL) [84]. In RCT, the electron micrographs of the same area of the grid are generated in tilted and untilted condition, giving two angles. A third angle is computed from the 2D alignment of chosen particle images. These three angles or views can then be used to compute an initial 3D volume. In CL, common lines of any two 2D averaged classes are found as a result of the Fourier transform of the original 3D object to compute their relative angles. This is suitable for a small set of atoms, as it generates an *ab initio* model of the structure. Larger datasets, with both 3D construction techniques, require a known model of the object of interest (such as an X-ray crystallography structure of the ribosome). Although cryo-EM is suitable to gather information on ribosomal dynamics, its resolution remains limited, and is currently being improved through both computational means and new camera technologies [89]. Cryo-EM is also a very labor-intensive method, although this is currently being solved by automation of some processing steps, such as particle classification.

1.5.3. SmFRET

FRET stands for Förster resonance energy transfer. This type of energy transfer occurs between fluorescent dyes showing spectral overlap, such that the acceptor dye is excitable by the wavelength of photons the donor dye emits as it fluoresces, and is very sensitive to the inter-dye distance. Hence the acceptor fluoresces upon coming to close contact (20-80 Å) with the donor. When

biomolecules are tagged with such FRET pairs, and the photons emitted by the acceptor dye detected, interrogation of interactions and dynamics become possible. As such, this method and the derivations of it have been very useful in analyses of protein conformation, protein-protein interactions and cellular localization of proteins [78,90].

FRET, especially in conjunction with single molecule technologies (smFRET), has also been extensively used in protein translation research, mostly pertaining to translational dynamics, as inter-dye distance can be monitored over time [78,91]. In setups with the ribosome, molecules of interest, either intrinsic or extrinsic to the ribosome, are labeled with FRET fluorophore pairs. This primary setup requires synchronization of molecules, which is challenging with multistep processes. This challenge has been overcome by incorporation of single molecule spectroscopy and microscopy (smFRET), allowing single photons to be detected at a time, which would result from a single FRET interaction. The ribosome is also immobilized on an optically transparent surface, solving the problem of fluorophore diffusion. As a process takes place, binding of molecules of interest (eg. tRNAs) may be detected by a series of fluorescence bursts and delays, allowing time and rate constants of dissociation and association to be resolved [78,92].

Although smFRET is a powerful quantitative technique for interrogation of translational and ribosomal dynamics, it relies heavily on known structures, and cannot be used for discovery of novel dynamic processes. Additional limitations come from the maximum possible distance between the fluorophores and fluorophore photobleaching. Surface immobilization, although conferring some advantages, may

also perturb behavior of systems, and may result in some nonspecific surface interactions. Currently, the method is also challenging and time consuming [78,84].

1.5.4. MD simulations

Molecular dynamics (MD) approaches computationally explore the time-dependent changes in the positions of atoms. Simulations are achieved by first modelling the molecular interactions within a macromolecule. This requires calculation of the total "potential" force acting on each atom, through bonded or non-bonded interactions. MD simulations are generally coupled to structural studies to be able to do these calculations, as well as obtaining information on the initial positions and velocities of all particles in the system. From this total force, the position, velocity and acceleration of each atom are calculated by solving for Newton's equations of motion. This process is repeated after computationally moving the atoms to their estimated position at a time step. After many iterations of this process, the results add up to a trajectory of the time evolution of the system at hand.

Defined this way, MD simulations provide a visualization option for dynamics studies. They have been used in conjunction with cryo-EM and smFRET, and facilitate "quasi atomic model" building. As described in Chapter 5: Conclusion and future directions, our RNA chemical modification studies are being used to help refine MD simulations of the yeast ribosome through the translational elongation cycle.

1.5.5. Chemical structure probing

All chemical structure probing methods have a common scheme of chemical treatment of RNA, which results in adduct formation on the RNA, and detection of the locations of such adducts by primer extension by a reverse transcriptase. Sequencing reactions are conducted in tandem for each region of interest. Conventionally, radioactively labeled primers and sequencing gels are employed for fragment analysis, providing single nucleotide resolution in reads of 100-200 nt long fragments.

1.5.5.1. Base specific chemicals

Traditional, base specific chemicals, DMS, CMCT, and kethoxal, have affinity for the basepairing edges of nucleotides, mostly the Watson-Crick edge. Hence they target non-basepaired regions of RNA molecules. The modification patterns obtained from treatment of RNA with these chemicals may indicate basepairing, tertiary contacts, or protein-RNA interactions. Due to the base specific nature of these chemicals, they have to be used in tandem to obtain complete structural information on RNA [93,94]. An additional step must also be performed to stop the reactions with these chemicals.

DMS (dimethyl sulfate) methylates the N-1 atom of adenosine and the N-3 of cytosine bases. It may modify adenines and cytosines that are single stranded, basepaired at the end of a helix, or in a base pair next to a GU pair [93,94]. DMS has affinity for DNA, as well. CMCT (1-cyclohexyl-(2-morpholinoethyl)carbodiimide metho-p-toluene sulfonate) modifies the N-3 atom of uracil, and to a smaller extent,

the N-1 of guanine. Kethoxal (β-ethoxy-α-ketobutyraldehyde) modifies the N-1 and N-2 atoms of guanine [93,94].

1.5.5.2. Hydroxyl radical footprinting

Another chemical probing method, hydroxyl radical footprinting, relies on the cleavage of unprotected regions of RNA by hydroxyl radicals. In addition to the general probing scheme mentioned above, this method requires the use of a system to continually generate such radicals. This is achieved through the Fenton reaction of Fe(II) EDTA with hydrogen peroxide and ascorbic acid. Hydroxyl radical footprinting can be used with DNA, RNA, or even proteins, as the radicals can break phosphodiester and peptide bonds. This method generates information on the tertiary structure of a molecule, specifically solvent accessibility, which makes it especially useful in identification of protein binding sites on nucleic acids. For such a purpose, tethering of the hydroxyl radical generating system on the protein of interest is necessary, and is commonly achieved through the use of BABE (bromoacetamidobenzyl-EDTA) in conjunction with reduced iron. BABE is a chelate labeling reagent that conjugates with sulfhydryl groups [95,96]. Another way to constantly generate hydroxyl radicals necessary for cleavage is achieved through irradiation with synchrotron X-ray beams. This is especially useful to track dynamic, rapid processes, such as ribonucleoprotein folding, as it provides analyses on timescales of 50-100 milliseconds [97].

1.5.5.3. In-line probing

Another method that may be employed to probe the RNA structure, specifically the local nucleotide dynamics, is in-line probing. This method does not

require any chemicals, and is not enzymatic, but is based on the natural tendency of RNA to degrade differentially according to its structure. Briefly, single stranded RNA is able to sample through a range of conformations, one of which is the "in-line" conformation of the 2'-oxygen, the phosphorus, and the adjacent 5'-oxygen. In this conformation, the 2'-oxygen acts as a nucleophile in the intramolecular displacement of the adjacent 5'-oxygen and cleaves the RNA linkage. In contrast to the flexible single stranded regions, the linkages in the highly structured regions of the RNA will be much less prone to this sort of cleavage [98].

1.5.5.4. SHAPE

SHAPE, selective 2'-hydroxyl acylation analyzed by primer extension, is a chemical probing method that provides for both structure and dynamics interrogation. The scheme is very similar to other chemical probing methods, however more than one chemical is suitable for SHAPE. The most important common property of SHAPE chemicals is that they react with 2'-hydroxyl groups, hence modifying all RNA nucleotides with equal specificity. Another common property is that they are self-quenching. Examples of these chemicals are N-methylisatoic anhydride (NMIA, half-life: 8.3 min at 37°C), 1-methyl-7-nitroisatoic anhydride (1M7, half-life: 14 sec at 37°C), and benzoyl cyanide (BzCN, half-life: 0.2 sec at 37°C) [99,100]. Unless the 2'-hydroxyl group of a nucleotide is constrained through basepairing, stacking or other interactions, the SHAPE chemical binds to the nucleotide (Figure 15), forming an adduct that cannot be resolved during primer extension by a reverse transcriptase. This results in fragments of varying lengths. If radioactively labeled primers are used, the fragments can be visualized on gels, and essentially single nucleotide resolution is

obtained. The use of non-base specific chemicals, and the 2'-hydroxyl reactivity essentially depending on local flexibility, gives an edge to SHAPE method compared to other chemical probing techniques such that it can be employed to obtain information on dynamics of all nucleotides on the RNA of interest. The SHAPE chemicals also have high dynamic ranges, hence the data obtained are highly quantifiable. There have been further improvements to this method (please see below).

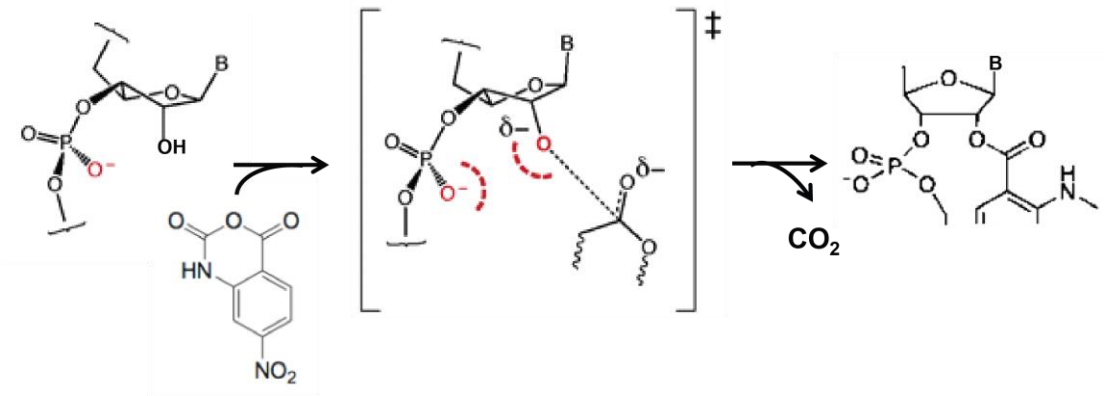

Figure 15. SHAPE reaction.

The ribose 2'-hydroxyl group attacks the carbonyl carbon of the SHAPE chemical, shown here is 1M7. This attack depends on the vicinity of the neighboring phosphate group, as its negative charge does not allow stable binding of the chemical to the 2'-hydroxyl group. After electron rearrangements, part of the anhydride chemical breaks off as carbon dioxide and the RNA nucleotide is covalently bound to an adduct. Modified from Merino et al, 2005 and Mortimer and Weeks, 2007 [100,101].

1.5.5.4.1. SHAPE chemistry

During the course of development of SHAPE method, it has been shown that the acylation of 2' position selectively in single stranded RNA nucleotides does not rely on solvent accessibility or electrostatic factors, but on local nucleotide flexibility, as the single stranded RNA tends to assume more conformations than RNA duplexes [102]. In other studies, the chemical reactivity of 2'-hydroxyl has found to be modulated by proximity of adjacent 3'-phosphodiester anion [101]. According to this, the 2'-hydroxyl reactivity of AMP is the highest, followed by, in decreasing order, cyclic

AMP, ATP, 3'-deoxy-ATP, 3'-O-methyl-ATP, adenosine 3'-ethyl phosphate (pAp-ethyl; unstructured RNA analogue with 2'-hydroxyl and 3'-phosphodiester monoanion) and pAp-ddC (dinucleotide analogue).

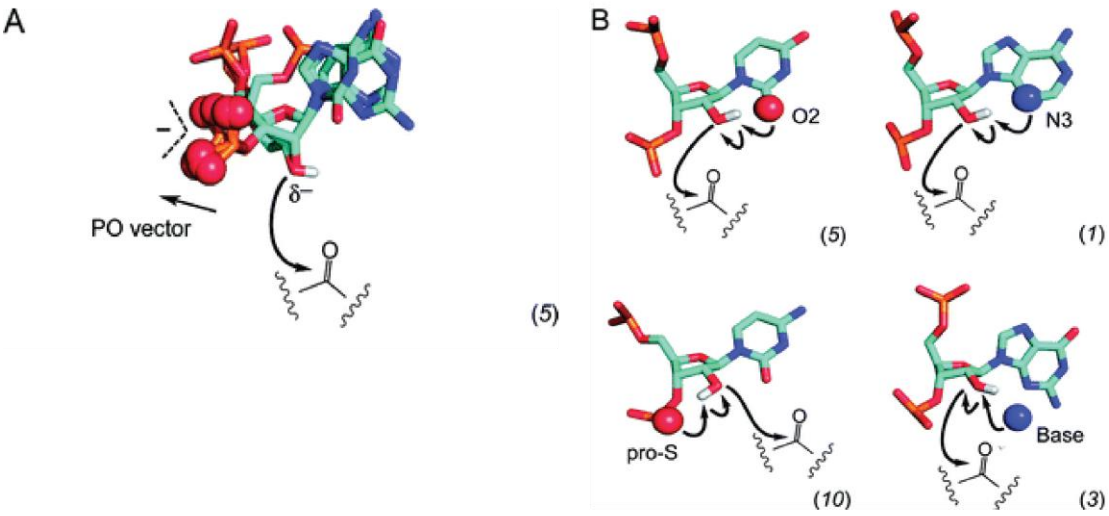

Figure 16. Mechanisms of RNA SHAPE chemistry.

A. Hyper-reactive nucleotides from McGinnis et al are superimposed to point out to the fact that the nonbridging oxygen groups of the backbone (and the permanent charge) are directed away from the 2′-OH group, and the 2'-oxyanion is stabilized this way. B. General base catalysis examples are shown. These include catalysis by the pyrimidine O2 (upper left), purine N3 (upper right), pro-S oxygen (lower left), and alkaline solvent (lower right). For each panel, the number of occurrences observed in SHAPE analysis of 16S rRNA crystals is given in parentheses. Phosphate group oxygens are thought to have "pro-chirality" as substitution of one results in S chirality ("pro-S") and the other in R chirality ("pro-R") [103]. Image modified from McGinnis et al, 2012 [104].

An attempt to show which conformations of the 2'-hydroxyl and the neighboring positions are permissive to chemical binding comes from a study in which SHAPE has been performed on 16S rRNA crystals [104]. The hyper-reactive nucleotides resulting from in-crystal SHAPE have mostly fallen into one or more of these categories: A) long PO-to-2'-OH distance (nucleotides mostly in C3'-endo ribose conformation), B) short 2'-OH to pyrimidine O2 / purine N3 distance (nucleotides only in C2'-endo ribose conformation), and C) short 2'-OH to non-bridging O distance (nucleotides mostly in C2'-endo ribose conformation). The first category is in accordance with previous studies [101], while the latter two indicate that

the 2’-hydroxyl reactivity may be modulated by the pyrimidine O2 or purine N3 group and the nonbridging phosphate oxygen, respectively. These observations and functional group substitution experiments from the above study indicates general base catalysis as a mechanism for the increased reactivity of 2’-hydroxyl with SHAPE chemicals (Figure 16).

1.5.5.4.2. Highthroughput SHAPE (hSHAPE)

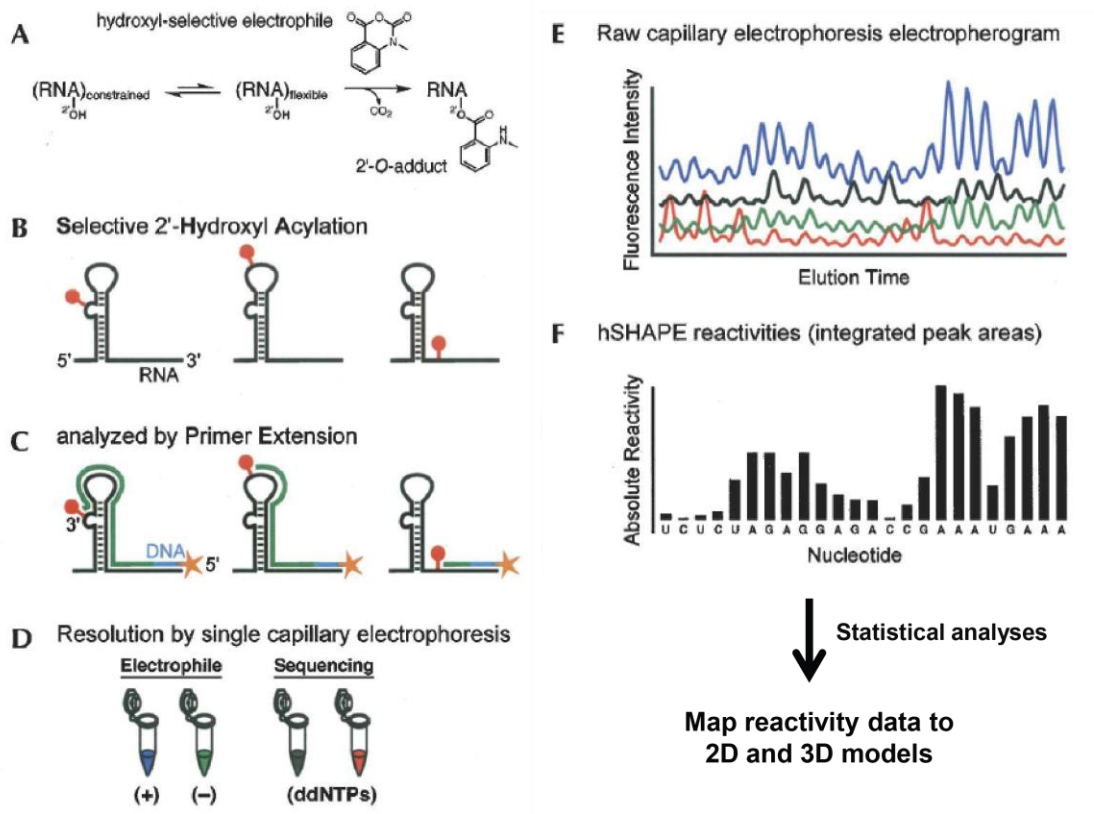

Figure 17. Scheme of highthroughput selective 2’-hydroxyl acylation analyzed by primer extension.

A. The RNA of interest is treated with a hydroxyl-selective electrophile, 1-methyl-7-nitroisatoic anhydride in our experiments. The chemical binds to the 2’-hydroxyl groups of nucleotides based on local flexibility. **B.** Unconstrained regions of the RNA, such as bulges, loops and single stranded stretches interact with the SHAPE chemical, resulting in 2’-O-adducts (red knobs). **C.** These adducts cannot be resolved by the reverse transcriptase during primer extension, using fluorescently labeled primers (blue with yellow stars). **D.** Four primer extension reactions are conducted per primer region, separated by the fluorescent tag. One tube contains the chemical treated RNA, another contains the vehicle control RNA (DMSO treated), and the remaining two contain untreated RNA and are for sequencing reactions. For rRNA hSHAPE, we have 20 primer sets and use dideoxynucleotides (ddNTPs) corresponding to the two most common nucleotides of a region for sequencing reactions [105]. **E.** The fragments resulting from primer extension are resolved by capillary electrophoresis and the

electropherograms are analyzed by ShapeFinder. This analysis entails correct alignment of the corresponding chemical treated and vehicle control peaks with the RNA sequence. **F.** Integrated peak areas (area under chemical treated peak minus area under the corresponding control peak) obtained from ShapeFinder are put through statistical analyses and mapped onto 2D and 3D maps of the ribosome. Image modified from Vasa et al, 2008 [106].

As with all chemical probing techniques, visualization of fragments obtained from SHAPE was carried out by gel electrophoresis until recently. Today, this powerful technique is coupled to capillary electrophoresis, making it high throughput (hence "hSHAPE") since the read lengths have increased from 100-200 nts to 400-600 nts. Fluorescently labeled primers are also employed, eliminating the need for radioactively labeled materials. These improvements enhance the accuracy of quantitative analyses related to hSHAPE, make it easier, faster and more automated. The hSHAPE scheme is shown in Figure 17. The methodology we use is described in detail in Chapter 6. Other improvements to the SHAPE technique are listed in Chapter 2.

1.6. Project rationale and aims

The extensive use of the biophysical techniques discussed above has resulted in an accurate view of the static structure of the ribosome and the steps in translation; yet uncovering the dynamic nature of this complex machinery and the allosteric communication pathways within it remains a challenge. While providing valuable and accurate structure information, X-ray crystallography is limited by the formation of high quality crystals. Cryo-electron microscopy, while having provided insight into different conformational states of the ribosome, is still limited by resolution. Single molecule FRET has been especially useful in determining the tRNA movements during translation, but is limited by the maximum possible distance between the

fluorescent probes. Chemical probing of rRNA structure has the advantage of simplicity and can provide a good understanding of how the rRNA structure changes. However, the traditional chemicals used in this approach have limitations such as high noise, difficult optimization, the need for reaction quenching and low dynamic range. These and other technical details have limited the use of traditional chemical probing technology to probing of only short stretches (about 100 nucleotides at a time) of rRNA.

Since relatively small changes in the secondary and tertiary structure of rRNA might allow transmission of information between different regions of the ribosome, probing of rRNA structure with an enhanced technique can give valuable insight into ribosome dynamics. hSHAPE is a high-throughput technique with single nucleotide resolution, and can provide data on both overall rRNA dynamics and changes in individual functional sites. It is not base specific in contrast to other chemical probing methods and targets the 2'-OH of all RNA nucleotides. The chemical used in this work, 1-methyl-7-nitroisatoic anhydride (1M7), has a high dynamic range, is self-quenching and yields high signal to noise ratios, making the method easy to optimize [100]. After application of this technique on different elongation complexes and through computational modeling, the allosteric communication pathways throughout the ribosome can be uncovered in the context of the translation elongation cycle. Such knowledge will ultimately contribute tremendously to our understanding of the ribosome and structure/function relationships.

In this context, this work aims to improve hSHAPE analyses for use with eukaryotic rRNA, and to interrogate rRNA dynamics using this method in initiation

and elongation complexes, with the ultimate aim of uncovering the binding site of eukaryotic initiation factor 5 (eIF5) on the SSU, and generating a complete, dynamic view of the translation elongation cycle.

Chapter 2: The evolution of hSHAPE analyses

2.1. Background and rationale

Ribonucleic acid (RNA) is a complex biomolecule that mediates, catalyzes, and regulates many processes during gene expression. The catalytic roles of RNA can be illuminated by analyses of an RNA molecule's complex tertiary structures, which can be determined by X-ray crystallography and nuclear magnetic resonance spectroscopy. For molecules without available atomic resolution structures, secondary structure prediction is typically the first step toward elucidating functional higher order interactions. Single stranded RNA forms numerous secondary structures including duplexes, hairpins, bulges, internal loops and junctions. These can be predicted and probed by computational (phylogenetic comparative sequence analysis or covariation analysis), and biochemical approaches (enzymatic and chemical structure probing) respectively. Biochemical methods are based on the partially selective interaction of small molecules or ribonucleases with single stranded, unstructured RNA regions and detection of these interactions by primer extension to probe local RNA structure, flexibility and solvent accessibility [8,107,108].

Selective 2'-hydroxyl acylation analyzed by primer extension (SHAPE) is a chemical probing method in which a hydroxyl selective, self-quenching electrophile is employed to interrogate local RNA flexibility [109]. When coupled with primer extension protocols employing fluorescently labeled primers and capillary electrophoresis [110] (thus rendering it high throughput - hSHAPE), reads in the range of 400-600 nt long can be generated with single nucleotide resolution. Data may then

be analyzed using ShapeFinder [111], and processed through fitted baseline adjustment, mobility shift correction, signal decay correction, scaling and peak alignment. The output consists of an integrated peak value, or the reactivity value, for each nucleotide. Overall, the technique yields high signal to noise ratios and has a high dynamic range. Modifications to the method include employing electrophiles improved for a shorter reaction time [100,112], coupling of hSHAPE with multiplexed deep sequencing [113,114], or the use of a two-capillary system [115], all of which increase the strength of the technique.

There have been major improvements to the process of RNA structure determination by SHAPE. These include improving the algorithms associated with RNA secondary structure determination [116], improving the signal decay correction associated with primer extension electropherogram analyses [117,118], and merging mutational analyses with SHAPE chemistry to arrive at the most reliable secondary and tertiary structure predictions in the absence of X-ray crystallography data [119–121]. What remains common to all these studies is the method of normalization, which comprises of box-plot analysis to remove peaks greater than 1.5 times the interquartile range above the 75th quartile and division of all SHAPE reactivities by the average of the highest 10% of intensities after removal of outliers [116,122]. This approach loses a considerable amount of information and does not lend itself well to visualization of complex structures such as ribosomal RNA (rRNA) in the context of the ribosome. One attempt at improving the normalization of SHAPE reactivities involves separately normalizing the background and signals by their corresponding median values before background subtraction using a series of algorithms named Fast

Analysis of SHAPE Traces (FAST) [123]. However this does not overcome the skewed data distributions associated with application of SHAPE on eukaryotic rRNA, which interferes with normalization and causes loss of data.

One of the strengths of SHAPE chemistry is that its high dynamic range has the potential to retain high resolution information pertaining to the entropic environment of individual ribobases. Such information has a broad range of applications, including providing additional restraints upon molecular dynamics simulations, nucleotide resolution mapping of intra- and inter molecular complexes, and visualization of changes in entropic landscapes in macromolecules. As noted above, the problem is that current analytical methods lose much of this information. Here, we report a new method for normalization and analysis of hSHAPE data that maximizes information retention while minimizing background noise. The testbed for this method is the yeast ribosome, for which atomic resolution structures are available but for which the molecular dynamics remains incomplete. Application of this method to a well-defined series of yeast ribosome complexes reveals both previously known and unknown changes in rRNA entropic states that can be simply visualized.

2.2. Results

2.2.1. hSHAPE analyses v1.0

Our original hSHAPE analysis method, based mainly on previous methods [110], employs the raw reactivities or median normalized reactivities of rRNA nucleotides. Raw reactivities refer to the integrated peak values obtained from ShapeFinder after correction of negative values to "zero"s. Median normalized reactivities are generated by dividing the raw reactivities by the median value for a primer region. Both types of

data are then categorized into ranges based on the mean, the median, the mean plus one standard deviation and the mean plus two standard deviations prior to the merge of all primer regions together. The ranges are labeled as reactivity levels from 1 to 4, which can then be color coded and shown on secondary and tertiary rRNA structure maps. These reactivity levels are also used to compare data from different rRNAs, obtained from different ribosomal complexes in the context of this work, by simply taking the difference of the levels on a per nucleotide basis.

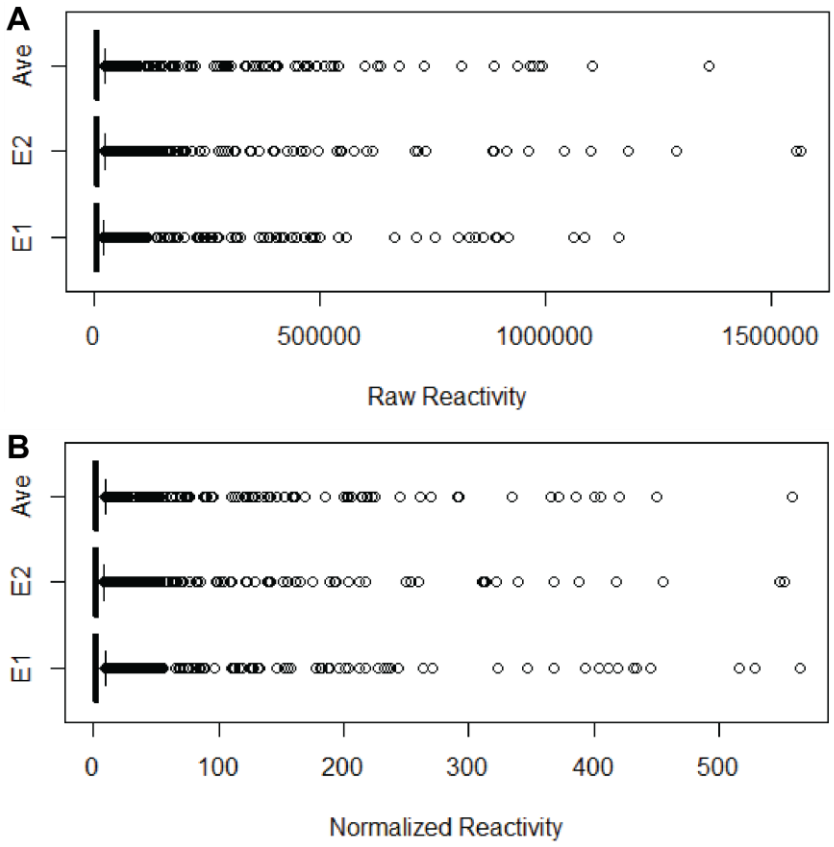

Figure 18. Box plot analyses indicate extremely skewed distribution of data.

A. Box plot analysis of the raw reactivity values from hSHAPE experiments. B. Box plot analysis of the median normalized values from hSHAPE experiments. E1 and E2 show the data from two runs of the empty small subunit, and Ave indicate the average of the two.

Evaluation of the results of these processes by box plot analyses indicate extremely skewed data, with a very large number of outliers above the maximum (Figure 18). Frequency histograms of the raw reactivities and median normalized

reactivities were also generated to further observe the data distribution, confirm the right skew of the data and the presence of extremely high outliers (Figure 19). These results illuminate the necessity to improve the data analysis step of hSHAPE.

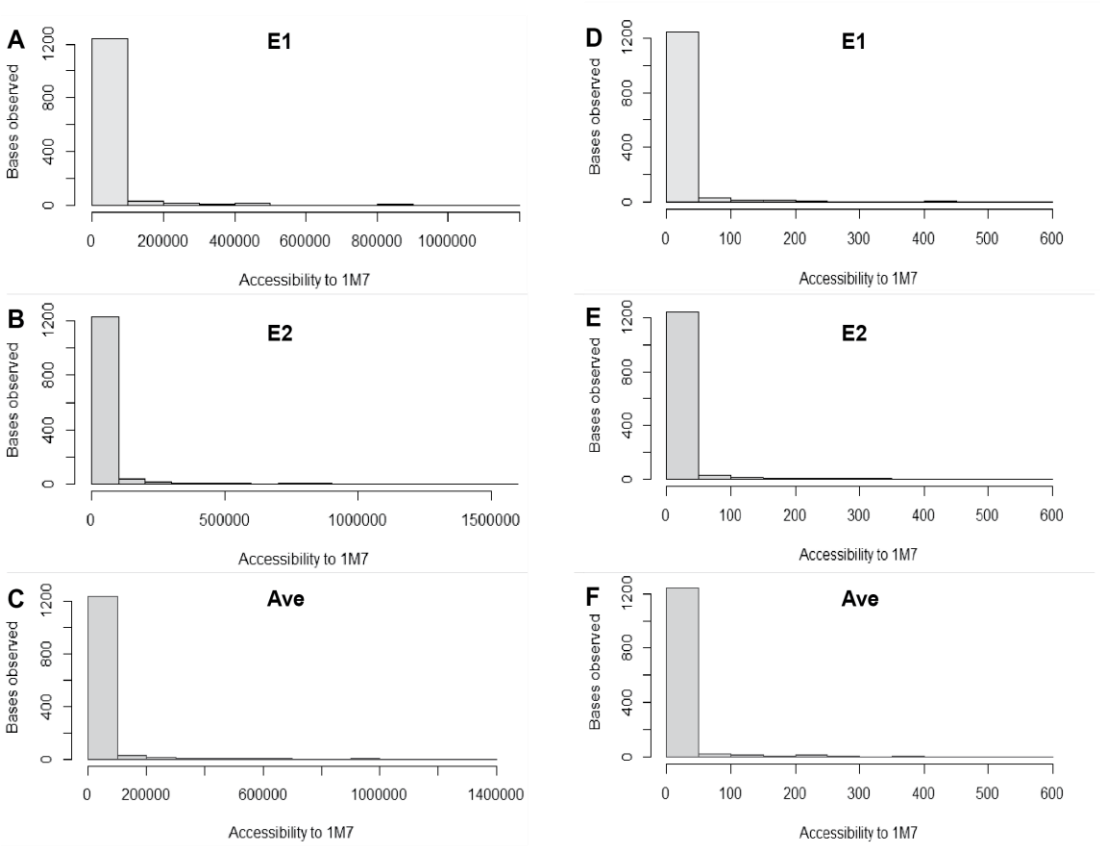

Figure 19. Frequency histograms also show extremely skewed distribution of data.

A-C. Histogram of the raw reactivity values from hSHAPE experiments. D-F. Box plot analysis of the median normalized values from hSHAPE experiments. E1 and E2 show the data from two runs of the empty small subunit, and Ave indicate the average of the two.

2.2.2. hSHAPE analyses v2.0

Examination of the data shown in Figure 18 and Figure 19 revealed that the unimodal and right-skewed distributions resemble lognormal data. Data transformation is a common application in genome-wide data analyses [124,125], however has not been reported in hSHAPE data analyses before. Thus, to improve the analyses scheme, the raw reactivity data were transformed by the natural log (ln)

before further processing, separately for each primer region. The resulting box-plot and histogram represent a tremendous improvement from the previous approach (Figure 20A and Figure 21A-C), revealing that the non-zero data adopted a normal distribution.

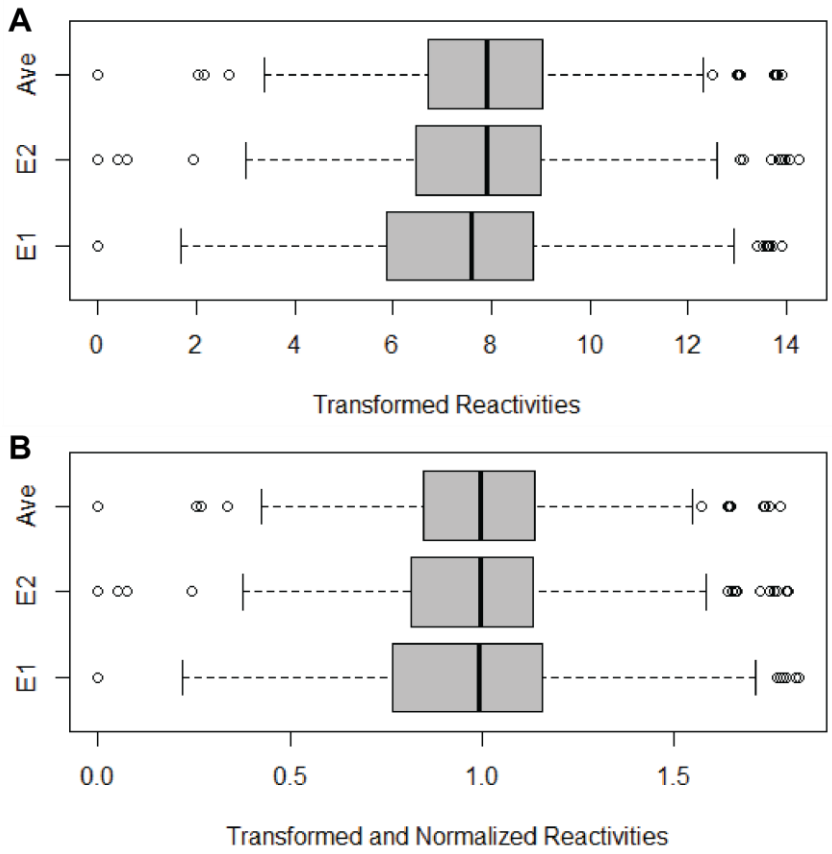

Figure 20. Box plot analyses show the data acquire a unimodal, symmetric distribution after natural log (ln) transformation and median normalization.

A. Box plot analysis of the ln transformed values from hSHAPE experiments. B. Box plot analysis of the ln transformed and median normalized values from hSHAPE experiments. E1 and E2 show the data from two runs of the empty small subunit, and Ave indicate the average of the two.

Next, median values for each primer region were employed to normalize the ln transformed data. The ln transformed value for each nucleotide was divided by the median of the region, and the data were merged. Box plot and histogram analyses show that the data distributions were very similar to that of ln transformed values, maintaining the normal distribution of non-zero data (Figure 20B and Figure 21D-F).

With these new analyses, assignment of reactivity levels for visualization purposes is performed following comparison of transformed, normalized values from different rRNAs, or different ribosomal complexes in the context of this work. For this comparison, the difference of the transformed, normalized values from different complexes is divided by the transformed, normalized value of the empty ribosome, on a per nucleotide basis. (This division step accounts for the overall reactivity of the ribosome.)

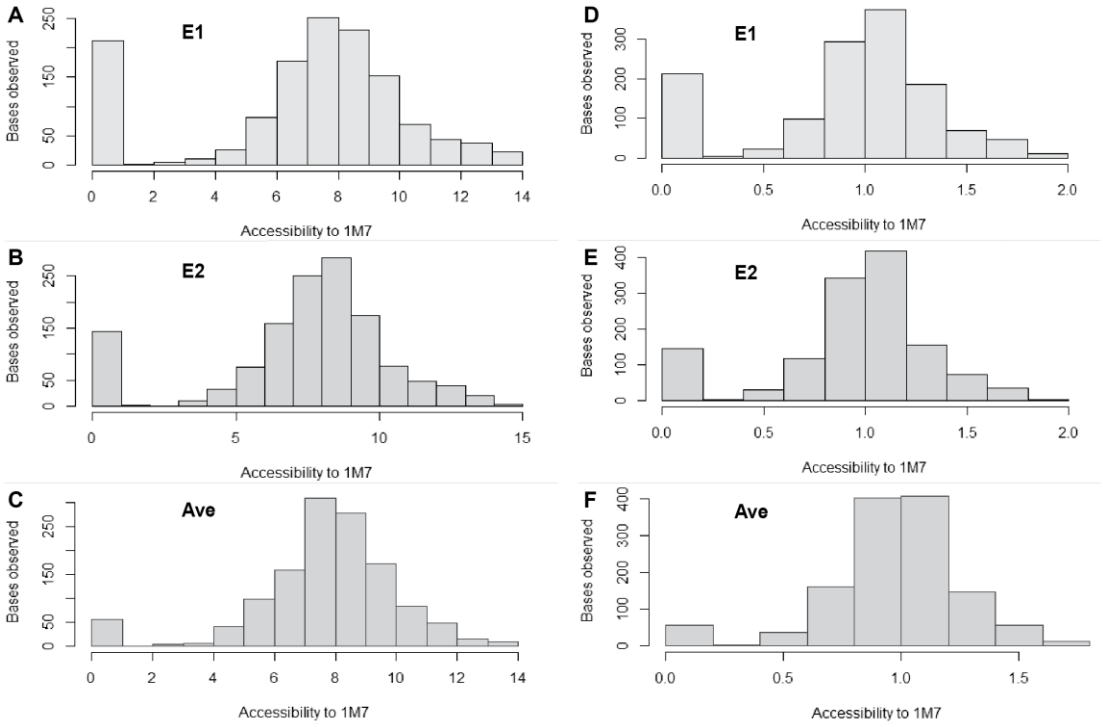

Figure 21. Frequency histograms also show improvement in data distribution upon ln transformation.

A-C. Histogram of the ln transformed values from hSHAPE experiments. D-F. Box plot analysis of the ln transformed and median normalized values from hSHAPE experiments. E1 and E2 show the data from two runs of the empty small subunit, and Ave indicate the average of the two.

For visualization purposes, a color code is employed that represents ranges of comparative reactivity levels. 15 levels of reactivity are chosen by grouping the data generated from comparison calculations, based on the frequency histograms.

Frequency intervals are used to determine the relative reactivity levels. A representative histogram is shown in Figure 22A. Level "0" (indicating no change between two complexes) comprises most of the data points (highest bars, roughly in the range of -0.25 to 0.25 for all complexes), followed by levels "-1" and "1." The most extreme levels "-7" and "7" (indicating a large decrease in reactivity and a high increase in reactivity, respectively, in one complex compared to the other) include the smallest number of data points. All other levels include approximately the same number of data points. The resulting color scale is shown in Figure 22B in the order of relative levels, colors, and comparative reactivity ranges.

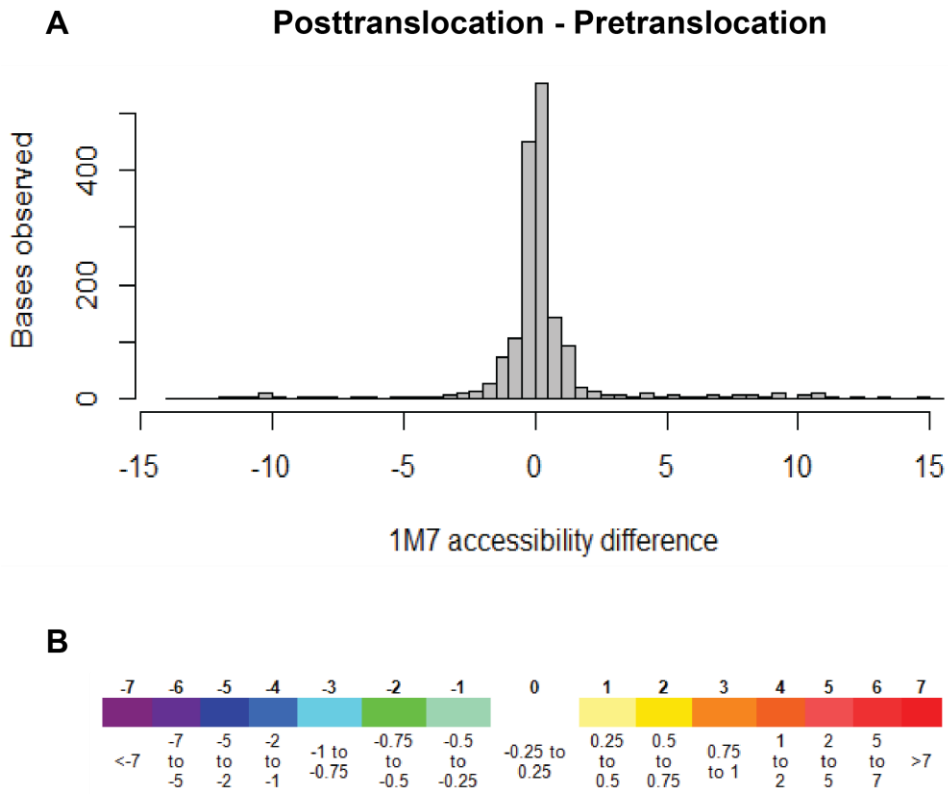

Figure 22. Difference calculations and data visualization.

A. Data distribution of the reactivity difference between posttranslocation and pretranslocation complex 18S rRNAs. For more information on the complexes, please refer to Chapters 4 and 6. B. The above data distribution was used to derive the color code shown here to be used in hSHAPE 2D and 3D difference maps.

The same color scale is maintained in the difference maps of complexes versus the empty ribosome as well, even though the data distribution of the results of the comparison calculations differ (Figure 23). As the reactivity of a nucleotide might decline to zero in a complex, reactivity level "-1" forms a natural limit to complex versus empty ribosome calculations, resulting in a non-normal data distribution after this comparison. We maintained the color code from comparisons of two complexes (Figure 22B), except level "-1" was assigned the color for level "-7"; to be able to visually compare and contrast difference maps of any nature and to indicate that level "-1" resembles the largest decrease in reactivity in certain cases (i.e. difference maps of complexes vs. empty ribosomes).

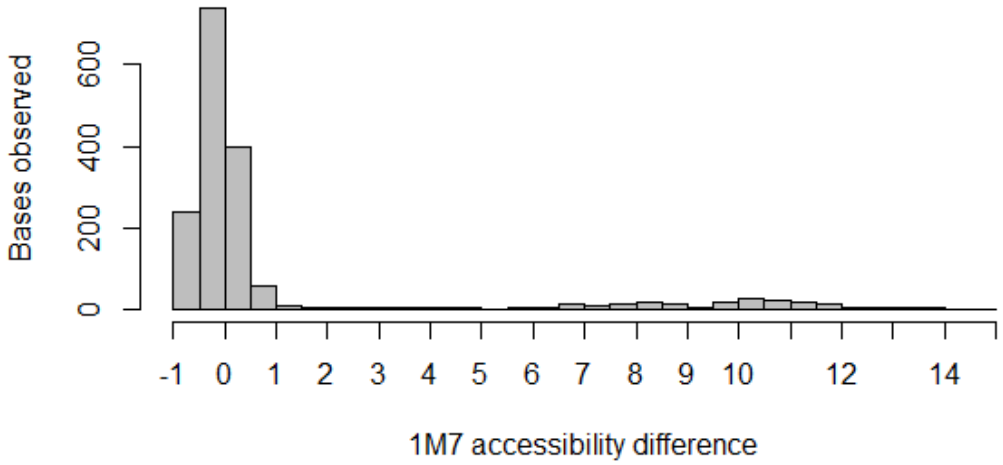

Figure 23. Data distribution of the reactivity difference between the P site occupied complex and the empty ribosome 18S rRNAs.

2.2.3. Application of method to ribosome complexes and discussion

hSHAPE is a powerful, highly quantifiable method to detect changes in RNA flexibility. It is easy to optimize, conduct and does not require specialized machinery. The signal to noise ratio is also very high with hSHAPE chemicals compared to other RNA structure probes. However, it should be noted that the use of fluorescently

labeled primers, while supplying an avenue to make the technique highthroughput and highly automated, introduces noise during primer extension. The effect of the noise increases non-linearly as the data sets become larger, such as with the 5000+ nucleotides of eukaryotic ribosomal RNA. To overcome the data distribution problems observed with hSHAPE and improve normalization for comparison of data from rRNAs of different eukaryotic ribosomal complexes, we suggest adding a simple natural log transformation step to the analyses.

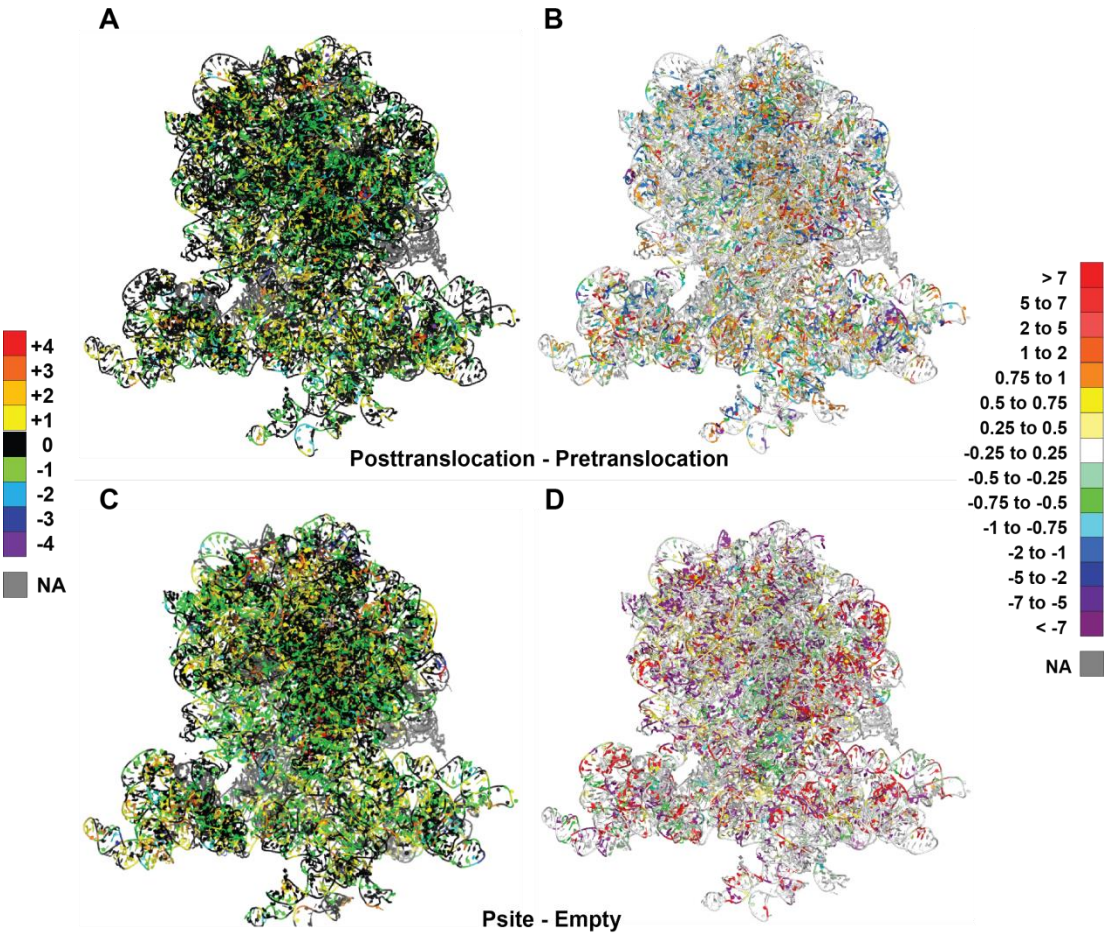

Figure 24. Representative results from the two statistical approaches.

The three dimensional structure is from Ben-Shem et al, 2011.[2] **(A-B)** The difference maps of posttranslocation and pretranslocation complexes **A.** after the first version of statistical analyses, **B.** after the updated statistical analyses. **(C-D)** The difference maps of P site occupied complex and the empty ribosome **C.** after the first version of statistical analyses, **D.** after the updated statistical analyses. The color code for the first version of analyses is shown on the left, for the updated analyses

on the right. For more information on the complexes, please refer to Chapter 4: Walking the ribosome through the translation elongation cycle and Chapter 6: Materials and methods.

Figure 24 compares the outputs from hSHAPE analyses before and after natural log transformation. The sample data are from the comparisons of various ribosomal complexes. Results with the first version of analyses are shown in panels A and C. These images are "noisy," and give the impression that the reactivities of almost all nucleotides have changed, albeit slightly, between the complexes of interest. However when the results from the improved analyses are examined (panels B and D), it is evident that large changes were masked by smaller changes in reactivity in the results of the previous analyses. The changes in reactivity localize to specific regions of the ribosome after the improved analyses are applied to the data, allowing more complex interpretations of the results.

Figure 25 focuses on the P stalk region in the difference map of posttranslocation vs pretranslocation complex, and compares the effects of the two analyses in this region. The updated method (B) has cleared up many of the "slight loss of reactivity" regions (indicated with green), which are present in abundance after the original analyses are applied (A). The updated analyses have also rendered some intersubunit bridge regions visible: A slight protection is now visible at the tip of H38 (B1a bridge), and protected nucleotides are visible in H69 and h44 (B2a bridge). Other stretches of reactivity decrease or increase are also now visible (unmarked), and should be examined further. While eukaryotic structures related to translocation are still under study by various groups [26,49,126,127], deprotection of the P stalk region and protection of intersubunit bridges are expected changes in the

ribosomes after translocation. Overall, the new analyses highlight the “true” reactivity changes and remove noise from results.

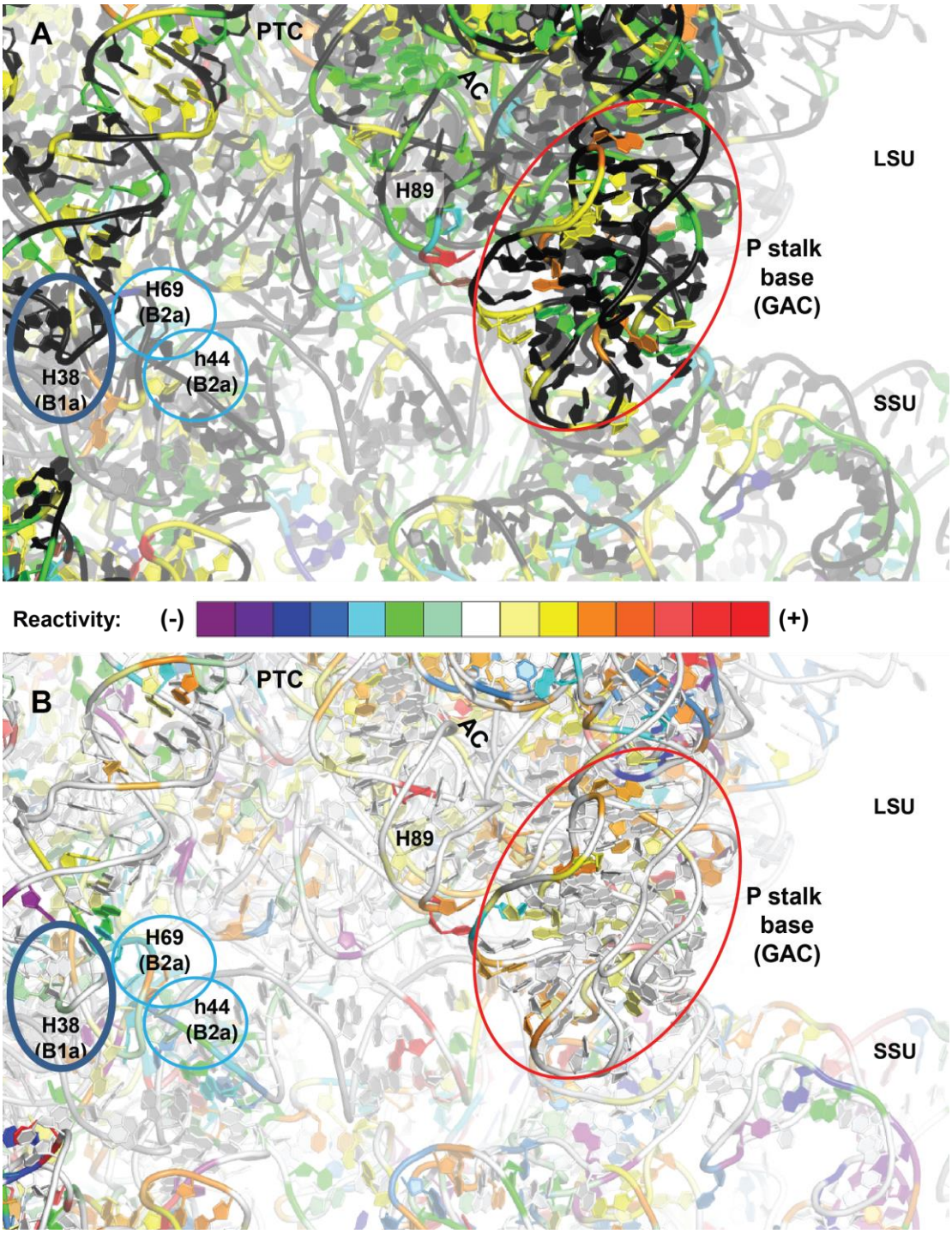

Figure 25. The P stalk in images generated by the two statistical approaches.

The P stalk area in the difference map of posttranslocation vs. pretranslocation complex is shown after **A.** the first version of analyses, **B.** the updated analyses. In this view the whole A site area is visible. P

stalk (red), H38 (dark blue), H69-h44 (light blue), H89, PTC and AC are labeled. The reactivity ladder belongs to the updated visualization, however warm colors indicate increase in reactivity and cool colors indicate decrease in reactivity in both approaches. Unchanged reactivity is indicated by the color black in the first version of analyses. PTC: peptidyl transferase center, AC: accommodation corridor, GAC: GTPase associated center.

While the improvements described here may be of great utility for ribosomal dynamics studies as shown in Figure 24 and Figure 25, users of hSHAPE are advised to test other transformation methods on their data, especially given that the data are "zero-heavy"; the original hSHAPE values are not of lognormal but of "delta" lognormal distribution [128,129]. In the context of this work, the zero values were chosen to be included in the data processing, as they may be biologically relevant and indicating regions of no reactivity. Ln(x+c) transformation, where c = 1 in this work, was useful for our purposes, as 99% of the raw reactivities obtained from hSHAPE experiments are approximately 10^2 to 1.5 x 10^6 times this constant. Along these lines, when data transformation was applied to median normalized reactivities instead of raw reactivities, the problems with data distribution persisted, as most of these values are only 0.5 to 500 times of the constant (data not shown).

Overall, hSHAPE quantification of large RNA dynamics can be improved through data transformation, and increases the amount of information extracted from ribosomal RNA studies. Improved hSHAPE analyses then may be applied to interrogation of rRNA flexibility in translation initiation and elongation complexes.

Chapter 3: hSHAPE analyses of translation initiation complexes

3.1. Background and rationale

As discussed in Chapter 1, eukaryotic translation initiation is complex, beginning with mRNA activation and 43S preinitiation complex (PIC) formation. 43S PIC is then recruited to the mRNA, and after further rearrangements, scanning and AUG recognition, translation starts. There are still many unknowns, including the structural dynamics of 43S PIC formation. Our current understanding of this process, based on structural, biochemical and yeast genetics approaches are summarized in Figure 26.

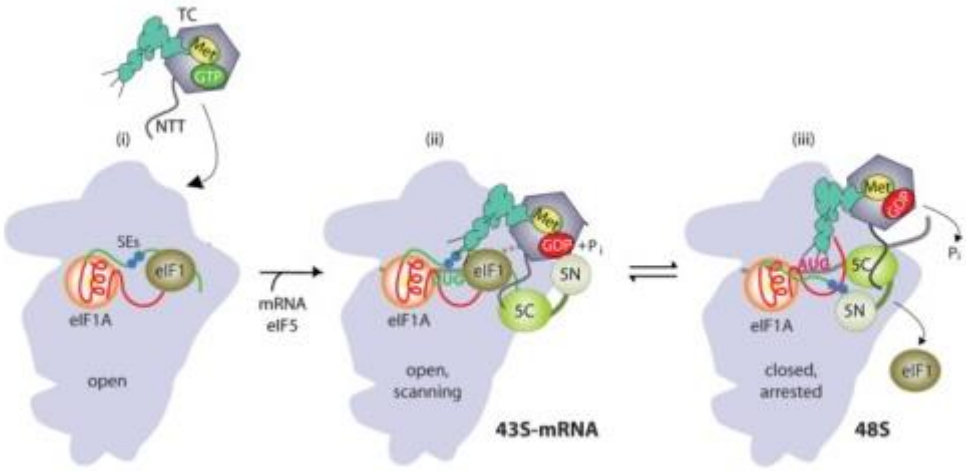

Figure 26. Model summarizing the interactions between different initiation factors and the structural rearrangements of the initiation complex.

(i) eIF1 and eIF1A binding rearranges the 40S to an open conformation which is capable of binding the ternary complex (TC) composed of eIF2, initiator tRNA and GTP. eIF1A CTT (green) monitors the P site and interacts with eIF1, while NTT (red) interacts with eIF1. The CTT has structural elements that have been shown to favor of scanning (SE: scanning enhancer). (ii) After eIF5 and mRNA binding, scanning starts. The complex is still in the open conformation, and the initiator tRNA is not fully at the P site – this is caused by the SE elements of eIF1A. eIF5 may be recruited through interactions of its NTD (5N) with eIF2, and its CTD (5C) with the NTT of eIF2 and the CTT of eIF1A. GTP hydrolysis occurs but inorganic phosphate (P_i) is not released. (iii) When the start codon is encountered, in a complex coordination of events, P_i is released possibly due to a dramatic change in eIF5 binding, allowing tRNA anticodon: start codon interactions and leading to displacement of eIF1A CTT. The change in eIF5 binding leads to eIF1 release as well and to the assumption of a closed conformation by

the 40S subunig. The closed conformation is not permissive to scanning. The displaced eIF1A CTT now interacts with 5N instead of 5C. Image modified from Saini et al, 2014 [130].

Cryo-EM structures of 40S bound with eIF1 and eIF1A have been reported [131–133]. The latest reported resolution is at 3.7Å. These show that eIF1 and eIF1A bind to different sides of h44 close to tRNA binding sites. eIF1A binds to the A site (40S shoulder); in fact, one of the roles of this factor is to prevent a tRNA from binding to the A site. eIF1A has unstructured amino and carboxyl terminal tails (NTT and CTT), and its CTT reaches and occludes the P site as well. The eIF1A-CTT may enable communication between this factor and eIF1, as eIF1 binds near the P site (40S platform), in accordance with its role in regulating the full localization of the initiator tRNA ASL into the P site. In the structures of 40S bound with eIF1 and eIF1A, gross conformational rearrangements are observed in comparison to empty 40S and to 48S PIC after start codon recognition [132–135]. The head/body/platform junction appears to be "open" in these structures, as well as the "latch" between h18 and h34 which clamps around mRNA upon start codon recognition. These data all indicate that the mRNA entry channel assumes an "open" conformation that allows the 43S PIC to scan along the mRNA in search of a start codon.

Other components of 43S PIC are eIF3, the ternary complex (TC = eIF2-GTP-Met-tRNA$_i^{Met}$) and eIF5. eIF3 is a very large, multisubunit complex, and recent X-ray crystallography structures of the yeast eIF3, coupled with cryo-EM reconstruction, cross-linking, mass spectrometry, and structure modeling, indicate that it clamps around the 40S subunit, perhaps coordinating the correct positioning of other initiation factors, including eIF1 and eIF1A [136]. Given that eIF3 is an essential element of the reconstituted yeast translation initiation system [19], it may possibly

function as more than an anti-association factor. However, assembly of 48S PIC in the absence of eIF3 has also been reported seemingly with no defects [137], thus providing insight into start codon recognition and the related structural rearrangements. Additionally, there are structural differences between yeast and mammalian eIF3 and the mammalian eIF3 structures have not been mapped to the predicted locations of eIF1, eIF5-CTD or eIF2 [134,138].

Initiator TC recruitment occurs through the interaction of eIF2α subunit with 40S, possibly through ribosomal protein uS7, and is enhanced by the other initiation factors of the 43S PIC. In yeast, eIF3 is thought to be in a position to monitor TC binding [134]. Overall, there are a plethora of interactions between the initiation factors that make up the 43S PIC that stabilize the complex and which may possibly enhances TC binding. These include (1) eIF5-CTD (carboxyl terminal domain) interactions with the eIF2β subunit-NTT, the eIF3c subunit-NTD (amino terminal domain), and eIF1; (2) eIF1 interactions with the eIF2β subunit-NTT and the eIF3c-NTD; and (3) eIF3a subunit-CTD interactions with the eIF2β subunit [134].

eIF5 is perhaps the most elusive of the initiation factors that are thought to form the 43S PIC. It is the GTPase activating protein (GAP) of eIF2, and is known to function in GTP hydrolysis by eIF2, regulation of inorganic phosphate release and stimulation of the closed conformation of 30S upon start codon recognition [80,130,139]; hence its functions are relatively well known on the 43S-mRNA and 48S PIC's. Its role in the 43S PIC seems to be to stabilize the complex through its interactions with other factors (mostly eIF2). However its exact binding location on the ribosome is not known and has not been reported. Biochemical assays indicate direct binding between

eIF5 (and / or its NTD/CTD) and SSU [19,140]. The latest cryo-EM structure of the 48S PIC indicates an additional density on the platform which is suspected to be eIF5 [137]. The GAP catalytic site of eIF5 is located on its NTD, while the CTD includes a HEAT domain shown to interact with eIF1, eIF2β and eIF3c-NTD. These two domains are held together by a linker region. There is no available structure of the complete eIF5, but the structures of its NTD and CTD are known [141,142]. Current known and estimated structural information on eIF5 is summarized in Figure 27.

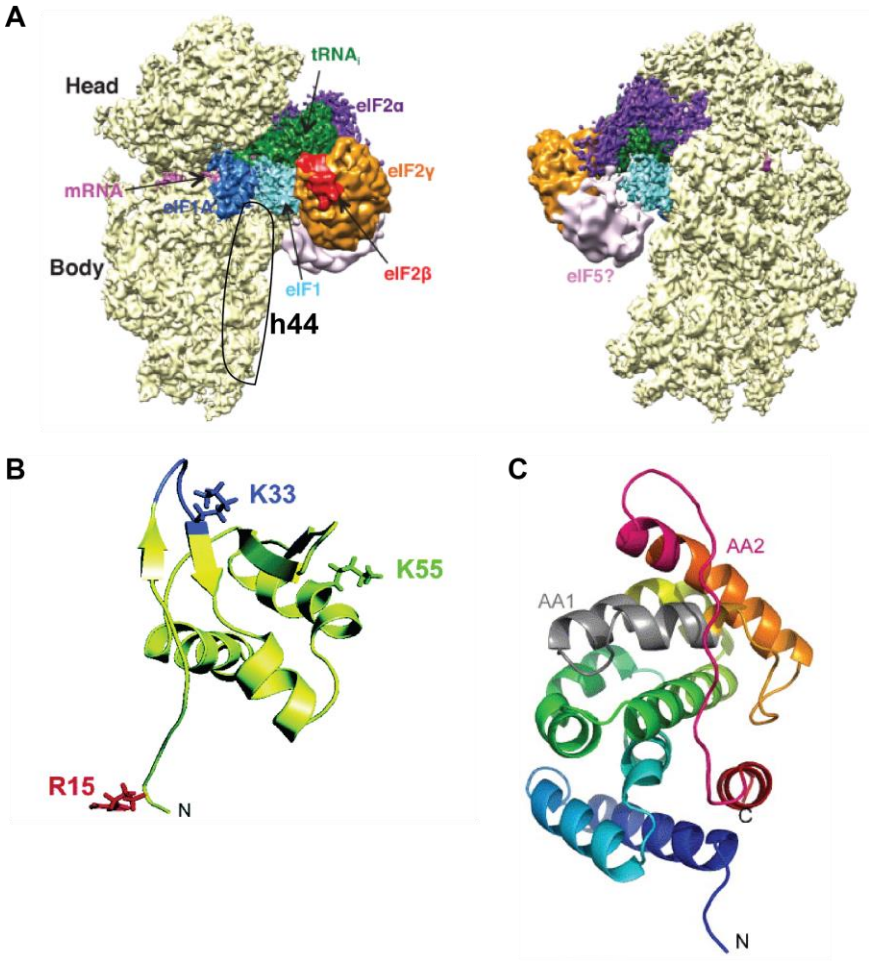

Figure 27. Possible location of eIF5 and the structure of the individual eIF5 domains.

A. 48S PIC structure and the densities identified on it. Most of the densities could be attributed to relevant factors (eIF1 - light blue, eIF1A - dark blue, eIF2 - orange, purple, red) or tRNA (green) or mRNA (bright pink). An unidentified density is marked in pale pink and this may belong to eIF5. This density is better seen on the right. h44 density has been labeled in black on the left. B. eIF5-NTD structure. R15 (red) is the catalytic residue for GAP function. Some other functionally important amino acids are also shown. C. eIF5-CTD structure. These eight helices form an expanded HEAT domain.

Aromatic and acidic amino acid boxes, AA1 (grey) and AA2 (red) are important for binding to eIF3 and eIF2. Images modified from Hussain et al, 2014, Conte et al, 2006, and Bieniossek et al, 2006 [137,141,142].

Our aim in this project was to use hSHAPE to map eIF5 onto different preinitiation complexes. We started with complexes of 40S with eIF1, eIF1A, with or without eIF5, as eIF1 and 1A are known to stably interact with 40S regardless of the presence or absence of other factors, thus forming an appropriate baseline for subsequent analyses. After discovering a potential footprint for eIF5 using this approach, we worked with complexes of 40S with eIF5 or eIF5-NTD or eIF5-CTD, obtaining different sets of protected regions. Our analyses suggest that eIF5 binding appears to change in the presence and absence of eIF1 and eIF1A, perhaps indicating that the initial eIF5 binding to the 40S requires guidance from other factors.

3.2. Results

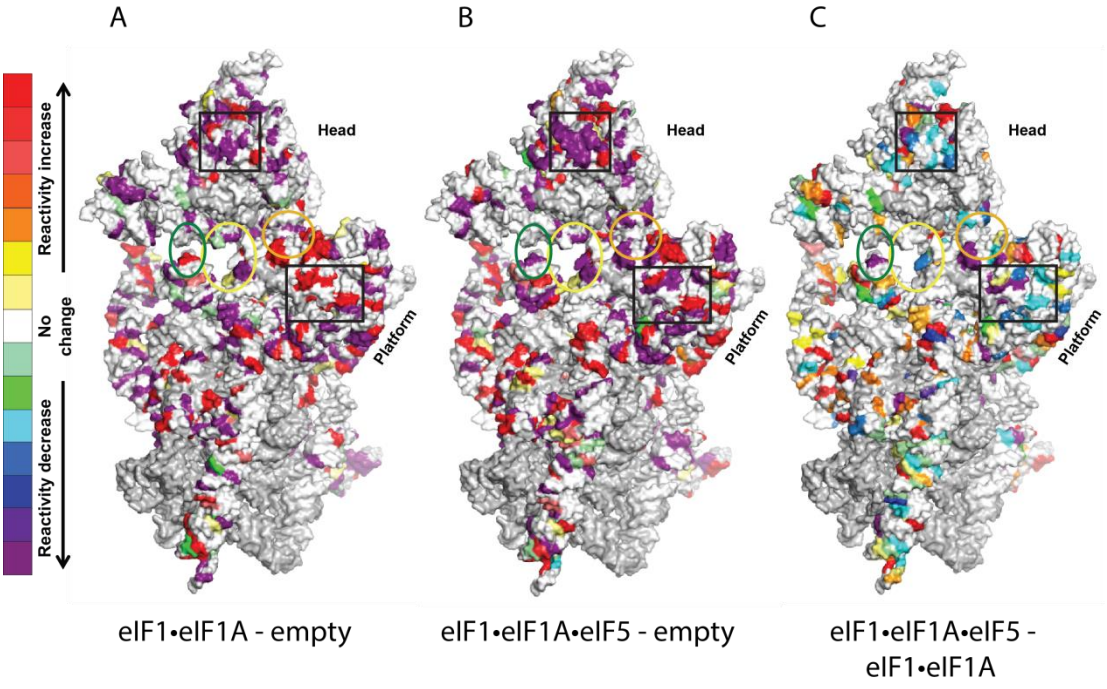

Figure 28. Building initiation complexes.

A. Difference map of the eIF1•eIF1A complex minus the empty SSU, **B.** Difference map of the eIF1•eIF1A•eIF5 complex minus the empty SSU, **C.** Difference map of the eIF1•eIF1A•eIF5 complex minus the eIF1•eIF1A complex, indicating the reactivity changes caused by eIF5. The view is from the

intersubunit face of the eukaryotic rRNA. The eIF1 (yellow-orange circle) and eIF1A (yellow ellipse) related changes are shown. The areas inside the black rectangles lose reactivity upon eIF5 binding. The green ellipse marks the "latch" area between h18 (shoulder) and h34 (head). There is a reactivity decrease on the h18 side upon eIF5 binding. The tertiary structure is from Ben-Shem et al, 2011[2].

To obtain a footprint of the eukaryotic initiation factor 5, structural analyses were performed on different initiation complexes of the yeast ribosome. These complexes were assembled by Fan Zhang at NIH. The first set of complexes to be probed were ribosomal small subunits of the yeast bound with eIF1, eIF1A, and/or eIF5. Results of these are shown in Figure 28 and Figure 29, from the intersubunit face and the solvent side, respectively. As can be seen in the panel A of Figure 28, binding of eIF1 and eIF1A causes flexibility changes in different places of the 18S rRNA. The known eIF1A binding site (on the neck, towards the platform) appears to have lost flexibility. The result of eIF1 binding, although not very clear in 40S-eIF1-eIF1A complex (Figure 28A), is also visible (on the neck, towards the shoulder). Addition of eIF5 causes protection in the head domain, the neck, at the back of the shoulder, as well as further protection on the shoulder. The changes in the neck domain, and the tips of helices 18 and 34 (the so-called "mRNA latch") may be indicative of assumption of a closed conformation by the 40S subunit (Figure 28B and C).

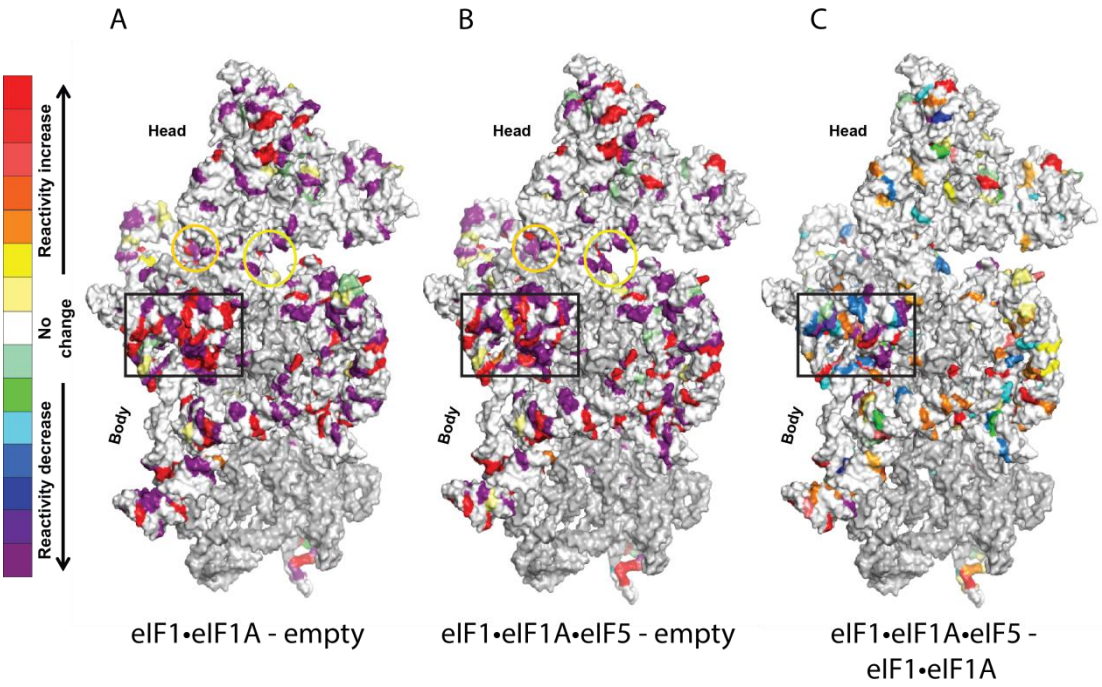

Figure 29. Building initiation complexes.

A. Difference map of the eIF1•eIF1A complex minus the empty SSU. **B.** Difference map of the eIF1•eIF1A•eIF5 complex minus the empty SSU. **C.** Difference map of the eIF1•eIF1A•eIF5 complex minus the eIF1•eIF1A complex, indicating the reactivity changes caused by eIF5. The view is from the solvent exposed side of the eukaryotic rRNA. eIF1 (yellow-orange circle) and eIF1A (yellow circle) related changes are shown. The reactivity of the area inside the black rectangle decreases upon eIF5 binding. The tertiary structure is from Ben-Shem et al, 2011.[2]

We repeated hSHAPE with complexes of 40S with only full length eIF5, eIF5-NTD or eIF5-CTD, as eIF5 can bind 40S on its own *in vitro* [80]. While we anticipated that this would provide a more accurate view of their respective binding sites, the protected regions observed for these domains were different than those observed with the previous set of complexes (the locations of black rectangles vs. blue ellipses in Figure 30 and Figure 31). The decreased reactivity in the head domain appears to have moved towards the top of this structure, accompanied with some additional loss of reactivity in the beak region (not marked in the figures). This loss of reactivity is seen more clearly in the full length eIF5 complex, rather than with only NTD or only CTD, with CTD reflecting more of this reactivity change than NTD. The reactivity change in the beak is more visible in the eIF5-CTD complex. A new

region of reactivity decrease is visible in the middle of the body domain (specifically on h44) in the full length eIF5 complex, compared to vacant 40S. This may be a protection pattern caused by the physical binding of the eIF5-NTD (Figure 30A and B vs. C). Another new region of reactivity decrease is visible towards the back of the shoulder and right below the beak (specifically helices 16 and 17). This pattern is strongest with the full length eIF5 complex and to some degree in the eIF5-CTD complex. The mRNA latch (at least the h18 component, marked by the green ellipse in Figure 30) also has decreased reactivity in the full length eIF5 complex.

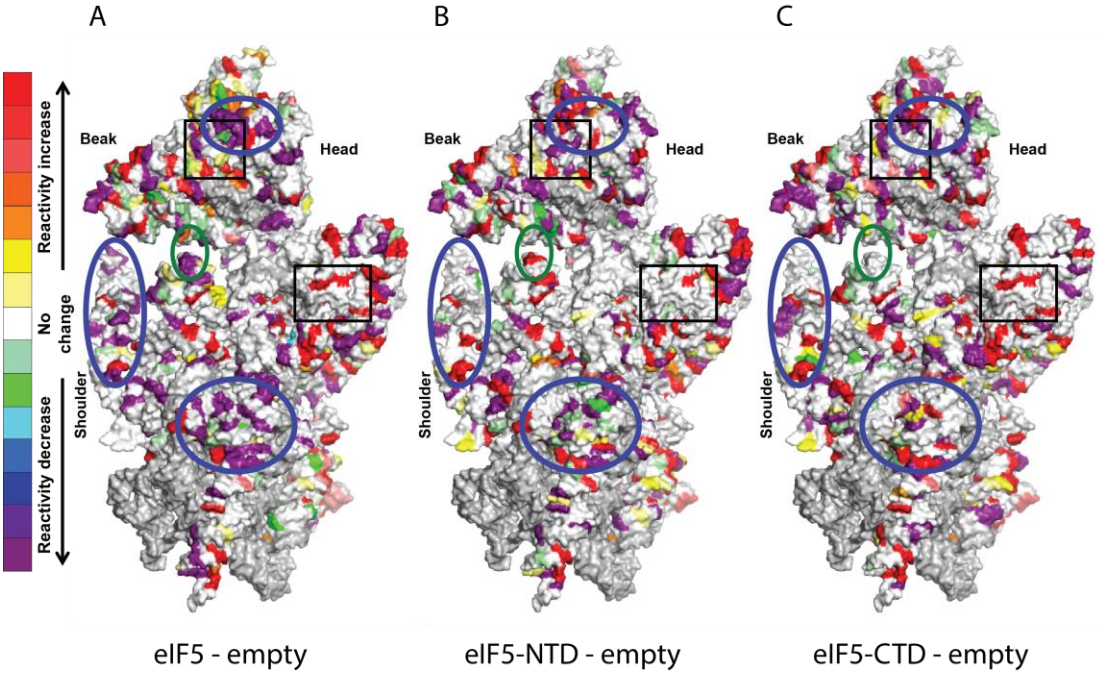

Figure 30. Difference maps of eIF5 complexes and empty SSU.

A. Difference map of full length eIF5 minus empty SSU, **B.** Difference map of the N terminus of eIF5 minus empty SSU, **C.** Difference map of the C terminus of eIF5 minus empty SSU. The view is from the intersubunit face of the eukaryotic rRNA. The black rectangles are used to show where protected regions were seen with the previous set of complexes. The regions of reactivity decrease from the current set of complexes are indicated with blue ellipses. The "latch" is indicated by a green ellipse. The tertiary structure is from Ben-Shem et al, 2011.[2]

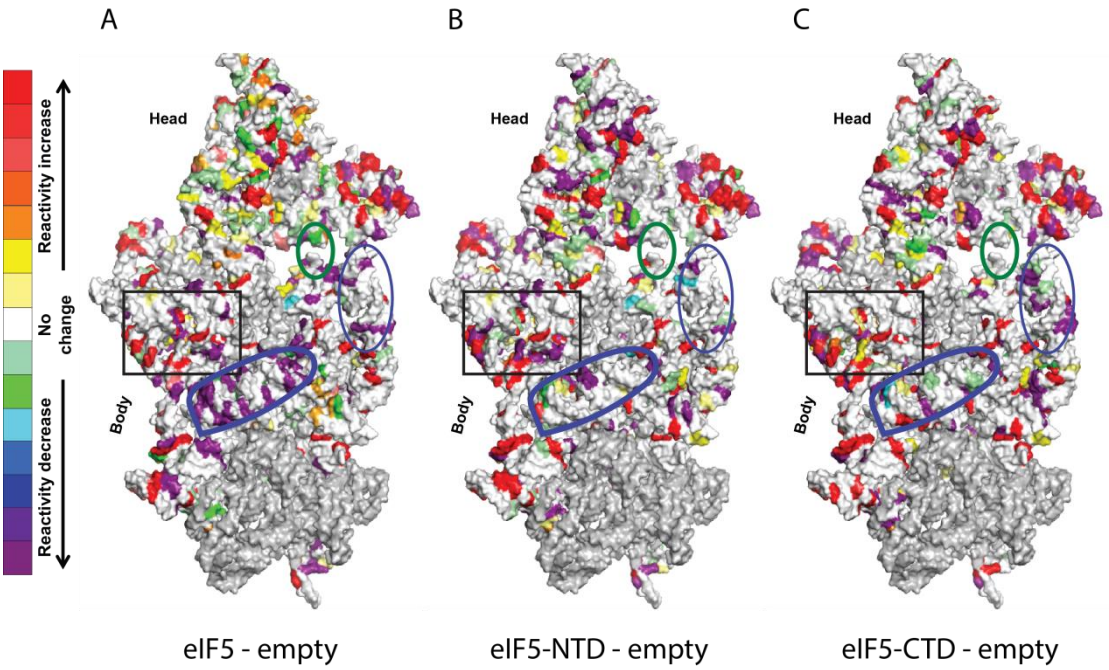

Figure 31. Difference maps of eIF5 complexes and empty SSU.

A. Difference map of full length eIF5 minus empty SSU, **B.** Difference map of the N terminal domain of eIF5 minus empty SSU, **C.** Difference map of the C terminal domain of eIF5 minus empty SSU. The view is from the solvent exposed side of eukaryotic rRNA. The black rectangle marks the place of the loss of reactivity seen in the previous set of complexes. The thick, blue ellipse indicates the loss of reactivity observed with the current set of complexes. The thin, blue ellipse marks the h16-17 loss of reactivity. The "latch" is marked with a green ellipse. The tertiary structure is from Ben-Shem et al, 2011.[2]

The location of decreased reactivity is observed at the solvent exposed face of 40S is also changed (the black rectangle vs. the thick, blue ellipse in Figure 31). Decreased reactivity is observed in h21 (part of expansion segment 6 in eukaryotes), to a greater extent with the complex containing full length eIF5, and to a lesser extent with the eIF5-CTD containing complex. Decreased reactivity in the h16-17 region is visible in this view as well, especially in the eIF5-CTD containing complex. Both components of the mRNA latch (h18-h34) show decreased reactivity in the presence of the full length eIF5 complex in this view.

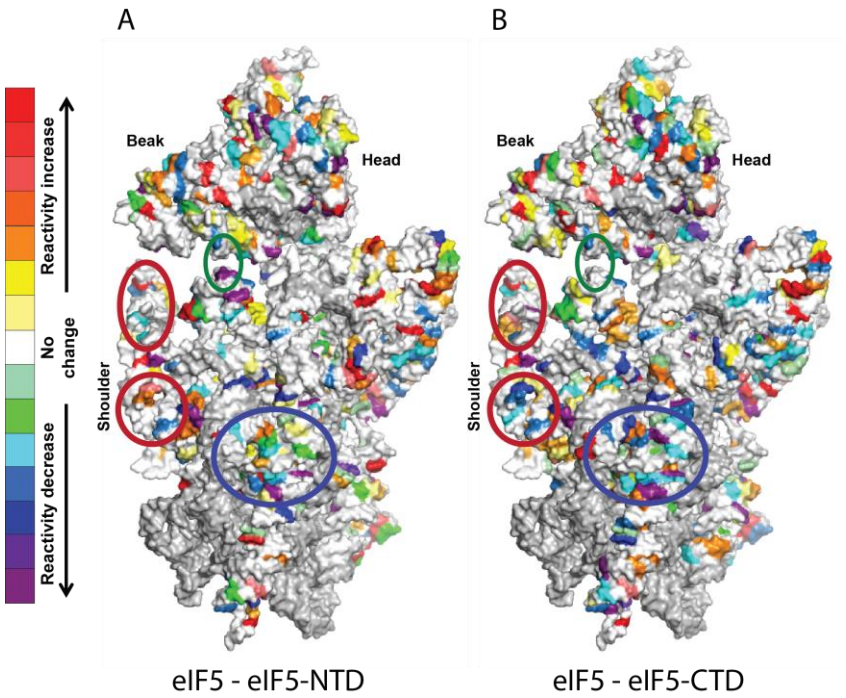

Figure 32. Difference maps of the full length eIF5 complex and NTD or CTD portion complexes.

A. Difference map of the full length eIF5 complex minus the eIF5-NTD complex, indicating the reactivity changes caused by the C terminal domain, **B.** Difference map of the full length eIF5 complex minus the eIF5-CTD complex, indicating the reactivity changes caused by the N terminal domain. The view is from the intersubunit face of the tertiary structure of eukaryotic rRNA at 3Å resolution. The latch (green ellipse), and the regions of reactivity decrease from h16 (dark red ellipse), h17 (dark red circle), and h44 (blue ellipse) are marked and show differences in reactivity between the two maps.

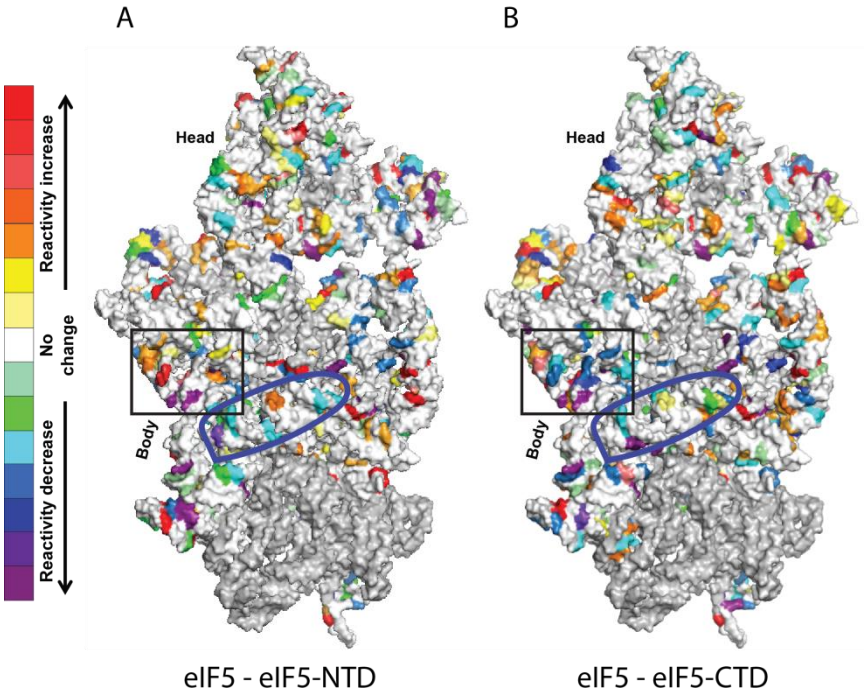

Figure 33. Difference maps of the full length eIF5 complex and NTD or CTD portion complexes.

A. Difference map of the full length eIF5 complex minus the eIF5-NTD complex, indicating the reactivity changes caused by the C terminal domain, **B.** Difference map of the full length eIF5 complex minus the eIF5-CTD complex, indicating the reactivity changes caused by the N terminal domain. The region of loss of reactivity from h21 is indicated with a blue ellipse. A region implicated in the previous set of complexes is shown with a black rectangle. The view is from the solvent exposed side of the tertiary structure of eukaryotic rRNA at 3Å resolution.

We generated difference maps of the complex containing the full length eIF5 vs. complexes with either eIF5-NTD or eIF5-CTD in an effort to observe the reactivity changes caused by specific domains (Figure 32 and Figure 33). In these maps, the differences between eIF5 vs eIF5-NTD should indicate changes caused by the CTD, and vice versa. We observed reactivity differences between eIF5 minus eIF5-NTD and eIF5 minus eIF5-CTD in the same regions discussed above. For example, components of the latch (green ellipse in Figure 32A vs B) show greater degrees of chemical reactivity loss in the eIF5 minus eIF5-NTD map than the eIF5 minus eIF5-CTD map, implicating the eIF5-CTD in this rearrangement. In contrast, the protected area from h44 (blue ellipse in Figure 32B vs A) is more extensive in the eIF5 minus eIF5-CTD difference map, implicating the eIF5-NTD as the cause. Additionally, the two eIF5 domains seem to affect helices 16 and 17 in an opposite manner (dark red ellipse and circle in Figure 32A vs B), with the CTD domain possibly affecting h16 more (Figure 32A), and the NTD affecting h17 more (Figure 32B). Another interesting observation is that some loss of reactivity on the platform is visible in Figure 32B (full length eIF5 vs CTD map - unmarked). This is the region we initially identified a possible footprint for eIF5, and may be of importance.

The h21 region shows slight differences between NTD vs CTD as well. eIF5-CTD may cause a greater extend to decrease in chemical reactivity in this region (Figure 33A vs B). The back of the beak loses reactivity in the presence of the eIF5-CTD as well (Figure 33A - unmarked). In the eIF5 vs eIF5-CTD map, decreased

reactivity is also observed in a region we identified with the previous set of complexes (Figure 33B - black rectangle). The previous regions of reactivity loss are only visible in difference maps of full length eIF5 vs eIF5-CTD complexes, indicating the effect of the eIF5-NTD on these regions (Figure 32B and Figure 33B).

3.3. Discussion

Eukaryotic translation initiation consists of 43S PIC formation, activated mRNA recruitment to the PIC, and scanning for a start codon in optimal context. One of the components of the 43S PIC is the eukaryotic initiation factor 5. The functions of eIF5 after mRNA recruitment, during scanning and start codon recognition have been well documented and most importantly relate to its interaction with eIF2 / initiation ternary complex (TC). Binding assays indicate a direct association between eIF5 and the ribosomal small subunit, however a binding site has not been described, and a common hypothesis is that it binds through initiation TC. The conformational changes that it is thought to induce would require interactions with the SSU directly as well, especially upon start codon recognition. In this work, we report a possible change in the binding site of eIF5 depending on the presence of other IF's (i.e. eIF1 and 1A), and find support for eIF5-induced conformational changes.

The hSHAPE results obtained with the 40S-1-1A and 40S-1-1A-5 complexes indicate two regions of decreased chemical reactivity located on the intersubunit face of 40S upon eIF5 binding: one in the head domain and the other on the platform. These are in accordance with theories on the location of eIF5, and the interacting eIF1A tail domain [80,130,139]. Additionally, the reactivity change observed in the "mRNA latch" in the same set of complexes may imply that the initiator TC binds to

open up the mRNA entry tunnel, thus enabling mRNA binding and consecutive scanning to take place.

hSHAPE results on 40S-eIF5 complexes without additional IF's show different regions of decreased chemical reactivity. The reactivity decrease on the head domain changes slightly and decreased reactivity is also seen in the middle of the body domain, specifically on h44. Another "new" region of reactivity decrease is visible towards the back of the shoulder and right below the beak (specifically helices 16 and 17), mostly in the full length eIF5 complex and to some degree in the eIF5-CTD complex. This is interesting as, induced by eIF1 and eIF1A, h16 is able to adopt "open" (extending away from 40S body) and "closed" (bending towards 40S beak) conformations that are thought to regulate mRNA entry and scanning [1]. We do not obtain directional information from hSHAPE, however, stabilization of h16 is still thought provoking. The results further indicate that the "mRNA latch" may be closed in the full length eIF5 complex. Together with stabilization of h16, the results may indicate a "closed" conformation of the 40S. This would be compatible with the known eIF5 functions during eukaryotic initiation, i.e. that is it is a regulator of scanning, and may imply that the entire repertoire of eIF's are needed on the 43S PIC to form the "open" conformation, balancing out the effect of eIF5. In fact, based on the results from the two sets of complexes, eIF1 and 1A may also be functioning to correctly position eIF5, eventually (with eIF2-TC in place for example) resulting in the 40S open conformation. Viewed as a whole, this may ensure the correct order of binding events.

Another, less exciting, explanation of the differences observed between the two sets of complexes might simply be that eIF5 does not bind as efficiently on 40S without eIF1 or 1A present. In fact, the dissociation constants for eIF5, eIF5-NTD and eIF5-CTD are quite high: 300 ± 50 nM, 250 ± 30 nM, and 1500 ± 500 nM, respectively [80]. These, in turn, imply either a high k_{off} value or a low k_{on} value, which would influence the length of time available for 1M7 reagent to react with the associated complexes. This may also explain the unclear effects of the individual domains alone (especially of CTD, as it has the highest dissociation constant).

While both explanations above are viable, another region of decreased reactivity located on the solvent side of the 40S subunit seems to support the former. h21 (part of expansion segment 6 in eukaryotes) shows decreased hSHAPE reactivity, mostly in the complex with full length eIF5 and to a lesser extent with eIF5-CTD. This is interesting as structural rearrangements have been observed in this area during transition from 40S to 43S, and are thought be associated with a rotation in the platform-body region [143], compatible with a closed conformation and regulating mRNA recruitment and scanning.

A preliminary model is shown in Figure 34, implicating eIF5 as a regulator of 40S rearrangements, and being led to its correct binding site by the eIF1A tail. Experiments with mutant eIF5 and the interacting eIF1A tail, as well as other structure probing approaches, will be necessary to test this model. Nonetheless, through hSHAPE studies, we are able to show reactivity changes induced by eIF5 in agreement with major rearrangements of 40S, possibly towards the closed conformation.

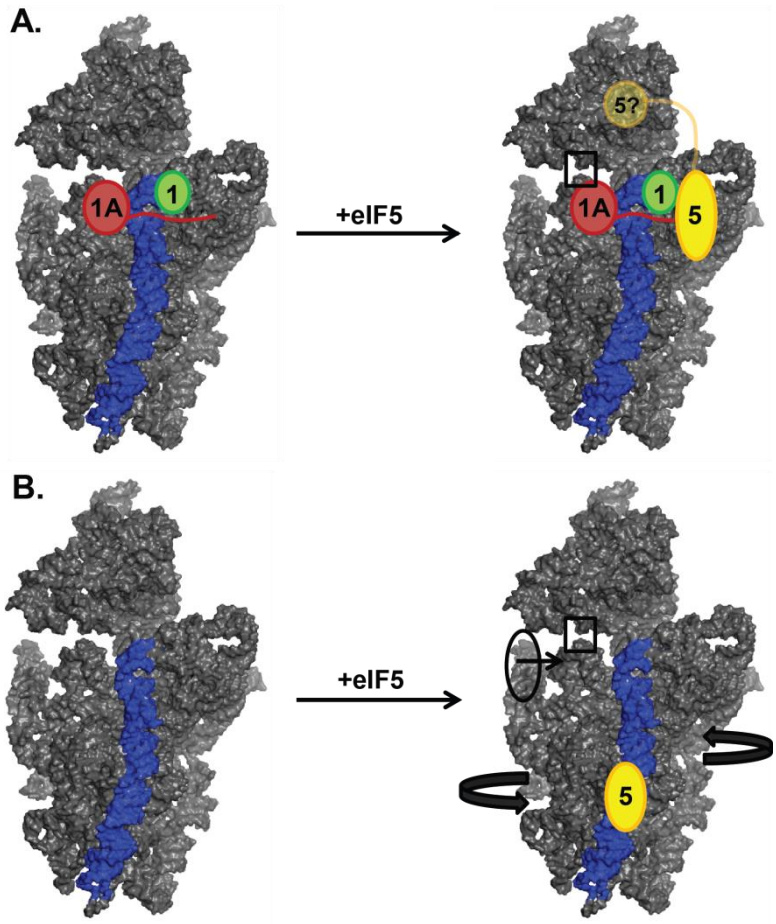

Figure 34. Possible eIF5 binding sites.

A. When eIF1 (green) and 1A (red) are bound to the ribosome, eIF5 (yellow) is "guided" to a site on the platform, possibly through interactions with eIF1A CTT. In the actual 43S PIC, interactions with eIF2-TC are also crucial. eIF1A CTT interacts with eIF5 NTD, hence the platform may be primarily the binding site of this domain, while eIF5 CTD may be binding to the head (possibly through interactions with eIF1A NTT [80]). eIF5 binding is accompanied by the "closing" of the mRNA latch (small rectangle). B. eIF5, having low affinity for the empty 40S, does not bind to its site on the platform without presence of eIF1 and 1A. Instead it possibly binds to a site in the middle of h44 (blue). This is accompanied by rearrangements resembling closed complex formation: mRNA latch closure, h16 stabilization, body-platform rotation.

Chapter 4: Walking the ribosome through the translation elongation cycle

4.1. Background and rationale

Translation elongation is a very dynamic process that involves both large and small scale structural rearrangements (please see Sections 1.2.2 and 1.4 for details). Most of these rearrangements have been well described in the catalytic sites of the ribosome, especially in bacteria. Eukaryotic studies are underway but are hindered by the resolution of the current methodologies (please see Section 1.5 for details). While large scale, low resolution studies indicate that translation elongation occurs is very similar in prokaryotes and eukaryotes, recent studies indicate some differences, including potential differences in tRNA binding sites and intersubunit motions [26,131,127]. Added to these are the facts that eukaryotic ribosomes are larger and have additional elements (e.g. expansion segments on rRNA). The observation of "subunit rolling" in mammalian ribosomes is especially intriguing [26], as it may indicate presence of communication pathways within eukaryotic ribosomes beyond the usual functional sites. In sum, these differences highlight the need for further studies on the eukaryotic elongation cycle and how ribosome structural dynamics map to each step of this process.

Given that the rRNA harbors important elements including the peptidyltransferase center, the decoding center and a large fraction of the intersubunit bridges, interrogation of rRNA dynamics could be beneficial to the study of eukaryotic translation elongation and for identifying potential functions of the "non-catalytic" regions of the ribosome. The budding yeast, *Saccharomyces cerevisiae*,

provides a powerful model system to assemble and study different eukaryotic ribosomal elongation complexes. As discussed in detail in Chapters 1 and 2, improved hSHAPE analyses have proven useful for detecting and visualizing changes in rRNA flexibility among different ribosomal complexes. Here we report the assembly and hSHAPE probing of seven ribosomal complexes that occur during the elongation cycle and discuss the important implications of these results. Previously described functional regions and intersubunit bridges are mentioned in detail for the rest of Section 4.1, as well as what is already known on eukaryote-specific elements. Section 4.2 starts with results from complex verification, and goes on to compare the hSHAPE data to known functional regions and intersubunit bridges, as well as to analyze eukaryote-specific elements. We conclude our analyses with a discussion on a network of communication pathways identified in our data.

4.1.1. Known functional regions of bacterial and eukaryotic rRNAs

There are a number of well-established paradigms upon which our work can be built. The first is based on classical studies from the Noller group in which bacterial ribosomes were subjected to chemical probing and hydroxyl radical cleavage studies [144–149]. These provide a strong foundation for identifying pre-"landmark" rRNA nucleotides whose protection patterns change upon binding of mRNA, tRNA or other transacting factors to the ribosome. The second are the numerous structural studies, including X-ray crystallographic and cryo-EM, of both bacterial and eukaryotic ribosomes in complex with the substrates and accessory proteins [84,135,143,150,151].

4.1.1.1. mRNA - rRNA interactions

The landmark mRNA/16S rRNA interactions in prokaryotic ribosomes are: U1381 (C1618 in yeast), C1395 (C1632 in yeast), G413 (A485 in yeast), U421 (U494 in yeast), G424 (G497 in yeast), A532 (A579 in yeast), G693 (G904 in yeast), U723 (C934 in yeast), A845 (U1060 in yeast), G1131 (U1362 in yeast), C1132 (U1363 in yeast), G1300 (C1537 in yeast), G1338 (G1575 in yeast). Such studies also pre-predicted mRNA binding sites on the 23S RNA: U1065 (A1240 in yeast; close to GAC) and U887 (A1025 in yeast; close to doman II) [152]. Structural studies of mammalian ribosomes and initiation complexes identified an mRNA cleft and latch on 18S rRNA, formed by the nucleotides C565, C575-U578, G904, U999, G1150-A1152, C1190-U1191, C1274, A1427, C1620-U1621, C1634-C1641, A1756-U1758, G1760-A1763, A1765-U1770, A1794 (all yeast numbers) [84,135,143,150].

4.1.1.2. tRNA - rRNA interactions

The rRNA nucleotides protected upon tRNA binding have been studied extensively in bacterial ribosomes [147,148,153–155]. The chemical probing results on these are summarized in Table 1. These studies have also indicated the presence of hybrid states of tRNAs [147,148,154].

In the early chemical probing and hydroxyl radical cleavage studies, binding of tRNAs to different sites on bacterial ribosomes were controlled by magnesium concentrations and the presence or absence of an mRNA template. In these conditions, the nucleotides taking part in E site binding were acylated or cleaved regardless of presence of mRNA. Hydroxyl radical cleavage experiments of the LSU identified nucleotides U1859-G1862 (A2219-A2222 in yeast), C1881-G1884

(A2224-C2227 in yeast), U2074-76 (U2416-G2418 in yeast), C2395-U2401 (C2765-C2773 in yeast), G2421-C2424 (G2793-G2796 in yeast), U2431-G2436 (G2800-G2805 in yeast) as residing in the E site. mRNA-dependent cleavages occurring under low Mg^{++} and mRNA-independent cleavages under high Mg^{++} indicated P site related interactions. These P site nucleotides in the LSU were: C1941-C1947 (C2284-C2290 in yeast), G1954-U1956 (U2297-A2299 in yeast), G1959-A1966 (G2302-A2309 in yeast), G2251-U2257 (G2619-A2626 in yeast), U2492-G2494 (U2861-G2863 in yeast), C2594-U2596 (C2963-U2965 in yeast), C2601-G2603 (C2970-G2972 in yeast). Strictly mRNA dependent cleavages were thought to be related to the A site. These A-site nucleotides in the LSU were: U1940-A1970 (G2283-A2313 in yeast), U2555-U2561 (U2924-A2930 in yeast), A2566-C2573 (U2935-C2942 in yeast), A2600 region (A2969 region in yeast), G2659-G2664 (G3026-G3031 in yeast) [149].

	16S	**18S**	**23S**	**25S**
A site	G529, G530, A1492, A1493, (A1408, G1494), A892(↑), G1405(↑), A532(↑), G926(↑), G1338(↑)	G577-78, C1646, A1755-57, A580(↑), U1117(↑), A1151(↑), U1643(↑), A1576(↑)	C2254, A2439, A2451, G2553, U2555, A2602, G1041, C1941, G1068, G1071, U2609, (A1916, A1918)	A1217, G1243, G1246, C2284, C2622, A2808, A2820, G2922, U2924, A2971, U2978, A2259, G2261
P site	G693, A794, C795, G926, G1401, (A532, G1338, A1339, G966, G529, G530)	A905, A1151, A1005, C1006-07, G1638, C1639, G577-78, A580, A1576-77, C1192	*G2252*, *G2253*, A2439, A2451, *U2506*, *U2584*, *U2585*, (A1916, A1918), A1926, G2505, A2602(↑)	G2620-21, A2808, A2820, U2269, G2874, U2875, U2953-54, A2259, G2261, A2971(↑)
E site			*C2394*, *G2112*, *G2116*, *(A2169)*	C2764, G2454, A2458, A2484

Table 1. Summary of protected and deprotected rRNA nucleotides upon tRNA binding.

These have been gathered from chemical probing studies on bacterial rRNA. Please see text for further detail, as well as tRNA binding sites emerging from hydroxyl radical cleavage studies and/or other structural studies. CCA-end dependent protections are shown in italics. EF-Tu dissociation dependent

protections (ie. A site tRNA CCA-end / acceptor stem dependent protections) are shown in grey. Deprotections are indicated with an "up arrow" in parentheses. Weakly protected nucleotides are in parentheses. Yeast nucleotides corresponding to the bacterial counterparts are also listed.

Structural studies on mammalian translation initiation complexes describe the SSU P site as nucleotides C1000-A1001, G1169-A1171, C1190-C1192, A1194-C1195, C1461-G1466, G1574-U1579, G1622, A1635-C1637 of 18S rRNA (all yeast numbers) [135]. A cryo-EM study of the mammalian pre-translocation complex identified nucleotides G577, G1179, C1274, A1756, G1757 as residing in the SSU A site; A1001, G1002, C1192, G1462, C1463, G1575, A1576, G1638, C1639, C1759, G1760 as constituting the SSU P site (or P/E); and G904-A906, C1162, A1577, U1578 as SSU E site bases. The same study identified nucleotides G1178, A1179, A1193, G1194, G2414-U2417, A2443, C2444, U2835, C2836, U2996, G2997, U3010 in the LSU A site (or A/P); U2408-U2410, U2423, A2424, U2771, C2772, G2778, A2779, A2813, G2814, U2861-G2863, U2978, U2979, A3129, A3130 in the LSU P site; and A2368-G2370, G2393, G2394, G2614, G2615, A2643 for the LSU E site (or P/E) [127].

4.1.1.3. Elongation factor - rRNA interactions

According to hydroxyl radical probing studies with bacterial ribosomes, the main nucleotides of the small subunit rRNA that are in close proximity with EF-G (eEF2 in eukaryotes) are: A33-G39 (U29-U35 in yeast), A160 (A156 in yeast), A440-G445 (G510-A515 in yeast), A495-C500 (A542-G548 in yeast), G537-G539 (A585-C587 in yeast), G790 (G1002 in yeast), U954 (C1180 in yeast), U1211-A1212 (U1443-A1444 in yeast), C1227-G1230 (C1461-G1464 in yeast), C1398-G1400 (C1636-G1638 in yeast) [156].

The same study shows that the sarcin-ricin stem-loop in domain IV (C2646-G2674 in bacteria; U3013-U3041 in yeast) and the region around A1070 (A1245 in yeast) interact with EF-G in the large subunit rRNA. Other EF-G interacting bases identified in this study include G2470-A2471 (G2839-C2840 in yeast), U2479-A2482 (G2848-A2851 in yeast), C1920-G1922 (C2263-C2265 in yeast), C1965 (C2308 in yeast), U1065-A1070 (A1240-A1245 in yeast), A1090-C1100 (U1265-C1275 in yeast), C2649-G2659 (A3016-G3026 in yeast), C2667-U2672 (C3034-C3039 in yeast) [156].

LSU rRNA protection sites of EF-G reported in a chemical probing study of bacterial ribosomes are as follows: A1067 (G1242 in yeast), A1069 (A1244 in yeast), G2655 (G3022 in yeast), A2660 (A3027 in yeast), G2661 (G3028 in yeast) [146]. The same study identified the following nucleotides as involved in EF-Tu (eEF1A in eukaryotes) dependent protections of LSU rRNA: G2655 (G3022 in yeast), G2661 (G3028 in yeast), A2660 (A3027 in yeast) and A2665 (A3032 in yeast) [146]. No SSU nucleotides are implicated in the chemical probing studies [146], hence the SSU nucleotides listed above may only be found in close proximity to, but not in direct contact with EF-G.

4.1.2. Changes in intersubunit bridges

Another topic of interest in the field are the locations of points of contact between the SSU and the LSU, i.e. the intersubunit bridges. These are emerging as functional centers as well, as translocation involves movement of the subunits relative to one another, resulting in structural changes the intersubunit bridges as the ribosome transits the elongation cycle. The intersubunit bridges have been identified and

characterized using many techniques, including crosslinking, chemical probing, mutagenesis, cryo-EM and X-ray crystallography [2,157–162]. Here all previously known intersubunit bridges are summarized.

In the nonrotated prokaryotic ribosome [161], the B1a bridge forms by the interaction of uS13 and nucleotides A886-C888 (G1024-A1026 in yeast) located at the tip of H38. In the rotated yeast ribosome [2], it forms by the interaction of 18S nucleotides U1239 and U1240, and 25S nucleotide A1025. The B1a bridge is broken in the hyper-rotated conformation [2].

B1b/c bridge forms by the interaction of uS13 and uL5 in both prokaryotes [161] and yeast [2], although in yeast uS19 also contributes to the formation of this bridge. In the hyper-rotated conformation of the yeast ribosome [2], different residues from the same proteins take part in the bridge formation.

The B2a intersubunit bridge is composed entirely of RNA:RNA interactions. In bacteria [161], it is formed by SSU nucleotides C1408-C1410, U1494-C1495 (C1646-A1648, U1758-C1759 in yeast, respectively) located in h44, and by the LSU H69 nucleotides A1913-C1914, A1918 (A2256-C2257, G2261 in yeast, respectively). In yeast [2], the interactions are more extensive but still mostly span h44 and H69 (18S: U1004, U1643-C1646, U1758-C1759, G1780; and 25S: A2255, C2257-2259, A2262-U2264). These interactions do not appear to be altered in the hyper-rotated ribosomes [2].

B2b is also an RNA:RNA bridge. In bacteria [161], it forms by (1) the interactions between h24 nucleotides G784-G785, C794 (U996-G997, C1006 in yeast) and H67, H69 nucleotides C1836-C1837, G1922 (C2195-C2196, C2265 in

yeast), and (2) the interactions between h45 nucleotides G1516-C1519 (G1780-C1783 in yeast) and H69, H71 nucleotides A1919-C1920, A1932 (A2262-C2263, A2275 in yeast). In yeast [2], the same helices take part in formation of this bridge, but the nucleotides change slightly: G994-U996, U1779-A1781 of 18S interact with C2195-C2196, G2272, A2275 of 25S. These interactions change further in the hyper-rotated form [2]: U996, U1779-A1781 of 18S interact with C2196-C2197, U2274-A2275 of 25S.

B2c is another RNA:RNA bridge. In bacteria [161], h24 and h27 nucleotides G770-U771, A900-G901 (U982-A983, A1125-G1126 in yeast) interact with H67 nucleotides C1832-C1833 (U2191-C2192 in yeast). These slightly change in the rotated yeast ribosomes [2]: U981-G984 of 18S interact with C2151, U2191-C2192 of 25S; further changes were observed in the hyper-rotated conformation [2]: U982-A983 of 18S interact with U2191 of 25S.

In bacteria [161], B3, also an RNA:RNA bridge, forms from the interactions of h44 nucleotides U1484-G1486 (G1748-A1750 in yeast) and H71 nucleotides C1947-G1948, A1960-C1961 (C2290-A2291, A2303-C2304 in yeast). In yeast [2], the same helices take part in the arrangement of this bridge, except the interactions are much more extensive: A1655-U1657, A1659, A1746-A1749 of 18S interact with A1922, G2124-A2126, C2290-U2292, U2294, U2301-A2303, G2305 of 25S. This is unchanged in hyper-rotated ribosomes [2]. This and observations from rotated prokaryotic ribosomes, have led to the hypothesis that B3 acts as a pivot during rotation [2,163]. However, this is challenged by the latest cryo-EM studies of mammalian ribosomes [26].

In prokaryotes [161], the B4 intersubunit bridge is formed by (1) the interactions of h20 nucleotides C763-G764 (C975-G976 in yeast) with H34 nucleotides C717-A718 (A848-C849 in yeast), and (2) the interactions of uS15 with the same H34 nucleotides. This changes considerably in the rotated yeast ribosomes [2]: G628, A630, A971-A973 of 18S interact with A846-A847 of 25S, and the proteins eL30 and uS15 interact. Furthermore, residues from uS15 also interact with nucleotide A847 of 25S. In the hyper-rotated ribosomes [2], uS15 interacts with G844-A847 of 25S rRNA, and G628, G972-A973 of 18S interact with A846-48 of 25S.

B5 is an extensive bridge in prokaryotes [161]. It forms by the interactions of (1) h44 nucleotides G1418-U1419 (U1656-U1657 in yeast) with H64 nucleotides C1768-U1769 (A2126-U2127 in yeast), (2) h44 nucleotides G1420-22 (G1658-A1660 in yeast) with uL14, and (3) h44 nucleotides G1474-U1476 (U1738-A1740 in yeast) with H62 nucleotides A1689-90 (A1921-22 in yeast) and H64 nucleotide G1989 (A2332 in yeast). In yeast [2], B5 forms by the interactions of C411, U1734 of 18S with uL14, and the interaction of A1667 of 18S with G1935 of 25S rRNA. In hyper-rotated ribosomes [2], A1667 of 18S also interacts with A1936 of 25S.

In nonrotated prokaryotic ribosomes [161], B6 forms through interactions between h44 nucleotides A1429-30, G1474-U1476 (A1667-G1668, U1738-A1740 in yeast) and H62 nucleotides A1689-90, G1702-A1705 (A1921-22, G1934-U1937 in yeast), and the interaction of G1431 of 16S (U1669 in yeast) with bL19. In rotated yeast ribosomes [2], bL19, which does not have a eukaryotic homologue, is replaced by eL24, and the 18S nucleotides that take place in this bridge are G1670 and U1724

only. This bridge remains unchanged in hyper-rotated ribosomes [2]. This bridge may rearrange upon "subunit rolling" in mammalian ribosomes [26].

B7a is formed by h23 nucleotides C698, G702 (C910, G913 in yeast) and H68 nucleotides A1848-G1849, G1896 (A2208-U2209, G2239 in yeast), in the nonrotated prokaryotic ribosome [161]. In the rotated yeast ribosome [2], U909-C910, G913 of 18S interact with A2207, G2239-40 of 25S. In the hyper-rotated state [2], U911, G913 of 18S interact with U2205 of 25S to hold this bridge together.

B7b (B7b/c in newer studies) is an RNA:protein bridge, and is formed mainly through uL2 interactions with h23 and h24 in both nonrotated prokaryotic and rotated eukaryotic ribosomes [2,161]. In prokaryotes [161], the specific nucleotides that take part are SSU G712-13, G773-A776 (A924-G925, G985-A988 in yeast). In the rotated yeast ribosome [2], SSU G986-87, U1012-A1013 interact with uL2, while SSU A983 interacts with eL43. This is changed considerably in hyper-rotated ribosomes [2]: SSU A892, G984, G986, A988 interact with uL2 and SSU A923, U982-A983, G985, G1122 interact with eL43.

B8 is the last universal bridge, and is formed by the interactions of h14 nucleotides G345-47 (G418-A420 in yeast) with uL14, in the prokaryotic nonrotated ribosome [161]. In the rotated yeast ribosome [2], C411-A412, and G419 interact with the homologous protein. In the hyper-rotated yeast ribosome [2], the interacting rRNA nucleotides remain unchanged, while the interacting residues from uL14 change slightly. This bridge may be rearranging upon "subunit rolling" in mammalian ribosomes [26].

The eukaryote specific bridges eB8, eB11-14 have only been described in the rotated structures of the eukaryotic ribosome [2,162]. eB8 is formed by the interactions of eS1 with nucleotides A2536 and U2537 of 25S rRNA. These change in hyper-rotated ribosomes to interactions between S1e and nucleotides G2533, A2535 of 25S, and eL43 [2]. This bridge may also rearrange upon "subunit rolling" in mammalian ribosomes [26]. eB11 forms through interactions between eS8 and the 25S nucleotides A2107, G3345, G3353-U3355, with changes to interactions with G3345-U3346, G3353-U3354 in hyper-rotated conformation [2]. eB12 is defined by interactions between uS17and 18S nucleotides U813-G815, A850-A855 with eL19, while in the hyper-rotated state [2], eS7 takes the place of uS17. eB13 forms through interactions between eS6 and uL3 and eL24 in the rotated eukaryotic ribosomes, while the 18S nucleotides G273-C275, U278, U280, A1712-A1714 also interact with eL24 in the hyper-rotated state [2]. This bridge may also rearrange upon "subunit rolling" in mammalian ribosomes [26]. Finally, eB14 forms by the interactions between 18S nucleotides G1112, G1114-G1118, A1125-G1127, C1641-G1642, G1654-A1655, C1773-U1775, G1777-78, A1782-U1785 and eL41. Another nucleotide, A1750 is added to the bridge in the hyper-rotated form [2], and the interacting residues of eL41 change slightly.

The metazoan ribosomes may have three more bridges, eB15-eB17, indicated in the cryo-EM structure of the 80S *Drosophila* ribosome, formed by the interactions between extended ES31L and protein eS27 and the interactions of extended ES27L and eS8 (rotated) or eS27 (nonrotated), respectively [162].

4.1.3. More structural insight into eukaryotic ribosomes

As previously noted in Chapter 1, there are eukaryote-specific ribosomal structures. Not only are there eukaryote-specific ribosomal proteins and eukaryote-specific extensions to universal proteins, but eukaryote-specific rRNA extensions exist. These are called "expansion segments". Expansion segments and their structures have been studied in the context of ribosome and rRNA evolution. They are generally located on the solvent exposed regions of the ribosome (Figure 35). In fact, as the eukaryote species complexity increases, an rRNA layer is observed to form on the ribosome. Possible functions of some expansion segments have been defined, such as interacting with extraribosomal factors and structures [82,164,165,166].

An example of a relatively well studied expansion segment is ES27L [164]. This is a long and very flexible region of LSU, comparable in flexibility to the L1 stalk, and is found opposite to the P stalk / GAC. At least three conformations of this region have been observed through cryo-EM in yeast, wheat germ, fruit fly and human ribosomes. ES27L extending towards the L1 stalk is named "$ES27L_{in}$", whereas extending towards the peptide exit tunnel is known as "$ES27L_{out}$". Another conformation observed in wheat germ and fruit fly ribosomes is "$ES27L_{int}$" in which ES27L is not as extended to the L1 stalk as human ES27L is. ES27L is thought to regulate access of nonribosomal factors, such as chaperones, modifying enzymes, SRP, or the translocon, to the exit tunnel.

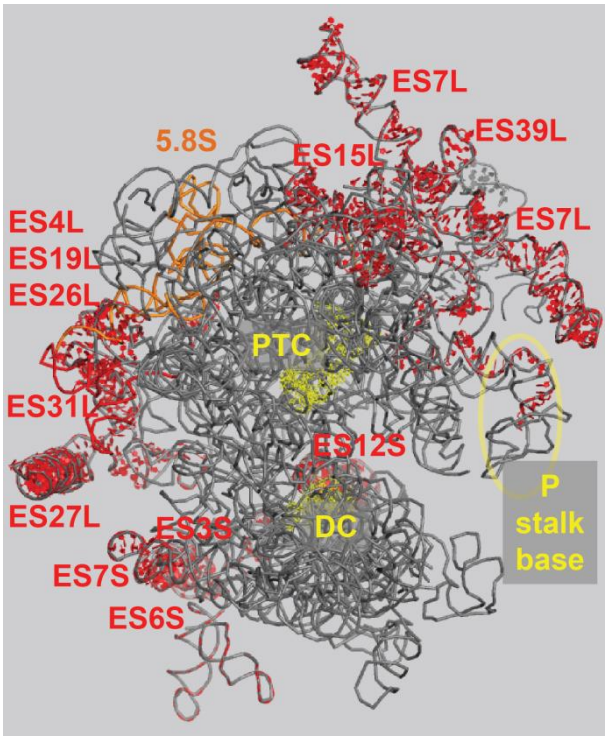

Figure 35. Expansion segments in 80S yeast ribosome.

Expansion segments are shown in red. Functional regions are shown in yellow for reference. ES: expansion segment, the "S" following the number denotes small subunit ES, whereas "L" denotes large subunit ES. PTC: peptidyl transferase center, DC: decoding center. Ribosome structure is from Armache et al, 2010 [167].

ES27L also interacts with other components of the ribosome, including another expansion segment, ES31L, and ribosomal proteins eL34 and eL38 [164]. The interplay between ES31L and ES27L has been observed to change depending on presence or absence of eEF2, *i.e.* the rotational status of the ribosome.

Another expansion segment, ES7S, located on SSU, is an extension of h26 and is part of the mRNA exit tunnel [82]. Yet another, ES7L, located on LSU, has been observed to contact Sbp2, selenocyteine insertion sequence binding protein-2, a crucial component of selenocysteine protein synthesis in humans [165,166]. Other than these the studies on expansion segments have stayed at the structural level [168–171]. ES3S and ES6S comprise most of the extended rRNA in SSU [82]. In LSU, majority of expansion segments are found grouped together, one such group forming behind the P

stalk (ES7L, ES39L), and another behind the L1 stalk (ES19L, ES20L, ES26L, ES31L) [164].

4.2. Results

4.2.1. Complex assembly and verification

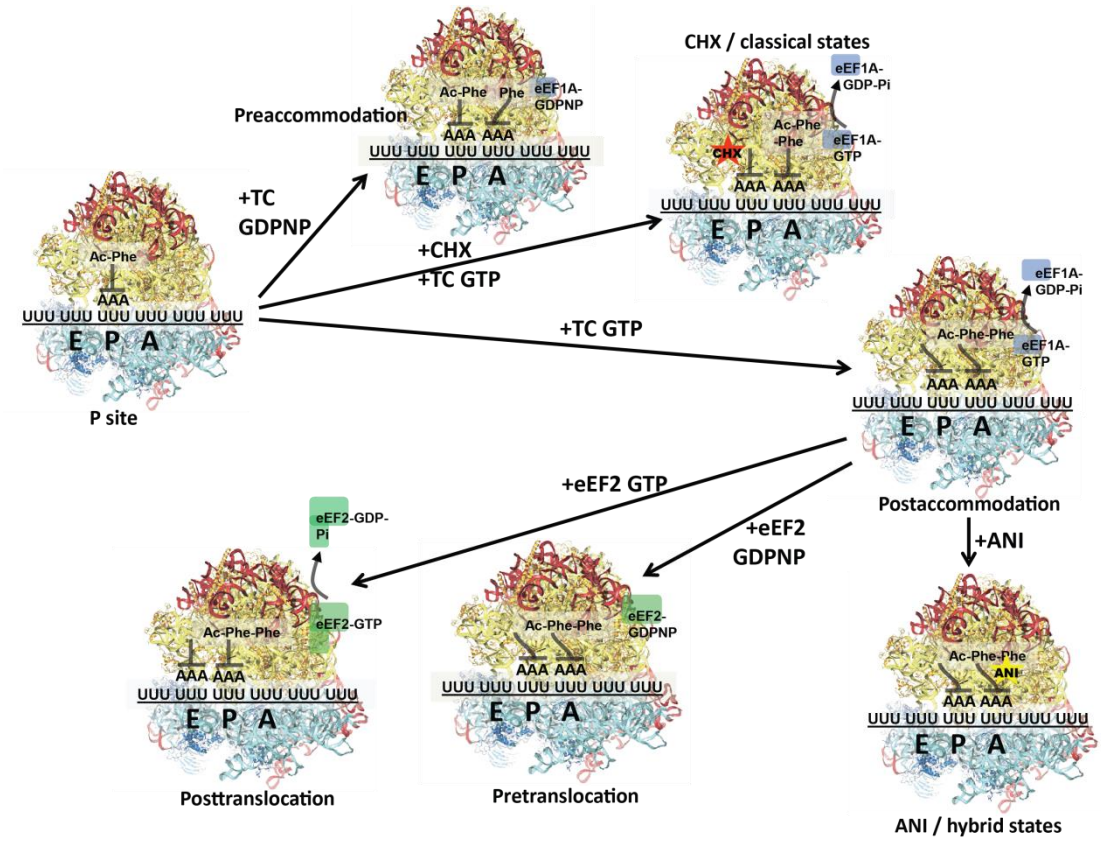

Figure 36. The complex assembly scheme.

The P site occupied complex (P site) is obtained by interacting empty 80S ribosomes with a peptidyl tRNA mimic (N-acetyl-phenylalanyl-tRNA or Ac-Phe-tRNA) and a template [polyuridylic acid or poly(U)]. From this complex, three others are obtained by addition of the ternary complex (TC) of eEF1A and phenylalanyl-tRNA (Phe-tRNA) with GDPNP (Pre-accommodation complex), or TC with GTP followed by an antibiotic (cycloheximide) (CHX / classical states complex), or TC with GTP only (Post-accommodation complex). From the Post-accommodation complex, the three final complexes are obtained by addition of another antibiotic (anisomycin) (ANI / hybrid states complex), or eEF2 with GDPNP (Pre-translocation complex), or eEF2 with GTP (Post-translocation complex).

Ribosomal complexes of the elongation cycle were assembled and verified prior to hSHAPE probing. Seven such complexes were assembled as described in Figure 36 and Chapter 6: Materials and methods. These are: (1) P site occupied

complex with a P site tRNA; (2) pre-accommodation complex with a P site tRNA and TC-GDPNP; (3) post-accommodation complex with A and P site tRNAs; (4) pre-translocation complex with A and P site tRNAs and eEF2-GDPNP(5) post-translocation complex with P and E site tRNAs; as well as two complexes with translation inhibitors (6) CHX complex with cycloheximide, A and P site tRNAs; and (7) ANI complex with anisomycin, A and P site tRNAs. In each of these complexes, the tRNA(s) should be in P/P state (P site occupied complex), P/P and A/T states (pre-accommodation), A/A-A/P and P/P-P/E states (post-accommodation), A/P and P/E states (pre-translocation), P/P and E/E states (post-translocation), A/A and P/P states (CHX), and A/P and P/E states (ANI). The tRNA states are also indicative of rotational status with "classical" A/A, P/P, E/E states occurring in nonrotated complexes, and "hybrid" A/P and P/E states occurring in rotated complexes.

A series of biochemical assays were performed to verify the assembled complexes. The results of tRNA binding assays are shown in Figure 37. Results of tRNA binding assays.. P site tRNA binding results are applicable to all complexes and indicate P site occupancy to be 90%. Separate A site binding assays were conducted for pre-accommodation (employing TC-GDPNP as the A site substrate), post-accommodation (employing TC-GTP as the A site substrate), and CHX complexes (incubating P site occupied complex with cycloheximide before using TC-GTP as the A site substrate); these indicate A site occupancy rates in the range of 55-65%. Results from post-accommodation complex are applicable to ANI, pre-translocation, and post-translocation complexes.

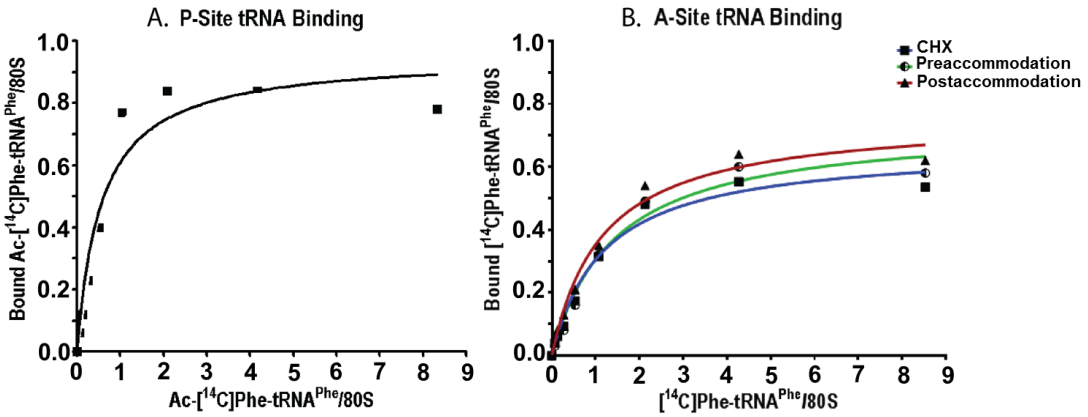

Figure 37. Results of tRNA binding assays.

P and A site binding assays were performed as described in Chapter 6: Materials and methods. The tRNA binding activity from different batches of ribosomes were comparable, at about (A) 85-90% for the P site, and (B) 55-65% for the A site. Separate A site tRNA binding reactions were performed for pre-accommodation, CHX and post-accommodation complexes.

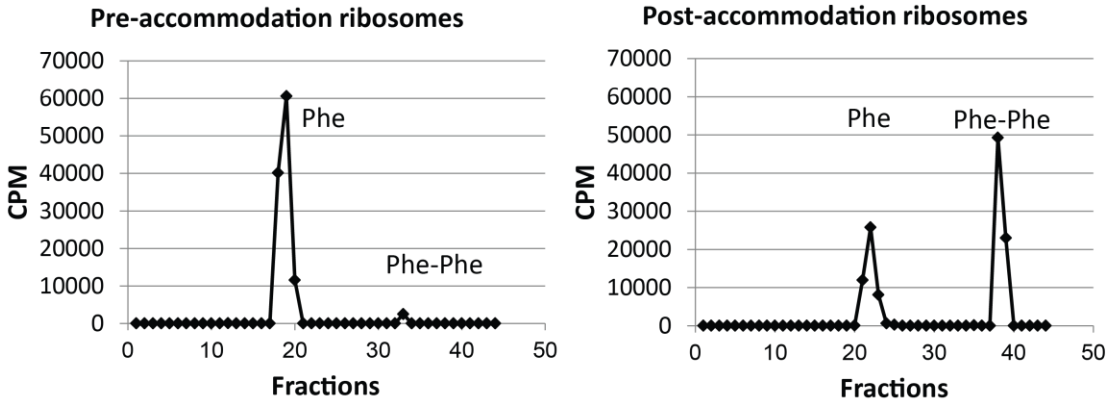

Figure 38. Results of dipeptide formation assays.

HPLC-based dipeptide formation assays were performed as described in Chapter 6: Materials and methods, for further verification of pre-accommodation (left) and post-accommodation (right) complexes. Dipeptide formation was observed in post-accommodation but not pre-accommodation complex, as expected. Quantification suggests a dipeptide yield of about 50%, consistent with the results from binding assays.

Pre-accommodation and post-accommodation complexes were further verified through an HPLC-based dipeptide formation assay [172], indicating whether or not peptidyl transfer has taken place in these complexes (Figure 38). According to this, pre-accommodation complex shows no significant dipeptide formation, whereas post-accommodation complex does show dipeptide in amounts comparable to the A and P site tRNA occupancy rates (about 50%).

The CHX and ANI complexes were further verified by base-specific structure probing of intersubunit bridge (B7a) to indicate their rotational statuses (Figure 39). Empty ribosomes are thought to freely rotate, whereas P site occupied complex is nonrotated, hence these were used as controls. Results from the CHX and ANI complexes indicate that these are nonrotated and rotated, respectively. These results also correlated with hSHAPE probing of this bridge.

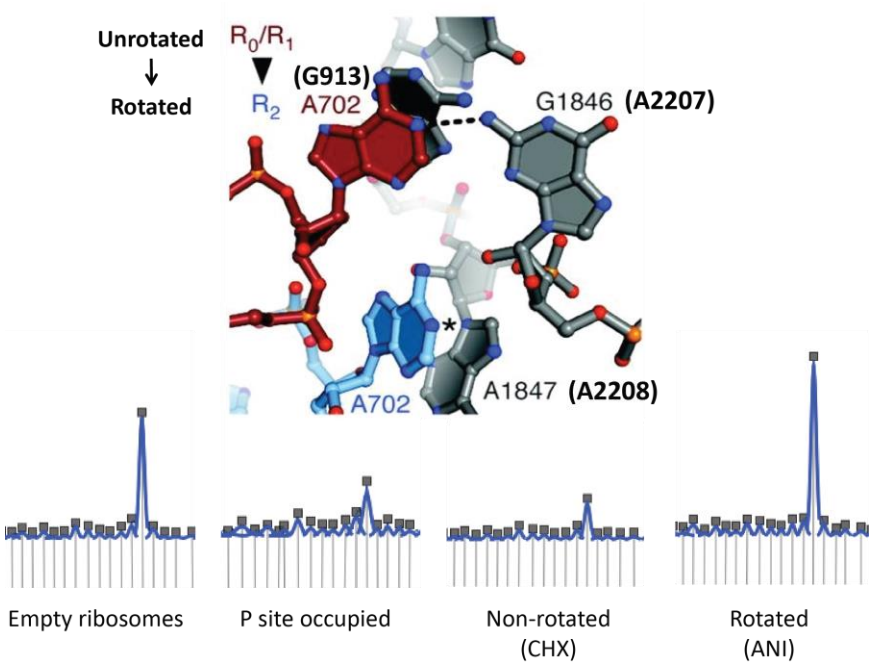

Figure 39. Rotational status of CHX and ANI complexes.

Kethoxal probing was performed as described in Chapter 6: Materials and methods, for further verification of CHX and ANI complexes. G913 (18S rRNA) component of B7a bridge (top) was probed with guanine-specific chemical kethoxal. Lower reactivity (smaller peaks in the electropherograms at the bottom) indicated a nonrotated bridge, where G913 and A2207 basepair. Higher reactivity (larger peaks) indicated a rotated bridge, where G913 and A2208 form a stacking interaction. Based on this, CHX is not rotated, and ANI is, as expected.

Pre-translocation and post-translocation complexes were further verified by (1) eEF2 binding assay, and (2) puromycin assay to detect the presence of an unoccupied A site (Figure 40). eEF2 was found to bind ribosomes with 70% efficiency, and the A site was unoccupied in 70% of post-translocation complexes, indicating that translocation occurred in all complexes that could bind eEF2. Since

puromycin binds to an open LSU A site, the reaction was conducted at 4°C to prevent binding to the pre-translocation complex, in accordance with similar studies in bacteria [173,174]. As a result, there was a clear difference between A-site occupancy of pre- and post-translocation complexes.

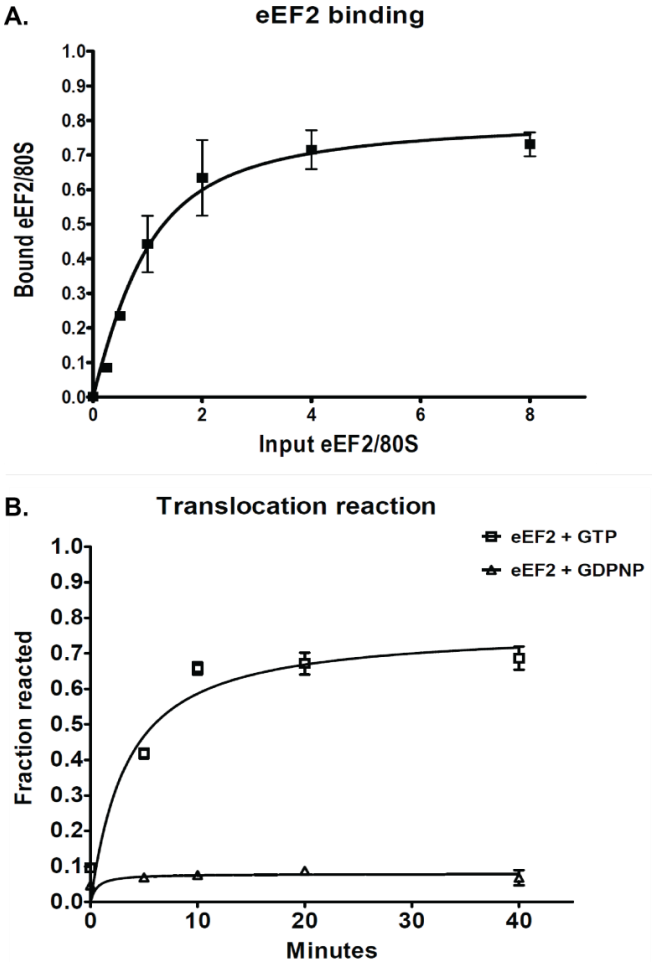

Figure 40. Results of eEF2 binding and puromycin (translocation) assays.

These assays were performed as described in Chapter 6: Materials and methods, to verify pre- and post-translocation complexes. A. eEF2 binding to ribosomes are about 70%. B. A site vacancy in the post-translocation state is about 70%, in accordance with eEF2 binding results, and higher than the pre-translocation state.

4.2.2. Identification of rRNA functional sites in hSHAPE data

After assembly and biochemical verification of complexes, hSHAPE was performed as described in Chapter 6. Results from known functional sites, obtained mostly from bacterial and mammalian ribosome studies were examined.

4.2.2.1. mRNA - rRNA interactions

SSU	Empty	P site	Average		SSU	Empty	P site	Average
A579	1.028081	0	0.476597		**G577**	1.399097	0	0.544874
G904	1.508937	1.043881	1.067043		**G904**	1.508937	1.043881	1.067043
C1537	1.066834	0.555762	0.935147		**C1274**	1.54062	0.929795	1.37215
G1575	1.19643	0.836136	0.656089		**C1620**	0.902895	0	0.953627
C1634	1.223311	0.852858	1.385665		**C1634**	1.223311	0.852858	1.385665
LSU					**A1635**	1.030116	0.540819	0.936215
A1025	1.674609	1.007647	1.506515		**C1636**	1.077452	0.740066	1.131201
A1240	1.074042	0.734931	0.802454		**C1637**	1.062668	0.549173	0.694238
					G1638	0.865004	0.18962	0.608664
					C1640	1.111845	0.657189	1.158289

Table 2. mRNA-rRNA interactions from hSHAPE data.

Left columns correspond to the comparison of bacterial studies to the hSHAPE data, right columns correspond to the comparison of mammalian studies to the hSHAPE data. Please see text for details. Empty: empty ribosome values, P site: P site occupied complex values, Average: average of the values from all complexes with an mRNA template. SSU: small subunit, LSU: large subunit. The values are obtained directly from complex comparison calculations (please see Chapter 6: Materials and methods).

The reactivity values we examined in the hSHAPE data in comparison with the mRNA-rRNA contact sites from previous studies were either the P site occupied complex values or the average values of all complexes compared to empty ribosomes (Figure 41 and Table 2). Of the nucleotides uncovered in prokaryotic ribosome chemical probing studies, A579, G904, C1537, G1575 of SSU, and A1025, A1240 of LSU were found to be protected in both P site occupied ribosomes, and overall in all complexes. Of the nucleotides uncovered in mammalian ribosome structural studies, G577, G904, C1274, A1635, C1637, G1638 of SSU were found to be protected in

both P site occupied ribosomes, and overall in all complexes. These nucleotides also show up in the difference map of P site occupied complex minus empty ribosome (Figure 41). There are also nucleotides that show protection overall, indicated by the average value from all complexes, compared to the empty ribosomes, but not in P site occupied ribosomes: C565, C575, A1427 of SSU. The mammalian ribosome structural studies have not uncovered any nucleotides from the LSU that might be affected by mRNA binding to ribosomes.

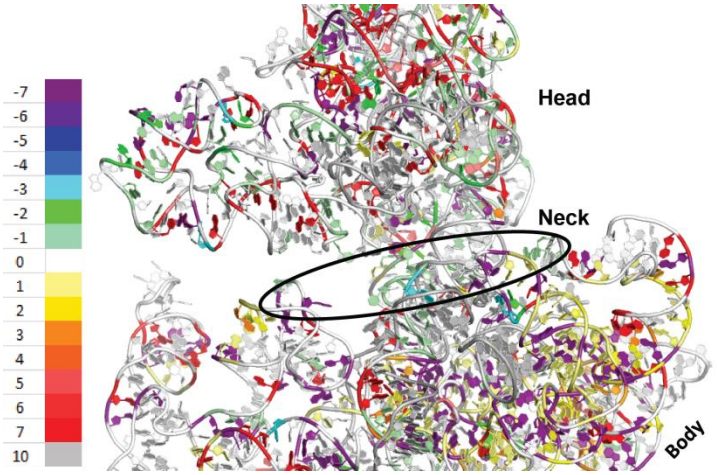

Figure 41. Changes in reactivity at the mRNA binding region.

Part of the 3D difference map of P site occupied complex vs. empty ribosome is shown above. Even though there are highly reactive nucleotides throughout, the reactivity of the neck region (and of the other mRNA interacting components) is low, possibly due to interactions with the mRNA template.

4.2.2.2. tRNA - rRNA interactions

First, the tRNA binding sites that emerged from bacterial chemical probing studies were examined in the hSHAPE data (Table 3). Protections at 18S P site residues are observed upon N-Ac-Phe-tRNA binding to yeast 80S. These occur at positions G577, A579, G904, A905, A1005, C1006, G1575, A1577, G1638, and can be seen in both numerical data and the difference maps. Some additional nucleotides show decreased reactivity values compared to empty ribosomes, but these do not appear in difference maps. Protection at 25S P site residues are also observed in the P

site occupied complex compared to empty ribosomes. These occur at positions U2269, A2820, and U2954. While no changes were observed at nucleotides G2620 or G2621, C2622 shows strong protection in this analysis. These nucleotides are all in the distal tip of Helix 80 which is known as the "P site loop," hence this may be an important protection. As with SSU nucleotides, some additional LSU nucleotides show decreased reactivity values but these are not present in difference maps.

Trapping the ribosome before accommodation (*i.e.* pre-accommodation complex) appears to render the 18S flexible in general. Unfortunately, most of the 18S A site (positions A1755-G1757) could not be probed due to their proximity to the 3' end of the SSU rRNA it is difficult to discern a clear A site signature on the small subunit with hSHAPE. However, it is clear that U578 is less reactive in the pre-accommodation complex relative to the P site occupied complex suggesting the start of A tRNA binding. In the color maps, most 25S A site residues become slightly more reactive or do not show changes in reactivity, with the exception of A2259 which becomes strongly protected compared to the P site occupied complex. A2259 is among the nucleotides the protection of which occurs independently of eEF1A (EF-Tu) dissociation.

SSU	Site	Empty	P site	Pre-acc	Post-acc	Pre-trans	Post-trans
G577	A, P	1.399097	0	1.176051	0.440576	0	1.107741
U578	A, P	0	0	0	1.154491	1.492553	1.409848
A579	P	1.028081	0	1.058643	0.359615	0	0.964728
G904	P	1.508937	1.043881	1.237881	1.070823	1.065315	0.917316
A905	P	1.399623	1.003750	0.955063	1.320124	0.670896	1.423297
A1005	P	0.976133	0.126593	1.218276	0.241482	0.360543	1.295051
C1006	P	0.615169	0.193700	0	0.837512	0	0.972633
G1575	P	1.196430	0.836136	0	0	1.434292	1.010017
A1577	P	0.987951	0.543608	1.107272	0	0.911948	0.922447
G1638	P	0.865004	0.189620	0.912904	0.968274	0.633609	0.338911
U1643	A (↑)	0	0	1.503339	1.285889	1.743357	0.593165
LSU		**Empty**	**P site**	**Pre-acc**	**Post-acc**	**Pre-trans**	**Post-trans**

A2259	A	0	0.822130	0	0	0	0.844950
G2261	A	1.326057	1.115180	1.479520	2.125404	1.170622	0
U2268	P	1.656955	0.649949	1.410646	1.177815	1.363268	1.335987
U2269	P	1.184619	0.544774	1.091499	1.439345	0	0.960000
G2454	E	1.073323	0.902117	1.164097	1.616188	1.200907	1.114971
A2458	E	1.564251	1.358675	1.705848	2.239336	1.440975	1.445277
A2484	E	0.999342	0.710854	1.068599	1.511473	1.130644	1.091234
C2622	A	1.079750	0	1.137126	1.064209	1.091083	1.074191
C2764	E	1.878895	0.986822	1.062229	1.071432	1.027051	0.505065
A2808	A, P	0	0	0.813131	1.177240	0	0.699794
A2820	A, P	1.506094	0.914349	1.201215	0	1.389515	1.227199
U2924	A	0.996548	1.900586	0.947680	1.006964	1.494715	0.998771
U2954	P	1.591385	0	1.370176	1.901525	2.047267	1.780146
A2971	A	1.595470	1.679157	1.528251	0	1.724749	1.658034
U2978	A	1.427609	1.174853	1.361624	0.863808	1.345808	1.502811

Table 3. hSHAPE data on tRNA binding sites from bacterial studies.

Please see text for details. Empty: empty ribosome values, P site: P site occupied complex values, Pre-acc: pre-accommodation complex values, Post-acc: post-accommodation complex values, Pre-trans: pre-translocation complex values, Post-trans: post-translocation complex values. SSU: small subunit, LSU: large subunit. The "Site" column indicates if the nucleotide belongs to the bacterial A, P, and/or E sites. The values are obtained directly from complex comparison calculations (please see Chapter 6: Materials and methods).

After GTP hydrolysis, accommodation and peptidyltransfer (i.e. in the post-accommodation complex), tRNA protection patterns become clearer, especially in the 18S rRNA. The 18S nucleotides that show increased protection are: A1005, A1576, A1577, U1643, and C1646. Nucleotides G577-A579, G904, G1575, which were protected in the previous complexes, also remain protected in post-accommodation complex. The 25S nucleotides that show continued and / or enhanced protection are: A2259, U2875, and G2794. These were protected in the pre-accommodation complex as well. The nucleotides showing increased protection or novel protection compared to the pre-accommodation complex are A2820, A2971, and U2978. Also, some E site tRNA interactions can be observed at nucleotides C2212, and A2802 [151].

The pre-translocation complex, *i.e.* ribosomes bound with eEF2 and prior to GTP hydrolysis, show continued or increased protection of tRNA binding related nucleotides, especially in the 25S rRNA. The 25S rRNA protections occur at

positions G2261, U2269, C2284, G2620, G2621, A2808, U2875, and U2953. Nucleotides A1217 and G1243 are also protected, and even though chemical probing studies list these in the A site (Table 1), other structural studies implicate them in transacting factor binding [33,47]. Some of the listed protections are unexpected as they should interact with the A site tRNA more than the P site or E site tRNAs according to chemical probing studies (Table 1). The key A site residues A2971 and U2978 become reactive again, with values comparable to empty ribosomes. This observation clashes with studies from the Noller laboratory [144,147,148], however it might also indicate an empty LSU A site, as would be expected. The loss of reactivity at nucleotides G2454, A2458, A2484, and an overall protected L1 stalk base (H76-78), indicates E site tRNA protections. We also observed novel or enhanced protections at A905, C1006, and G1638 of 18S.

SSU A site	Empty	P site	Pre-acc	Post-acc	Pre-trans	Post-trans
G577	1.399097	0	1.176051	0.440576	0	1.107741
P or P/E						
C1000	0.958233	0	0.995246	1.179447	1.203922	1.155918
G1002	1.164849	0	1.379372	1.3597	1.416736	1.400864
G1462	0	0.978274	0.970021	1.220028	1.136653	1.09194
G1575	1.19643	0.836136	0	0	1.434292	1.010017
G1638	0.865004	0.18962	0.912904	0.968274	0.633609	0.338911
C1639	0	0	0	0.986505	1.051786	1.488376
E site						
G904	1.508937	1.043881	1.237881	1.070823	1.065315	0.917316
A905	1.399623	1.00375	0.955063	1.320124	0.670896	0.423297
A906	0	1.063726	0.83807	0	1.580771	0.956454
LSU **A or A/P**	**Empty**	**P site**	**Pre-acc**	**Post-acc**	**Pre-trans**	**Post-trans**
A1179	0.964898	0.685139	1.261124	0.426619	1.181147	0
G2414	0.849775	0.706048	1.06291	0	1.086422	0.892657
U2416	0.864446	0.52094	0.611094	0	0	0
U2996	1.483941	1.664498	1.568466	0	1.628608	1.64789
G2997	0	0	1.04262	0.840714	0.977197	0
P site						
U2408	0.935348	0	0.945575	1.012484	0	0.946127
A2424	1.024822	0	0.94651	1.11736	1.019969	0.916552

G2778	1.028703	0	0.32769	0.929118	0.956259	0.849439
A2779	1.068401	0	0	1.344604	1.202072	1.20289
A3130	1.152856	0	0	1.077206	0	1.014833
E or P/E						
A2368	0.851326	0.720796	0.781305	0	0.80203	0
G2369	0.977028	0.652577	1.005705	1.412935	0	0.914007
G2393	0.914806	0	0.868926	1.319257	0.91636	0.992166
G2614	0.885197	1.294668	0.97423	1.295094	0.962226	1.067243
A2643	1.007919	1.077436	0.906561	1.299254	1.010257	0.936591

Table 4. hSHAPE data on tRNA binding sites from the mammalian ribosome.

Empty: empty ribosome values, P site: P site occupied complex values, Pre-acc: pre-accommodation complex values, Post-acc: post-accommodation complex values, Pre-trans: pre-translocation complex values, Post-trans: post-translocation complex values. SSU: small subunit, LSU: large subunit. rRNA nucleotides that are thought to interact with A, P, E tRNAs, as well as tRNAs in hybrid A/P and P/E states are labeled. The values are obtained directly from complex comparison calculations (please see Chapter 6: Materials and methods).

In the post-translocation complex, we observed a more open A site compared to the pre-translocation complex, especially in 18S. SSU nucleotides G577 and A580 become reactive, indicative of an open A site. Also in the SSU, loss of reactivity is observed at G904, G1575, G1638, U1643 and C1646. These might be due to re-established P/P state binding, or in the case of U1643 and C1646 may indicate rearrangements of specific intersubunit bridges. In the 25S rRNA, positions A2259, C2284, and A2808, as well as nucleotides from H43-44 become reactive. A2971 and U2978 remain reactive, indicating an open A site. The E site remains protected, and a novel protection is seen at C2764.

Table 4 shows a comparison of the hSHAPE data to published mammalian tRNA binding sites [127]. Compared to the results from bacterial sites, higher numbers of complete loss of reactivity are seen with mammalian sites, especially in the P site occupied and post-accommodation complexes.

Examination of Table 3 and Table 4 reveal differences between bacterial and fungal tRNA binding sites on rRNA, and indicate that mammalian sites may be a better match to yeast sites, especially considering the distances of the listed

nucleotides from a model tRNA. Based on this, we employed the latest cryo-EM structures of yeast ribosomes to visually analyze the P tRNA binding site further [175]. The P site occupied vs empty ribosome differences were mapped onto the nonrotated 80S ribosome, and the protected nucleotides located close to the model P site tRNA were examined (Figure 42). By this analysis, G2249-A2252, C2265-U2268, A2309, C2622, C2646, C2654-A2656, C2693-A2695, G2968-A2969 emerge as the new nucleotides of the 25S (LSU) P site. Some of these (A2309, C2622, G2968-A2969) were found to be in proximity to the P site tRNA by the hydroxyl radical cleavage experiments of the bacterial large subunit [149]. G2620-21, A2808, A2820, U2953-54 remain unchanged between bacteria and yeast. C1000-G1002, C1463-C1465, A1576-U1579, C1636-C1637 emerge as the new nucleotides of the 18S (SSU) P site, and this is in accordance with mammalian ribosome structures [135,127]. Only interactions with A1576-77 are conserved from bacteria.

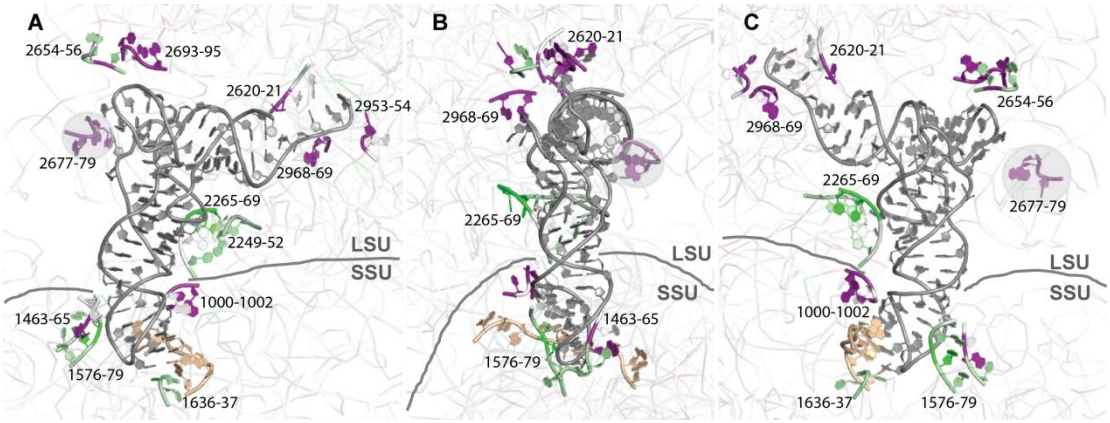

Figure 42. The yeast P site.

The nucleotides that have decreased reactivity in the P site occupied complex compared to the empty ribosome were mapped to the nonrotated yeast ribosome structure [175]. The model P site tRNA (grey) was used to locate the rRNA nucleotides that possibly interact with the tRNA. The labeled nucleotides in the figure are located 3-12 Å away from different parts of the tRNA (except G2677-A2679, shown with a transparent circle, which are 18 Å away on the average). The model mRNA is shown in tan. Please see text for nucleotide identities.

Analysis of post-translocation complex vs. empty ribosome reveals differences with the described P site. G2250-51, C2265, G2619, A2694-96, A2808, A2820, A2969 in the LSU, and G1466, A1576, G1638 in the SSU remain unchanged between P site occupied complex and the post-translocation complex. The post-translocation complex reveals additional decreases in hSHAPE reactivity at SSU C1644, U1647 and LSU A1006, C2285, C2405, G2623, A2647, U2668, A2680-U2681, G2863. Of these C2285 and G2863 are in proximity to the P site related cleavages from bacterial studies, making the bacterial 50S P site still a better match for the yeast 60S P site than the mammalian one. All the listed nucleotides from both complexes are in close proximity (averaging at 10 Å) with the model P/P tRNA.

4.2.2.3. Elongation factor - rRNA interactions

The complexes that retain an elongation factor are the pre-accommodation (eEF1A) and pre-translocation (eEF2) complexes. Therefore, we examined the nucleotides that were found to be protected in these complexes upon elongation factor binding in chemical probing experiments in bacteria. In the GAC, A1244, and G3028, A3032 of the SRL show protection in the difference map of the pre-accommodation and P site occupied complexes. A3032 shows protection in the hSHAPE difference map of the pre-translocation and post-accommodation complexes (Table 5).

Chemical probing						
LSU	**Empty**	**P site**	**Pre-acc**	**Post-acc**	**Pre-trans**	**Post-trans**
A1244	1.202057	0.574830	0	0	1.116745	1.106730
G3028	0	1.145025	0.961712	0.908052	1.093411	1.195303
A3032	0.710629	1.244453	1.042951	0.806668	0.608918	0.938253
Hydroxyl radical cleavage						
SSU	**Empty**	**P site**	**Pre-acc**	**Post-acc**	**Pre-trans**	**Post-trans**
U29	0.975940	1.171044	0.960857	0.561885	0	0.821889
U33	0.898435	1.167619	1.073215	0.732314	0.388697	1.078317

G34	0	0.723018	0.944016	0.490194	0	1.043170
G510	0.821488	0	0.965594	1.004035	0	0
A511	1.114740	1.074892	0.969845	1.033155	0	0
A512	0.982187	1.086948	0	0.968909	0	0
U513	1.166411	1.150214	0.702178	0.959734	1.139413	0.998140
G514	1.189051	1.120822	0.928289	1.013778	0	0.739962
A544	1.170754	1.049323	0.733191	0.878903	1.198156	0
U547	0.965420	1.092893	0.776802	1.003396	0.460939	0
G548	0.993852	0.985371	0.905813	0.867271	0	0
G586	0.829594	1.075882	0.905225	1.007972	0.732587	0.919999
C587	0.833604	0	0	0.991647	0	0.853817
A1444	0	1.245539	1.103465	1.045523	0.945114	1.591058
C1461	0	0	1.122910	0	1.230382	1.141285
G1462	0	0.978274	0.970021	1.220028	1.136653	1.091940
G1464	1.237013	0	1.133840	0.828773	0	0.841558
G1638	0.865004	0.189620	0.912904	0.968274	0.633609	0.338911
LSU	**Empty**	**P site**	**Pre-acc**	**Post-acc**	**Pre-trans**	**Post-trans**
G1243	1.760012	0	0.951139	1.679863	0.964481	1.150582
A1244	1.202057	0.574830	0	0	1.116745	1.106730
A1270	1.293568	0.713459	0	1.074548	1.318914	1.315441
C2308	1.120530	0.952449	1.447967	1.842303	1.363942	1.324106
C2849	1.076941	1.156672	0.896894	0.891885	0.588945	0.838247
G2850	0	0.949812	1.015095	1.488754	0	0.900230
A2851	1.073177	1.365186	1.060798	1.038430	0.923093	1.085299
A3017	0	1.025394	0.997964	0	0.712744	1.327650
C3018	0	1.086792	0.780153	0	0	0.935807
U3019	0.859554	1.188375	0	1.198593	0.722542	0
U3023	0.926946	1.089361	0	0.858891	0.713559	0.989456
A3024	0.903170	1.054250	0.695538	0.856185	0.986207	0.901661
C3025	0.000000	1.086760	0.980006	1.112488	0.778146	1.032909
G3026	0.928263	0.773983	0.869914	1.244164	0.975608	1.100397
A3035	0	1.063433	0	0.947684	1.005874	1.114901
G3036	1.003952	0.928459	0	1.006930	0.841481	0.852623
U3038	0	1.255474	1.135425	0.780687	1.050342	0

Table 5. EF binding sites from chemical probing studies.

Empty: empty ribosome values, P site: P site occupied complex values, Pre-acc: pre-accommodation complex values, Post-acc: post-accommodation complex values, Pre-trans: pre-translocation complex values, Post-trans: post-translocation complex values. SSU: small subunit, LSU: large subunit. The values are obtained directly from complex comparison calculations (please see Chapter 6: Materials and methods).

X-ray crystallographic structures of the bacterial ribosome with EF-Tu (stabilized by kirromycin) or EF-G (stabilized by fusidic acid) were also examined for nucleotides that interact with the elongation factors [33,47]. In the hSHAPE data, SSU nucleotides G430, C431, and LSU nucleotides A1270, C2844, G3028, A3032 emerge

as eEF1A (EF-Tu) interacting nucleotides. SSU nucleotides U52, C433, G434, A436, A441, C442, and LSU nucleotides G1243, G3030-A3032 emerge as eEF2 (EF-G) interacting nucleotides. Results are shown in Table 6.

X-ray crystallography							
SSU	**Factor**	**Empty**	**P site**	**Pre-acc**	**Post-acc**	**Pre-trans**	**Post-trans**
U52	EF-G	0.994683	0.814413	1.000532	0.721838	0	0.729098
G430	EF-Tu	1.132694	1.039492	0.405961	1.070965	0.998279	1.220954
C431	EF-Tu	0	0.944068	0.534706	0	1.310621	1.247968
C433	EF-G	1.078705	1.168738	0.970594	0.529084	0	1.336763
G434	EF-G	0	1.086352	1.115286	0.966473	0.107163	0
A436	EF-G	1.206836	1.099728	1.454033	1.463126	0	1.447335
A441	EF-G	1.035357	1.102187	0.978408	1.068419	0	0
C442	EF-G	0.896014	1.080354	0.908404	0.980458	0.742448	1.062566
LSU	**Factor**	**Empty**	**P site**	**Pre-acc**	**Post-acc**	**Pre-trans**	**Post-trans**
G1243	EF-G	1.760012	0	0.951139	1.679863	0.964481	1.150582
A1270	EF-Tu	1.293568	0.713459	0	1.074548	1.318914	1.315441
C2844	EF-Tu	1.240611	1.553191	1.160410	1.470473	1.971848	1.143636
G3028	EF-Tu	0	1.145025	0.961712	0.908052	1.093411	1.195303
G3030	EF-G	0.829820	1.157142	0.968730	0.499957	0	1.023816
G3031	EF-G	0.609064	1.144072	1.008770	0.739089	0	0
A3032	EF-Tu, EF-G	0.710629	1.244453	1.042951	0.806668	0.608918	0.938253

Table 6. EF binding sites from X-ray crystallography structures.

Empty: empty ribosome values, P site: P site occupied complex values, Pre-acc: pre-accommodation complex values, Post-acc: post-accommodation complex values, Pre-trans: pre-translocation complex values, Post-trans: post-translocation complex values. SSU: small subunit, LSU: large subunit. Nucleotides implicated in binding of specific elongation factors are labeled in the "Factor" column. EF-Tu is the bacterial counterpart of eEF1A, EF-G is the bacterial counterpart of eEF2. The values are obtained directly from complex comparison calculations (please see Chapter 6: Materials and methods).

Comparison of the whole GAC (nucleotides 1230-1280) in all complexes yielded interesting results. There is a decrease in reactivity of this region in the P site occupied complex compared to empty ribosomes, followed by increase in reactivity in the pre-accommodation and, to a lesser extent, post-accommodation complexes (Figure 43). The reactivity decreases again in the pre-translocation complex, in accordance with eEF2 binding, and increases in specific bases in the post-translocation complex. The results from sarcin-ricin loop (SRL; nucleotides around 3020-30 in the above tables) indicate an overall loss of reactivity in pre-

accommodation and pre-translocation complexes, in accordance with EF binding, hence the deviance in the reactivity of the corresponding GAC's is thought provoking.

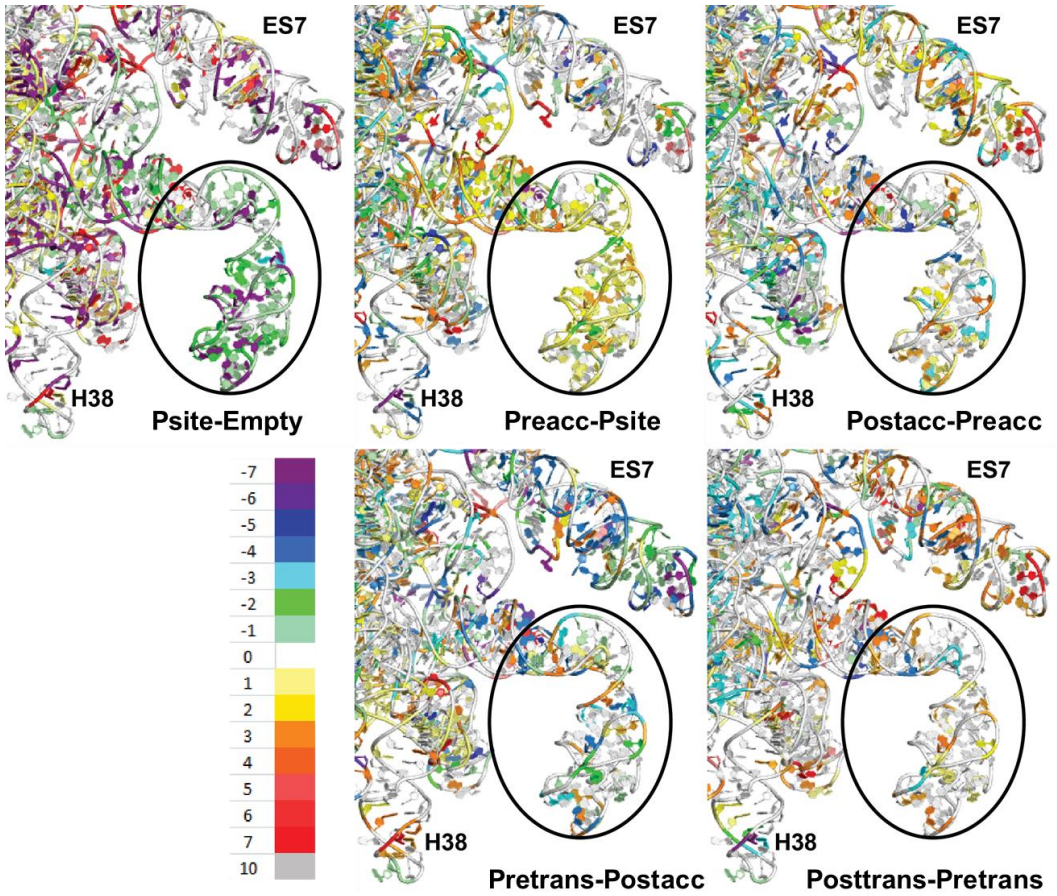

Figure 43. P stalk base (GTPase associated center, GAC) in the difference maps.

Upper row left to right: P site occupied - empty, pre-accommodation - P site occupied, post-accommodation - pre-accommodation difference maps. Lower row left to right: pre-translocation - post-accommodation, post-translocation-pre-translocation difference maps. P stalk base is circled.

4.2.3. Intersubunit bridges

The hSHAPE data were also compared with structural studies from bacteria and yeast that identified LSU:SSU contacts, i.e. intersubunit bridges, in nonrotated and rotated ribosomes, respectively [2,161]. Nonrotated complexes (P site occupied, CHX, post-translocation complexes) were mainly compared to the empty ribosomes and the complexes that are immediately before or after them, to evaluate the bridges

from nonrotated structures. Rotated complexes (post-accommodation, ANI, pre-translocation) were used in the evaluation of rotated ribosome bridges. An nonrotated / rotated ribosome bridge component was assumed to be visible in hSHAPE data if any of the nonrotated / rotated complexes showed protection compared to the empty ribosomes and the other complexes surrounding them. We only considered the rRNA components, as hSHAPE does not give data on proteins. These results are summarized in Table 7 and Table 8.

SSU	Bridge	Empty	P site	Post-acc	Pre-trans	Post-trans	CHX	ANI
C1646	B2a	0.86574	0.812653	1.1208662	1.997161	0.895131889	0.8498122	0.98274652
U1647	B2a	1.372284	1.057123	1.6139609	0.8485179	0	1.6351251	1.38117491
A1648	B2a	0	0.742094	1.1133393	1.6802686	1.588106108	1.0646258	0.71909374
G997	B2b	0.860241	0	1.0414039	1.1617747	1.007135251	1.1099782	0.93796598
C1006	B2b	0.615169	0.1937	0.8375123	0	0.972632686	0	1.02024292
U982	B2c	0.840464	0	1.1998926	0.9471848	1.238487449	1.2533042	1.18279604
A983	B2c	0.887246	1.055425	1.0466288	0.9057969	1.08382522	0.9540696	1.02080427
A1125	B2c	0.987227	0	1.2357653	1.5300019	0.740117114	0	0.8400954
G1126	B2c	0.938292	1.21013	0.8838819	0.9293682	1.015187456	0	0.92730647
G976	B4	0.575106	0	1.086813	1.0538135	1.246054331	0.8116136	0.60522325
G1658	B5	0.923964	0	1.1386782	1.0804183	0.932762866	1.1155992	1.30347527
A1660	B5	0	0	0.8819223	0	0.960882592	0.7230418	1.4543778
U1738	B5, B6	0	0	1.0290032			0	0.88136261
C1739	B5, B6	0		0.9020902			1.0537561	1.12512227
A1667	B6	0.767705	0.69241	0.8728328	0	0.833540216	0.6982577	1.34177178
G1668	B6	0.714619	0	0.8697098	0	0.730278628	0.8622518	0.91567792
U1669	B6	0	0.357769	0.882194	0.9626738	0.727681563	1.0102266	1.48336323
C910	B7a	0.778511	0.973588	0	1.1725574	0	0	0.89769034
G913	B7a	1.210575	0.970306	1.3410615	1.4194958	0	0.9552165	1.28318313
G914	B7a	0.918626	0.862648	0	1.0614172	0	0.8893325	0.79972507
G925	B7b	0.711435	0	0	0.8698684	1.057758313	0.8889053	0.88565041
G985	B7b	0.864954	1.056574	1.0360825	1.0577368	1.162144775	0.9615991	0.99307325
G986	B7b	0.582086	1.109588	0.9386496	0.8580121	0.832449337	0	1.0021138
G987	B7b	0.881483	0	1.1338049	1.2882377	1.247737575	1.1666039	1.11202167
G419	B8	1.05883	0	1.4406986	0.8919211	0.968572086	1.0668742	0.95748056
A420	B8	1.228887	0	1.7342675	0.4392027	0.95474109	1.3536546	0.9589811
LSU	Bridge	Empty	P site	Post-acc	Pre-trans	Post-trans	CHX	ANI
A1025	B1a	1.674609	1.007647	2.117648	1.6129892	1.048101287	1.0372475	1.99149157
A1026	B1a	1.682716	1.528939	2.2137263	1.7148504	1.375389568	1.0343607	2.09227145
A2256	B2a	1.289989	0.385102	0.6972292	0.8441767	1.407282296	0	0
C2257	B2a	1.429314	0	2.0814382	1.4846587	1.028994542	1.0996502	1.58934739
G2261	B2a	1.326057	1.11518	2.1254041	1.1706219	0	1.4751843	1.78384405

C2196	**B2b**	0.918888	0	0	0.552581	0.783829875	0.8032884	0
A2262	**B2b**	1.269554	0	1.8641947	1.356294	1.08741044	1.2967673	1.38128648
C2265	**B2b**	1.166487	0.82812	1.0906709	1.1640379	1.288430234	0.8209109	0
A2275	**B2b**	1.030825	0	1.4941747	0	1.093299901	1.3906824	0
C2192	**B2c**	0.971161	0	0	0.769856	0	0.9621819	0.96012941
C2290	**B3**	1.021718	0.765861	1.6213262	1.2229734	1.147171389	1.0716945	1.10985335
A2291	**B3**	1.069814	0.913487	1.484852	1.3096802	1.133128308	0.9413655	0.86338599
A2303	**B3**	0.792156	0.824726	1.2298419	0.877768	0	0	0.8179269
C2304	**B3**	0	0	0	0	1.022986958	0	0.75423998
C849	**B4**	0	0.990276	0.7764342	0	0.739915883	0.6506956	0.8063262
A2332	**B5**	0.79065	0	1.4466433	0.9000802	0.863621087	1.0152965	0
G1934	**B6**	0.883854	1.024268	0.8707546	1.1903695	1.023360696	1.1747014	1.40425196
A2208	**B7a**	1.396026	0.758025	1.2931782	1.1020973	0.927880223	0.8090739	1.59736329
U2209	**B7a**	1.635583	1.356684	2.2219065	1.4285737	1.531487289	1.7098194	1.77030469
G2239	**B7a**	1.120313	0.904275	1.5196005	1.1541604	0.771308043	1.075435	1.07088127

Table 7. hSHAPE data on bacterial, nonrotated conformation bridges.

The bridge components were obtained from Yusupov et al, 2001 [161]. The bridge column indicates which intersubunit bridge the nucleotide belongs to. Expected decreases in reactivity in the nonrotated complexes are highlighted green. The values are obtained directly from complex comparison calculations (please see Chapter 6: Materials and methods).

The bridge components at which all complexes of a specific rotational status showed loss of reactivity compared to the complexes of the "opposing" status were especially valuable; strikingly, these are very few in number. We also observed that the nonrotated complexes, especially the P site occupied complex, showed the highest number of expected reactivity levels in the bridges. These findings are consistent with the notion that there may be "sub-rotational conformations" occurring throughout elongation and that the intersubunit interface may be more "fluid" in structure than previously thought. These sub-conformations may manifest themselves as (A) the formation of some bridges but not others, or, (B) the formation of some interactions that make up a bridge but not others, or, (C) combinations of both. As indicated by the better fit of nonrotated complex hSHAPE data to the list of nonrotated bridges, compared to the rotated complex data and rotated bridges, there may be fewer "sub-nonrotated" conformations than rotated ones.

The eukaryotic bridges implicated in "subunit rolling", *i.e.* B6, B8, eB8, and eB13, were also examined [26]. Some effects were also to be expected in eB11 and eB12. While this analysis captured some changes in these bridges (highlighted grey in Table 8), we note that they also overlap with SSU rotation.

SSU	Bridge	Empty	P site	Post-acc	Pre-trans	Post-trans	CHX	ANI
C1644	B2a	1.197942	0.80129	1.2385371	0	0.57737618	0.2824204	0.99134972
G1645	B2a	1.191097	0.68625	0.7017392	1.5028355	0.33794883	0.5609593	0
U982	B2c, B7b/c	0.840464	0	1.1998926	0.9471848	1.23848745	1.2533042	1.18279604
A1655	B3, eB14	1.172668	0.91913	1.1980247	1.1473936	1.13295112	1.103525	0
A1746	B3	1.107333		0.4917296			1.18558	
G1747	B3	1.155208		0.7777143			1.0384968	
G1748	B3	0.849402		0			0.8211643	
A1749	B3	0.805794		0.6787745			0.9816615	
G628	B4	0.983325	0.95369	1.1084418	0.9176349	1.28509855	0.9806069	0.98876165
C411	B5, B8	0.979727	0	0	0	0.92383781	0	1.15636695
A1667	B5	0.767705	0.69241	0.8728328	0	0.83354022	0.6982577	1.34177178
U1734	B5	0.777364	0	1.0561588	0		1.163628	0.6512412
G1670	B6	0	0.87795	0.9599856	0	0	1.0997787	0
U909	B7a	0.804306	0.9771	0.6761169	0.9856134	1.02802159	0.764185	0.77536369
C910	B7a	0.778511	0.97359	0	1.1725574	0	0	0.89769034
U911	B7a	1.442609	1.14016	1.6040537	1.435276	1.30660978	1.2548329	0.81765021
A923	B7b/c	0.541091	0	0.9651395	0.288727	0.7841185	0.6040875	0.89618312
G986	B7b/c	0.582086	1.10959	0.9386496	0.8580121	0.83244934	0	1.0021138
U1012	B7b/c	0.740227	0	1.092217	0	1.0207736	1.1491892	1.20778133
G1122	B7b/c	0.895671	1.20101	1.2928013	1.4566045	1.15371639	1.2369045	0
A412	B8	1.406518	1.16878	0.7639067	1.1158622	1.16966659	1.1471297	1.23205285
U851	eB12	1.109696	1.09448	0.9380267	0	1.02969013	0.7401936	0.72600599
G273	eB13	1.066791	1.14048	1.3061394	0.9359146	1.22184896	1.053235	1.12253314
G274	eB13	0	0	1.5934351	1.2150526	1.46781917	0	0.82992983
C275	eB13	1.300059	1.52884	2.1362754	2.1539131	2.38308732	1.8034771	1.47732532
A1714	eB13	0.946517	0.71593	0	0.9875311	0	0.9851416	0
G1114	eB14	0.299353	1.13198	0.9823288	0.9257716	0.95046597	0.9258818	1.03726958
U1115	eB14	0	0	1.0249099	0.8024211	1.03311253	1.0592058	1.16080222
G1126	eB14	0.938292	1.21013	0.8838819	0.9293682	1.01518746	0	0.92730647
G1127	eB14	0.847594	1.25346	0.8140357	0.749936	0	0.4022362	0.68906548
C1641	eB14	0.947436	0.74338	0.3160873	1.9428717	1.42852197	0.9327305	1.08301684
G1642	eB14	0.862858	0.81917	0.7312791	0	1.55778182	0.9029685	1.11540635
LSU	Bridge	Empty	P site	Post-acc	Pre-trans	Post-trans	CHX	ANI
A2259	B2a	0	0.82213	0	0	0.84494963	0	1.60620842
C2263	B2a	0.920025	0.72067	0	0	0.59286677	0.801735	0.84492549
C2196	B2b	0.918888	0	0	0.552581	0.78382988	0.8032884	0
C2197	B2b	0.956444	0	1.3292934	0.914977	1.02848798	1.0841475	0
A2275	B2b	1.030825	0	1.4941747	0	1.0932999	1.3906824	0

C2192	**B2c**	0.971161	0	0	0.769856	0	0.9621819	0.96012941
A1922	**B3**	0.858229	1.1692	0.7506318	1.062651	1.01319101	0.9216749	0.8793968
A2291	**B3**	1.069814	0.91349	1.484852	1.3096802	1.13312831	0.9413655	0.86338599
U2301	**B3**	0.876703	0.89921	1.0899571	0	0.98564701	0.743509	0.97125693
G2302	**B3**	0.995543	0.89406	0	1.008746	0.97549001	1.1056209	1.02460239
G2305	**B3**	1.342081	1.17167	2.0275786	1.2708593	1.37998697	1.4428183	0
G844	**B4**	1.033777	1.29458	1.1662149	1.3124769	1.28052769	1.2576829	0
A848	**B4**	1.371455	1.20915	0.8673768	0	1.12450725	1.0884484	1.02659477
G1935	**B5**	1.027573	1.16948	0.8775504	1.2388827	1.01987166	1.1395794	1.49197697
A1936	**B5**	1.139345	1.23549	0.6964552	1.0620109	1.02945407	0.9721565	1.14264889
G2240	**B7a**	1.181148	0.755	1.6445104	1.2295566	1.21894703	1.2051912	0
G2533	**eB8**	0.821709	0	0	0	0	0.8387015	0
A2535	**eB8**	1.071347	0.68267	0	1.0482945	1.07665899	1.0188318	0.92474591
G3345	**eB11**	0.967349		0			0.9833053	

Table 8. hSHAPE data on eukaryotic, rotated conformation bridges.

The bridge components were obtained from Ben-Shem et al, 2011 [2]. The bridge column indicates which intersubunit bridge the nucleotide belongs to. Bridges implicated in subunit rolling are highlighted in grey. Expected decreases in reactivity in the rotated complexes are highlighted green. The values are obtained directly from complex comparison calculations (please see Chapter 6: Materials and methods).

Since there were more unexpected data on the intersubunit bridges than the regions examined in the earlier sections, and since intersubunit rearrangements remain an active field of research in eukaryotic ribosomes, we examined our data from one more angle. A difference map of empty 80S and 40S was generated (Figure 44), to highlight the reactivity decreases caused by subunit association. As expected, most of these are found on the known subunit interface of the ribosome, clustering in the SSU h44, and in the head and platform domains. Interestingly, the SSU nucleotide numbers so identified were not a perfect match to the known list of yeast intersubunit bridges [2].

We then focused on the same nucleotides in all difference maps (Figure 45), with surprising results. Except for the platform and a small portion of h44, the possible "interface nucleotides" are very reactive in the nonrotated, P site occupied complex compared to empty ribosomes. In the pre-accommodation complex, most of these become even more reactive compared to the P site complex, whereas in the

post-accommodation complex a portion of the head domain and most of h44 have decreased reactivity compared to pre-accommodation ribosomes. The nucleotides become more reactive again in the pre-translocation complex compared to post-accommodation ribosomes. Decreased reactivity in the post-translocation complex is visible but not dramatic. Finally, the rotated complex with hybrid state tRNAs shows decreased reactivity in the head domain and in parts of h44 compared to the nonrotated complex with classical state tRNAs.

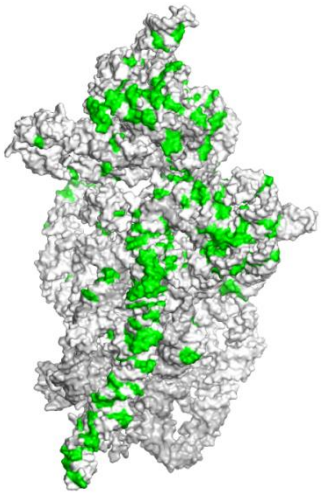

Figure 44. Regions of protection on 18S rRNA upon subunit joining.

The nucleotides that have lost reactivity in 18S rRNA after 60S joining (*i.e.* difference map of 80S vs 40S) are highlighted in green and mostly map to the subunit interface.

These rather unexpected results reveal some novel insights into ribosome structural dynamics. First, a region on the platform located close to one nucleotide of the B7b/c bridge, becomes protected upon subunit association and in nonrotated, P site occupied ribosomes. Second, the rearrangements observed in the subunit interface suggest that the pre-accommodation complex may be in a rotated state. Finally, different bridges or regions of the intersubunit interface are affected in different complexes, regardless of rotational status, supporting the notion that the ribosome may acquire many different rotated and nonrotated sub-states.

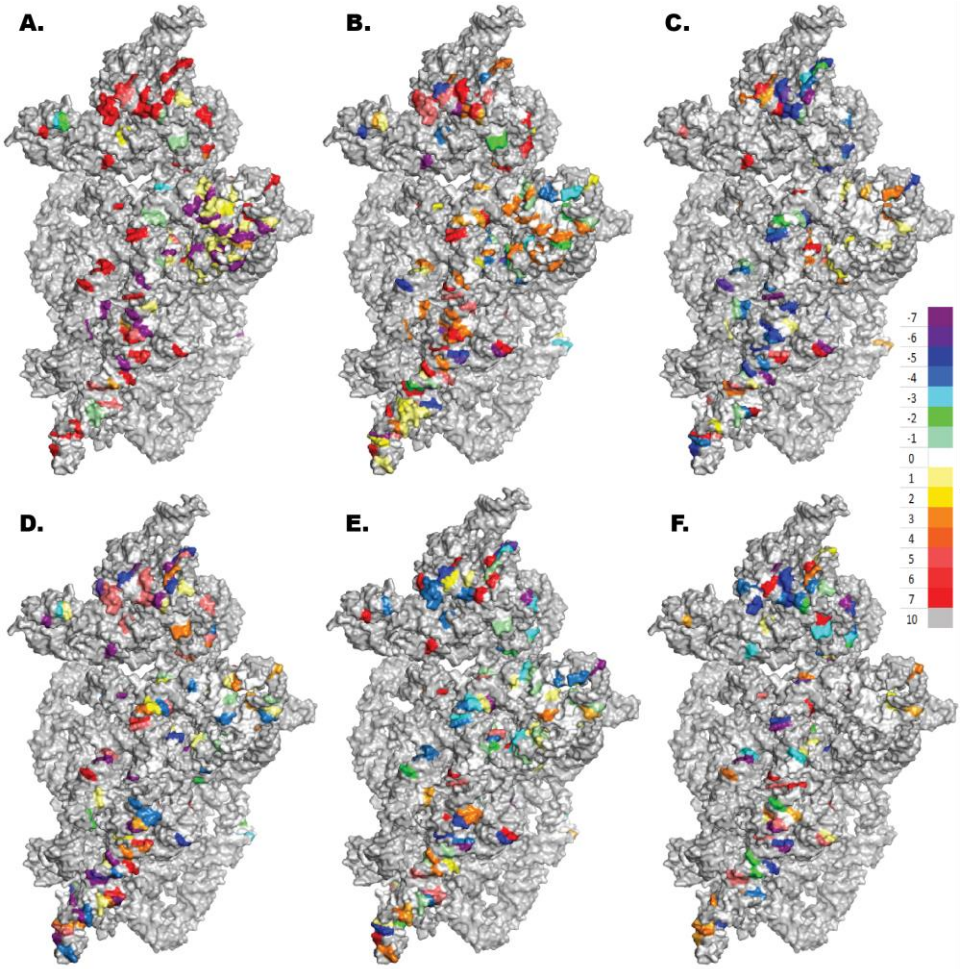

Figure 45. The reactivity changes in 60S interacting nucleotides of the SSU through the elongation cycle.

The regions obtained from the difference map of empty 80S and 40S (Figure 44) were examined in the difference maps of elongation cycle complexes. A. P site occupied complex vs. empty ribosome, B. Pre-accommodation vs. P site occupied complex, C. Post-accommodation vs. Pre-accommodation complex, D. Pre-translocation vs. Post-accommodation complex, E. Post-translocation vs. Pre-translocation complex, F. Complex with hybrid state tRNAs (ANI) vs. Complex with classical state tRNAs (CHX).

4.2.4. Expansion segments

The eukaryote specific components of the rRNA are known as expansion segments (ES). Graphing the hSHAPE reactivities of ES's from different elongation complexes yielded interesting results. Overall, most ES's show accommodation-specific changes in reactivity, such that the reactivity decreases or increases as ribosomes progress from the P site occupied complex to the post-accommodation

complex. Graphs of ES's that display the most dramatic changes are shown in Figure 46. These are ES3S from SSU, ES7L from the P stalk region, ES27L from the "back" of LSU, across from the P stalk, and ES31L from the L1 stalk region. Further analyses indicate that the reactivity returns to pre-accommodation levels in pre-translocation and post-translocation complexes for ES7L, ES27L and ES31L. For ES3S, it stays roughly at the post-accommodation levels.

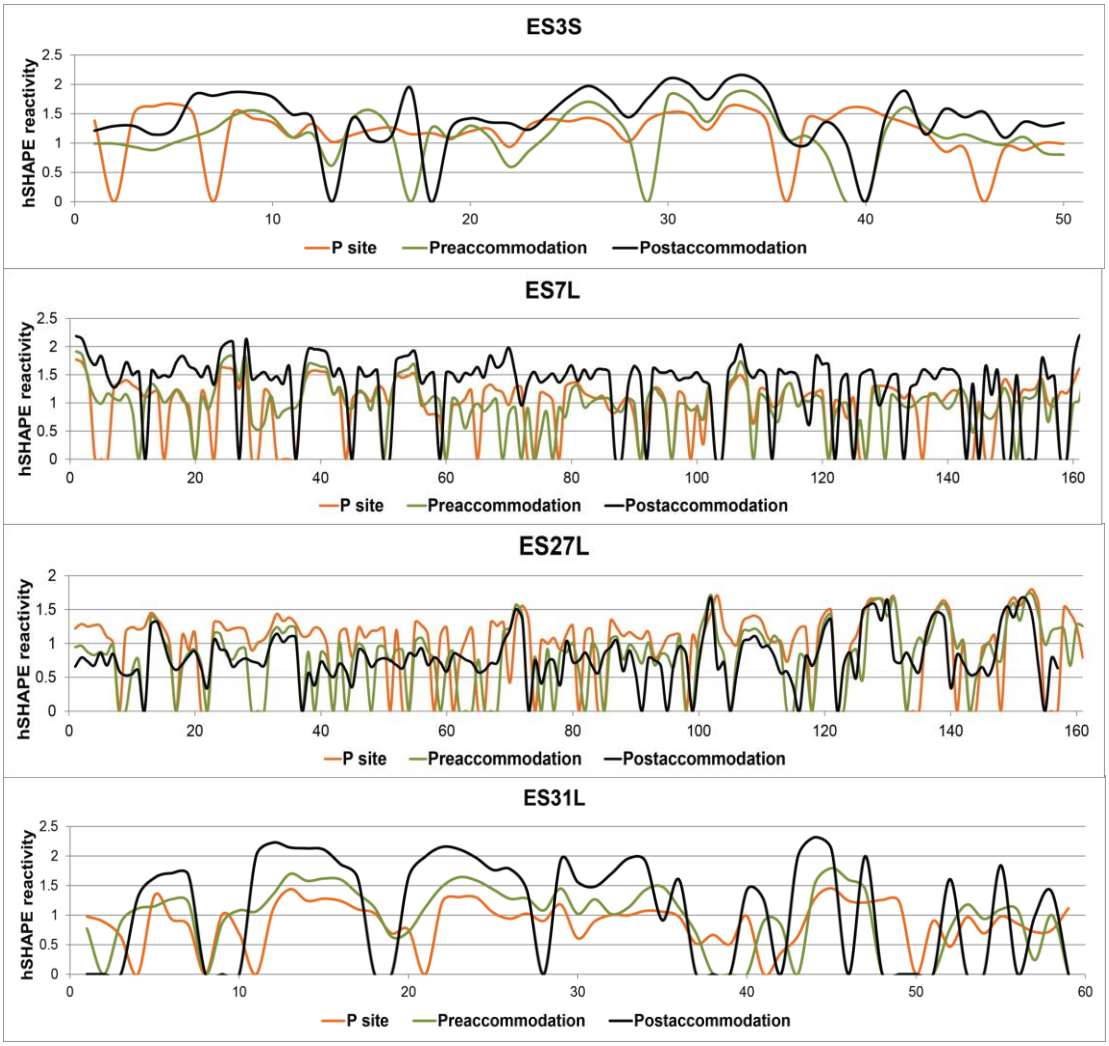

Figure 46. hSHAPE reactivity of different expansion segments in the accommodation related complexes.

The reactivities of ES3S, ES7L, ES27L and ES31L in P site occupied, preaccommodation and postaccommodation complexes are shown, and indicate overall increase or decrease in reactivity as accommodation proceeds.

These results indicate that expansion segments go through structural rearrangements during elongation, most notably during accommodation, suggesting potential roles for these eukaryote-specific elements at this step of translation.

4.2.5. Allosteric communication pathways

The ribosome is a very large protein-RNA complex and the functions of only few regions are well understood. It is generally assumed that the whole molecule is required for structural stability and that the main communication occurs between DC, PTC, and GAC, through tRNAs and transacting factors. However, studies have found that mutations within these regions may cause changes in rRNA structure extending into other regions [176–178]. Furthermore, ribosomal protein mutations that map to regions that are away from catalytic sites can affect both ribosome function and structure [179–182]. These indicate that information may be transferred to and from functional sites to distal regions of the ribosome, possibly through allostery. To find such "allosteric communication pathways" in the hSHAPE data, patterns of reactivity changes were examined. Nucleotides that did not show reactivity changes in one or more difference maps were omitted.

These analyses reveal that there is no single nucleotide whose reactivity continually increases or decreases as the ribosome progresses through the elongation cycle. There are also no nucleotides that only lose reactivity in pre-accommodation complex, or only in post-accommodation complex, or only in pre-translocation complex, or only in post-translocation complex. A single nucleotide, A3008, of LSU H94 is only deprotected in P site occupied ribosomes. There are no nucleotides that only lose reactivity in P site occupied ribosomes; this was expected since most or all

features of this complex are present in all of the other complexes as well (e.g. all of the complexes contain both a tRNA in the P-site and an mRNA).

Specific patterns were observed that highlight the relatively direct effects of (1) trans-acting factor binding, (2) rRNA structural rearrangements that occur during a specific step (e.g. accommodation or translocation), (3) structural rearrangements that occur between steps (i.e. accommodation and translocation). A five-symbol annotation is used to label the patterns, where (-) denotes a reactivity decrease while (+) denotes an increase, and the order of (-)s and (+)s match the difference maps: P site occupied vs empty → pre-accommodation vs P site occupied → post-accommodation vs pre-accommodation → pre-translocation vs post-accommodation → post-translocation vs pre-translocation.

The most common two patterns in the hSHAPE data are (-+-+-) and (+-+-+), i.e. the nucleotides sharing these patterns go through reactivity increases or decreases, respectively, only in pre-accommodation and pre-translocation complexes. Of the 5354 total nucleotides examined, 60 and 76 nucleotides, respectively, share these patterns. These patterns are mainly related to EF binding. The cyclical nature of these patterns is especially thought provoking as it may reinforce idea that of the sequential binding of these transacting factors ensures the unidirectionality of eukaryotic elongation.

4.2.5.1. Trans-acting factor binding patterns

As discussed in the previous section, the (-+-+-) and (+-+-+) patterns were of great interest (Table 9). Mapping of these enabled us to identify connections between nucleotides located in different functional regions, including H69 (decoding, the B2a

bridge), H82 (the P and E sites), H88 (the E site), H90 (the A site), and the SRL. Nucleotides from these regions showed decreased reactivity upon factor binding. Other known important regions were also highlighted as a result of different nucleotides either decresing or gaining reactivity upon factor binding: these include h23 (the B7b/c bridge), and h44 (decoding, and many bridges).

Helices	(-+-+-)		Helices	(+-+-+)		Helices	(--+-+)		Helices	(++-+-)
	5.8S			**5.8S**			**18S**			**18S**
SS	A41		H6	C57		B h24	C1006		h6a	C99
SS	A61			**18S**		h34	C1279		B h8	U144
SS	U74		h6	A86		B h42	U1552		B h13	C402
SS	G75		ES3	210		h43	A1592		SS	C435
	18S		ES3	236			**25S**		h17	C530
B h5	U44		B ES3	246		H42	C1216		B h23	U896
B h6	A65		h11	U318		H43	C1254		B h34	A1275
h6	C87		h11	G325		SS	C1257		h34	C1280
SS	U101		h11	G329		H41	U1336		h35	G1292
SS	U137		h11	C338		*SS*	*G1493*		h35	C1327
h8	G154		h11	G356		*H54*	*U1626*		h39	C1339
h9	A182		h12	G363					SS	U1413
h12	G365		h12	U374					h38	U1415
SS	A425		h12	C382					h41	U1532
B h18	G552		h16	G487					B h42	A1543
h20	U632		h22	G879					h42	G1548
ES6	C696		h23	U921					B h42	G1553
h23	G901		h23a	C937					B h43	C1596
B h23a	A939		B h22	A952					B h43	U1598
B h27	A1131		SS	A963					B h43	C1599
SS	A1287		h20	U968					h43	C1606
B h39	U1347		h27	C1128					SS	U1613
h39	U1350		B h33	A1244					h28	U1617
h39	G1364		h33	C1248					B h28	C1618
SS	C1634		h34	G1271					h28	U1621
h44	G1713		h40	G1408					h28	U1626
h44	G1718		h38	G1418					h28	U1627
h44	U1724		h41	G1498					h44	A1648
	25S		B h41	G1523					h44	G1649
B H11	G33		h43	U1604					h44	U1669
H17	G171		h44	G1680						**25S**
H17	G244		h44	U1682					B H11	A35
H16	G258		h44	U1725					B H11	G41
B H21	G282			**25S**					H41	A1182
B H31	A761		H11	U44					SS	A1190
H31	G774		H13	A89					*H50*	*A1498*
H33	U905		B H13	A99					*H50*	*G1517*
H37	G964		H15	G139					*H50*	*U1518*

ES12	G1089		H15	G143					*SS*	*U1555*
B H41	A1179		H14	A319					*SS*	*C1556*
H46	U1384		H2	U414					*H53*	*C1598*
H26a	A1446		ES7	G495					*H54*	*G1624*
H26a	U1448		ES7	G505					*B H59*	*C1761*
H47	*U1470*		ES7	U506					H76	U2505
H52	*C1550*		ES7	G510					H97	G3109
ES19	*U1564*		ES7	C515					H98	G3288
ES19	*G1565*		B ES7	A521					H98	G3289
H53	*C1597*		ES7	C539					H101	C3324
H54	*U1616*		ES7	U587						
ES26	*C1633*		ES7	C599						
H55	*G1652*		B ES7	G600						
H57	*A1676*		B H30	G726						
H58	*G1727*		H27	G787						
ES27	U1992		B H35	U871						
H67	C2192		H33	A904						
H61	C2350		H41	G1172						
H93	A2969		*H57*	*U1682*						
H96	G3052		*H54*	*A1823*						
H96	G3083		ES27	G1968						
ES39	C3249		ES27	G1987						
SS	A3299		H69	U2254						
H101	G3327		SS	U2334						
			H82	U2650						
			SS	G2658						
			H86	A2721						
			H88	A2769						
			H74	A2813						
			H90	G2939						
			H90	G2947						
			B 95	C3025						
			H96	G3059						
			B H96	G3080						
			H97	U3111						
			ES39	C3190						
			ES39	G3200						
			H98	U3287						
			B H100	A3307						
			B H101	U3329						

Table 9. Nucleotides involved in reactivity change patterns related to EF binding and dissociation.

The first two patterns focus on changes upon factor binding, the second two focus on factor dissociation. Eukaryote-specific components are shown in light blue. Known functional components (e.g. involved in tRNA binding / intersubunit bridges / decoding center / P and L1 stalks / peptide exit tunnel) are shown in dark blue. A nucleotide close to the PTC but not part of the known functional regions is shown in red. Nucleotides belonging to a domain at the back of the LSU (roughly opposite from the central protuberance) are italicized (please see the discussion section). SS denotes nucleotides from single stranded regions. A "B" in front of a helix name indicates the nucleotide is located in a loop or other single stranded portion of the helix.

We also examined (--+-+) and (++-+-) as other patterns related to trans-acting factors (Table 9). These appear be more related to factor dissociation than binding. A striking result from this analysis is the increase in reactivity of nucleotides located in the SSU head domain. Many nucleotides of the head domain become unreactive upon factor dissociation (i.e. in post-accommodation and post-translocation complexes). This may be a consequence of factor dissociation, of the simultaneous events taking place at these steps (e.g. rotation), or of both. As expected, the P stalk base shows decreased reactivity upon elongation factor binding (H42-44).

As the results discussed in Section 4.2.2.3. Elongation factor - rRNA interactions suggest, the reactivity of the EF binding site (especially the P stalk base) changes dramatically in the P site occupied complex compared to the empty ribosome. The (--+-+) and (++-+-) patterns may also be indicative of nucleotides that are affected in both P site occupied complex and the trans-acting factor bound complexes. In this case, the above interpretation might be modified from "EF dissociation" to "loss/gain of reactivity in P stalk base / GAC" as the cause of the changes listed in Table 9 (patterns (--+-+) and (++-+-)).

4.2.5.2. Patterns indicating rearrangements at a specific step

Next, we focused on nucleotides belonging to reactivity change patterns in accordance with rearrangements during the accommodation or translocation steps of elongation. For this analysis, patterns in which decreased reactivity was observed in only one complex were compared to their "partners" at specific steps in the elongation cycle (Table 10 and Table 11).

Helices	(+-+++)		Helices	(++-++)
	18S			**18S**
h10	C282		h3	C31
SS	A1139		h4	C36
h44	G1695		h26	G1046
	25S		SS	A1137
H41	C1183		SS	A1321
ES27	G1998		h42	U1567
H95	A3035		h28	G1629
H96	U3058		h44	A1678
ES39	G3199			**25S**
			H83	C2708

Table 10. Nucleotides involved in reactivity change patterns related to accommodation.

Eukaryote specific components are shown in light blue. Known functional components are shown in dark blue. Nucleotides close to the PTC but not part of the known functional regions are shown in red. SS denotes nucleotides from single stranded regions. A "B" in front of a helix name indicates the nucleotide is located in a loop or other single stranded portion of the helix.

Comparison of accommodation complexes using this rubric suggest that more communication pathways may be active in the pre-accommodation complex than post-accommodation, indicated by the number of nucleotides belonging to functionally important helices. The pattern (+-+++) may reflect eEF1A specific rearrangements as well. In this case, the identification of nucleotides in ES27 and ES39 suggest some specific involvement of these expansion segments in accommodation. Additionally, the eB13 intersubunit bridge that is involved in subunit rolling in mammalian ribosomes, may slightly rearrange in the pre-accommodation complex. The only LSU nucleotide that follows the (++-++) pattern (i.e. decreased reactivity in post-accommodation complex) is 2708, which is located in H83, part of the central protuberance (known to go through rearrangements upon tRNA binding [183,184]).

Similar to the results from accommodation complexes, additional communication pathways may be active in the eEF2-bound pre-translocation complex than post-translocation. The pattern (+++-+) may reflect eEF2 specific

rearrangements. In this case, the presence of a nucleotide from ES7 suggests some specific involvement of this expansion segment in translocation. Contrary to the pre-accommodation complex, there may also be some involvement of the PTC in the pre-translocation complex (red items in Table 11). No LSU nucleotide was observed to undergo a decrease in reactivity only in the post-translocation complex. This is an interesting, yet understandable observation, as most rearrangements between pre- and post-translocation complexes would be expected to take place in the SSU due to intersubunit rotation and translocation of mRNA:tRNA interaction by one codon on the SSU neck. Accordingly, most of the nucleotides following the (++++-) pattern are from the head and neck region of the SSU.

Helices	(+++-+)		Helices	(++++-)
	5.8S			**18S**
H4	U27		h16	C484
	18S		h39	G1352
B h23	U886		B h42	A1556
SS	A1256		h28	G1622
h34	G1267		h44	C1706
h42	U1564			
h44	G1690			
h44	G1692			
	25S			
SS	G400			
ES7	U540			
H46	C1411			
H68	A2220			
SS	A2280			
SS	C2362			
B H73	A2397			
H83	G2662			
H97	U3107			
SS	G3173			
SS	C3181			

Table 11. Nucleotides involved in reactivity change patterns related to translocation.

Eukaryote specific components are shown in light blue. Known functional components are shown in dark blue. Nucleotides close to the PTC but not part of the known functional regions are shown in red. SS denotes nucleotides from single stranded regions. A "B" in front of a helix name indicates the nucleotide is located in a loop or other single stranded portion of the helix.

4.2.5.3. Patterns indicating rearrangements in-between steps of the elongation cycle

Patterns of changes in base reactivity that suggest rearrangements leading to a switch between accommodation and translocation were also examined. For this analysis, patterns that showed opposing reactivity changes in accommodation and translocation complexes were identified (Table 12). There are no nucleotides belonging to the (---++) pattern, i.e. no nucleotides that are protected in P site occupied, pre-accommodation, post-accommodation complexes, yet deprotected in translocation complexes.

Helices	(+++--)		Helices	(-++--)		Helices	(+--++)
	18S			**5.8S**			**18S**
ES6	G845		SS	G63		B h1	G10
	25S			**18S**		h2	U12
H25	U430		h11	G330		h3	U27
SS	G1646			**25S**		B h7	U304
H68	U2226		SS	G420		h18	G561
B H72	G2377		SS	G421		h23	A884
SS	U3319		ES7	G474		B h23	U916
			ES7	G538		SS	U1232
			ES7	G575			**25S**
			H27	C670		H11	U32
			H30	G728		H39	U1138
			H31	A751		H60	U1871
			H33	G826		H63	G1949
			H45	A1363		ES27	G2042
			H46	G1379		ES27	C2064
			H46	C1396		SS	C2797
			B H68	A2198		H94	C3004
			H68	G2236		H95	A3017
			B H69	C2257		B H95	G3028
			B H69	U2260		H96	G3085
			H69	A2262		B H97	A3106
			H26a	C2359		H99	U3297
			H73	G2395			
			H76	G2442			
			H75	A2601			
			H84	C2682			
			B H85	A2694			
			H101	C3321			

Table 12. Nucleotides involved in reactivity change patterns related to a switch from the accommodation to translocation steps of elongation.

In these patterns, accommodation and translocation complexes have opposing changes in reactivity (e.g. nucleotides losing reactivity through accommodation, but gaining through translocation are indicated by the last pattern). No nucleotide belonged to the pattern (---++). Eukaryote specific components are shown in light blue. Known functional components are shown in dark blue. Nucleotides close to the PTC but not part of the known functional regions are shown in red. SS denotes nucleotides from single stranded regions. A "B" in front of a helix name indicates the nucleotide is located in a loop or other single stranded portion of the helix.

One possible structural switch may be reflected by decreased reactivity in ES27 and ES7 in the accommodation and translocation complexes, respectively. Additionally, PTC rearrangements appear to be more highly implicated in translocation rather than accommodation (red nucleotides in Table 12). Decreased reactivity in a nucleotide of H76 in pattern (-++--) is in accordance with L1 stalk rearrangements related to E site tRNA interactions and translocation [185,186]. Interestingly, this pattern of decreased reactivity is also observed in the P site occupied complex, and thus it may be more appropriate to interpret this as a change that is not present in accommodation, rather than one present in translocation. Different bridges are impacted at different steps, too, such as B2a (H69) and eB11 (H101) in translocation, and B7b/c (h23) in accommodation.

4.3. Discussion

The eukaryotic translation elongation cycle is similar to its bacterial counterpart, with the same main steps and homologous transacting factors. However, given the increased size of the eukaryotic ribosome and the recently described novel intersubunit motions in mammalian ribosomes, the differences may be greater than previously thought. In this study, we walked the ribosome through an entire round of elongation, and using hSHAPE to determine the changes in rRNA flexibility, we obtained a complete dynamic view of the rRNA bases in the elongating ribosome.

Our analyses included validation by comparison to previously reported changes localized in conserved functional regions, to novel changes in eukaryote-specific regions of the ribosome. We also identified the nucleotides that share reactivity change patterns throughout the elongation cycle, supporting the model of linked long range interactions that constitute complex-wide information exchange pathways.

The hSHAPE analyses of ribosomes harboring tRNAs reveal that the yeast P site shares "hybrid" features between bacterial and mammalian sites (Figure 42, Table 13). In the 40S subunit, the yeast P site protection data closely matches the tRNA/rRNA interactions observed in mammalian cryo-EM structures. In contrast, the yeast 60S P site hSHAPE protection patterns are a better match to the 50S P site/tRNA cleavage patterns obtained from bacterial hydroxyl radical cleavage studies. These findings may provide some novel insight into the evolution of the ribosome, suggesting that the 40S subunit was first reengineered in the eukaryotes to accommodate a more intricate initiation process, followed by further evolution of the 60S subunit in higher eukaryotes. Results obtained from the posttranslocation complexes reinforce the similarities between the yeast and bacterial P sites (through hydroxyl radical cleavage), while highlighting the differences between the respective P sites in the small subunits (most dramatically observed by loss of reactivity at SSU nucleotides A1001-G1002). One caveat to this comparison however is the differences between hSHAPE and hydroxyl radical cleavage: the former modifies specific nucleotides while the latter targets both exposed bases and their near-neighbors. Overall, further experimentation and higher resolution structures will be required in order to define the yeast P site, as well as A and E sites at atomic resolution,

improving on the low resolution structures available currently [187–190]. Archaeal ribosomes may be another intermediate to examine [191], however the available high resolution structures do not contain the fully associated 70S archaeal ribosome and rely heavily on the eubacterial ribosome as a model [192–195].

Prokaryotic P site		Mammalian P site	
SSU	**LSU**	**SSU**	**LSU**
G577-A580	C2284-C2290	C1000-G1002	U2408-U2410
A905	U2297-A2299	G1169-A1171	U2423-A2424
A1005-C1007	G2302-A2309	C1190-C1192	U2771-C2772
A1151	G2619-A2626	A1194-C1195	G2778-A2779
C1192	A2808	C1461-G1466	A2813-G2814
A1576-77	A2820	G1574-U1579	U2861-G2863
G1638-C39	U2861-G2863	G1622	U2978-79
	U2953-54	A1635-C1639	A3129-30
	C2963-G2972		

Table 13. Comparison of the matches between the observed yeast P site and the prokaryotic / mammalian P sites.

Nucleotides from previous bacterial and mammalian studies are listed, and the nucleotide ranges that match the observed yeast P site (based on the results from both P site occupied complex and posttranslocation complex) are marked in green. We cannot obtain data between 18S nucleotides G1140-G1200 (grey) by hSHAPE due to presence of highly modified bases in the region, inducing strong stops in the primer extension reaction.

Analyses of the hSHAPE data pertaining to the intersubunit bridges indicate that one size does not fit all, as there seem to be major rearrangements or reactivity differences in the bridge regions among ribosomes of similar rotational status (*i.e.* rotated or nonrotated). This implies that the notions of "rotated" and "nonrotated" states are overly simplistic. Indeed, time-resolved cryo-EM has revealed over 50 conformations of the bacterial ribosome [196], and other studies have identified tRNA binding "substates" wherein various portions of tRNAs make interactions with the ribosome that are "in-between" previously defined tRNA binding sites [51,197,126]. Hence our hSHAPE data reinforce the notion that the ribosome can assume numerous "sub-rotational statuses".

Analyses of the data pertaining to the expansion segments indicate consistent rearrangements in most of these elements as translation elongation progresses from the P site occupied complex to postaccommodation complex. This suggests that they undergo dynamic rearrangements during the process of aa-tRNA accommodation. An interesting pattern revealed by hSHAPE is that some expansion segments either lose (eg. ES27L) or gain (eg. ES3S, ES7L, ES31L) reactivity in their entirety through the accommodation process, but that during translocation, only shorter stretches show reactivity changes.

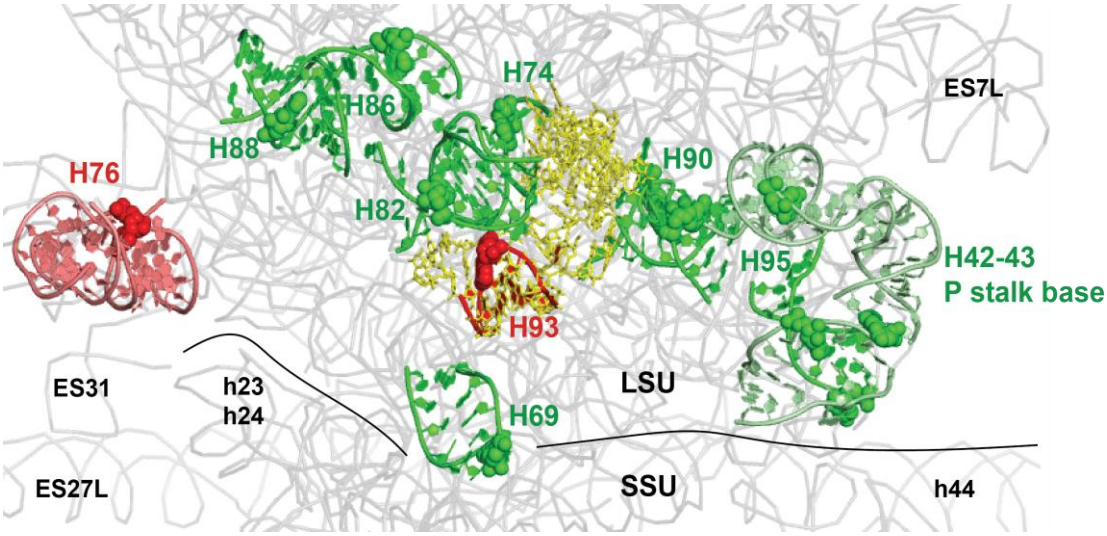

Figure 47. Pathway between EF binding site and tRNA binding sites.

Please see text for details. In this view, tRNA binding sites are visible between the 40S (SSU) head and 60S (LSU) central protuberance. Nucleotides (spheres) which are only protected in factor bound complexes and the helices in which they are located are shown in bright green. Nucleotides protected in both factor bound complexes and P site occupied complex (and the corresponding helices) are shown in pale green. Nucleotides that are only reactive in factor bound complexes (and the corresponding helices) are shown in red. Nucleotides reactive in both factor bound complexes and P site occupied complex (and the corresponding helices) are shown in light red. The peptidyltransferase center is shown in yellow. The green helices, except H69, lie in a "branched line" covering parts of all tRNA binding sites, bridging these and the EF binding site.

Analyses of the patterns of reactivity changes in the hSHAPE data also appears to indicate, that elongation factor binding (either eEF1A or eEF2) triggers similar reactivity changes in a set of nucleotides located in different helices. These

include but are not limited to h23 and h44 in the SSU, and H69, H82, H88, H90, SRL, H101 in the LSU. The reactivity of these nucleotides all change in the same direction as the ribosome progresses from one complex to the other. In addition, they are all protected in both the pre-accommodation and pre-translocation complexes. These observations suggest the existence of a physical linkage or "information exchange pathway" encompassing the EF binding site, the afforementioned functionally important helices, and others that we do not know the function of. Some of the helices that are revealed in this analysis, including h23, h38, h39, h41, h43, H74, H82, H86, and H88, are a remarkable match to a previously defined communication pathway spanning the two subunits through B1b/c intersubunit bridge that were identified using mutants of ribosomal protein L11 [179].

As Figure 47 shows, the hSHAPE data provides a pathway between the elongation binding site (P stalk and H95 - sarcin ricin loop) and A, P and E sites. Nucleotides from H42, H43, H95, H90, H69, H74, H82, H86 and H88 lose reactivity in the factor bound complexes (Section 4.2.5.1). H42 and 43 also have low reactivity in the P site occupied complex compared to empty ribosomes. H42-43 and H95/SRL form part of the elongation factor binding site. H90 forms part of the accommodation corridor leading to the A site of peptidyltransferase center / PTC. H69 forms part of the decoding center, as well as part of the B2a bridge. H74 is in close proximity to the PTC and seems to form a bridge towards H86 and H88 which harbors part of the E site. H82 is also in close proximity to the PTC and forms part of the P site. Nucleotides from H76 and H93 gain reactivity in the factor bound complexes. H76 also has high reactivity in the P site occupied complex compared to empty ribosomes.

H76 forms part of the L1 stalk base and is associated with E site tRNA movements. H93 forms part of the A site. Taken as a whole, we suggest an allosteric communication pathway that starts at the EF binding site, reaches into the PTC, and from there separates into branches, one of which spans the A, P and E sites, and a second that may employ the A site tRNA to reach to H69 and across the B2a bridge to the decoding center.

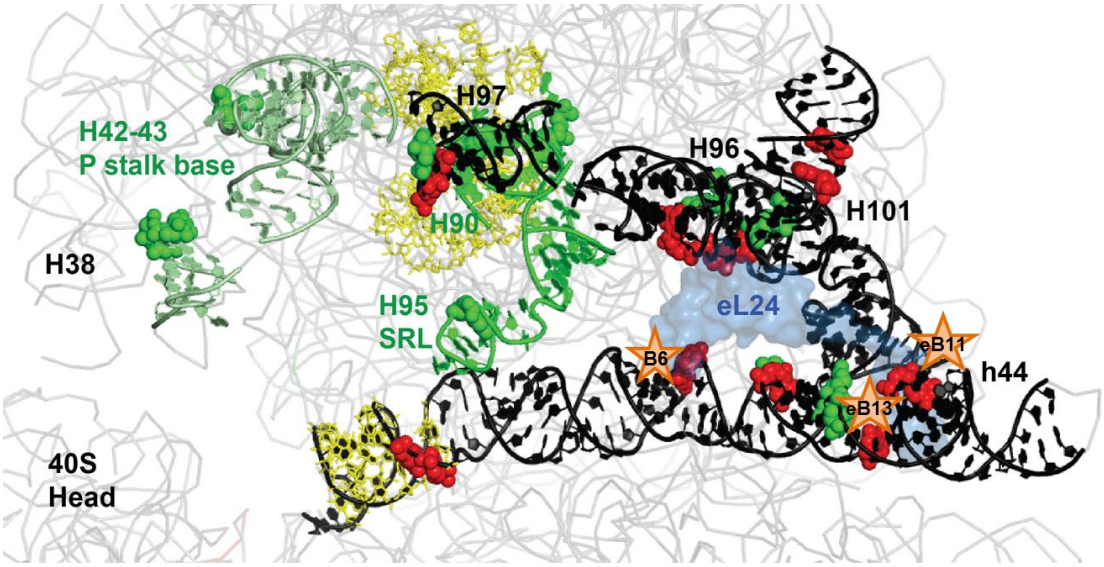

Figure 48. Pathways between EF binding site and the intersubunit bridges B6, eB11, eB13.

Please see text for details. Coloring is the same as Figure 47, with additions. Helices that harbor both protected and reactive nucleotides are shown in black. Proteins are shown in blue. Peptidyltransferase and decoding centers are shown in yellow. Bridges are shown as orange stars. Information may flow through H96 to bridges B6, eB13 (through eL24 and h44), or eB11 (through H101 and eS8 - not present in this structure) towards the SSU from H95/SRL.

The flexibility of select nucleotides in H76 (following different patterns of reactivity changes) may be due to the bending of the L1 stalk towards or away from the E site, depending upon the step of elongation. Different conformations may be exposing different nucleotides of this helix to chemical attack. On the other hand, the flexibility of select nucleotides in H93 may be due to changes in the occupancy of the LSU A site, possibly acting as a sensor for the A site tRNA on the suggested pathway. The opposing reactivity of H69 may be on par with the role of H93, or lack

thereof, since, in contrast to the LSU, the SSU A site is not vacant in any of the factor bound complexes.

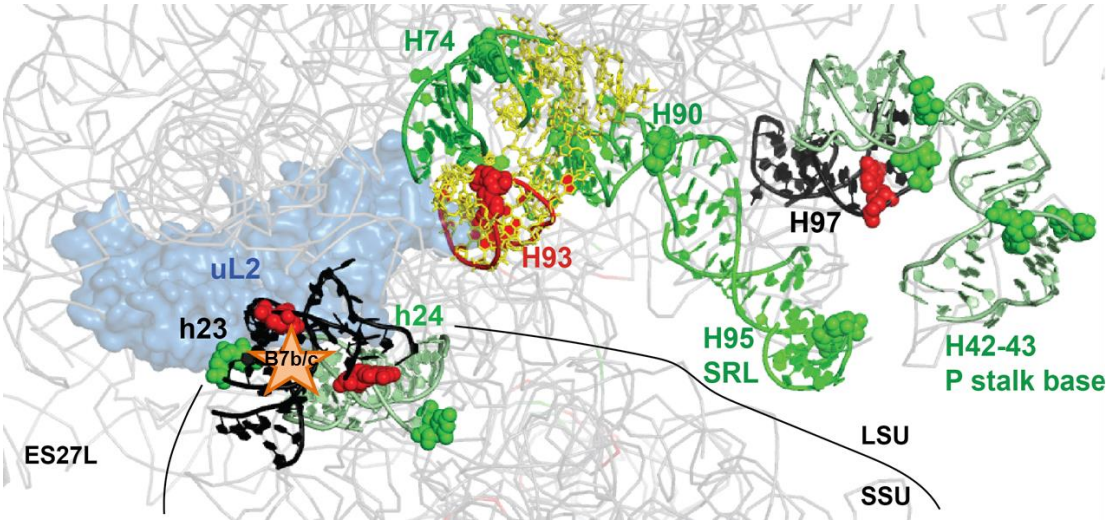

Figure 49. Pathway between EF binding site and the intersubunit bridge B7b/c.

Please see text for details. Coloring is the same as Figure 47 and Figure 48. Another bridge implicated in the reactivity change pattern results is B7b/c. Information may flow to SSU through uL2 - h23/24 interaction from EF binding site. Components that bridge uL2 and EF binding site are H97, H90 and H74.

Examination of the same sets of nucleotides suggests the presence of additional pathways connecting EF binding to intersubunit bridges. Factor binding, especially eEF2, causes major rearrangements in the bridge regions hence these pathways are of great interest. Figure 48 shows a potential pathway governing part of the bridges B6, eB11 and eB13. H95/SRL may connect to H101 through H96, which have low reactivity nucleotides in close proximity, possibly allowing interaction. H101 in turn interacts with eS8 (not present in the ribosome structures used), forming most of eB11. H96 also contacts eL24, which interacts with h44 in return to form parts of B6 and eB13 bridges. All these bridges have been implicated in subunit rolling of the mammalian ribosomes. The increase in reactivity on H96 and h44 clusters around eL24 contact points, hence in factor bound complexes B6 and eB13

may be dramatically rearranged. This is partially in accordance with the results of Section 4.2.3.

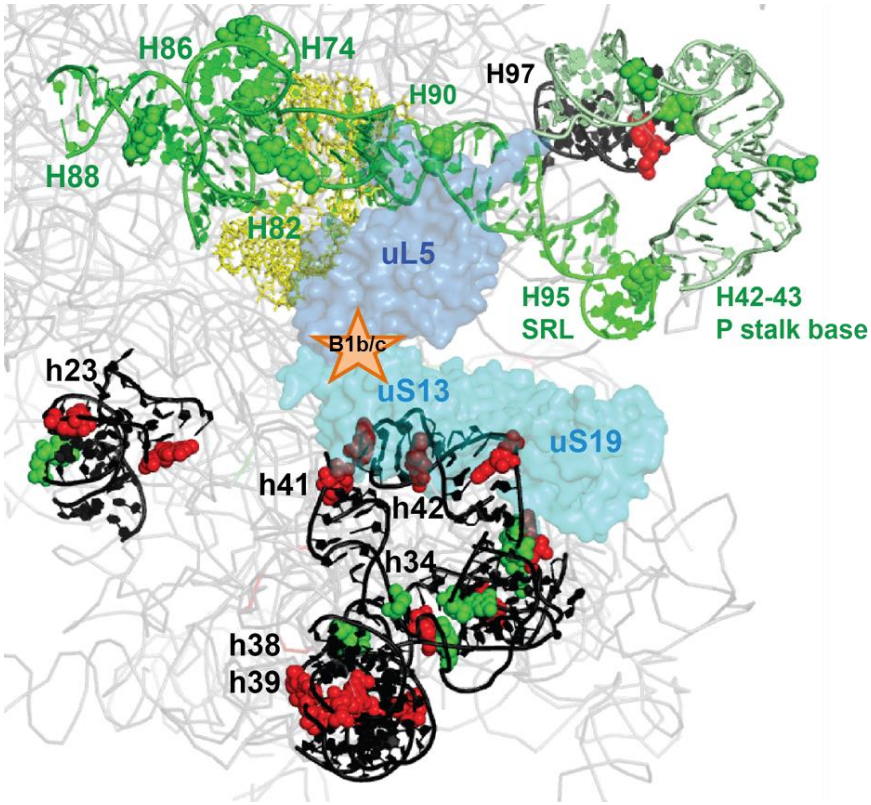

Figure 50. Comparison of hSHAPE data to the B1b/c pathway.

Please see text for details. Coloring is the same as Figure 47 and Figure 48. Information may be flowing through B1b/c from LSU towards the SSU. The opposing reactivities indicate "switch"es throughout elongation. h23 reactivity changes may be due to rearrangements of B7b/c rather than B1b/c.

The hSHAPE data also reveal a cluster of h44 nucleotides close to the decoding center that go through reactivity changes in correlation with EF binding and dissociation. This, together with the reactivity change seen at the tip of H69, and the reactivity changes in h11 and h12 of SSU, may indicate how the decoding center is networked with the whole ribosome. SSU helices 11 and 12 lie in close proximity to h44 decoding center [198], even though their exact roles in translation, if any, are not known.

Figure 49 shows a possible allosteric communication pathway between the EF binding site and B7b/c bridge. Upon EF binding, rearrangements occur in H90 both through H95/SRL and H97. This passes onto H74 which is in close proximity to uL2. uL2 in turn contacts h23-24 of small subunit to form B7b/c. The presence of nucleotides of opposing reactivities at the h23-uL2 interface may be indicative of a switch from nonrotated to rotated conformations (and vice versa) upon factor binding (and dissociation).

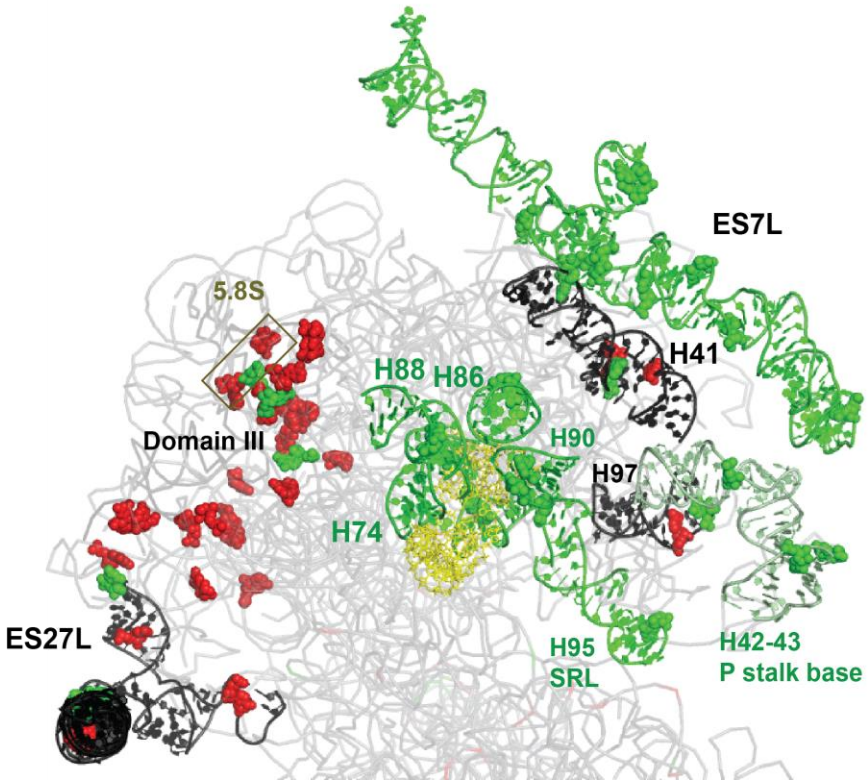

Figure 51. Pathways between EF binding site and the expansion segments ES7L, ES27L.
Please see text for details. Coloring is the same as Figure 47 and Figure 48. Information may flow through H41 from P stalk to ES7L, while Domain III may be important in a pathway towards ES27L.

As mentioned previously, the helices and loop regions that were described to take place in a communication pathway governing the B1b/c bridge [179] aligned well with the hSHAPE data and patterns of reactivity changes in the current study (Figure 50). Nucleotides from h23, h34, h38, h39, h41, h42, H82, H84, and H88 were

identified as participating in this pathway. Additional nucleotides mapped to regions in-between helices, implicating H74 and H86 as well. In our data, even though nucleotides from H84 display decreased reactivity in one or both complexes with an elongation factor, there is a point at which no noticeable reactivity change occurs. We do not recover nucleotides that show no reactivity change at any given point with the pattern search yet, hence H84 nucleotides are not classified into patterns currently. Improving the pattern search to include lack of changes in reactivity may solve this problem, supporting the B7b/c bridge branch of our network of pathways, and may enable other previously described communication pathways [181,199] to surface in our data.

The B1b/c bridge pathway in the hSHAPE data may be extending from EF binding sites, passing through the PTC, and then moving through H82 to the central protuberance and uL5. In fact, a nucleotide in a single stranded region between H82 and H83, A2658, loses reactivity in the factor bound complexes, and is in close proximity to uL5. uL5 in turn contacts uS13. Both uS13 and another interacting protein, uS19, then contact h41 and 42, and the "information" is transferred further into the SSU to h34, 38 and 39. According to our data, h23 is part of a pathway governing the B7b/c bridge. Hence an explanation for the presence of a h23 nucleotide in the previously described B1b/c pathway may be that the uL5 mutations introduced cause a shift in rotational equilibrium, impacting the B7b/c bridge as well.

We also identified pathways that connect the EF binding site and expansion segments ES7L and ES27L (Figure 51). The results from Sections 4.2.4 and 4.2.5, and the location of ES7L impart a potential role to this expansion segment in EF

binding. In addition to this, H41 may contact both the P stalk helices and ES7L, allowing information flow. For a potential ES27L pathway, the solvent exposed "back" of the SSU, specifically Domain III, may be important. Most nucleotides from this domain (which contacts 5.8S rRNA, and contains Helices 47-59 including H50 - part of the peptide exit tunnel) are reactive in the factor bound complexes, and lose reactivity upon factor dissociation. Thus, a communication pathway between PTC/H74 and ES27L may form in the absence of EFs.

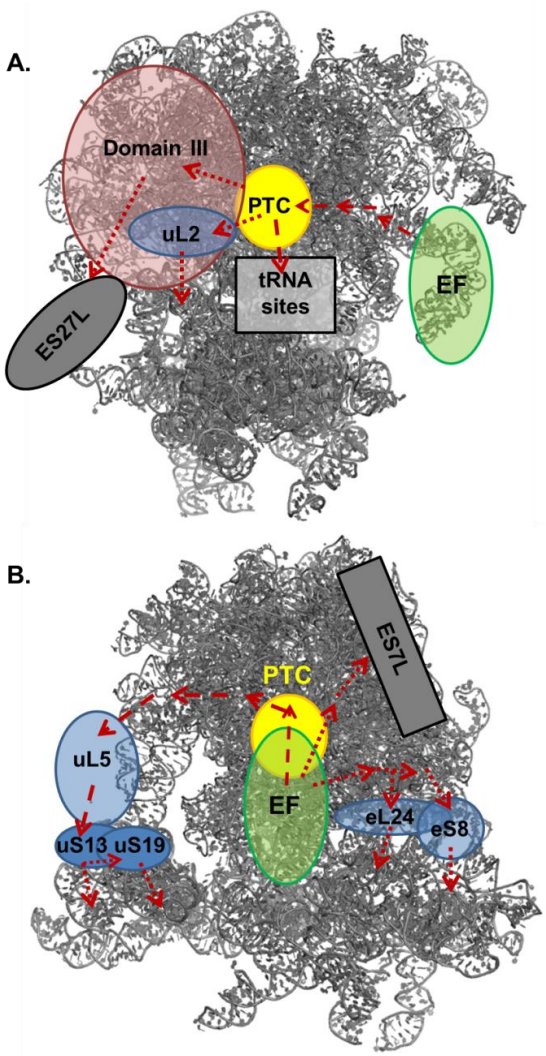

Figure 52. Possible network of elongation factor binding related communication pathways in yeast ribosomes.

According to this model, "information" is generally received by the PTC from EF binding sites and is then distributed to different parts of the ribosome, including bridges and expansion segments. A. View

through the tRNA binding sites. PTC may distribute signals to tRNA binding sites, and/or to SSU through B7b/c bridge, and/or to the "back" of the ribosome, to Domain III and ES27L. B. View through the P stalk. PTC may distribute signals to SSU through B1b/c and/or B6, eB11, eB13 bridges as well. There may also be a path from the P stalk / SRL to ES7L that does not employ the PTC. These pathways may also be acting in reverse (please see text).

Figure 52 summarizes the possible allosteric information exchange pathways that allow different functional regions of the ribosome to communicate with one another as the ribosome progresses through the elongation cycle. This model suggests that EF binding and/or dissociation may influence individual intersubunit bridge conformations, supporting the hypothesis that the ribosome goes through many different rotational statuses throughout the elongation cycle. Further work, including mutational analyses, probing of ribosomal mutants by hSHAPE, and improvements to computational algorithms employed, are required to further map the dynamic features of these intra-ribosomal communication networks.

Pattern searching is a very recent and promising addition to analyses of hSHAPE results. Hence there is room for improvement. As noted above, the search should not remain limited to reactivity increases or decreases in difference maps, but should also include instances of no change. This way, in-depth pathways may be obtained, e.g. it may be possible to "connect the dots" from H90 to H74, as this information transmission pathway lies at the center of our current model. In fact, preliminary manual pattern searching in PTC reveals bases C2821 and U2865-66 as nucleotides that lose reactivity in factor bound complexes, lowering the distance between H74 and H90 to about 8Å from 30Å. Nucleotide C2821 continues to lose reactivity in the posttranslocation complex, while U2865-66 do not show a change in reactivity between pre- and postaccommodation complexes, hence not appearing in the results of our current pattern search. These and other nucleotides of the PTC

should be subjected to more complex analyses for patterns of reactivity changes, since they may be important not only in bridging the EF binding site to other locations but in many more pathways possibly not related to the effects of EF binding.

Even though in the scope of this work we focused on patterns that are quite specific to certain events, some of the patterns obtained may be reflective of more than one type of rearrangement in the complexes, such as rotational status and / or elongation factor binding and / or conformational changes occurring at specific steps of elongation (*i.e.* accommodation or translocation), hence opening our results to different interpretations. Still, nucleotides sharing the same pattern through the elongation cycle may implicate allosteric changes in reactivity between diverse regions of the ribosome, including non-catalytic sites, and should be explored further through mutational and structural analyses.

Finally, our findings may be summarized in a list:

- mRNA binding results (Table 2, Figure 41) are in accordance with the reported and expected changes in the literature [135,200], validating our experimental approach.
- Elongation factor binding results (Tables 5 and 6) are generally in accordance with the reported and expected changes as well [33,201,188,202]. There are nucleotides that deviate from the expected changes which should be examined further. A major unexpected finding is the protection of the P stalk base in the P site occupied ribosomes Figure 43. Given the possible communication pathways that connect the P stalk base and / or the sarcin-ricin loop to the small subunit (Figures 48-50), this may be due to the effects of the rotational status of this complex on the elongation factor

binding site. This, in turn, would indicate the possibility that the network of communication pathways shown in Figure 52 may be active in both directions; whereby different regions of the ribosome influence elongation factor binding site rearrangements.

- tRNA binding results (Tables 3 and 4) both revealed nucleotides that act in accordance with the reported and expected changes in the literature [127,149], and ones that deviated from these. Visual analyses of the yeast P site employing a model tRNA [175] (Table 13 and Figure 42) revealed the possibility that the P site of the yeast may be an intermediate between the bacterial and mammalian P sites (please see above for details).
- Intersubunit bridge results (Tables 7 and 8, Figure 44) were quite different than what was expected in the literature [2,203], with the P site occupied complex giving the best fit to the list of reported intersubunit contact points in the nonrotated conformation. We conclude that the interface between the two ribosomal subunits is more "fluid" than what has been reported until now, in X-ray crystallography studies and in low resolution cryo-EM studies, revealing the presence of multiple rotated and nonrotated conformations (please see above for details). This may be possible by the different elongation factor binding site rearrangements we see with various complexes, and, in turn, the individual effects of these rearrangements on intersubunit bridges, through the revealed network of communication pathways. Molecular dynamics simulations of our data (please see Chapter 5: Conclusion and future directions) and examination of our elongation complexes with high resolution cryo-EM may shed more light on the data obtained from the intersubunit bridges.

- Our data provide novel insight into the rearrangements of the expansion segments of the rRNA throughout the elongation cycle (Figure 46), indicating possible roles of these in accommodation specifically (please see above for details). The revealed network of communication pathways further imply that ES7L rearrangements may be related to elongation factor binding (Figure 51).
- The data are also a rich source for examination of nucleotides that lose or gain reactivity together at the same steps of the elongation cycle (Tables 9-12). Highlighting these in the three dimensional structure of the yeast ribosome reveals a network of possible communication pathways with the elongation factor binding sites at the center (Figures 47-52). Our main hypothesis states that, upon elongation factor binding, information flows from the factor binding site to the peptidyl transferase center, where it is distributed further to different regions of the ribosome. There are pathways of information flow that do not pass through the peptidyl transferase center as well. A more comprehensive interpretation of all of our major findings indicate that these pathways may also be functioning in reverse, such that the rearrangements at intersubunit bridges (*i.e.* the rotational status) of the ribosome may be influencing the rearrangements of the elongation factor binding site.

Chapter 5: Conclusion and future directions

Recent structural advances in the disciplines of ribosome structural biology and translation have yielded an accurate, high resolution static view of ribosomes from different species, including the eukaryotic model organism *S. cerevisiae*. The race is now on to uncover as much information on ribosomal dynamics as possible, to generate a more complete view of this highly dynamic machinery and to connect structural changes to functional consequences.

In this project, our aim was to use rRNA flexibility as a tool to obtain information on ribosomal dynamics. To this end, our main system was the eukaryotic elongation cycle. Comparison of our results with bacterial studies revealed significant differences, adding to a line of work that is revealing eukaryotic elongation to be more complex in some ways than the bacterial counterpart. Important implications of this work include (1) differences in tRNA binding sites, (2) an improved view of rotation and intersubunit motions, (3) possible communication networks linking the elongation factor binding sites with various regions of the ribosome, including intersubunit bridges and eukaryote-specific elements.

Paving the way to these important observations were modifications to the method used to detect changes in rRNA flexibility, hSHAPE. Chapter 2 describes these improvements. To the present advantages of this method, including the ease of optimization and the high dynamic range of the non-base specific chemicals employed, new ones were added, including accurate data normalization and decreasees in data loss, making hSHAPE suitable for use with eukaryotic rRNA.

Chapter 3 shows that the improved hSHAPE analyses can be used to detect fine changes in rRNA flexibility, which indicated that the different initiation complexes examined resembled the closed, scanning-repressive state of the small subunit. We also attempted to locate the binding site of eukaryotic initiation factor 5, and observed different candidate sites depending on presence or absence of other initiation factors on the small subunit.

We performed detailed analyses on rRNA derived from complexes resembling different steps of translation elongation cycle in Chapter 4. We used functional regions, such as tRNA binding sites, to validate our method, then expanded to examine an area of active research in the field with analyses of intersubunit bridges, and finally delved into the unknown with analyses of the dynamics of the eukaryotic expansion segments, and generated preliminary maps of potential allosteric communication pathways.

Our approach, while giving us promising results for future, was not without pitfalls. One very important problem is that we worked with heterogeneous populations of complexes, as indicated by the results from biochemical assays. The P site occupancy of our ribosomes was about 90%; leaving 10% of empty ribosomes with each complex we built on top of the P site occupied ones. The A site occupancy was even lower at about 60%; leaving about 30% of complexes with only a P site tRNA in our experiments. Translocation may have introduced more variables, as the efficiency of this was slightly larger than 60%, at 70%, meaning that on top of the post-accommodation complexes, eEF2 could have reacted with 10% more of the ribosome population in our preparations. These only account for experimental

heterogeneity; resulting from technical problems with ribosome purification and / or binding of various substrates and elongation factors to the ribosome. Cryo-EM and sm-FRET studies indicate that there are naturally occurring heterogeneous populations of ribosomes, as well: for example there are pre-accommodation ribosomes with slightly but noticeably different conformations (e.g. before or after codon recognition) [26]. Overall, both different natural populations of ribosomes and the substoichiometric occupancies of these populations by the substrates of interest (*eg*. A site tRNA binding) may have effects on our rRNA probing results, decreasing the signal magnitude.

The most direct way to address the problem of naturally occurring heterogeneous ribosome populations would be to employ single molecule techniques. However, there may be relatively simpler solutions to experimental heterogeneity. Use of differentially tagged ribosomes and substrates may be an option. Crosslinking would be necessary for affinity purification of complexes since complex assembly *in vitro* relies on a state of equilibrium with bound and unbound substrates. Another option may be coupling massively parallel sequencing with hSHAPE [204], allowing for detection of chemical adducts on single RNA strands, similar to mutational profiling. The technique is currently applicable to short RNA molecules, as identifying two different primer reads as coming from the same RNA molecule is challenging. For hSHAPE of rRNA, optimization could be possible by performing this only on empty ribosomes at first, obtaining all possible locations the chemical could bind to in any of the reads, especially focusing on identifying regions such as the bridges, and then

subtracting these from other complexes as we advance. Still, solving this problem will be challenging.

Another problem with the hSHAPE analyses of rRNA is that currently we employ 3' end primers that are complementary to the 3' end of rRNA, causing us to lose some data from these ends. This could be solved by ligation of a short stretch of RNA after the hSHAPE reaction and RNA purification, before primer extension, and employing 3' end primers that are complementary to this "linker."

A general problem with assembly of translation complexes *in vitro* is use of high magnesium concentrations (10-15 mM), which are actually inhibitory to translation compared to *in vivo* conditions (1-2 mM) [205]. The translation inhibition may be related to changes in conformation of ribosomes under high magnesium levels. This is a current problem with all ribosomal dynamics studies, as it would require purification of complexes from cell lysates, which only yields a handful of complexes as some states are possibly very short-lived. Another potential problem that impacts the value of our results for translation in vivo is our starting complex. Due to the relative simplicity of translation initiation in bacteria, studies have been conducted where elongation complexes have been built after initiation takes place. Replicating this with eukaryotic ribosomes is challenging. *In vitro* reconstituted eukaryotic translation initiation systems are now available, and have been shown to allow subunit joining to yield 80S ribosomes [19,206]. In fact, they have also been used to reconstitute elongation and termination events [207]. While it would potentially be lucrative to adapt this system to structural probing, it may introduce too much heterogeneity to the ribosome populations, and overwhelm the potential solutions to

the hetereogeneity problem. The use of an mRNA template with Kozak sequence [175], while less exciting than using *in vitro* reconstituted yeast translation systems, may provide a slight relief to the problem of "artificial" start complex. This would at least mimic the interactions of the rRNA with the full start codon context.

There are also challenges to the use of hSHAPE data directly for insight into ribosomal dynamics. One such challenge is the lack of information on ribosomal protein dynamics. Compared to bacterial ribosomes, both the rRNA and the ribosomal protein repertoire of the eukaryotic ribosomes increase, with additional sequences added to both types of molecules. In fact, the ratio of the total amounts of rRNA and proteins in the ribosome increases from 2:1 to 1:1 in yeast. Ribosomal proteins are thought to have active roles in eukaryotic translation [180,208–210], and some eukaryote-specific proteins engage in eukaryotic intersubunit bridges, indicating that proteins may be dictating the intersubunit motions to a larger degree in eukaryotes. Added to the fact that the protein components of the dynamic P (L7/L12 in bacteria) and L1 stalks are known to be functionally important in all domains of life, data based on rRNA may be losing valuable information on ribosomal dynamics. It may be possible to recover some of this information through coupling hSHAPE with predictive tools.

Another hSHAPE-specific challenge is the importance of the same regions in rRNA for more than one process, e.g. different intersubunit bridges may partially overlap with each other or with tRNA binding sites. A similar challenge results from the fact that hSHAPE is sensitive to all nucleotide interactions, including stacking and basepairing, as well as any other source of stabilization of nucleotides. Hence upon

encountering reactivity changes, it is difficult to estimate if the change is due mostly to variations in the same plane with the nucleotide (i.e. basepairing) or in different planes (i.e. stacking and others). This may be solved through careful, computational, delineation of all "forces" acting on rRNA nucleotides, and interpretation of data to include all possible explanations. Three dimensional visualization and analyses of hSHAPE data would be very valuable to overcome the listed protocol-specific challenges.

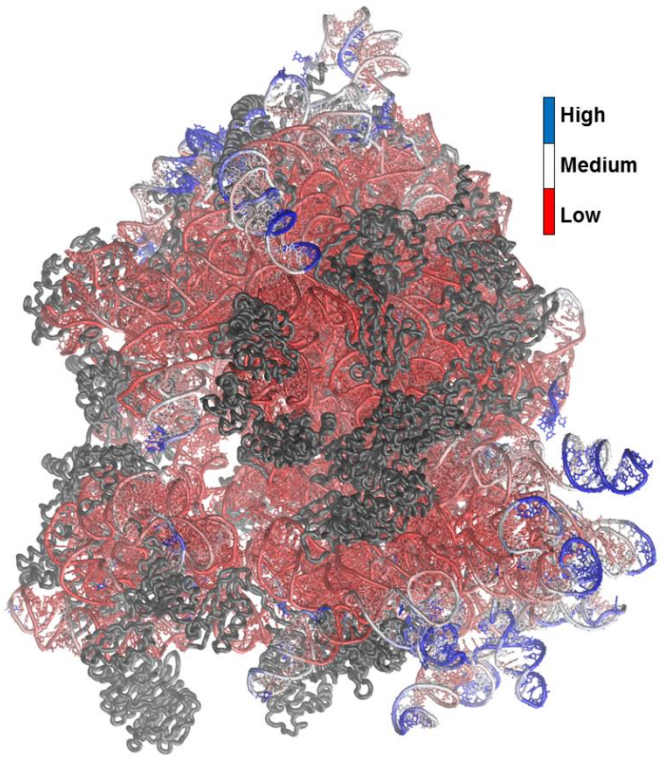

Figure 53. MD-SHAPE analysis of the empty 80S ribosome.

Please see text for details. The flexibility color code is shown on the right. Proteins are shown in grey. Exposed rRNA regions are highly flexible, whereas regions covered by proteins are not. These analyses, with improved coloring, will be very useful in determination of the underlying causes of flexibility changes, including protein-RNA interactions as potential causes of such changes. Image generated by our collaborators, Dr. Serdal Kirmizialtin and Dr. Karissa Sanbonmatsu (LANL).

Along these lines, one of the current directions of this project is to use our data to impose additional constraints in molecular dynamics simulations. As explained in Chapter 1, the simulations require calculation of the total force acting on

each atom and molecule of a system and tracking of the changes in positions of said atoms and molecules in a time-dependent manner. MD simulations are initially based on published structures resembling the complexes of interest. We suggest that they can be fine-tuned by the high resolution hSHAPE data. hSHAPE reactivities may be added to the total force calculations by conversion into "pseudo"-free energy values [116,211], in the same way they are used for structure prediction. Since the simulations are based on other structural studies, they are useful in predicting ribosomal protein dynamics as well, and nicely indicate whole domain movements vs. base flipping in rRNA. As such, MD-SHAPE will be valuable in generating a "movie" of ribosomal dynamics changes in a set of elongation complexes. Automated mining of the three dimensional information contained in simulations would also be another direction to consider to obtain lists of position changes of all nucleotides allowing classifications of different motions and simplifying comparisons of simulations of different complexes. Purely visual comparisons are also possible directly with MD-SHAPE. While MD simulations are most valuable as trajectories of movements, Figure 53 shows a static view of the empty ribosome after MD-SHAPE, implicating protein-RNA interactions as major causes of the flexibility differences throughout the ribosome as exposed surfaces are highly flexible. Hence MD simulations will possibly be useful in identifying the reasons underlying flexibility changes in elongation complexes as well.

Another computational direction we would like to take with this project is to define the hSHAPE reactivities in voxels - volumetric pixels of a certain size. This is both an attempt to simplify and improve visualization of our data, and definition of

the voxels in hydrogen-bonding distances (i.e. about 3.5 x 3.5 x 3.5 $Å^3$ to contain interacting nucleotides in the same voxel) would allow us to have a sense of which interactions may be rearranging as the reactivities change from one complex to the next. Figure 54 shows visualization of our data in voxels of 6 x 6 x 6 $Å^3$ coupled to volumetric rendering highlighting the maximum flexibility value among the group of nucleotides contained in a single voxel. According to this, in post-accommodation complex the 25S rRNA undergoes rearrangements whereas in the pre-translocation complex it is the 18S rRNA that undergoes changes. Even at this preliminary resolution, this analysis is already useful in visualization. Obtaining information on which nucleotides are "trapped" in each voxel would allow for further analyses and discovery of communication pathways throughout the ribosome in the context of translation elongation.

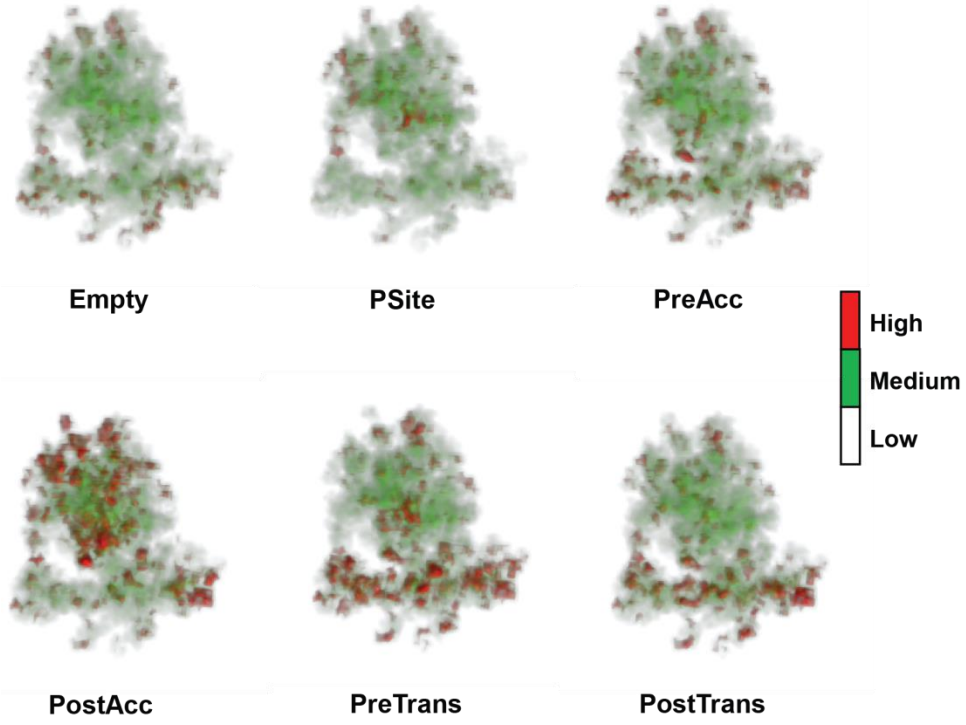

Figure 54. The hSHAPE data visualized in voxels.

25S and 18S rRNAs are visualized from the P stalk side. The entire volume of the ribosome is divided into voxels of 6Å dimensions. For each voxel, the maximum flexibility value among the nucleotides contained inside is computed. In the image, volumetric rendering is used to show maximum flexibility values of each voxel. The more flexible a voxel is, the more opaque it is. The color code for the flexibilities is shown on the right. Image generated by our collaborators, Dr. Sujal Bista and Dr. Amitabh Varshney (UMIACS, UMD).

Other than the computational directions we are starting to take through collaborations with Los Alamos National Laboratories and Computer Sciences Department at University of Maryland, a future direction of this project is to use the biochemical and structural tools that were employed here, for "walking" mutant ribosomes through the elongation cycle. This could potentially be a part of the mutational analyses of ribosomal mutants, and would show (1) at precisely which step the mutant ribosome performs poorly and (2) due to which conformational change, compared to wild type ribosomes. Currently, hSHAPE is being used on only empty mutant ribosomes. Ribosomal mutants may also be employed to check for the authenticity of the communication pathways obtained computationally. In fact, the current repertoire of ribosomal mutants from our laboratory could be employed for this initially. Another way to validate these communication pathways may be through repeating our project with ribosomes from other organisms.

The results of this project identify hSHAPE as a valuable technique for studies of ribosomal dynamics. Improvement to address the issues listed above, as well as following through with the future directions, has the potential to take similar studies to a whole new level, finally obtaining a high resolution dynamic map of the yeast ribosome.

Chapter 6: Materials and methods

Strains.

Yeast strain JD1370 (*MATa trp1 ura3 leu2 PEP4::HIS3 NUC1::LEU2)* was used for purification of ribosomes. Yeast strains TKY865 (renamed to JD1540; *MATα leu2-3,112 his4-713 ura3-52 trp1Δ tef2Δ2 tef1::LEU2 met2-1 pTKB779 (TRP1 2u TEF1-His6)* and TKY675 (renamed to JD1334; *MATα ade2 leu2 ura3 his3 trp1 eft1::HIS3 eft2::TRP pEFT1-LEU2 -CEN*) were kind gifts from Dr. Terry G. Kinzy (Rutgers University) and were used to purify eukaryotic elongation factors 1A and 2 (eEF1A and eEF2), respectively. Bacterial strain M15 pREP4-pJD833, cloned by Dr. Sharmishtha Musalgaonkar from our laboratory, was used to purify phenylalanyl tRNA synthetase.

Ribosome preparation.

Ribosome purification was essentially performed as previously described [212] followed by puromycin treatment to remove tRNAs [213]. In brief, yeast strain JD1370 was grown to an OD595 of 1.2 in 2L of YPAD. Cells were broken using 0.5 mm glass beads at 4°C with a Biospec Mini bead beater. Cellular debris was removed by centrifugation at 30,000xg for 30 minutes in a Beckman-Coulter Optima Max E ultracentrifuge. The S30 supernatant was purified using Sulfolink resin. After elution from the column, ribosomes were treated with 1 mM GTP and 1 mM puromycin (pH 7.0) at 30°C for 30 minutes. This was followed by overnight centrifugation in a high salt glycerol cushion (20 mM HEPES-KOH pH 7.6, 60 mM NH_4Cl, 500 mM KCl, 10 mM $Mg(OAc)_2$, 2 mM DTT, 25% glycerol) at 100,000xg. The ribosome pellets were resuspended in the presence of 20 mM Mg^{++} and incubated at 4°C for 1 hour to

ensure maximal subunit association. The resuspension, diluted 1:1 in a buffer without Mg^{++} to lower the final concentration of the ion to 10 mM, was passed through a 10-30% sucrose cushion (20 mM HEPES-KOH pH 7.6, 100 mM KCl, 10 mM $Mg(OAc)_2$, 2 mM DTT) at 45,000xg for 15 hours. 80S fractions were collected. After buffer exchange (to 20 mM HEPES-KOH pH 7.6, 50 mM NH4Cl, 10 mM $Mg(OAc)_2$, 1 mM DTT, 25% glycerol), 80S ribosomes were quantified and stored at -80°C.

Elongation factor purification.

Yeast strains JD1540 and JD1334 were grown to an OD595 of 1.5 in 2L of YPAD. Cell lysis was essentially the same as the ribosome purification procedure, except the buffer composition was 20 mM sodium phosphate buffer, pH 7.6, 500 mM NaCl and 10 mM imidazole. Cellular debris and ribosomes were removed by centrifugation at 100,000xg for 3 hours at 4°C. The supernatants were filtered through a 0.2 micron syringe filter. Filtered eEF1A supernatant was mixed and incubated with Qiagen Ni-NTA agarose and washed under gravity flow. His-tagged eEF1A was eluted in presence of 250 mM imidazole. Eluates from different preparations were pooled. Imidazole was removed by buffer exchange. eEF1A activity was determined by A site tRNA binding assays (described below). Filtered eEF2 supernatant was passed through a 5-ml GE Healthcare HisTrap HP column and washed using a peristaltic pump. His-tagged eEF2 was eluted in presence of 250 mM imidazole. Imidazole was removed by buffer exchange. eEF2 activity was determined through ADP ribosylation by diphtheria toxin and ribosome binding assay [210]. Protein concentrations were determined by Bradford assay.

Aminoacyl-tRNA synthetase purification.

Bacterial strain M15 pREP4-pJD833 was grown to OD600 = 0.5 and induced by 1mM IPTG for six hours prior to collection of cell pellets. Cells were washed with 20 mM sodium phosphate buffer, pH 7.6, 500 mM NaCl, 10 mM imidazole. Lysozyme was added to a concentration of 0.1 mg/ml and sonication was employed to lyse cells. The rest of the procedure was essentially the same as elongation factor purification. Briefly, cellular debris was removed by ultracentrifugation and the supernatant was incubated with Ni-NTA agarose and washed under gravity flow. His-tagged aminoacyl-tRNA synthetase was eluted in the presence of 250 mM imidazole. Imidazole was removed by buffer exchange. Protein concentration was determined by Bradford assay. The activity was determined by small scale aminoacylation reactions and detected as incorporation of [^{14}C] phenylalanine, under increasing protein amount.

tRNA charging.

CCA-adding enzyme was purified by Dr. Alexey Petrov, an alumnus of our laboratory, by salting out different fractions of S30 supernatants of Baker's yeast. The activity was determined by Dr. Sharmishtha Musalgaonkar based on quantification of [α-^{32}P] ATP incorporation in both time-course assays and under increasing enzyme amount.

Yeast $tRNA_{Phe}$ was incubated with 10x ATP and CTP in 50 mM Glycine-NaOH, pH 9.0, 20 mM $MgCl_2$ and 1 mM DTT. 0.3 µg of CCA-adding enzyme was added to the reaction per pmole tRNA. Pyrophosphatase was also employed to remove the inhibitory byproduct pyrophosphate from the reaction (one unit liberates 1

μmole of inorganic orthophosphate per min at pH 7.2 at 25°C). The reaction took place at 30°C for 24 min. 300 mM sodium acetate, pH 5.0, was used to stop the reaction, as well as phenol-chloroform extraction to remove proteins. CCA-repaired tRNA was collected by overnight ethanol precipitation and resuspension of pellet in 3 mM sodium acetate. When pyrophosphatase was not used, this solution was passed through a G25 column to remove pyrophosphate before moving on to aminoacylation.

CCA-repaired tRNA was incubated with 10x non-radioactive phenyalanine or 3x [^{14}C] phenylalanine, in 100 mM HEPES-KOH, pH 7.6, 10 mM ATP, 10 mM KCl, 20 mM $MgCl_2$ and 1 mM DTT. 0.5 μg of aminoacyl-tRNA synthetase was added per pmole of tRNA. Pyrophosphatase was also employed. The reaction took place at 30°C for 30min. The next steps were similar to the CCA repair procedure, to obtain phenylalanyl tRNA (phenol-chloroform extraction, ethanol precipitation). The tRNA pellet was resuspended in 3 mM sodium acetate and 10 mM $MgCl_2$. To obtain N-acetyl-phenylalanyl tRNA, directly after stopping aminoacylation, fresh acetic anhydride was added to a concentration of 5% (V/V). This was incubated on ice for 1 hour. Addition of acetic anhydride and incubation were repeated, and phenol-chloroform extraction and ethanol precipitation proceeded. The tRNA pellet was resuspended in 3 mM sodium acetate and 10 mM $MgCl_2$.

High performance liquid chromatography (HPLC) was employed to purify aminoacylated or acetylated and aminoacylated tRNA from deacyl tRNA. A Bakerbond Wide-Pore™ C4 column (250 x 4.6 mm) was equilibrated with buffer A (20 mM ammonium acetate pH 5.0, 400 mM NaCl and 10 mM magnesium acetate). Sample was injected and eluted over a linear gradient of 0-50% buffer B (buffer A in

60% methanol) with a flow rate of 0.5 ml/min. The specific steps are: 1. buffer A for 15 min, 2. linear gradient of buffer B from 0-10% until the 20^{th} min, 3. linear gradient of buffer B from 10-50% until the 90^{th} min, 4. run 50% buffer B for 10 min. The aminoacylated fractions eluted around 85 min, the acetylated-aminoacylated fractions around 95 min, and the deacylated tRNA fractions around 60min. Fractions of interests were pooled, ethanol precipitated and resuspended, and stored at -80°C. Depending on the phenylalanine species, either concentration or radioactivity was measured to quantify the charged tRNAs.

Ribosome/tRNA interactions.

To assay binding of aminoacyl-tRNA to the ribosomal A-site, 2 sets of reactions were set up in parallel. A mix containing 100 µg of polyuridylic acid (poly(U)), 500 pmoles of ribosomes, a 4-fold molar excess of $tRNA^{Phe}$, all in binding buffer (80 mM Tris-HCl, pH 7.4 at 30^{o} C, 160 mM NH_4Cl, 15 mM magnesium acetate, 2 mM spermidine, 0.5 mM spermine, 6 mM β-mercaptoethanol) in 150 µl total volume was prepared and incubated for 30 min at 30°C to block the P-site. To prepare the ternary complex ($[^{14}C]$Phe-$tRNA^{Phe}$•eEF1A•GTP), 100 µg of eEF1A, 1mM GTP, 512 pmoles $[^{14}C]$-Phe-$tRNA^{Phe}$ were mixed in 60 µl total volume binding buffer and incubated for 30 min at 30^{o}C. After incubation, serial 2-fold dilutions of the ternary complex reaction mix were prepared, resulting in 8 fractions containing decreasing amounts of ternary complex (128 - 1 pmoles), in 15 µl each. An equal amount of the ribosome mix (25 pmoles of ribosomes, 15 µl) was added to each dilution, followed by incubation for 30 min at 30^{o}C. The mixtures were applied onto pre-wetted nitrocellulose Millipore HA (0.45 micron) filters, washed with binding

buffer, and radioactivity was measured via scintillation counting. Background control reactions without ribosomes were performed at each ligand dilution and subtracted from experimental ones. Binding data were fitted into "single binding site with ligand depletion" models using GraphPad Prism. To test binding of tRNA to the P-site, N-acetyl-[^{14}C]-Phe-tRNA^{Phe} was used as the ligand, without prior incubation with tRNA^{Phe}, and 11 mM magnesium acetate was used in the binding buffer. Assays were conducted for each complex.

Ribosome/eEF2 interaction.

5 pmoles ribosomes were incubated with increasing concentrations of eEF2 (0.5 – 64 pmoles), 10 µg of polyU, and 4x molar excess of [^{14}C] NAD over ribosomes in 50 µl total volume of binding buffer (50 mM Tris-HCl pH 7.5, 50 mM ammonium acetate, 10 mM magnesium acetate, 2 mM DTT, 100 µM GDPNP) at 30°C for 20 minutes. Diphtheria toxin (0.2 µg) was added, and reactions were incubated for 30 min at 30°C. After precipitation with TCA (final concentration 15% V/V) and 15 min incubation on ice, reaction mixtures were applied onto GF/C filters, washed with 5% TCA, and the amount of [^{14}C]-ADP ribosylated eEF2 was determined by scintillation counting. Counts resulted from unbound eEF2 and were subtracted from total eEF2 to obtain the amounts bound.

Ribosomal complex assembly for hSHAPE analyses.

Elongation: 50 pmoles of 80S yeast ribosomes programmed with 100 µg polyuridine were used for all complexes. Complex assembly conditions were based on binding assays. To assemble P-site occupied ribosomes, 150 pmoles of N-acetyl-phenylalanyl (Phe) tRNA^{Phe} were incubated with ribosomes in binding buffer (80 mM

HEPES pH 7.5, 50 mM NaCl, 11 mM magnesium acetate, 6 mM β-mercaptoethanol) at 30°C for 30 minutes. For pre- and post-accommodation ribosome assembly, P-site occupied ribosomes were incubated with a ternary complex of eEF1A-GDPNP-Phe-tRNA^{Phe} or eEF1A-GTP-Phe-tRNA^{Phe}, respectively, in binding buffer with 15 mM magnesium acetate at 30°C for 30 minutes. Ternary complexes were prepared by incubating 250 pmoles of Phe-tRNA^{Phe}, 1 nmole of eEF1A and 1 mM GDPNP or GTP. The hybrid states complex was prepared by incubating post-accommodation ribosomes with 1 mM anisomycin. The accommodation intermediate complex and the classical states complex were prepared by incubating P-site occupied ribosomes with 1 mM anisomycin or 1 mM cycloheximide, respectively, before addition of the ternary complex and then proceeding with the remainder of post-accommodation ribosome preparation. To assemble pre- and post-translocation ribosomes, post-accommodation ribosomes were prepared in large scale (starting with 500 pmoles ribosomes) and centrifuged for 2 hours at 4°C at 100,000xg through 25% glycerol cushion in binding buffer with 15 mM magnesium acetate. The ribosome complex pellets were resuspended in binding buffer with 15 mM magnesium acetate and quantified. 50 pmoles were incubated with 300 pmoles eEF2 and 1 mM GDPNP or GTP.

Initiation: These complexes were assembled by Fan Zhang (NIH). 50 pmoles of empty 40S was used as baseline. 100 pmoles eIF1, 100 pmoles eIF1A, and 250 pmoles eIF5 were added to 50 pmoles 40S for assembly of the complexes 40S-eIF1-eIF1A and 40S-eIF1-eIF1A-eIF5. The reactions proceeded in reconstitution buffer (30 mM HEPES-KOH pH7.4, 100 mM potassium acetate, 3 mM magnesium acetate

and 2 mM DTT) for 15 min at 26°C. 150 pmoles of full length eIF5 or 150 pmoles of eIF5-NTD or 450 pmoles of eIF5-CTD were added to 50 pmoles 40S for assembly of 40S-eIF5, 40S-eIF5-NTD, or 40S-eIF5-CTD, respectively. The reactions proceeded in reconstitution buffer for 6 min at 26°C.

Dipeptide formation analysis by HPLC.

The analysis of dipeptide formation by HPLC was adapted from Marquez et al, 2004 [172]. Complexes to be tested were assembled using 50 pmoles P-site occupied ribosomes and ternary complexes made of 250 pmoles [^{14}C]-Phe-tRNA^{Phe}, 1 nmole eEF1A and 1mM GTP or GDPNP. Phenol-chloroform extraction was performed. The aqueous phase was collected and was used in ethanol precipitation overnight. Pellets obtained from ethanol precipitation were treated with 0.5M NaOH to hydrolyze RNA. The mixtures were neutralized with 1M HCl, loaded onto a Thermo Scientific Hypersil™ C18 column (150 x 4.6 mm) equilibrated with 0.1% trifluoroacetic acid (TFA), and were subjected to reverse phase HPLC. A binary linear gradient was applied at 0.5 ml/min using 0.1% TFA as Buffer A and 60% acetonitrile in 0.1% TFA as Buffer B. Fractions of 900 µl were collected and the radioactivity measured by liquid scintillation. The results were plotted.

Translocation assay.

The puromycin assay to test for translocation was adapted from Rheinberg and Nierhaus, 1986, and Nierhaus, 1990 [173,174]. 250 pmoles post-accommodation complex prepared with [^{14}C]-Phe-tRNA^{Phe} tRNA were passed through A-site tRNA binding buffer (80 mM Tris-HCl, pH 7.4 at 30^{o} C, 160 mM NH_4Cl, 15 mM $Mg(OAc)_2$, 2 mM spermidine, 0.5 mM spermine, 6 mM β-mercaptoethanol) with 25%

glycerol at 100,000xg for 2 hours, to remove unbound tRNAs and the eEF1A. The amount of complex collected was measured through detecting radioactivity by scintillation counting. For the translocation assay, 5 pmoles of radioactively labeled post-accommodation complex was incubated with 35 pmoles eEF2 with 1 mM GTP, or 35 pmoles eEF2 with 1 mM GDPNP, or no eEF2 (used as background control). Translocation proceeded for 5 minutes at 30°C. The puromycin reaction was conducted at 4°C [173,174]. 10 mM puromycin was added to each tube and the reactions were stopped at 0, 5, 10, 20 and 40 min by ethyl acetate extraction. The organic layer containing puromycin was collected and the radioactivity was measured by scintillation counting.

1M7 treatment.

1M7 treatment was performed as previously described [210]. The complexes were divided into two aliquots. For "reaction" samples, 1M7 was added to a final concentration of 6mM. For "control" samples, the same volume of anhydrous DMSO was added. Reactions proceeded for 10 minutes at 30°C and subsequently were precipitated overnight in 70% ethanol and 300 mM sodium acetate. rRNAs were purified using RNAqueous Micro kit (Ambion). rRNA concentrations were determined using a Nanodrop 1000.

Kethoxal treatment.

The complexes to be tested were prepared from 100 pmoles of ribosomes and divided into four aliquots. For "reaction" samples, 0.5 µl, 1 µl, and 2 µl of kethoxal (diluted 1:100 in ethanol) were used. For "control" samples, 1 µl ethanol was used. Reactions proceeded for 10 minutes at 30°C and were quenched in 250 mM

potassium borate, pH 7.0, and 150 mM sodium acetate. rRNAs were precipitated, purified and quantitated as described above.

hSHAPE extension.

Primer extensions were performed as previously described [210]. Four primers were constructed by Dr. Jonathan Leshin, an alumnus of our laboratory, with the following fluorescent molecules for each region: 6-FAM labeled primers were used for the 1M7 treated samples, VIC labeled primers were used for the DMSO treated samples, and NED and PET labeled primers were used for sequencing reactions. To 1 µg of rRNA, 2.5 pmoles of primer was added. The samples were incubated at 65°C for 5 minutes then 50°C for 5 minutes. A master mix was made of 5 units Superscript III Reverse Transcriptase (Invitrogen), 0.5 mM dNTP mixture, 1X Superscript Buffer (Invitrogen) and 5 mM DTT and added to the samples to a final volume of 10 µl. In addition, 1 mM of appropriate ddNTP was added to the sequencing samples.[105] Samples were incubated at 50°C for one minute, 52°C for 45 minutes and 65°C for 5 minutes. The four extension reactions for each region were combined and precipitated overnight in 70% ethanol at -20°C. Samples were washed twice with 70% ethanol and resuspended in Hi-Di Formamide (Applied Biosystems) and sent for fragment analyses using capillary electrophoresis at Genewiz.

ShapeFinder analysis.

hSHAPE data were aligned to rRNA sequences using ShapeFinder [210,105,106]. Fitted baseline adjustment, mobility shift correction, signal decay correction, scaling, alignment features of the software were employed and the aligned peaks were fitted into a Gaussian function. Integrated peak values were obtained as the areas under

1M7 treated peaks minus the areas under corresponding negative control peaks, and used for further analyses (please see below).

Box-plot analysis.

Integrated peak values (1M7 reactivity values for every nucleotide of the ribosome) obtained from ShapeFinder were corrected for negative values and analyzed by box-plots in R 3.1.0 using robust statistics. The following features of the integrated peak data (x_1-x_n) were determined: the minimum allowed value (Q_{min}), the 25th percentile (Q_{25}), the sample median ($\tilde{x}$), the 75th percentile (Q_{75}), the maximum allowed value (Q_{max}), and the interquartile range (IQR), where:

$$Q_{25} = \begin{cases} x_{((n+1)/4)}, & \text{if } n \text{ is odd} \\ \frac{x_{n/4} + x_{n/4+1}}{2}, & \text{if } n \text{ is even} \end{cases} \quad \textbf{1}$$

$$\tilde{x} = \begin{cases} x_{((n+1)/2)}, & \text{if } n \text{ is odd} \\ \frac{x_{n/2} + x_{n/2+1}}{2}, & \text{if } n \text{ is even} \end{cases} \quad \textbf{2}$$

$$Q_{75} = \begin{cases} x_{(3(n+1)/4)}, & \text{if } n \text{ is odd} \\ \frac{x_{3n/4} + x_{3n/4+1}}{2}, & \text{if } n \text{ is even} \end{cases} \quad \textbf{3}$$

$$IQR = Q_{75} - Q_{25} \quad \textbf{4}$$

$$Q_{min} = Q_{25} - 1.5 * IQR \quad \textbf{5}$$

$$Q_{max} = Q_{75} + 1.5 * IQR \quad \textbf{6}$$

As nonreactive nucleotides (*i.e.* integrated peak values of "zero") were expected, outliers were identified as values above Q_{max} and were removed in the first

version of hSHAPE data analyses. A need for data transformation was evident from the box plot analyses, and led to improved data analyses as explained below.

Data processing and normalization.

Natural log transformation was employed for data processing for improved analyses. For each data point in the dataset x_1-x_n (zero-corrected integrated peak values from a single primer region), the transformed values y_1-y_n were defined as:

$$y_{1,\ldots},y_n = \ln((x_{1,\ldots},x_n)+c), \text{ where } c=1 \qquad \mathbf{7}$$

The transformed datasets y_1-y_n from each primer region were normalized by the median for that region and merged to obtain transformed, normalized data for the whole yeast ribosomal RNA except 5S rRNA. The merged data were analyzed by box-plots and resulted in unimodal, symmetric distributions. Outliers were identified and removed as described above.

Complex comparison.

To compare reactivity values from different 80S ribosomal complexes, the following calculations were performed:

$$\text{Complex vs. Empty 80S} = \frac{(\text{Complex} - \text{Empty 80S})}{\text{Empty 80S}}, \quad \text{per nucleotide} \qquad \mathbf{8}$$

$$\text{Complex A vs. Complex B} = \frac{(\text{Complex A} - \text{Complex B})}{\text{Empty 80S}}, \quad \text{per nucleotide} \qquad \mathbf{9}$$

Data grouping and frequency histograms.

For visualization purposes, a color code was employed that represented ranges of comparative reactivity values, or reactivity levels. 15 levels were chosen by grouping the data based on frequency in MS Excel and plotting the corresponding histograms in R 3.1.0 (Figures 22 and 23). According to this, the values obtained

from the above complex comparison calculations lay in the interval -15 to 15 for all complexes. Frequency intervals were used to determine the relative reactivity levels. Level "0" (indicating no change between two complexes) comprised most of the data points (highest bars, values between -0.25 to 0.25). The most extreme levels "-7" and "7" (indicating a large decrease in reactivity and a high increase in reactivity, respectively, in one complex compared to the other) included the smallest number of data points (values below -7 and above 7, respectively). All other levels included approximately the same number of data points. The resulting color scale is shown in Figure 22B in the order of relative levels, colors, and comparative reactivity ranges.

Generation of difference maps of eukaryotic rRNA.

The color-coded comparative reactivity values were mapped onto the 3.0 Å X-ray crystallography structure of *Saccharomyces cerevisiae* ribosome [2] using a PyMOL script [105], and the secondary structure mapping was performed by the online tool, Ribovision, following the instructions of the developers [11].

Pattern discovery on the hSHAPE data.

MS Excel was employed to examine patterns of reactivity changes in the hSHAPE data. 32 patterns were scanned for in five difference maps (P site occupied vs empty, preaccommodation vs P site occupied, postaccommodation vs preaccommodation, pretranslocation vs postaccommodation, posttranslocation vs pretranslocation). Only reactivity decreases and increases in sequence were scanned for, and made up the 2^5 (=32) possible patterns.

Appendix: 2D difference maps

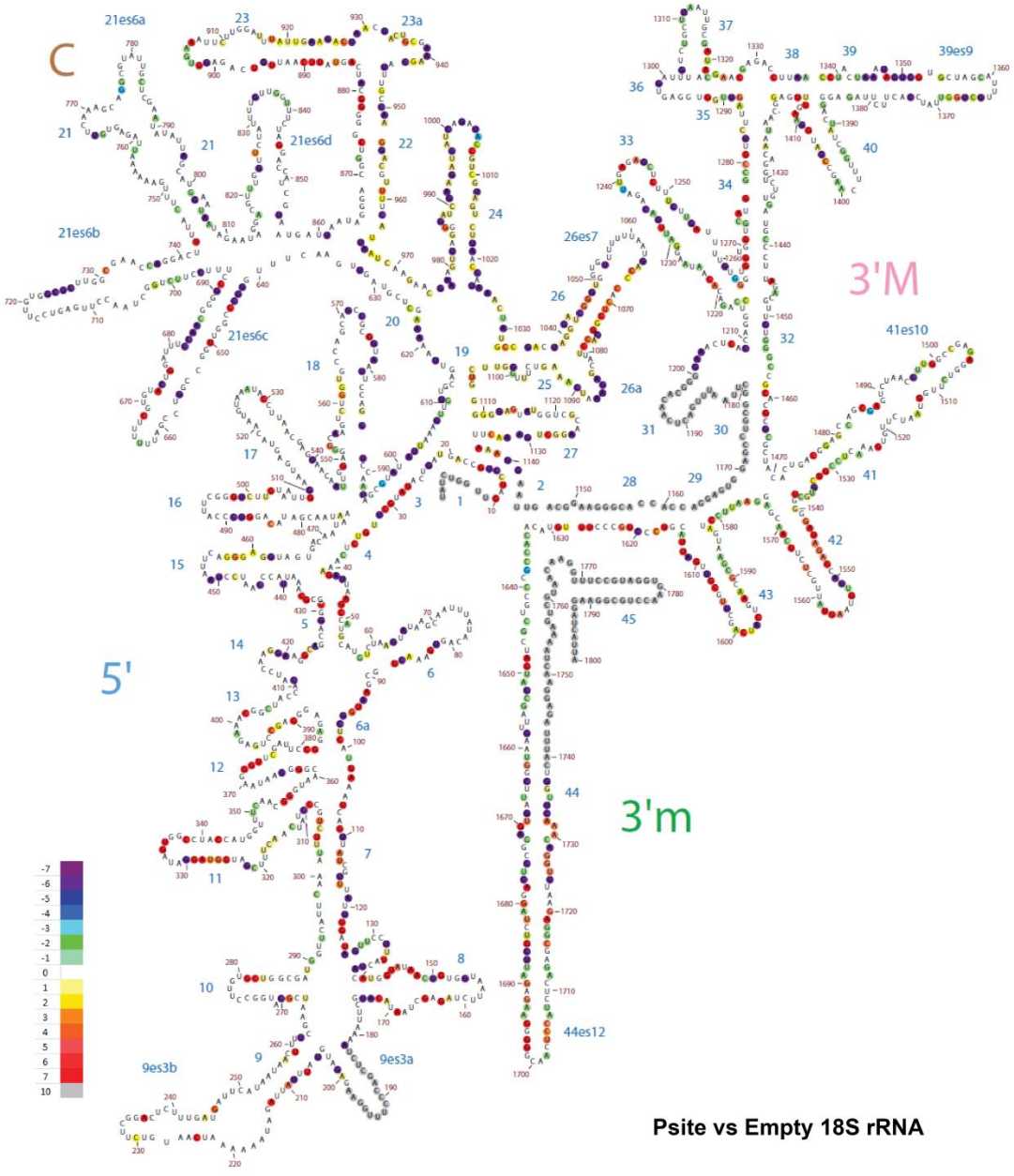

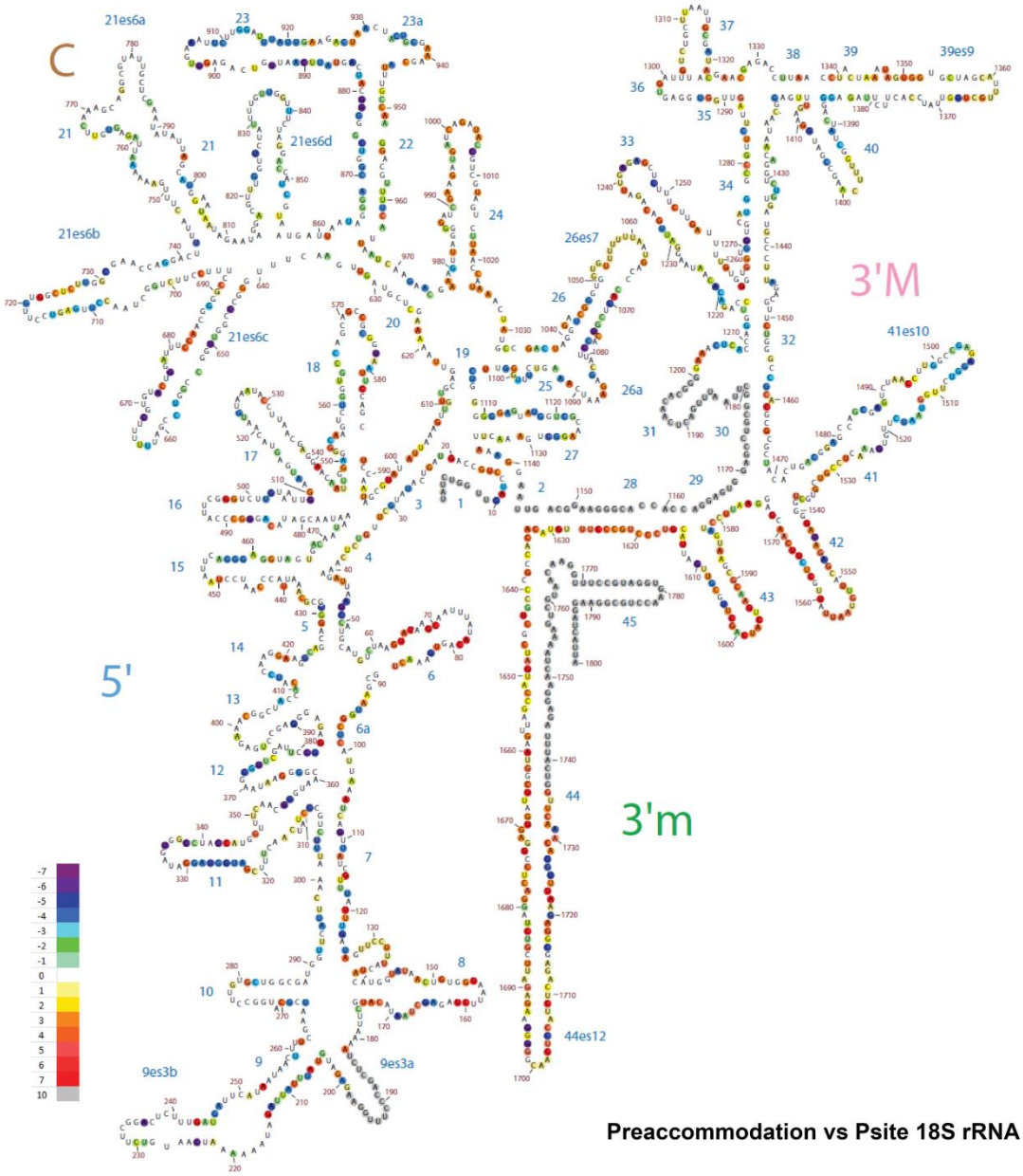
C
5'
3'M
3'm
21es6a
23
23a
21
21es6d
22
24
21es6b
26es7
21es6c
18
19
25
26
26a
20
17
27
2
1
3
16
28
29
41es10
15
4
14
5
6
42
43
45
13
6a
12
44
11
7
8
10
44es12
9es3b
9
9es3a
Preaccommodation vs Psite 18S rRNA

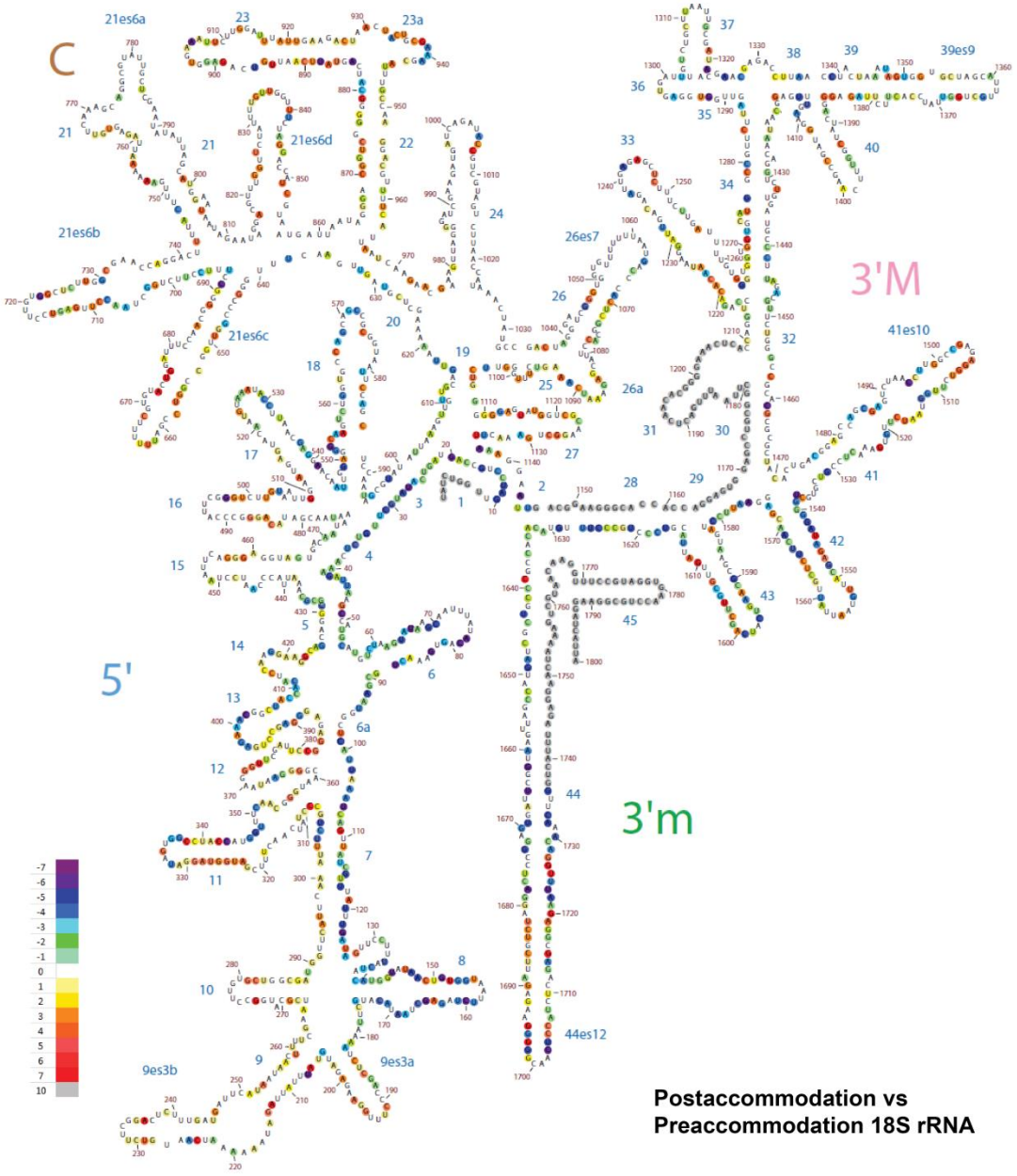
C
5'
3'M
3'm
21es6a
21es6b
21es6c
21es6d
23
23a
22
24
26es7
26
26a
25
27
41es10
39es9
44es12
9es3a
9es3b
Postaccommodation vs
Preaccommodation 18S rRNA

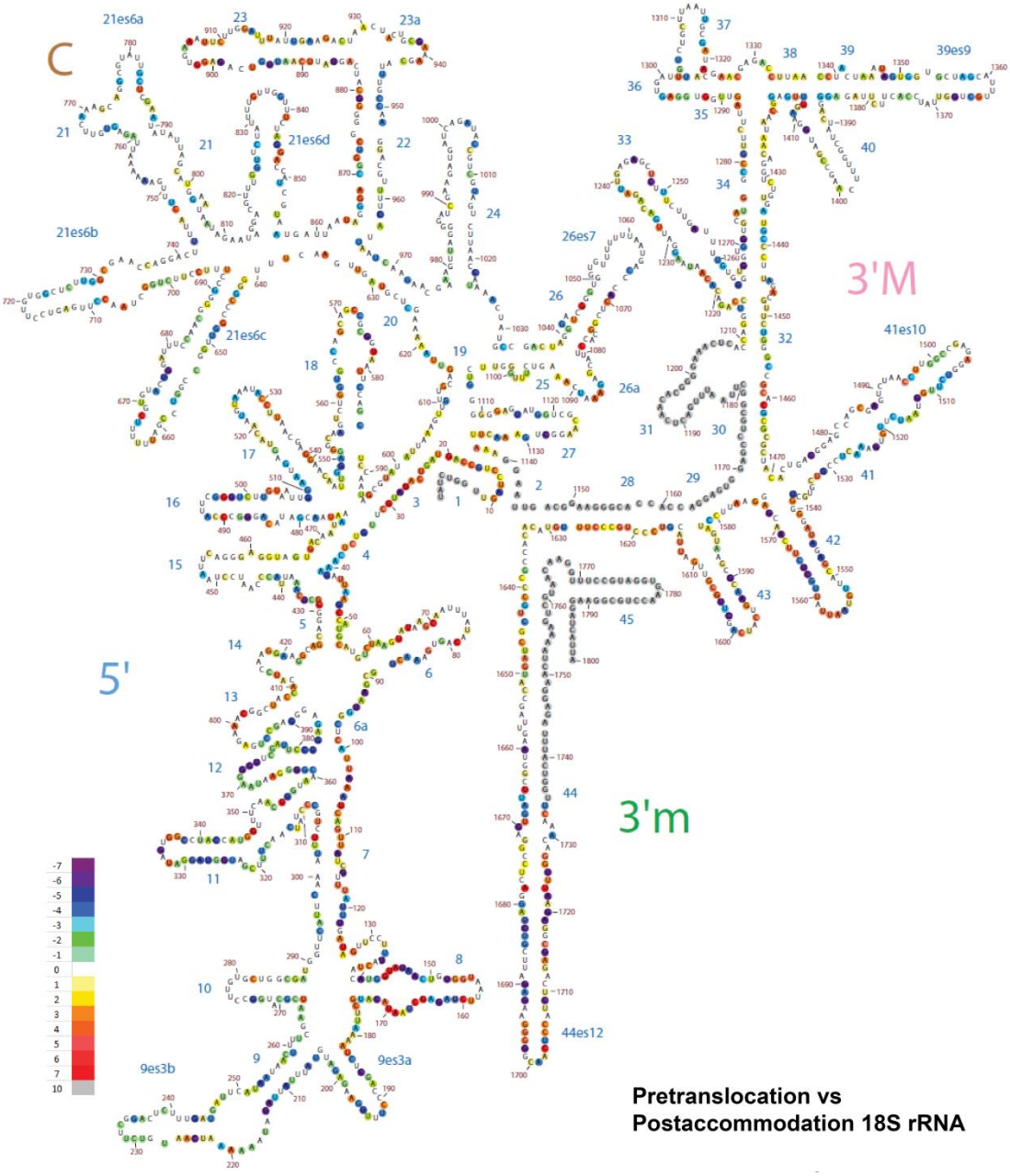
C
21es6a
23
23a
21
21es6d
22
24
21es6b
26es7
3'M
21es6c
26
26a
41es10
5'
3'm
44es12
9es3b
9es3a
Pretranslocation vs
Postaccommodation 18S rRNA

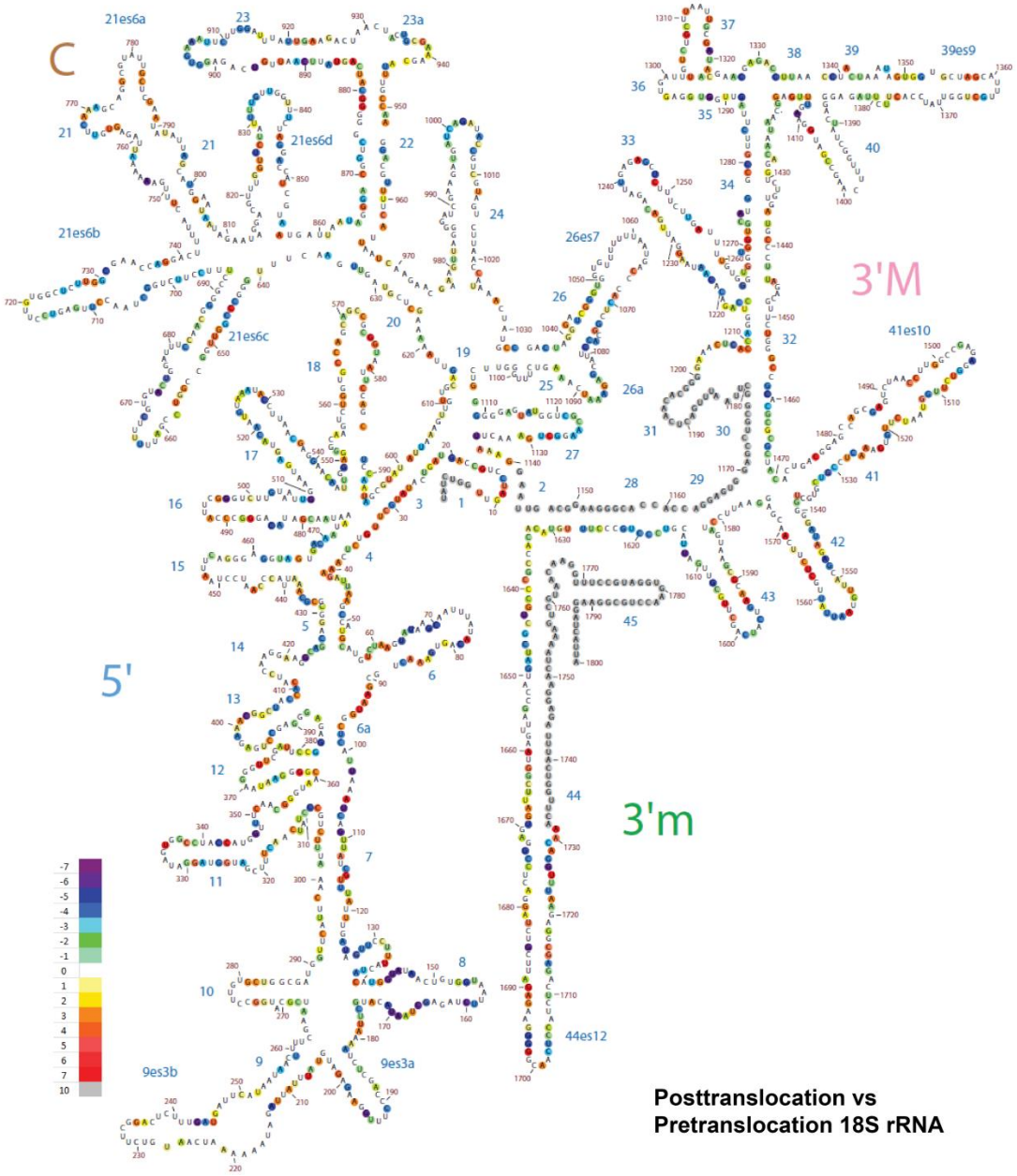

Posttranslocation vs Pretranslocation 18S rRNA

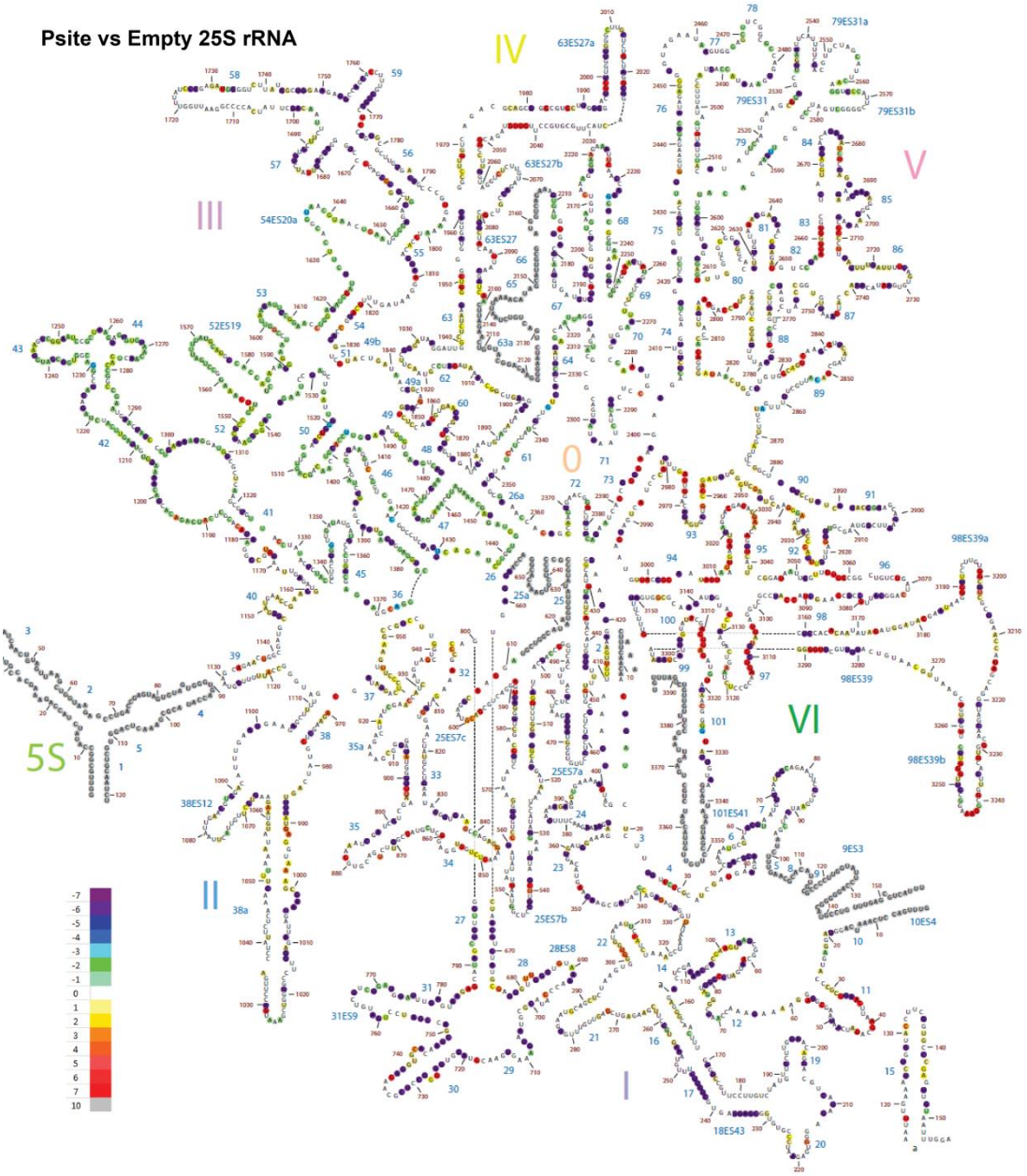
Psite vs Empty 25S rRNA
IV
V
III
0
VI
5S
II
I
63ES27a
79ES31a
79ES31
79ES31b
63ES27b
54ES20a
63ES27
52ES19
49b
49a
63a
26a
25a
98ES39a
98ES39
98ES39b
25ES7c
25ES7a
38ES12
101ES41
9ES3
10ES4
25ES7b
28ES8
31ES9
18ES43
-7
-6
-5
-4
-3
-2
-1
0
1
2
3
4
5
6
7
10

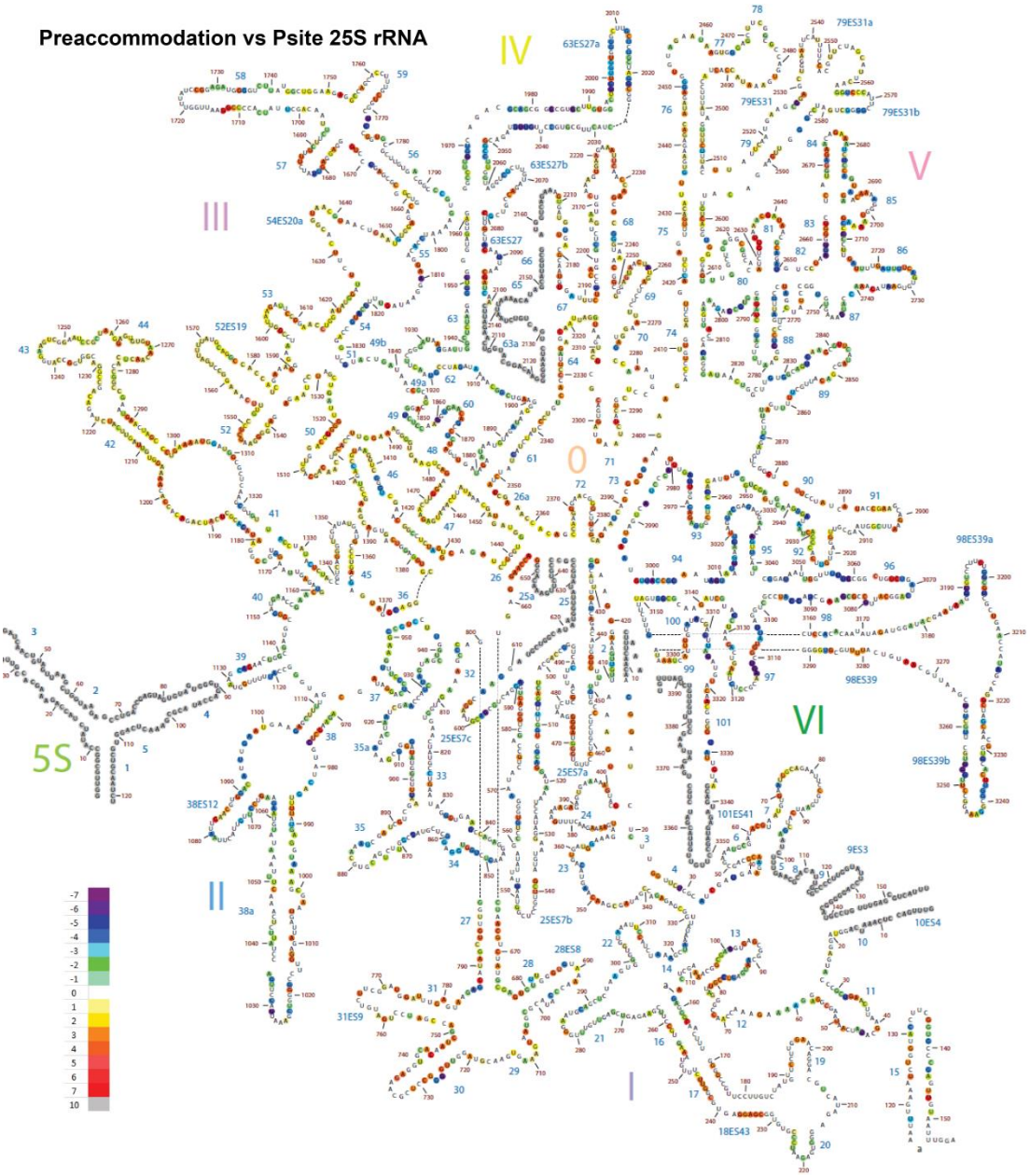
Preaccommodation vs Psite 25S rRNA
IV
V
III
0
VI
5S
II
I
63ES27a
79ES31a
79ES31
79ES31b
63ES27b
54ES20a
63ES27
52ES19
53a
49a
49b
26a
25a
98ES39a
98ES39
98ES39b
25ES7c
25ES7a
25ES7b
28ES8
31ES9
38ES12
38a
35a
101ES41
9ES3
10ES4
18ES43
-7
-6
-5
-4
-3
-2
-1
0
1
2
3
4
5
6
7
10

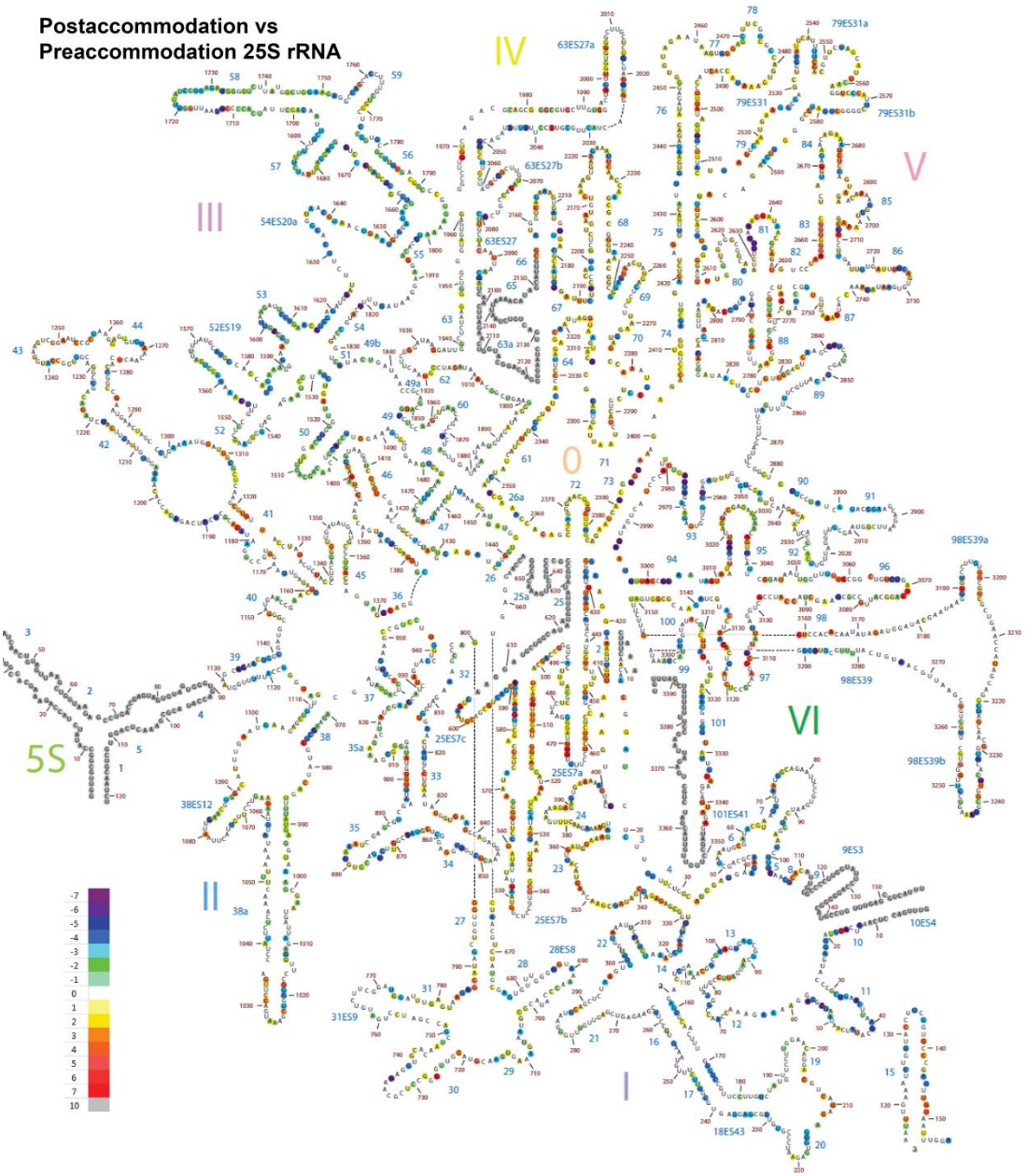
Postaccommodation vs
Preaccommodation 25S rRNA
IV
V
III
0
VI
5S
II
I
63ES27a
79ES31a
79ES531
79ES31b
63ES27b
54ES20a
63ES27
52ES19
49b
49a
63a
26a
25a
98ES39a
98ES39
98ES39b
25ES7c
25ES7a
25ES7b
101ES41
9ES3
10ES4
38ES12
38a
28ES8
31ES9
18ES43
-7
-6
-5
-4
-3
-2
-1
0
1
2
3
4
5
6
7
10

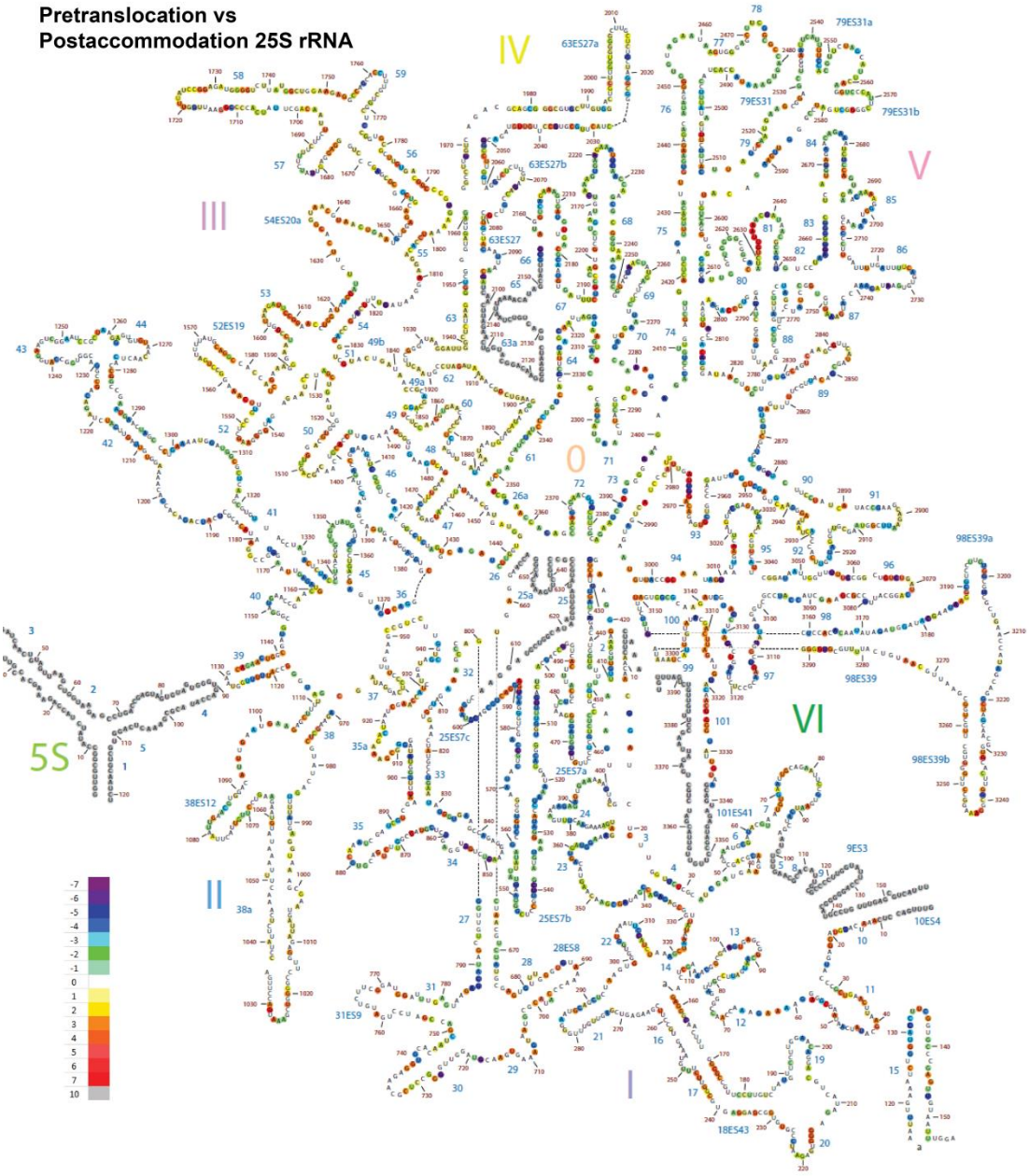
Pretranslocation vs
Postaccommodation 25S rRNA
IV
V
III
0
VI
5S
II
I
63ES27a
79ES31a
79ES31
79ES31b
63ES27b
54ES20a
63ES27
52ES19
49b
49a
26a
25a
98ES39a
98ES39
98ES39b
25ES7c
25ES7a
25ES7b
101ES41
9ES3
10ES4
38ES12
38a
35a
28ES8
31ES9
18ES43
-7
-6
-5
-4
-3
-2
-1
0
1
2
3
4
5
6
7
10

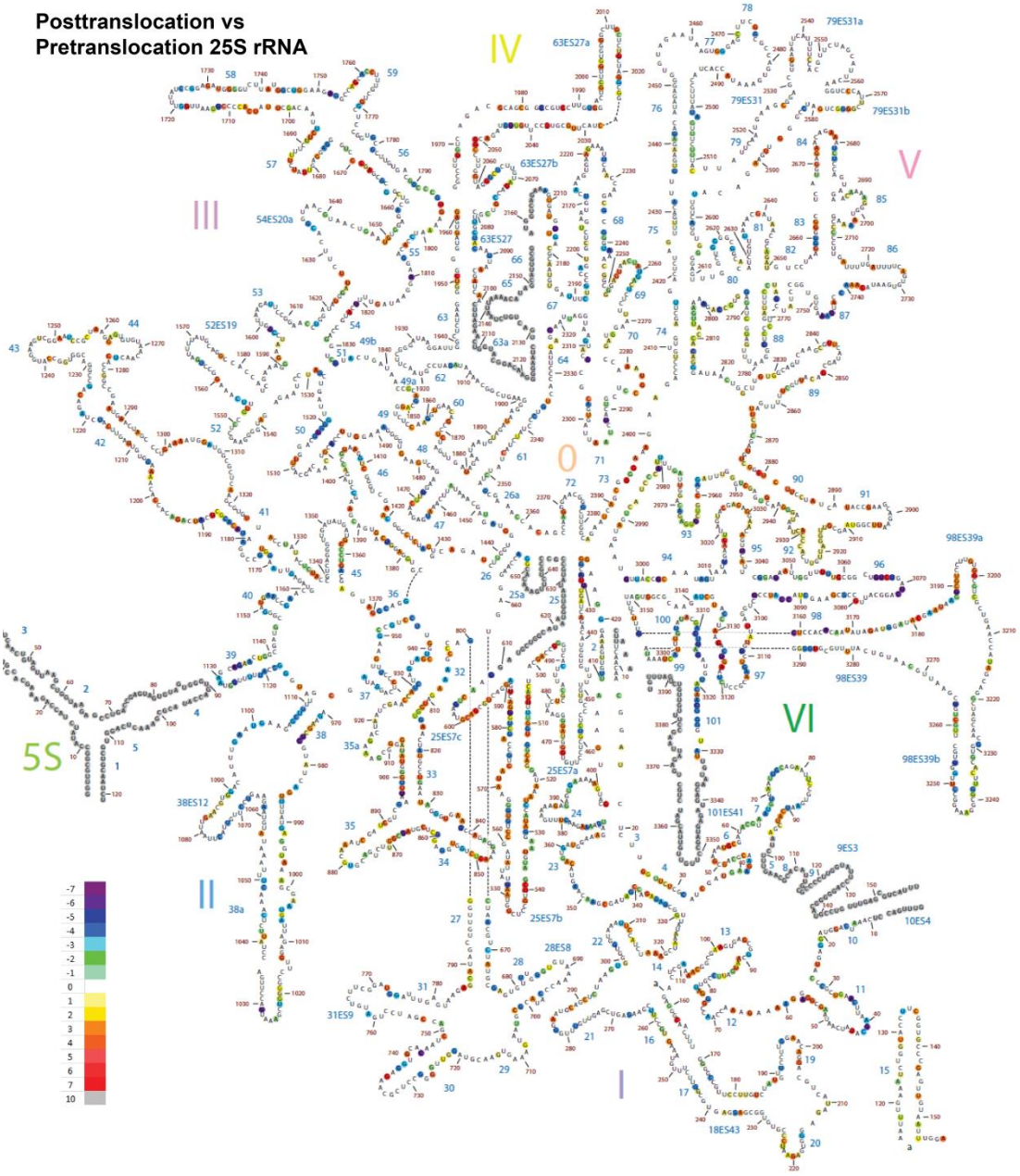
Posttranslocation vs
Pretranslocation 25S rRNA
IV
V
III
0
VI
5S
II
I
-7
-6
-5
-4
-3
-2
-1
0
1
2
3
4
5
6
7
10

Bibliography

1. Melnikov, S. *et al.* One core, two shells: bacterial and eukaryotic ribosomes. *Nat. Struct. Mol. Biol.* **19,** 560–7 (2012).

2. Ben-Shem, A. *et al.* The structure of the eukaryotic ribosome at 3.0 Å resolution. *Science* **334,** 1524–9 (2011).

3. Jack, K. *et al.* rRNA pseudouridylation defects affect ribosomal ligand binding and translational fidelity from yeast to human cells. *Mol. Cell* **44,** 660–666 (2011).

4. Baxter-Roshek, J. L., Petrov, A. N. & Dinman, J. D. Optimization of ribosome structure and function by rRNA base modification. *PLoS One* **2,** e174 (2007).

5. Decatur, W. A. & Fournier, M. J. rRNA modifications and ribosome function. *Trends Biochem. Sci.* **27,** 344–351 (2002).

6. Persaud, C. *et al.* Mutagenesis of the modified bases, m(5)U1939 and psi2504, in Escherichia coli 23S rRNA. *Biochem. Biophys. Res. Commun.* **392,** 223–7 (2010).

7. Kimura, S. & Suzuki, T. Fine-tuning of the ribosomal decoding center by conserved methyl-modifications in the Escherichia coli 16S rRNA. *Nucleic Acids Res.* **38,** 1341–52 (2010).

8. Noller, H. F. RNA structure: reading the ribosome. *Science (80-.).* **309,** 1508 (2005).

9. Moore, P. B. Structural motifs in RNA. *Annu. Rev. Biochem.* **68,** 287–300 (1999).

10. Petrov, A. S. *et al.* Secondary structures of rRNAs from all three domains of life. *PLoS One* **9,** e88222 (2014).

11. Bernier, C. R. *et al.* RiboVision suite for visualization and analysis of ribosomes. *Faraday Discuss.* **169,** 195–207 (2014).

12. *Metagenomics: Current Innovations and Future Trends*. 295 (Horizon Scientific Press, 2011). at <http://books.google.com/books?id=YGc1P0RiAOgC&pgis=1>

13. Farwell, M. A., Roberts, M. W. & Rabinowitz, J. C. The effect of ribosomal protein S1 from Escherichia coli and Micrococcus luteus on protein synthesis in vitro by E. coli and Bacillus subtilis. *Mol. Microbiol.* **6,** 3375–83 (1992).

14. Bernstein, J. R., Bulter, T., Shen, C. R. & Liao, J. C. Directed evolution of ribosomal protein S1 for enhanced translational efficiency of high GC Rhodopseudomonas palustris DNA in Escherichia coli. *J. Biol. Chem.* **282,** 18929–36 (2007).

15. Simonetti, A. *et al.* A structural view of translation initiation in bacteria. *Cell. Mol. Life Sci.* **66,** 423–36 (2009).

16. Simonetti, A. *et al.* Structure of the 30S translation initiation complex. *Nature* **455,** 416–420 (2008).

17. Marintchev, A. in *Biophysical approaches to translational control of gene expression* 83–101 (2013).

18. Jackson, R. J., Hellen, C. U. T. & Pestova, T. V. The mechanism of eukaryotic translation initiation and principles of its regulation. *Nat. Rev. Mol. Cell Biol.* **11,** 113–27 (2010).

19. Acker, M. G., Kolitz, S. E., Mitchell, S. F., Nanda, J. S. & Lorsch, J. R. Reconstitution of yeast translation initiation. *Methods Enzymol.* **430,** 111–45 (2007).

20. Pestova, T. V & Kolupaeva, V. G. The roles of individual eukaryotic translation initiation factors in ribosomal scanning and initiation codon selection. *Genes Dev.* **16,** 2906–22 (2002).

21. Acker, M. G., Shin, B.-S., Dever, T. E. & Lorsch, J. R. Interaction between eukaryotic initiation factors 1A and 5B is required for efficient ribosomal subunit joining. *J. Biol. Chem.* **281,** 8469–75 (2006).

22. Ceci, M. *et al.* Release of eIF6 (p27BBP) from the 60S subunit allows 80S ribosome assembly. *Nature* **426,** 579–84 (2003).

23. Sengupta, J. *et al.* Identification of the versatile scaffold protein RACK1 on the eukaryotic ribosome by cryo-EM. *Nat. Struct. Mol. Biol.* **11,** 957–962 (2004).

24. Nilsson, J., Sengupta, J., Frank, J. & Nissen, P. Regulation of eukaryotic translation by the RACK1 protein: a platform for signalling molecules on the ribosome. *EMBO Rep.* **5,** 1137–41 (2004).

25. Paek, K. Y. *et al.* Translation initiation mediated by RNA looping. *Proc. Natl. Acad. Sci.* **112,** 201416883 (2015).

26. Budkevich, T. V *et al.* Regulation of the mammalian elongation cycle by subunit rolling: a eukaryotic-specific ribosome rearrangement. *Cell* **158,** 121–31 (2014).

27. Youngman, E. M., Cochella, L., Brunelle, J. L., He, S. & Green, R. Two distinct conformations of the conserved RNA-rich decoding center of the small ribosomal subunit are recognized by tRNAs and release factors. *Cold Spring Harb. Symp. Quant. Biol.* **71,** 545–9 (2006).

28. Demeshkina, N., Jenner, L., Westhof, E., Yusupov, M. & Yusupova, G. A new understanding of the decoding principle on the ribosome. *Nature* 1–5 (2012). doi:10.1038/nature10913

29. Ogle, J. M., Murphy, I. V, Frank, V., Tarry, M. J. & Ramakrishnan, V. Selection of tRNA by the ribosome requires a transition from an open to a closed form. *Cell* **111,** 721–732 (2002).

30. Ogle, J. M., Carter, A. P. & Ramakrishnan, V. Insights into the decoding mechanism from recent ribosome structures. *Trends Biochem. Sci.* **28,** 259–66 (2003).

31. Jenner, L., Demeshkina, N., Yusupova, G. & Yusupov, M. Structural rearrangements of the ribosome at the tRNA proofreading step. *Nat. Struct. Mol. Biol.* **17,** 1072–8 (2010).

32. Demeshkina, N., Jenner, L., Westhof, E., Yusupov, M. & Yusupova, G. New structural insights into the decoding mechanism: translation infidelity via a G·U pair with Watson-Crick geometry. *FEBS Lett.* **587,** 1848–57 (2013).

33. Schmeing, T. M. *et al.* The crystal structure of the ribosome bound to EF-Tu and aminoacyl-tRNA. *Science* **326,** 688–94 (2009).

34. Hiller, D. a, Singh, V., Zhong, M. & Strobel, S. a. A two-step chemical mechanism for ribosome-catalysed peptide bond formation. *Nature* **476,** 2–6 (2011).

35. Kuhlenkoetter, S., Wintermeyer, W. & Rodnina, M. V. Different substrate-dependent transition states in the active site of the ribosome. *Nature* **476,** 351–4 (2011).

36. Rodnina, M. V. The ribosome as a versatile catalyst: reactions at the peptidyl transferase center. *Curr. Opin. Struct. Biol.* **23,** 595–602 (2013).

37. Borman, S. Protein Factory Reveals its Secrets. *Chem. Eng. News* **85,** 13–16 (2007).

38. Zaher, H. S., Shaw, J. J., Strobel, S. a & Green, R. The 2'-OH group of the peptidyl-tRNA stabilizes an active conformation of the ribosomal PTC. *EMBO J.* 1–9 (2011). doi:10.1038/emboj.2011.142

39. Bieling, P., Beringer, M., Adio, S. & Rodnina, M. V. Peptide bond formation does not involve acid-base catalysis by ribosomal residues. *Nat. Struct. Mol. Biol.* **13,** 423–428 (2006).

40. Polacek, N., Gaynor, M., Yassin, A. & Mankin, A. S. Ribosomal peptidyl transferase can withstand mutations at the putative catalytic nucleotide. *Nature* **411,** 498–501 (2001).

41. Lang, K., Erlacher, M., Wilson, D. N., Micura, R. & Polacek, N. The role of 23S ribosomal RNA residue A2451 in peptide bond synthesis revealed by atomic mutagenesis. *Chem. Biol.* **15,** 485–92 (2008).

42. Voorhees, R. M. & Ramakrishnan, V. Structural basis of the translational elongation cycle. *Annu. Rev. Biochem.* **82,** 203–36 (2013).

43. Weinger, J. S., Parnell, K. M., Dorner, S., Green, R. & Strobel, S. A. Substrate-assisted catalysis of peptide bond formation by the ribosome. *Nat. Struct. Mol. Biol.* **11,** 1101–1106 (2004).

44. Youngman, E. M., Brunelle, J. L., Kochaniak, A. B. & Green, R. The active site of the ribosome is composed of two layers of conserved nucleotides with distinct roles in peptide bond formation and peptide release. *Cell* **117,** 589–599 (2004).

45. Frank, J. & Agrawal, R. K. A ratchet-like inter-subunit reorganization of the ribosome during translocation. *Nature* **406,** 318–22 (2000).

46. Julián, P. *et al.* Structure of ratcheted ribosomes with tRNAs in hybrid states. *Proc. Natl. Acad. Sci. U. S. A.* **105,** 16924–7 (2008).

47. Gao, Y.-G. *et al.* The structure of the ribosome with elongation factor G trapped in the posttranslocational state. *Science* **326,** 694–9 (2009).

48. Ortiz, P. A., Ulloque, R., Kihara, G. K., Zheng, H. & Kinzy, T. G. Translation elongation factor 2 anticodon mimicry domain mutants affect fidelity and diphtheria toxin resistance. *J. Biol. Chem.* **281,** 32639 (2006).

49. Frank, J. Intermediate states during mRNA-tRNA translocation. *Curr. Opin. Struct. Biol.* **22,** 778–85 (2012).

50. Fischer, N., Konevega, A. L., Wintermeyer, W., Rodnina, M. V & Stark, H. Ribosome dynamics and tRNA movement by time-resolved electron cryomicroscopy. *Nature* **466,** 329–333 (2010).

51. Zhou, J., Lancaster, L., Donohue, J. P. & Noller, H. F. How the ribosome hands the A-site tRNA to the P site during EF-G-catalyzed translocation. *Science* **345,** 1188–91 (2014).

52. Andersen, C. B. F. *et al.* Structure of eEF3 and the mechanism of transfer RNA release from the E-site. *Nature* **443,** 663–668 (2006).

53. Dever, T. E. & Green, R. The elongation, termination, and recycling phases of translation in eukaryotes. *Cold Spring Harb. Perspect. Biol.* **4,** a013706 (2012).

54. Zhou, J., Korostelev, A., Lancaster, L. & Noller, H. F. Crystal structures of 70S ribosomes bound to release factors RF1, RF2 and RF3. *Curr. Opin. Struct. Biol.* **22,** 733–42 (2012).

55. Hirokawa, G. *et al.* The role of ribosome recycling factor in dissociation of 70S ribosomes into subunits. *RNA* **11,** 1317–28 (2005).

56. Peske, F., Rodnina, M. V & Wintermeyer, W. Sequence of steps in ribosome recycling as defined by kinetic analysis. *Mol. Cell* **18,** 403–412 (2005).

57. Fan-Minogue, H. *et al.* Distinct eRF3 requirements suggest alternate eRF1 conformations mediate peptide release during eukaryotic translation termination. *Mol. Cell* **30,** 599–609 (2008).

58. Frolova, L. Y. *et al.* Mutations in the highly conserved GGQ motif of class 1 polypeptide release factors abolish ability of human eRF1 to trigger peptidyl-tRNA hydrolysis. *RNA* **5,** 1014–20 (1999).

59. Frolova, L. *et al.* Eukaryotic polypeptide chain release factor eRF3 is an eRF1- and ribosome-dependent guanosine triphosphatase. *RNA* **2,** 334–41 (1996).

60. Pisarev, A. V, Hellen, C. U. T. & Pestova, T. V. Recycling of eukaryotic posttermination ribosomal complexes. *Cell* **131,** 286–99 (2007).

61. Pisarev, A. V *et al.* The role of ABCE1 in eukaryotic posttermination ribosomal recycling. *Mol. Cell* **37,** 196–210 (2010).

62. Skabkin, M. A., Skabkina, O. V, Hellen, C. U. T. & Pestova, T. V. Reinitiation and other unconventional posttermination events during eukaryotic translation. *Mol. Cell* **51,** 249–64 (2013).

63. Uchida, N., Hoshino, S.-I., Imataka, H., Sonenberg, N. & Katada, T. A novel role of the mammalian GSPT/eRF3 associating with poly(A)-binding protein in Cap/Poly(A)-dependent translation. *J. Biol. Chem.* **277,** 50286–92 (2002).

64. Jackson, R. J., Hellen, C. U. T. & Pestova, T. V. *Termination and post-termination events in eukaryotic translation. Advances in protein chemistry and structural biology* **86,** 45–93 (Elsevier Inc., 2012).

65. Shoemaker, C. J., Eyler, D. E. & Green, R. Dom34:Hbs1 promotes subunit dissociation and peptidyl-tRNA drop-off to initiate no-go decay. *Science (80-.).* **330,** 369–372 (2010).

66. Becker, T. *et al.* Structure of the no-go mRNA decay complex Dom34-Hbs1 bound to a stalled 80S ribosome. *Nat. Struct. Mol. Biol.* **18,** 715–720 (2011).

67. Becker, T. *et al.* Structural basis of highly conserved ribosome recycling in eukaryotes and archaea. *Nature* **482,** 501–506 (2012).

68. Gao, N. *et al.* Mechanism for the disassembly of the posttermination complex inferred from cryo-EM studies. *Mol. Cell* **18,** 663–74 (2005).

69. Preis, A. *et al.* Cryoelectron microscopic structures of eukaryotic translation termination complexes containing eRF1-eRF3 or eRF1-ABCE1. *Cell Rep.* **8,** 59–65 (2014).

70. Shoemaker, C. J., Eyler, D. E. & Green, R. Dom34:Hbs1 promotes subunit dissociation and peptidyl-tRNA drop-off to initiate no-go decay. *Science* **330,** 369–72 (2010).

71. Skabkin, M. A. *et al.* Activities of Ligatin and MCT-1/DENR in eukaryotic translation initiation and ribosomal recycling. *Genes Dev.* **24,** 1787–801 (2010).

72. Sohmen, D., Harms, J. M., Schlünzen, F. & Wilson, D. N. Enhanced SnapShot: Antibiotic inhibition of protein synthesis II. *Cell* **139,** 212–212.e1 (2009).

73. Sohmen, D., Harms, J. M., Schlünzen, F. & Wilson, D. N. SnapShot: Antibiotic inhibition of protein synthesis I. *Cell* **138,** 1248.e1 (2009).

74. Tsai, A. *et al.* The impact of aminoglycosides on the dynamics of translation elongation. *Cell Rep.* **3,** 497–508 (2013).

75. De Loubresse, N. G. *et al.* Structural basis for the inhibition of the eukaryotic ribosome. *Nature* **513,** 517–522 (2014).

76. Hansen, J. L., Moore, P. B. & Steitz, T. A. Structures of five antibiotics bound at the peptidyl transferase center of the large ribosomal subunit. *J. Mol. Biol.* **330,** 1061–1075 (2003).

77. Rakauskaite, R. & Dinman, J. D. Mutations of highly conserved bases in the peptidyltransferase center induce compensatory rearrangements in yeast ribosomes. *RNA* **17,** 855–64 (2011).

78. Petrov, A., Chen, J., O'Leary, S., Tsai, A. & Puglisi, J. D. Single-molecule analysis of translational dynamics. *Cold Spring Harb. Perspect. Biol.* **4,** a011551 (2012).

79. Zeng, X., Chugh, J., Casiano-Negroni, A., Al-Hashimi, H. M. & Brooks, C. L. Flipping of the ribosomal A-site adenines provides a basis for tRNA selection. *J. Mol. Biol.* **426,** 3201–13 (2014).

80. Nanda, J. S., Saini, A. K., Muñoz, A. M., Hinnebusch, A. G. & Lorsch, J. R. Coordinated movements of eukaryotic translation initiation factors eIF1, eIF1A, and eIF5 trigger phosphate release from eIF2 in response to start codon recognition by the ribosomal preinitiation complex. *J. Biol. Chem.* **288,** 5316–29 (2013).

81. Hinnebusch, A. G. & Lorsch, J. R. The mechanism of eukaryotic translation initiation: new insights and challenges. *Cold Spring Harb. Perspect. Biol.* **4,** a011544– (2012).

82. Jenner, L., Ben-Shem, A., Demeshkina, N., Yusupov, M. & Yusupova, G. in *Biophysical approaches to translational control of gene expression* (ed. Dinman, J. D.) 1–25 (Springer New York, 2013).

83. Sanbonmatsu, K. Y., Blanchard, S. C. & Whitford, P. C. in *Biophysical approaches to translational control of gene expression* 51–68 (Springer New York, 2013).

84. Datta, P. & Chatterjee, A. in *Biophysical approaches to translational control of gene expression* 27–50 (Springer New York, 2013).

85. Whitford, P. C. *et al.* Accommodation of aminoacyl-tRNA into the ribosome involves reversible excursions along multiple pathways. *RNA* **16,** 1196–204 (2010).

86. Sanbonmatsu, K. Y., Joseph, S. & Tung, C. S. Simulating movement of tRNA into the ribosome during decoding. *Proc. Natl. Acad. Sci.* **102,** 15854 (2005).

87. *Biophysical approaches to translational control of gene expression*. (Springer New York; 1 edition, 2013). doi:10.1007/978-1-4614-3991-2

88. Perutz, M. F. in *Nobel Lectures Chemistry* 653–673 (Elsevier Publishing Company, 1964).

89. Bai, X.-C., Fernandez, I. S., McMullan, G. & Scheres, S. H. W. Ribosome structures to near-atomic resolution from thirty thousand cryo-EM particles. *Elife* **2,** e00461 (2013).

90. Roy, R., Hohng, S. & Ha, T. A practical guide to single-molecule FRET. *Nat. Methods* **5,** 507–16 (2008).

91. Blanchard, S. C. Single-molecule observations of ribosome function. *Curr. Opin. Struct. Biol.* **19,** 103–9 (2009).

92. Wang, Y., Xiao, M. & Li, Y. Heterogeneity of single molecule FRET signals reveals multiple active ribosome subpopulations. *Proteins* **82,** 1–9 (2014).

93. *RNA-Protein Interactions : A Practical Approach: A Practical Approach*. 366 (Oxford University Press, 1998). at <http://books.google.com/books?id=ObiBuB_s24cC&pgis=1>

94. Weeks, K. M. Advances in RNA structure analysis by chemical probing. *Curr. Opin. Struct. Biol.* **20,** 295–304 (2010).

95. Hermanson, G. T. *Bioconjugate Techniques*. 1200 (Academic Press, 2013). at <http://books.google.com/books?id=6aO-207lhdgC&pgis=1>

96. Heilek, G. M., Marusak, R., Meares, C. F. & Noller, H. F. Directed hydroxyl radical probing of 16S rRNA using Fe(II) tethered to ribosomal protein S4. *Proc. Natl. Acad. Sci. U. S. A.* **92,** 1113–6 (1995).

97. Woodson, S. A., Deras, M. L. & Brenowitz, M. Time-resolved hydroxyl radical footprinting of RNA with X-rays. *Curr. Protoc. Nucleic Acid Chem.* Chapter 11, Unit 11.6 (2001).

98. Regulski, E. E. & Breaker, R. R. In-line probing analysis of riboswitches. *Methods Mol. Biol.* **419,** 53–67 (2008).

99. Leshin, J. A., Meskauskas, A. M. & Dinman, J. D. in *Biophysical approaches to translational control of gene expression* 69–81 (Springer New York, 2013).

100. Mortimer, S. a & Weeks, K. M. A fast-acting reagent for accurate analysis of RNA secondary and tertiary structure by SHAPE chemistry. *J. Am. Chem. Soc.* **129,** 4144–5 (2007).

101. Merino, E. J., Wilkinson, K. A., Coughlan, J. L. & Weeks, K. M. RNA structure analysis at single nucleotide resolution by selective 2'-hydroxyl acylation and primer extension (SHAPE). *J. Am. Chem. Soc.* **127,** 4223–4231 (2005).

102. Chamberlin, S. I. & Weeks, K. M. Mapping Local Nucleotide Flexibility by Selective Acylation of 2‘-Amine Substituted RNA. *J. Am. Chem. Soc.* **122,** 216–224 (2000).

103. Roat-Malone, R. M. *Bioinorganic Chemistry: A Short Course*. 243 (John Wiley & Sons, 2007). at <https://books.google.com/books?id=g--28L1G-MkC&pgis=1>

104. Mcginnis, J. L., Dunkle, J. A., Cate, J. H. D. & Weeks, K. M. The Mechanisms of RNA SHAPE Chemistry. (2012).

105. Leshin, J. A., Heselpoth, R., Belew, A. T. & Dinman, J. D. High throughput structural analysis of yeast ribosomes using hSHAPE. *RNA Biol.* **8,** 478–487 (2011).

106. Vasa, S. M., Guex, N., Wilkinson, K. a, Weeks, K. M. & Giddings, M. C. ShapeFinder: a software system for high-throughput quantitative analysis of nucleic acid reactivity information resolved by capillary electrophoresis. *RNA* **14,** 1979–90 (2008).

107. McGinnis, J. L., Duncan, C. D. S. & Weeks, K. M. High-throughput SHAPE and hydroxyl radical analysis of RNA structure and ribonucleoprotein assembly. *Methods Enzymol.* **468,** 67–89 (2009).

108. Batey, R., Rambo, R. & Doudna, J. Tertiary Motifs in RNA Structure and Folding. *Angew. Chem. Int. Ed. Engl.* **38,** 2326–2343 (1999).

109. Wilkinson, K. A., Merino, E. J. & Weeks, K. M. Selective 2’-hydroxyl acylation analyzed by primer extension (SHAPE): quantitative RNA structure analysis at single nucleotide resolution. *Nat. Protoc.* **1,** 1610–6 (2006).

110. Wilkinson, K. a *et al.* High-throughput SHAPE analysis reveals structures in HIV-1 genomic RNA strongly conserved across distinct biological states. *PLoS Biol.* **6,** e96 (2008).

111. Vasa, S. M., Guex, N., Wilkinson, K. A., Weeks, K. M. & Giddings, M. C. ShapeFinder : A software system for high-throughput quantitative analysis of nucleic acid reactivity information resolved by capillary electrophoresis (2008). doi:10.1261/rna.1166808

112. Mortimer, S. a & Weeks, K. M. Time-resolved RNA SHAPE chemistry: quantitative RNA structure analysis in one-second snapshots and at single-nucleotide resolution. *Nat. Protoc.* **4,** 1413–21 (2009).

113. Lucks, J. B. *et al.* Multiplexed RNA structure characterization with selective 2'-hydroxyl acylation analyzed by primer extension sequencing (SHAPE-Seq). *Proc. Natl. Acad. Sci. U. S. A.* **108,** 11063–8 (2011).

114. Loughrey, D., Watters, K. E., Settle, A. H. & Lucks, J. B. SHAPE-Seq 2.0: systematic optimization and extension of high-throughput chemical probing of RNA secondary structure with next generation sequencing. *Nucleic Acids Res.* gku909– (2014). doi:10.1093/nar/gku909

115. Karabiber, F., McGinnis, J. L., Favorov, O. V & Weeks, K. M. QuShape: rapid, accurate, and best-practices quantification of nucleic acid probing information, resolved by capillary electrophoresis. *RNA* **19,** 63–73 (2013).

116. Low, J. T. & Weeks, K. M. SHAPE-directed RNA secondary structure prediction. *Methods* **52,** 150–8 (2010).

117. Kladwang, W., VanLang, C. C., Cordero, P. & Das, R. Understanding the errors of SHAPE-directed RNA structure modeling. *Biochemistry* **50,** 8049–56 (2011).

118. Yoon, S. *et al.* HiTRACE: high-throughput robust analysis for capillary electrophoresis. *Bioinformatics* **27,** 1798–805 (2011).

119. Siegfried, N. A., Busan, S., Rice, G. M., Nelson, J. A. E. & Weeks, K. M. RNA motif discovery by SHAPE and mutational profiling (SHAPE-MaP). *Nat. Methods* **11,** 959–65 (2014).

120. Kladwang, W., VanLang, C. C., Cordero, P. & Das, R. A two-dimensional mutate-and-map strategy for non-coding RNA structure. *Nat. Chem.* **3,** 954–62 (2011).

121. Tian, S., Cordero, P., Kladwang, W. & Das, R. High-throughput mutate-map-rescue evaluates SHAPE-directed RNA structure and uncovers excited states. *RNA* **20,** 1815–26 (2014).

122. Kladwang, W. *et al.* Standardization of RNA chemical mapping experiments. *Biochemistry* **53,** 3063–5 (2014).

123. Pang, P. S., Elazar, M., Pham, E. a & Glenn, J. S. Simplified RNA secondary structure mapping by automation of SHAPE data analysis. *Nucleic Acids Res.* **39,** e151 (2011).

124. Fang, G. *et al.* Genome-wide mapping of methylated adenine residues in pathogenic Escherichia coli using single-molecule real-time sequencing. *Nat. Biotechnol.* **30,** 1232–9 (2012).

125. Xing, H., Mo, Y., Liao, W. & Zhang, M. Q. Genome-wide localization of protein-DNA binding and histone modification by a Bayesian change-point method with ChIP-seq data. *PLoS Comput. Biol.* **8,** e1002613 (2012).

126. Ramrath, D. J. F. *et al.* Visualization of two transfer RNAs trapped in transit during elongation factor G-mediated translocation. *Proc. Natl. Acad. Sci. U. S. A.* **110,** 20964–9 (2013).

127. Budkevich, T. *et al.* Structure and Dynamics of the Mammalian Ribosomal Pretranslocation Complex. *Mol. Cell* **44,** 214–224 (2011).

128. Crow. *Lognormal Distributions: Theory and Applications*. 387 (CRC Press, 1987). at <https://books.google.com/books?id=B8kNa1khS4QC&pgis=1>

129. Wang, S. C. Analysis of Zero-Heavy Data Using a Mixture Model Approach. (Virginia Tech, 1998). at <http://vtechworks.lib.vt.edu/handle/10919/30357>

130. Saini, A. K. *et al.* Eukaryotic translation initiation factor eIF5 promotes the accuracy of start codon recognition by regulating Pi release and conformational transitions of the preinitiation complex. *Nucleic Acids Res.* **42,** 9623–40 (2014).

131. Lomakin, I. B. & Steitz, T. A. The initiation of mammalian protein synthesis and mRNA scanning mechanism. *Nature* **500,** 307–11 (2013).

132. Passmore, L. A. *et al.* The eukaryotic translation initiation factors eIF1 and eIF1A induce an open conformation of the 40S ribosome. *Mol. Cell* **26,** 41–50 (2007).

133. Weisser, M., Voigts-Hoffmann, F., Rabl, J., Leibundgut, M. & Ban, N. The crystal structure of the eukaryotic 40S ribosomal subunit in complex with eIF1 and eIF1A. *Nat. Struct. Mol. Biol.* **20,** 1015–7 (2013).

134. Hinnebusch, A. G. The scanning mechanism of eukaryotic translation initiation. *Annu. Rev. Biochem.* **83,** 779–812 (2014).

135. Lomakin, I. B. & Steitz, T. A. The initiation of mammalian protein synthesis and mRNA scanning mechanism. *Nature* **500,** 307–11 (2013).

136. Erzberger, J. P. *et al.* Molecular Architecture of the 40S·eIF1·eIF3 Translation Initiation Complex. *Cell* **158,** 1123–35 (2014).

137. Hussain, T. *et al.* Structural Changes Enable Start Codon Recognition by the Eukaryotic Translation Initiation Complex. *Cell* **159,** 597–607 (2014).

138. Hashem, Y. *et al.* Structure of the mammalian ribosomal 43S preinitiation complex bound to the scanning factor DHX29. *Cell* **153,** 1108–19 (2013).

139. Luna, R. E. *et al.* The interaction between eukaryotic initiation factor 1A and eIF5 retains eIF1 within scanning preinitiation complexes. *Biochemistry* **52,** 9510–8 (2013).

140. Algire, M. A. *et al.* Development and characterization of a reconstituted yeast translation initiation system. *RNA* **8,** 382–397 (2002).

141. Conte, M. R. *et al.* Structure of the eukaryotic initiation factor (eIF) 5 reveals a fold common to several translation factors. *Biochemistry* **45,** 4550–8 (2006).

142. Bieniossek, C. *et al.* The crystal structure of the carboxy-terminal domain of human translation initiation factor eIF5. *J. Mol. Biol.* **360,** 457–65 (2006).

143. Gilbert, R. J. C. *et al.* Reconfiguration of yeast 40S ribosomal subunit domains by the translation initiation multifactor complex. *Proc. Natl. Acad. Sci.* **104,** 5788 (2007).

144. Moazed, D. & Noller, H. F. Interaction of tRNA with 23S rRNA in the ribosomal A, P, and E sites. *Cell* **57,** 585–597 (1989).

145. Moazed, D. & Noller, H. F. Binding of tRNA to the ribosomal A and P sites protects two distinct sets of nucleotides in 16 S rRNA. *J. Mol. Biol.* **211,** 135–45 (1990).

146. Moazed, D. & Robertson, J. M. Interaction of elongation factors EF-G and EF-Tu with a conserved loop in 23S RNA. *Nature* **334,** 362–364 (1988).

147. Moazed, D. & Noller, H. F. Sites of interaction of the CCA end of peptidyl-tRNA with 23S rRNA. *Proc. Natl. Acad. Sci.* **88,** 3725–3728 (1991).

148. Moazed, D. & Noller, H. F. Intermediate states in the movement of transfer RNA in the ribosome. *Nature* **342,** 142–148 (1989).

149. Joseph, S. & Noller, H. F. Mapping the rRNA neighborhood of. **15,** 910–916 (1996).

150. Fraser, C. S., Berry, K. E., Hershey, J. W. B. & Doudna, J. A. eIF3j is located in the decoding center of the human 40S ribosomal subunit. *Mol. Cell* **26,** 811–9 (2007).

151. Khade, P. & Joseph, S. Functional interactions by transfer RNAs in the ribosome. *FEBS Lett.* **584,** 420–6 (2010).

152. Wollenzien, P., Expert-Bezancon, A. & Favree, A. Sites of Contact of mRNA with 16S rRNA and 25S rRNA. *Biochemistry* **30,** 1788–1795 (1991).

153. Moazed, D. & Noller, H. F. Binding of tRNA to the ribosomal A and P sites protects two distinct sets of nucleotides in 16 S rRNA. *J. Mol. Biol.* **211,** 135–45 (1990).

154. Moazed, D. & Noller, H. F. Interaction of tRNA with 23S rRNA in the ribosomal A, P, and E sites. *Cell* **57,** 585–597 (1989).

155. Moazed, D. & Noller, H. F. Transfer RNA shields specific nucleotides in 16S ribosomal RNA from attack by chemical probes. *Cell* **47,** 985–994 (1986).

156. Wilson, K. S. & Noller, H. F. Molecular movement inside the translational engine. *Cell* **92,** 337–349 (1998).

157. Mitchell, P., Osswald, M. & Brimacombe, R. Identification of intermolecular RNA cross-links at the subunit interface of the Escherichia coli ribosome. *Biochemistry* **31,** 3004–3011 (1992).

158. Merryman, C., Moazed, D., Daubresse, G. & Noller, H. F. Nucleotides in 23S rRNA protected by the association of 30S and 50S ribosomal subunits1. *J. Mol. Biol.* **285,** 107–113 (1999).

159. Merryman, C., Moazed, D., McWhirter, J. & Noller, H. F. Nucleotides in 16S rRNA protected by the association of 30S and 50S ribosomal subunits. *J. Mol. Biol.* **285,** 97–105 (1999).

160. Maivali, U. Definition of bases in 23S rRNA essential for ribosomal subunit association. *RNA* **10,** 600–604 (2004).

161. Yusupov, M. M. *et al.* Crystal structure of the ribosome at 5.5 A resolution. *Science* **292,** 883–96 (2001).

162. Anger, A. M. *et al.* Structures of the human and Drosophila 80S ribosome. *Nature* **497,** 80–5 (2013).

163. Zhang, W., Dunkle, J. a & Cate, J. H. D. Structures of the ribosome in intermediate states of ratcheting. *Science* **325,** 1014–7 (2009).

164. Wilson, D. N. & Doudna Cate, J. H. The structure and function of the eukaryotic ribosome. *Cold Spring Harb. Perspect. Biol.* **4,** a011536– (2012).

165. Kossinova, O., Malygin, A., Krol, A. & Karpova, G. The SBP2 protein central to selenoprotein synthesis contacts the human ribosome at expansion segment 7L of the 28S rRNA. *RNA* **20,** 1046–56 (2014).

166. Caban, K. & Copeland, P. R. Selenocysteine insertion sequence (SECIS)-binding protein 2 alters conformational dynamics of residues involved in tRNA accommodation in 80 S ribosomes. *J. Biol. Chem.* **287,** 10664–73 (2012).

167. Armache, J.-P. *et al.* Cryo-EM structure and rRNA model of a translating eukaryotic 80S ribosome at 5.5-A resolution. *Proc. Natl. Acad. Sci. U. S. A.* **107,** 19748–53 (2010).

168. Alkemar, G. & NYGÅRD, O. Secondary structure of two regions in expansion segments ES3 and ES6 with the potential of forming a tertiary interaction in eukaryotic 40S ribosomal subunits. *RNA* **10,** 403 (2004).

169. Alkemar, G. & Nygård, O. Probing the secondary structure of expansion segment ES6 in 18S ribosomal RNA. *Biochemistry* **45,** 8067–78 (2006).

170. Larsson, S. L. & Nygård, O. Proposed secondary structure of eukaryote specific expansion segment 15 in 28S rRNA from mice, rats, and rabbits. *Biochemistry* **40,** 3222–31 (2001).

171. Nygård, O., Alkemar, G. & Larsson, S. L. Analysis of the secondary structure of expansion segment 39 in ribosomes from fungi, plants and mammals. *J. Mol. Biol.* **357,** 904–16 (2006).

172. Marquez, V. *et al.* Maintaining the Ribosomal Reading Frame:: The Influence of the E Site during Translational Regulation of Release Factor 2. *Cell* **118,** 45–55 (2004).

173. Rheinberger, H. J. & Nierhaus, K. H. Allosteric interactions between the ribosomal transfer RNA-binding sites A and E. *J. Biol. Chem.* **261,** 9133–9 (1986).

174. Nierhaus, K. H. The allosteric three-site model for the ribosomal elongation cycle: features and future. *Biochemistry* **29,** 4997–5008 (1990).

175. Svidritskiy, E., Brilot, A. F., Koh, C. S., Grigorieff, N. & Korostelev, A. A. Structures of Yeast 80S Ribosome-tRNA Complexes in the Rotated and Nonrotated Conformations. *Structure* **22,** 1210–8 (2014).

176. Burakovsky, D. E. *et al.* Mutations at the accommodation gate of the ribosome impair RF2-dependent translation termination. *RNA* **16,** 1848–53 (2010).

177. Sergiev, P. V. V *et al.* The conserved A-site finger of the 23 S rRNA: Just one of the intersubunit bridges or a part of the allosteric communication pathway? *J. Mol. Biol.* **353,** 116–123 (2005).

178. Rakauskaite, R. & Dinman, J. D. An arc of unpaired “hinge bases” facilitates information exchange among functional centers of the ribosome. *Mol. Cell. Biol.* **26,** 8992–9002 (2006).

179. Rhodin, M. H. J. & Dinman, J. D. An Extensive Network of Information Flow through the B1b/c Intersubunit Bridge of the Yeast Ribosome. *PLoS One* **6,** e20048 (2011).

180. Rhodin, M. H. J. & Dinman, J. D. A flexible loop in yeast ribosomal protein L11 coordinates P-site tRNA binding. *Nucleic Acids Res.* **38,** 8377–8389 (2010).

181. Meskauskas, A. & Dinman, J. D. A molecular clamp ensures allosteric coordination of peptidyltransfer and ligand binding to the ribosomal A-site. *Nucleic Acids Res.* **38,** 7800–13 (2010).

182. Koosha, H., Cameron, D., Andrews, K., Dahlberg, A. E. & March, P. E. Alterations in the peptidyltransferase and decoding domains of ribosomal RNA suppress mutations in the elongation factor G gene. *RNA* **6,** 1166–73 (2000).

183. Agrawal, R. K., Lata, R. K. & Frank, J. Conformational variability in Escherichia coli 70S ribosome as revealed by 3D cryo-electron microscopy. *Int. J. Biochem. Cell Biol.* **31,** 243–54 (1999).

184. Malhotra, A. *et al.* Escherichia coli 70 S ribosome at 15 A resolution by cryo-electron microscopy: localization of fMet-tRNAfMet and fitting of L1 protein. *J. Mol. Biol.* **280,** 103–16 (1998).

185. Fei, J., Kosuri, P., MacDougall, D. D. & Gonzalez, R. L. Coupling of ribosomal L1 stalk and tRNA dynamics during translation elongation. *Mol. Cell* **30,** 348–359 (2008).

186. Trabuco, L. G. *et al.* The role of L1 stalk-tRNA interaction in the ribosome elongation cycle. *J. Mol. Biol.* **402,** 741–60 (2010).

187. Spahn, C. M. T. *et al.* Structure of the 80S ribosome from Saccharomyces cerevisiae–tRNA-ribosome and subunit-subunit interactions. *Cell* **107,** 373–386 (2001).

188. Taylor, D. J. *et al.* Structures of modified eEF2 80S ribosome complexes reveal the role of GTP hydrolysis in translocation. *EMBO J.* **26,** 2421–2431 (2007).

189. Taylor, D. J. D. J. *et al.* Comprehensive molecular structure of the eukaryotic ribosome. *Structure* **17,** 1591–1604 (2009).

190. Spahn, C. M. T. *et al.* Domain movements of elongation factor eEF2 and the eukaryotic 80S ribosome facilitate tRNA translocation. *EMBO J.* **23,** 1008–1019 (2004).

191. Petrov, A. S. *et al.* Evolution of the ribosome at atomic resolution. *Proc. Natl. Acad. Sci. U. S. A.* **111,** 10251–10256 (2014).

192. Schroeder, S. J., Blaha, G., Tirado-Rives, J., Steitz, T. A. & Moore, P. B. The structures of antibiotics bound to the E site region of the 50 S ribosomal subunit of Haloarcula marismortui: 13-deoxytedanolide and girodazole. *J. Mol. Biol.* **367,** 1471–1479 (2007).

193. Greber, B. J. *et al.* Cryo-EM structure of the archaeal 50S ribosomal subunit in complex with initiation factor 6 and implications for ribosome evolution. *J. Mol. Biol.* **418,** 145–60 (2012).

194. Schmeing, T. M. *et al.* A pre-translocational intermediate in protein synthesis observed in crystals of enzymatically active 50S subunits. *Nat. Struct. Mol. Biol.* **9,** 225–230 (2002).

195. Yonath, A. The search and its outcome: high-resolution structures of ribosomal particles from mesophilic, thermophilic, and halophilic bacteria at various functional states. *Annu. Rev. Biophys. Biomol. Struct.* **31,** 257–73 (2002).

196. Fischer, N., Konevega, A. L., Wintermeyer, W., Rodnina, M. V & Stark, H. Ribosome dynamics and tRNA movement by time-resolved electron cryomicroscopy. *Nature* **466,** 329–33 (2010).

197. Yamamoto, H. *et al.* EF-G and EF4: translocation and back-translocation on the bacterial ribosome. *Nat. Rev. Microbiol.* **12,** 89–100 (2014).

198. Ramakrishnan, V., Brodersen, D. E., Carter, A. P., Wimberly, B. T. & Clemons Jr., W. M. Crystal structure of the 30s ribosome. (2001).

199. Rakauskaite, R., Dinman, J. D. & Rakauskait\.e, R. rRNA mutants in the yeast peptidyltransferase center reveal allosteric information networks and mechanisms of drug resistance. *Nucleic Acids Res.* **36,** 1497 (2008).

200. Berk, V., Zhang, W., Pai, R. D. & Cate, J. H. D. Structural basis for mRNA and tRNA positioning on the ribosome. *Proc. Natl. Acad. Sci.* **103,** 15830 (2006).

201. Stark, H. *et al.* Ribosome interactions of aminoacyl-tRNA and elongation factor Tu in the codon-recognition complex. *Nat. Struct. Mol. Biol.* **9,** 849–854 (2002).

202. Gao, Y.-G. *et al.* The structure of the ribosome with elongation factor G trapped in the posttranslocational state. *Science* **326,** 694–9 (2009).

203. Yusupov, M. M. *et al.* Crystal structure of the ribosome at 5.5 Å resolution. *Science.* **292,** 883 (2001).

204. Homan, P. J. *et al.* Single-molecule correlated chemical probing of RNA. *Proc. Natl. Acad. Sci. U. S. A.* **111,** 13858–13863 (2014).

205. Shenvi, C. L., Dong, K., Friedman, E. M., Hanson, J. A. & Cate, J. H. D. Accessibility of 18S rRNA in human 40S subunits and 80S ribosomes at physiological magnesium ion concentrations - implications for the study of ribosome dynamics. *RNA* **11,** 1898-1908 (2005).

206. Algire, M. A. *et al.* Development and characterization of a reconstituted yeast translation initiation system. *RNA* **8,** 382–97 (2002).

207. Eyler, D. E. & Green, R. Distinct response of yeast ribosomes to a miscoding event during translation. *RNA* **17,** 925–32 (2011).

208. Graifer, D. & Karpova, G. Roles of ribosomal proteins in the functioning of translational machinery of eukaryotes. *Biochimie* **109C,** 1–17 (2014).

209. Musalgaonkar, S., Moomau, C. A. & Dinman, J. D. Ribosomes in the balance: structural equilibrium ensures translational fidelity and proper gene expression. *Nucleic Acids Res.* **42,** 13384–92 (2014).

210. Sulima, S. O. *et al.* Eukaryotic rpL10 drives ribosomal rotation. *Nucleic Acids Res.* **42,** 2049–63 (2014).

211. Deigan, K. E., Li, T. W., Mathews, D. H. & Weeks, K. M. Accurate SHAPE-directed RNA structure determination a SHAPE experiment can be interpreted as a pseudo-free energy high accuracy . Free energy minimization , by using SHAPE pseudo-. **2008,** (2008).

212. Leshin, J. A, Rakauskaitė, R., Dinman, J. D. & Meskauskas, A. Enhanced purity, activity and structural integrity of yeast ribosomes purified using a general chromatographic method. *RNA Biol.* **7,** 354–60 (2010).

213. Triana, F., Nierhaus, K. H. & Chakraburtty, K. Transfer RNA binding to 80S ribosomes from yeast: evidence for three sites. *Biochem. Mol. Biol. Int.* **33,** 909 (1994).